Institute of Translational Medicine

Department of Molecular and Clinical Cancer Medicine

EVALUATION OF UHRF1 AND THE ANTIOXIDANT RESPONSE PATHWAY IN PANCREATIC CANCER AND THE PREDICTION OF RESPONSE TO TREATMENT

Thesis submitted in accordance with the requirements of the University of Liverpool for the degree of Doctor in Philosophy by

Thompson GANA

October 2017

Supervisors: Prof. Eithne Costello, Dr William Greenhalf and

Dr Lakis Liloglou

DECLARATION

I certify that this is an original piece of work undertaken at the University of Liverpool. Except where stated otherwise, all work included in this thesis was undertaken by myself. This work has not been submitted or used at any other University.

To my parents and siblings
and
To the company of my unseen and very special friends that have kept me hale and hearty

ABSTRACT

Pancreatic ductal adenocarcinoma (PDAC) is one of the most lethal cancers, characterised by very poor survival. The cellular defence protein Nrf2 is a mediator of oncogenesis in pancreatic cancer, although its role in this cancer type is not fully understood. UHRF1 is a nuclear protein involved in epigenetic regulation. Our laboratory recently established that UHRF1 suppresses Keap1, an important negative regulator of the Nrf2 pathway.

The aim of this study was to explore how UHRF1 contributes to Nrf2 function in pancreatic cancer cells and in pancreatic stellate cells, and to determine whether UHRF1 or NQO1, a downstream marker of Nrf2 activity could be predictive of PDAC treatment response. Depletion of UHRF1 from PDAC cells was associated with transcriptional upregulation of *KEAP1*, decreased levels of Nrf2 and Nrf2-regulated downstream proteins (NQO1 and AKR1C1), increased oxidative stress in the form of lower glutathione levels and increased reactive oxygen species. UHRF1 depletion enhanced cell cycle arrest, and concomitant depletion of UHRF1 and Keap1 reversed this effect, restored Nrf2 levels and reversed the increase in reactive oxygen species.

The expression of UHRF1 in human pancreatic stellate cells (hPSCs) was limited to a small subset of cells. Analysis in Nrf2-null mouse pancreatic stellate cells was precluded by the fact that these cells, unlike their wild-type counterparts could not be maintained in culture. Histological analysis of the pancreata of Nrf2-null mice revealed early signs of pancreatitis.

Germline single nucleotide polymorphisms (SNPs) were analysed in patients with advanced PDAC (n=140) from TeloVac and ViP clinical trials. The *NQO1* rs1800566 CC homozygous major genotype was associated with poor survival (p=0.01) and the combined *NQO1* rs1800566 and *SRXN1* rs6053666 SNPs were prognostic of survival in these patients (p=0.039). No SNP–related differences in survival for *NRF2* rs2886162 and *SRXN1* rs6053666 variants were observed (p=0.405 and p=0.634 respectively).

To determine whether UHRF1 or NQO1 expression are predictive of PDAC patient response to treatment, tissue microarrays from 349 patients randomized to chemotherapy in the ESPAC-3 trial (plus controls from ESPAC-1) were analysed by immunohistochemistry for these proteins. Patients were dichotomized into low and high expression for nuclear UHRF1 and cytoplasmic NQO1 levels respectively and groups compared using Kaplan-Meier curves, log-rank tests, and Cox proportional hazards models.

UHRF1 was expressed in 181 of 199 (90.9%) PDAC tumours. Its levels were not associated with survival in the observation only group, or in either 5FU/folinic acid or gemcitabine treated groups (p=0.882, p=0.34 and p=0.92 respectively). Interestingly, an inverse relationship between UHRF1 and diabetes was apparent (p=0.005).

NQO1 was expressed in the cytoplasm of 197 (95.2%) PDAC tumours. NQO1 levels were not associated with survival for the patents in the observation only group (p=0.301). However, median survival for patients treated with gemcitabine was 13.7 (95% CI 10.2 to 16.8) months for those with low NQO1 expression versus 24.2 (95%

CI 16.3 to 29.5) months for those with high NQO1 expression (p=0.01). For the 5FU/folinic acid group, median survival was 13.4 (95% CI 10.9 to 19.6) and 21.8 (95 % CI 16.9 to 25.7) months for those with low and high NQO1 levels respectively (p=0.08). Multivariable Cox proportional hazard analysis in gemcitabine treated patients, revealed that NQO1 expression was not an independent predictive factor in gemcitabine-treated (p=0.19) patients.

In summary, UHRF1 regulates Nrf2 in PDAC. UHRF1 levels are not prognostic, nor are they predictive of response to treatment in this disease. Interestingly, UHRF1 levels are inversely associated with diabetes, a finding that merits further study. By contrast, the *NQO1* SNP rs1800566 is prognostic in advanced PDAC patients and NQO1 protein expression is not an independent predictive marker of response to adjuvant gemcitabine treatment in PDAC patients.

ACKNOWLEDGEMENTS

Looking back in time through this mentally inspiring and physically challenging academic journey, I find myself indebted to all of those with whom I have had the pleasure of working with during these years.

Foremost, I would like to express my heartfelt gratitude to my supervisor, Professor Eithne Costello for her guidance, motivation and patience; she inspired me to think and work independently from which I have gained a wealth of experience. I would like to also thank other members of my supervisory team, Dr William Greenhalf and Dr Lakis Liloglou for their constructive criticism and insightful comments. My sincere thanks also goes to Professor Fiona Campbell with whom I spent many hours over several days scoring the tissue microarray immunohistochemistry slides.

Special thanks to Dr Anthony Evans for introducing me to several statistical softwares and together with Dr Karen Aughton both proof read my thesis draft; I cannot thank you both well enough for all your support. Other research staffs have been wonderful and deserve special mention too: Dr Lawrence B. Barrera, Dr Claire Jenkinson, Dr Wafa Abu-Alainin, Dr Adedamola O. Olayanju, Dr Paul Sykes, Dr Li Yan, Dr Taha Elmitwalli, Dr Lucy Oldfield, Dr Elinor Chapman, Dr Asmaa Salman, Dr Peppy Emeagi, Dr Victoria Shaw, Mr Tom Hanna; you have introduced me to new research skills and I owe my gratitude to you all.

I also want to acknowledge the friendship of fellow research colleagues: Mr Kulbir Mann, Mr Rohith R. Gopala, Ms Andrea Sheel, Mr Eyas Mohammed, Dylan Williams, Ms Frances Oldfield, Mr Summit Nandi, the companionship in short and long time

was worthwhile. I am also grateful to Dr Elizabeth Garner, Katie Bullock, Leigh Shannon, Natalie Coplin, Patricia Gerard, Timothy Dickson and Dr John Stanbury for their technical and logistic support.

I would also like to thank CRUK Liverpool Cancer Trials Unit for permission to use and include clinical trial data in this thesis. I am grateful to Institute of Translational Medicine (ITM), University of Liverpool and Hospitals Management Board, Niger State, Government of Nigeria for funding my research. I am also indebted to ITM postgraduate research team for giving me a memorable student experience here at the University of Liverpool.

Finally, I would like to thank my parents Mr and Mrs E.K. Gana and my siblings Henry, Patience, Moses and Solomon for their loving support while I have been away from them for many years. Last but not the least, I am grateful to my Uncle and his family Dr and Dr (Mrs) H.B. Gana for accommodating and supporting me during my programme here and to Dr and Mrs P. Gana and Dr and Mrs S. Yisa for their kind gestures during my stay in the UK.

PUBLICATIONS AND POSTERS:

Findings of the first result chapter (chapter 3) have been published in a peer reviewed journal:

Abu-Alainin, W., **Gana, T**., Liloglou, T., Olayanju, A., Barrera, L. N., Ferguson, R., Campbell, F., Andrews, T., Goldring, C., Kitteringham, N., Park, B. K., Nedjadi, T., Schmid, M. C., Slupsky, J. R., Greenhalf, W., Neoptolemos, J. P. and Costello, E. (2016), **UHRF1 regulation of the Keap1–Nrf2 pathway in pancreatic cancer contributes to oncogenesis.** J. Pathol., 238: 423–433. doi: 10.1002/path.4665

The findings of the first result chapter (chapter 3) have been presented at the following research meeting:

Oral Presentation
UHRF1 regulates the Keap1-Nrf2 cellular defence pathway in pancreatic cancer, European Pancreatic Club Conference, Toledo, Spain, 23 -26 June 2015.

The findings of the third result chapter (chapter 5) have been presented at the following research meeting:

Poster Presentation
Correlation of protein abundance and Single Nucleotide Polymorphism of *NRF2, NQO1* and *SRXN1* with patient survival in pancreatic cancer, Annual University of Liverpool Postgraduate Poster day, University of Liverpool, United Kingdom, June 2016

LIST OF ABBREVIATIONS

5FU	5-fluorouracil
AKR	Aldo-keto reductases
APSCs	Activated pancreatic stellate cells
ARE	Antioxidant response elements
BCA	Bicinchoninic acid
BIO	Biotinylated
BSA	Bovine serum albumin
CAF	Cancer associated fibroblast
CDKN2A	Cyclin dependent kinase inhibitor 2A
CI	Confidence interval
CKIs	Cyclin dependent kinase inhibitors
CpG	Cytosine-phosphate guanine
DAB	Diamidino-2-phenylindole
dFdC	2', 2' –difluorodeoxycytidine (Gemcitabine)
dFdCDP	Gemcitabine diphosphate
dFdCTP	Gemcitabine triphosphate
DMSO	Dimethyl sulfoxide
DNA	Deoxyribonucleic acid
DNMT1	DNA methyl transferase 1
DTT	Dithiothreitol
ECL	Enhanced chemiluminescence
ECM	Extra cellular matrix
EDTA	Ethylene diamine tetraacetic acid
EGFR	Epidermal growth factor receptor
EMT	Epithelial to mesenchymal transition
ESPAC	European Study Group for Pancreatic Cancer

FACS	Fluorescence-activated cell sorting
FBS	Fetal bovine serum
FAP	Fibroblast activation protein
FSP-1	Fibroblast specific protein-1
FAF	Fibrosis associated fibroblasts
FOLFIRINOX	Folinic acid, 5-FU, Irinotecan and Oxaliplatin
GCLc	Glutamate cysteine ligase catalytic subunit
GCLm	Glutamate cysteine ligase modulatory subunit
GS	Gluthathione synthetase
GSH	Reduced glutathione
GSR	Glutathione reductase
GSSG	Oxidized glutathione
HDAC	Histone deacetylase
HSCs	Hepatic stellate cells
HR	Hazard ratio
HRP	Horseradish peroxidase
ICBP 90	Inverted CCAAT box binding protein of 90 kDa
ICC	Immunocytochemistry
IHC	Immunohistochemistry
IPMN	Intraductal papillary mucinous neoplasm
JASPAC-1	Japan Adjuvant Study Group of Pancreatic Cancer 1
KM	Kaplan-Meier
Keap1	Kelch-like ECH-associated protein
KRAS	Kirsten rat sarcoma viral oncogene homolog
Maf	Masculoaponeurotic fibrosarcoma
MCN	Mucinous cyst neoplasm
NAF	Normal activated fibroblast
NQO1	NAD(P)H:quinone oxidoreductase 1

Nrf2	Nuclear factor erythroid 2-related factor 2
PAGE	Polyacrylamide gel electrophoresis
PanIN	Pancreatic intraepithelial neoplasia
PBS	Phosphate buffered saline
PC	Pancreatic cancer
PCR	Polymerase chain reaction
PCSs	Pancreatic stellate cells
PDAC	Pancreatic ductal adenocarcinoma
PHD	Plant homeo domain
PI	Propidium iodide
qPSCs	Quiescent pancreatic stellate cells
RING	Really interesting new gene
RNA	Ribonucleic acid
RNS	Reactive nitrogen species
ROS	Reactive oxygen species
RT	Reverse transcriptase
SDS	Sodium dodecyl sulphate
siRNA	Small interfering RNA
SRA	Set and ring associated domain
TeloVac	Telomerase vaccine
TMA	Tissue microarray
TTD	Tandem tudor domain
USP7	Ubiquitin specific peptidase 7
UBL	Ubiquitin-like domain
UHRF1	Ubiquitin-like with PHD and RING finger domains 1
VEGFR	Vascular endothelial factor receptor
ViP	Vandetanib in Pancreatic cancer
α-SMA	Alpha-smooth muscle actin

TABLE OF CONTENTS

1 GENERAL INTRODUCTION

1.1 Introduction

The pancreas is a vital organ that forms part of the gastrointestinal system and has digestive and hormonal functions. The digestive function of the pancreas is defined by the exocrine pancreas which makes up more than 95% of the pancreas and comprises acinar cells that secrete the digestive enzymes, the pancreatic ducts that deliver secreted enzymes to the small intestine, and the associated nerves, vessels and connective tissues. The endocrine pancreas (the islets) constitute 1-2% of the pancreatic mass and are responsible for hormonal synthesis and secretion of several hormones including insulin and glucagon[1]. Disturbances to the function of the pancreas can have severe consequences.

The term 'cancer' refers to the development of abnormal cell(s) that can arise from any tissue or organ characterized by uncontrolled cellular proliferation[2]. The transformation of normal cells into cancer cells which permits their proliferation, survival and spread is characterized by the acquisition of several biological traits[2]. Hanahan and Weinberg have described 10 hallmarks and facilitating characteristics commonly observed in cancers: enabling replicative immortality, sustaining proliferative signalling, resisting cell death, evading growth suppressors, inducing angiogenesis, activating invasion and metastasis, reprogramming cellular metabolism and evading immune destruction, all facilitated by tumour promoting inflammation and genome instability and mutation[2]. These properties although complex, are acquired by different cancers at various times during the multistep process leading to carcinogenesis.

Cancer is a major public health challenge worldwide; in 2012, an estimated 14.1 million new cancer cases and 8.2 million deaths from cancer occurred globally and this burden is expected to grow[3]. In Europe, an estimated 3.45 million new cancer cases and 1.75 million cancer related deaths were recorded in 2012[4]. In the United States, cancer is the second leading cause of death[5].

1.2 Pancreatic cancer

Pancreatic cancer is a leading cause of cancer related deaths in Europe and United States and the most lethal of gastrointestinal cancers[3-5] with an overall five-year survival of less than 7 %[6]. Surgical resection is potentially curative in patients that have cancers limited to the pancreas but despite surgical resection, the five-year survival in this group is still low though it has gradually improved from <18 %[7] to almost 29 %[8].

1.2.1 Epidemiological Trend

Sadly, there are currently no established screening tools for early detection of pancreatic cancer with an estimated 80 - 85 % of patients being diagnosed when the disease is advanced and no longer amenable to surgical resection[6,9]. In the early stages of PDAC patients have vague symptoms and present later with symptoms such as weight loss, jaundice, anorexia, fatigue and abdominal pain when the disease is advanced[10]. Both environmental (cigarette smoking, chronic pancreatitis, heavy alcohol consumption and long standing diabetes) and genetic factors (hereditary

pancreatitis and Peutz-Jeghers syndrome amongst others) have been implicated in pancreatic cancer development[11]. A 40-year trend in 5-year survival for pancreatic cancer in England from 1971 – 2011 showed a 1 % increase in survival from 2.3 – 3.3 %[12]. This is a very dismal prognosis. In Europe, an estimated pancreatic cancer incidence of 103,800 and mortality of 104,500 was recorded in 2012[4]. In the United States, pancreatic cancer is the fourth leading cause of cancer-associated death and is projected to be the second cause of cancer-related death by 2030[5,13]. The dismal prognosis associated with pancreatic cancer is attributable to late diagnosis and/or presentation and the blunted response to currently available therapeutics[6,14]. The intense stromal reaction and cancer heterogeneity have potentially contributed to this poor response[15,16]. Understanding these complexities will be beneficial towards defining therapies, diagnostic and therapeutic biomarkers that will improve pancreatic cancer management.

1.2.2 Treatment trials for pancreatic cancer

Gemcitabine and 5-fluorouracil (5-FU) have been for many years the two chemotherapeutic agents predominantly used in the treatment of pancreatic cancer in both adjuvant (after surgical resection) and advanced and metastatic (nonresectable) settings[7,17-20]. Gemcitabine (2', 2' –difluorodeoxycytidine – dFdC) is a prodrug that requires intracellular activation (phosphorylation) by deoxycytidine kinase to the active metabolites gemcitabine diphosphate (dFdCDP) and triphosphate (dFdCTP)[21,22]. 5-FU is a fluoropyrimidine that is an active antimetabolite[23]. Although

gemcitabine and 5-FU differ in their mechanisms of action, they both interfere with DNA synthesis[22,23].

The European Study Group for Pancreatic Cancer (ESPAC) have undertaken clinical trials to assess the benefit of adjuvant therapy in pancreatic cancer patients[7,8,18,19]. ESPAC-1 trial demonstrated a need for adjuvant chemotherapy with a statistically significant survival benefit[18]; the estimated 5-year survival rate for patients who had adjuvant chemotherapy with 5-FU versus resection and no chemotherapy (observation only) was 21.1% (95% CI 14.6–28.5) and 8% (95% CI 3.8–14.1) respectively while patients receiving adjuvant chemoradiotherapy did not fare any better to the observation arm with an estimated 5-year survival of 10% (95% CI 6.1–17.0). Following on from ESPAC-1, ESPAC-3 clinical trial was undertaken to determine the superiority of either 5-FU plus folinic acid to gemcitabine in terms of overall patient survival, progression-free survival and quality of life in the adjuvant setting[7]; in comparison to gemcitabine, 5-FU did not show any significant survival benefit with a medium survival of 23 months in both treatment arms. The estimated 5-year survival was 17.5% (95% CI 14.0–21.2) and 15.9% (95% CI 12.7–19.4) in gemcitabine and 5-FU plus folinic acid group respectively. Similarly, the progression-free survival and global quality of life scores was not significantly different between both treatment arms. On the toxicity profile however, gemcitabine had a better safety profile with fewer treatment related serious adverse events than 5-FU plus folinic acid. Continued efforts to improve overall survival for patients in adjuvant setting led to ESPAC-4 trial which examined the efficacy and safety of gemcitabine plus capecitabine combination therapy with gemcitabine monotherapy[8]. Capecitabine is

a 5-FU prodrug. This results of the trial were recently reported and showed a statistically significant difference in median overall survival of 28 months (95% CI 23.5–31.5) for gemcitabine plus capecitabine group compared with 25.5 (95% CI 22.7–27.9) months in the gemcitabine only group [hazard ratio (HR) 0.82; 95% CI 0.68–0.98, p=0.032]. The estimated 5-year survival rate was 28.8% (95% CI 22.9–35.2) for patients in the gemcitabine plus capecitabine group and 16.3% (95% CI 12.7–19.4) for gemcitabine group. Although more adverse events were recorded for the gemcitabine plus capecitabine group, they were within an acceptable level of toxicity[8]. The findings from ESPAC-4 are encouraging and come with the recommendation that chemotherapy with gemcitabine plus capecitabine should be the standard of care following surgery for pancreatic ductal adenocarcinoma (PDAC). The Japan Adjuvant Study Group of Pancreatic Cancer 1 (JASPAC-1) was undertaken to assess the efficacy of S-1 (an orally acting prodrug of fluorouracil) to gemcitabine[24]. This study showed that S-1 had a superior survival advantage with an estimated overall 5-year survival of 44.1% (95% CI 36.9–51.1) in the S-1 group compared with 24.4% (95% CI 18.6–30.8) in the gemcitabine group. While this result is interesting, several factors need to be considered when attempting to translate this finding to an European population. These include differences in race and the performance status (a quantification of general well-being in cancer patients with a 0 status denoting perfect health and 5 death) of patients enrolled into the study as 69% of patients in the JASPAC-1 trial had a low performance status of 0 compared with 42% in ESPAC-4[8,24].

In patients with advanced or metastatic pancreatic cancer, combination chemotherapy has also shown benefits[25-28]. An open label randomized phase III trial demonstrated a better performance for gemcitabine plus capecitabine than gemcitabine alone with an improved response rate (19.1% versus 12.4%) and progression-free survival (HR 0.78; CI 0.66–0.93)[25]. Another phase III trial compared the efficacy and safety of folinic acid, 5-FU, irinotecan and Oxaliplatin (FOLFIRINOX) with gemcitabine in metastatic pancreatic cancer in patients with good performance scores of 0 or 1 on a scale of 0–5 with higher scores indicative of disease severity[26]. This study demonstrated FOLFIRINOX therapy was superior to gemcitabine only therapy: the median overall survival of 11.1 months in the FOLFIRNOX arm compared with 6.8 months for gemcitabine therapy (HR 0.57; 95% CI 0.45–0.73); median progression-free survival was 6.4 months in the FOLFIRINOX group and 3.3 months in the gemcitabine group (HR 0.47; 95% CI 0.37–0.59); the objective response rate was also higher in the FOLFIRINOX group at 31.6% versus 9.4% in the gemcitabine group and the 1-year survival in the FOLFIRINOX group was approximately 50% compared with 9.4% in the gemcitabine group. FOLFIRINOX was however associated with increased toxicity. A phase 3 clinical trial assessing the efficacy and safety of the combination albumin bound paclitaxel (nab-paclitaxel) plus gemcitabine demonstrated a better performance than gemcitabine monotherapy in patients with advanced pancreatic cancer[27]: here the median overall survival was 8.5 months in nab-paclitaxel-gemcitabine group compared with 6.7 months in the gemcitabine group (HR 0.72; 95% CI 0.62–0.83); the median progression free survival was 5.5 months in nab-paclitaxel-gemcitabine group versus 3.7 months in the gemcitabine

group (HR 0.69; 95% CI 0.58–0.82) and the response rate was 23% versus 7% in nab-paclitaxel-gemcitabine group and gemcitabine group respectively but more adverse events were recorded in the nab-paclitaxel-gemcitabine group. In a separate phase 2 clinical Groupe Coopérateur Multidisciplinaire en Oncologie (GERCOR) trial, the efficacy and safety of combination chemotherapy involving Nab-paclitaxel plus either gemcitabine or simplified leucovorin with fluorouracil in metastatic pancreatic cancer was undertaken[28]. In this study the primary endpoint was progression free survival at 4 months with a target of 50% to qualify for future phase 3 trial. At 4 months greater than 50% of patients in both treatment arms were progression free with tolerable toxicities recorded. Emerging vaccine therapies have been tried in pancreatic cancer. A telomerase vaccine (TeloVac) trial assessing the efficacy and safety of sequential and simultaneous telomerase vaccination (GV1001) in combination with chemotherapy (gemcitabine plus capecitabine) was undertaken in patients with locally advanced or metastatic cancer[29]; this study randomized patients 1:1:1 into 3 groups: chemotherapy alone (gemcitabine plus capecitabine), chemotherapy plus sequential GV1001 (sequential chemoimmunotherapy) or chemotherapy plus concurrent GV1001 (concurrent chemoimmunotherapy); the reported median overall survival was not significantly different between chemotherapy group (7.9 months, 95% CI 7.1–8.8) and sequential chemoimmunotherapy (6.9 months, 95% CI 6.4–7.6), HR 1.19; 98.25% CI 0.97–1.48) or concurrent chemoimmunotherapy group (8.4 months, 95% CI 7.3 – 9.7), HR 1.05; 98.25% CI 0.85 – 1.29. More recently, a phase 2 double blind Vandetanib in Pancreatic cancer (ViP) trial was undertaken[30]. Vandetanib is a rearranged during transfection (RET) tyrosine kinase inhibitor with

marked vascular endothelial factor receptor (VEGFR) and epidermal growth factor receptor (EGFR) inhibitory signalling activity all involved in the pathogenesis of pancreatic cancer[30,31]. Vandetanib has also shown improvement in overall survival in patients with medullary carcinoma of the thyroid[32]. The ViP trial compared the clinical efficacy of vandetanib plus gemcitabine (vandetanib group) and placebo plus gemcitabine (placebo group) with overall survival as the primary outcome[30]. This study did not show an improvement in overall survival with a median survival of 8.83 months and 8.95 months in the vandetanib and placebo group respectively (HR 1.21; 80.8 % CI 0.95–1.53). Moreover, more adverse events were recorded for vandetanib group. Taken together, the studies outlined above demonstrate a superior advantage for combination-based chemotherapy over monotherapy.

1.2.3 Pancreatic cancer biology

Uncontrolled proliferation of cells, one of the hallmarks of cancer[2], is the result of abrogated cell cycle check points or disruption in growth signalling pathways[33]. Normal cell cycle check points and/or signalling pathways are physiologically regulated by activation or repression of relevant genes and/or proteins but dysfunctional modifications to either the DNA nucleotide sequence (genetic changes) or modifications to the genome without changes to the nucleotide sequence (epigenetic changes) can contribute to cancer formation[34,35].

1.2.3.1 Pancreatic cancer genetics

Pancreatic cancer is a heterogeneous disease characterized by several molecular and histological changes; both primary and metastatic tumours have distinct clonal subpopulations contributing to the heterogeneity in pancreatic cancer[15,36-39]. Global genomic analyses of 24 pancreatic cancers identified an average of 63 genetic alterations and most were due to point mutations[15]; these mutations altogether defined a set of 12 core signalling pathways that were altered although not every pancreatic cancer has an alteration in all 12 pathways. The 12 pathways include: KRAS signalling, DNA damage control, apoptosis, integrin signalling, hedgehog signalling, regulation of invasion, homophilic cell adhesion, G1/S phase transition regulation, c-Jun N-terminal kinase signalling, small GTPase-dependent signalling, TGF-β signalling and Wnt/Notch signalling. Genomic analyses of 99 pancreatic cancer patient tumours identified 2,016 non-silent mutations while another study analysed 100 pancreatic cancer tissues and reported 7,888 non-silent mutations in 5,424 genes[38,39]. These variations in pancreatic cancer genomes highlight the complexity of this disease.

PDAC is the most common (approximately 85%) of all pancreatic cancers arising from ductal epithelium; other pancreatic cancers include neuroendocrine carcinoma and intraductal papillary mucinous neoplasm (IPMN) with invasive cancer[40]. PDAC has also been hypothesized to arise from acinar cells in a process called acinar-to-ductal metaplasia (ADM)[41]. The established model for the development of PDAC begins with a normal ductal epithelium progressing to precancerous (pancreatic intraepithelial neoplasia – PanIN) lesions and finally to established primary invasive carcinomas[42];

the PanIN grades 1-3 are histologically distinct and genetic mutations seen in invasive PDAC can be seen in these precancerous lesions. Low grade PanIN-1 through intermediate grade PanIN-2 to high grade PanIN-3 lesions are associated with accumulating genetic alterations [42] PanIN-1 are associated with Kirsten rat sarcoma viral oncogene homolog (*KRAS)* mutation; PanIN-2 in addition shows mutations in the *p16* gene while PanIN-3 lesions demonstrate accumulated mutations including the *p53* gene. This progression model is well supported by the findings that approximately two-thirds of genetic mutations are shared between PanINs and invasive carcinomas[43]. Other precancerous lesions thought to precede PDAC development include IPMN and MCN (mucinous cyst neoplasm) which also have shared and distinct mutations from PDAC[44].

Frequently mutated genes that characterize PDAC include oncogene the *KRAS* and tumour suppressor genes cyclin-dependent kinase inhibitor 2A *(CDKN2A/p16^{INK4a}),* tumour protein p53 *(TP53)* and deleted in pancreatic cancer-4 (*DPC-4)*[11,15,38,44]; *KRAS* is the most commonly activated oncogene with more than 90% of pancreatic adenocarcinomas harbouring oncogenic *KRAS* mutation KRas, a small GTPase protein involved in signal transduction from growth factors and cell surface receptors; *KRAS* encodes 2 splice variants KRAS1, a pseudogene and KRAS2, a protooncogene. The commonly encountered *KRAS* mutation involves the *KRAS2* oncogene and typically occurs at codon 12 resulting in a gain-of-function mutation that constitutively yields active KRas even in the absence of cell surface receptor activation or other signals[45,46]. The result is continued activation of its target signalling pathways such as RAF-mitogen activated kinase (MAPK) pathway and phosphoinositide 3-kinase (PI3K)

pathway which regulates cell division, proliferation, gene expression and survival[44]. Of note is that *KRAS* mutations are also observed in chronic pancreatitis and healthy individuals [47] which underscores the fact that additional genetic and/or epigenetic events are needed to ultimately transform cells.

To understand the significance of oncogenic activating mutations of *KRAS* in pancreatic cancer, Collins *et al.*[48] used genetically modified mice that allowed for pancreas-specific inducible and reversible expression of KRas oncoprotein. Doxycycline in drinking water induced KRas while doxycycline-free drinking water switched off KRas activity. Using this model, the effect of KRas activity under different experimental conditions such as in caerulein-induced pancreatitis and p53 mutations could be examined. After caerulein-induced pancreatitis, KRas induction for 3 weeks led to the development of PanIN and fibrotic stroma while KRas inactivation following the 3 week period resulted in full pancreatic tissue recovery. When KRas was switched on for a longer duration of 5 weeks, the pancreatic tissue was composed mostly of PanIN lesions and fibrotic response and KRas inactivation resulted in apoptosis of the PanIN lesions and persistence of fibrosis. In p53 mutant mice that had developed pancreatic cancer, inactivation of KRas caused apoptosis and tumour regression with residual fibrosis. Taken together, these findings indicate that *KRAS* is required for both initiation and maintenance of pancreatic cancer in mice. Cyclin dependent kinase inhibitor 2A or inhibitor of CDK4 (*CDKN2A/p16^{INK4a}*)is the most commonly inactivated tumour suppressor gene in pancreatic cancer which encodes CDKN2A/p16^{INK4a}; CDKN2A protein plays a role in cell cycle regulation by preventing the phosphorylation of retinoblastoma protein[44]. The genetic alterations mentioned

above and others such as telomere shortening, breast cancer type 2 (BRCA2) or ataxia-telangiectasia mutated (ATM) mutations contribute to PDAC progression[15,44].

1.2.3.2 Epigenetics

Epigenetic changes modify the genome by suppressing or inducing gene expression without changes in the DNA nucleotide sequence; well recognized epigenetic mechanisms include DNA methylation, histone modifications and microRNAs[49]. Notably, epigenetic modifications have been observed in both normal cells and diseased cells such as cancer[50-53]. Aberrant DNA methylation patterns are one of the epigenetic landscapes of cancer. DNA hypomethylation is often associated with a gain in functional activation of transcription of a particular gene while hypermethylation leads to gene silencing. Both hypomethylation and hypermethylation of several genes including oncogenes and tumour suppressor genes respectively have been reported in several cancers[54].

The best studied epigenetic modification in pancreatic cancer is DNA methylation which is the addition of a methyl group at carbon 5 position of the cytosine ring resulting in 5-methyl cytosine[49,55]. The addition of a methyl group occurs on cytosines preceding a guanosine in the DNA sequence (CpG dinucleotide). More often, these CpGs are found in clusters (CpG islands) within the proximal promoter regulatory regions of genes. DNA methyltransferases (DNMTs), in particular DNMT1 is responsible for the addition and maintenance of the methylation pattern from parent

strand to newly synthesized daughter strand[56]. Methylation of these CpG islands within the promoter region of genes is generally correlated with gene silencing (Figure 1.1) mediated by disrupting the binding of transcription factors and most importantly, by attracting methyl-CpG binding domain (MBD) proteins to activate heterochromatin formation[57,58]. The 3 members of the MBD suppressive proteins are MBD, UHRF and zinc finger proteins[55]. UHRF1 is the focus of this thesis and is discussed further.

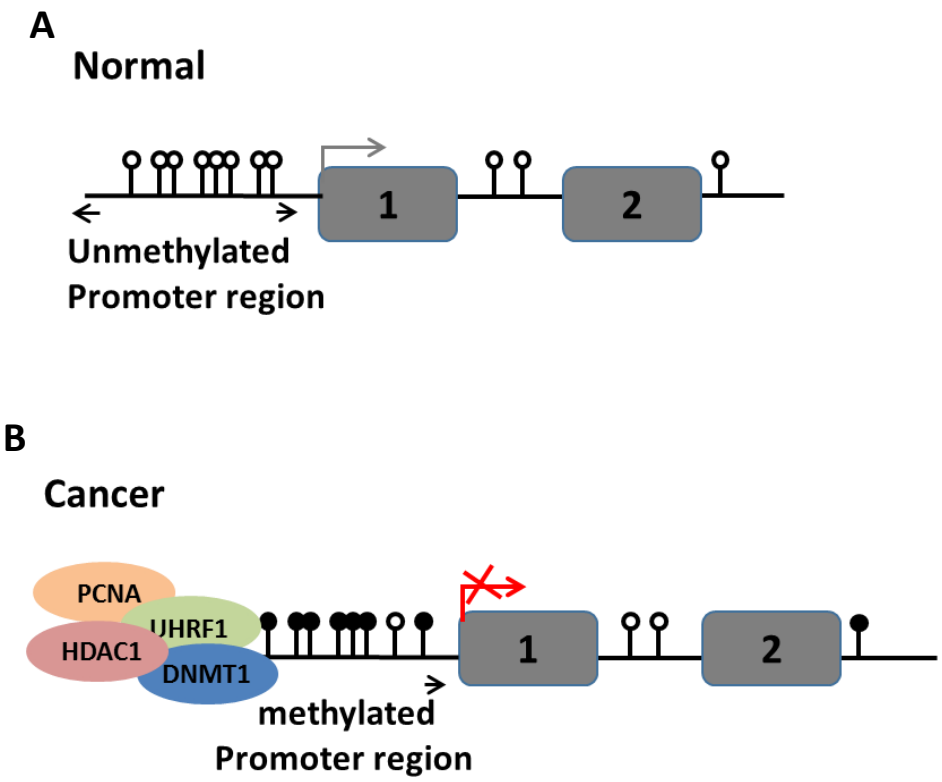

Figure 1.1. Gene silencing in association with promoter hypermethylation. (A) The unmethylated promoter of a hypothetical gene at exon 1 is actively transcribed. **(B)** Transcriptional repression of gene; gene silencing correlates with methylation of CpG within the promoter regions. The methylation of the CpGs and subsequent gene repression requires the cooperation of UHRF1, Dnmt1, proliferating cell nuclear antigen (PCNA) and histone deacetylase inhibitor 1 (HDAC1).

In order to identify gene targets and understand the functional relevance of aberrant methylation in pancreatic cancer, Sato *et al.* used methylation-specific (MSP) PCR to determine the methylation status of genes in 4 pancreatic cancer cell lines after treatment with 5 - aza - 2'- deoxycytidine (5 Aza-dC) a demethylating agent. They found greater than 5 fold induction of 475 genes in cancer cell lines compared with nonneoplastic normal human ductal epithelial (HPDE) cell lines[50]. They further examined the methylation status of 11 genes in a panel of 42 pancreatic cancers (laser microdissected) and reported aberrant methylation of all 11 genes with no methylation in a panel of 10 normal pancreatic duct epithelia (laser microdissected). Some genes hypermethylated in most (85%) of the 42 pancreatic cancers examined include *UCHL1, NPTX2, SARP2, CLDN5* and *Reprimo*[50]. In another study, Sato *et al.* examined the relevance of DNA hypomethylation in pancreatic cancer and reported methylation of 19 genes in normal pancreatic duct epithelia (laser microdissected)[51]. When examined in primary pancreatic cancerous tissue, 7 (claudin 4, lipocalin 2, 14-3-3 sigma, S100A4, mesothelin, trefoil factor 2 and prostate stem cell antigen) of the 19 genes were hypomethylated and overexpressed. These studies indicate hypomethylation and hypermethylation are frequent events in pancreatic cancer with functional relevance in affected genes.

In support of the studies by Sato *et al.* above[50,51], *p16* tumour suppressor gene inactivation by promoter hypermethylation is well established in pancreatic cancer and studies by Schutte *et al.* have demonstrated p16 inactivation by genetic and epigenetic mechanisms occurring in more than 95% of pancreatic cancer[53]. Progression through G1 phase of the cell cycle in normal cells requires the

inactivation of Rb (retinoblastoma) protein through phosphorylation by cyclin D1 and Cdk4 (cyclin dependent kinase 4) complex. p16 protein competitively binds to Cdk4 disrupting Cdk4-cyclin D1 complex. Inactivation of p16 leads to loss of cell cycle check and uninhibited progression of cells through G1 that can perpetuate tumourigenesis[53].

To determine if epigenetic changes occurs early in tumourigenesis, Sato *et al.* investigated methylation patterns in 65 laser microdissected PanIN lesions using methylation specific PCR (MSP); they reported aberrant methylation involving 8 genes in 68% of PanIN lesions[52]. This finding shows that early PanIN lesions also harbour epigenetic changes; these and many other genetic and epigenetic modifications can culminate in the initiation and progression of PDAC.

1.2.4 Ubiquitin-like with PHD and RING finger domains (UHRF)

As mentioned above, UHRF is one of the 3 members of the MBD suppressive proteins that play a role in DNA methylation. Four members of the UHRF family of proteins UHRF1, UHRF2, UHRF3 and UHRF4 have been described but most of the published data relate to UHRF1 with some limited data available for UHRF2[59]. UHRF2 is structurally similar to UHRF1 but the two proteins differ in expression patterns[60]; UHRF2 is widely expressed in differentiated human tissues and poorly expressed in human cancers whereas UHRF1 is expressed in proliferating embryonic stem cells and several cancers . It is suggested that UHRF2 might function as a tumour suppressor given that its overexpression led to growth inhibition and its levels were downregulated during partial hepatectomy[59]. UHRF1 is the focus of this thesis.

1.2.5 UHRF1

UHRF1 is a 793 amino acid multi-domain nuclear protein, also known as inverted CCAAT box-binding protein of 90 kDa (ICBP90) that binds to one of the several topoisomerase II alpha gene promoters[61]. It is important in cell cycle progression and growth[62-64] and in maintaining epigenetic modifications such as DNA methylation[65], histone methylation[66], histone ubiquitination[67] and histone deacetylation[68]. UHRF1 plays a vital role in linking epigenetic markers – histone post-translational modifications and DNA methylation which are required for normal gene expression and cellular processes[66,69].

Five domain structures have been described for UHRF1 (Figure 1.2)[70]. Through its SET and RING associated (SRA) domains, it maintains inherited epigenetic methylation patterns by binding to hemi-methylated DNA during replication subsequently recruiting DNMT1 to copy the methylation pattern to newly synthesized daughter strand[65,68]. A proposed mechanism for the UHRF1 and DNMT1 interaction has been described by Arita *et al.* as a base-flipping mechanism[71]; here, the SRA domain of UHRF1 recognising and binding to hemi-methylated cytosine in the CpG, leads to the formation of SRA-DNA complex which flips 5-methyl cytosine out of the parent strand of the DNA helix permitting DNA binding to UHRF1. This is followed by flipping out of the unmethylated cytosine on the newly synthesized daughter strand into the catalytic domain of DNMT1 to become methylated (Figure 1.2)[71].

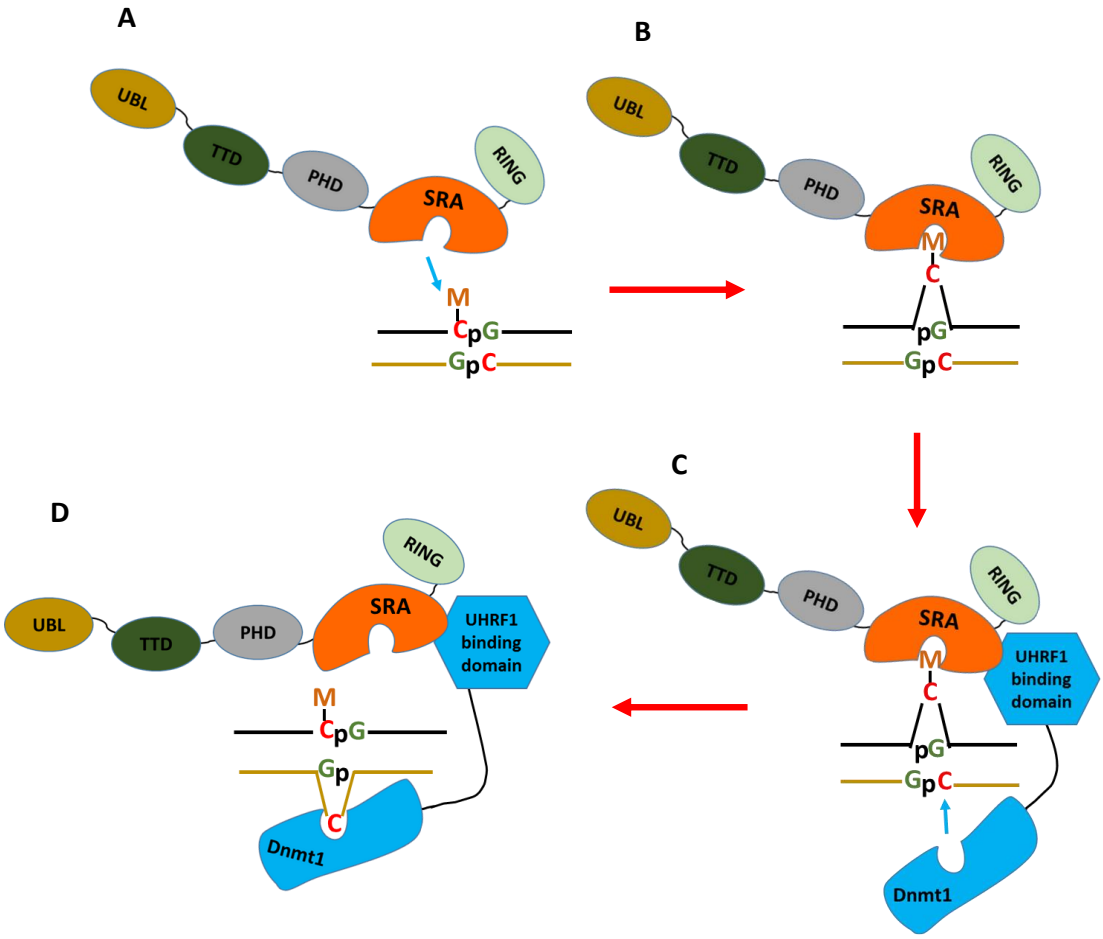

Figure 1.2. Schematic diagram of the cooperation between UHRF1 and Dnmt1 in DNA methylation maintenance. (A) Recognition of hemi-methylated cytosine on parent strand by the SRA domain of UHRF1. **(B)** Methylated cytosine flipped out into the SRA domain. **(C)** Recruitment of Dnmt1 by UHRF1. **(D)** Unmethylated cytosine on daughter strand is flipped out of the DNA helix after transfer of hemi-methylated DNA to Dnmt1. UHRF1 domains: UBL – Ubiquitin-like; TTD - Tandem tudor domain; PHD - Plant homeodomain; SRA - Set and ring associated domain and RING – Really interesting new gene domain. Dnmt1 – DNA methyl transferase 1. Adapted from Hashimoto *et al*. 2009[70] and Arita *et al*. 2008[71]

Further studies have demonstrated that in addition to the SRA domain of UHRF1, the tandem tudor domain (TTD) and/or plant homeodomain (PHD) of UHRF1 are able to target DNMT1 for DNA maintenance methylation[68].

In addition, UHRF1 interacts with and binds to histone deacetylase 1 (HDAC1) through its SRA domain[66,68]. The SRA domain has also been shown to participate in histone 3

(H3) methylation. The Really Interesting New Gene (RING) domain has E3 ubiquitin ligase activity responsible for histone ubiquitination[72]. These UHRF1 domain interactions enhance heterochromatin formation that structurally silences gene transcription[66]. It is not yet known whether these domains act in unison or independently[70].

1.2.6 UHRF1 regulation

In response to DNA damage, p53 up regulates p21 which down regulates UHRF1 by deactivating E2F1 transcription factor that directs UHRF1 transcription[63]. UHRF1 is also able to silence p21 by recruiting histone methyl transferase, DNMT1 and HDAC1 to the promoter site of p21[66]. UHRF1 has binding sites for retinoblastoma protein (pRB) which functions as a tumour suppressor by inhibiting cell cycle progression at G1/S transition[73]; overexpression of UHRF1 has led to pRB downregulation and increased the S and G2/M phase cell fractions of serum-starved lung fibroblasts[74]. UHRF1 through its RING domain ubiquitinates itself (autoubiquitination) and DNMT1 but ubiquitin specific peptidase 7 (USP7), also known as herpes virus associated ubiquitin specific protease (HAUSP) is able to deubiquitinate both UHRF1 and DNMT1 which stabilizes both proteins by preventing their proteasomal degradation[72,75].

1.2.7 UHRF1 in cancers

In a study to demonstrate the role of UHRF1 in oncogenesis, Unoki *et al.* demonstrated that in cancer cells, UHRF1 was found bound to the methylated

promoter regions of tumour suppressor genes such as *p16*^{INK4A} and *p14*^{ARF} genes[68]. The expression of UHRF1 occurs in proliferating cells but not in dormancy and its level has been shown to peak in late G1 and G_2M phases of the cell cycle in proliferating non-cancer cells whereas, cancer cells show increased and sustained UHRF1 expression throughout the cell cycle[61,62]. UHRF1 has been reported to be overexpressed in many cancers including lung cancer[76], bladder cancer[77], breast[62], colon cancer[78] and pancreatic[79,80] and has been suggested as such to be a potential target for treatment as functional studies demonstrate increased cell death with UHRF1 knockdown[64] and its expression is associated with poorer prognosis in some cancers[76,77].

Previous work by Crnogorac-Jurcevic *et al.*, undertaken in collaboration with our research group reported overexpression of UHRF1 in pancreatic cancer compared to chronic pancreatitis and normal pancreas[79]. Subsequent work by Abu-Alainin *et al.* from within our research group showed that 86% (114 of 132) of PDAC tissues overexpressed UHRF1; when UHRF1 expression was grouped as negative (score 0) or positive (score 1,2 or 3), a statistically significant association was found between positive UHRF1 tumours and larger tumour size but no association was found with patient outcome[80]. In recent reports, KRas has been shown to lie upstream of UHRF1 where it drives UHRF1 expression[80,81].

In summary, UHRF1 is involved in the maintenance of epigenetic changes and aberrant changes to these normal epigenetic processes can lead to cancer.

1.2.8 Keap1-Nrf2 defence pathway

Cells have developed defence mechanisms to defend themselves and overcome perturbations arising from chemical or oxidative stress[82]. A prominent defence mechanisms that maintains and reinstates cellular homeostasis is the Kelch-like ECH-associated protein (Keap1) and nuclear factor-erythroid 2-related factor 2 (Nrf2) pathway[82,83]. Nrf2 is a transcription factor and it functions to activate the transcription of several antioxidant proteins, detoxifications enzymes and xenobiotic transporters in addition to other functions in lipid synthesis, proliferation and inflammation[84]. Examples of such cytoprotective proteins include but are not limited to aldo-keto reductases (AKR), glutamate cysteine ligase catalytic subunit (GCLc), glutamate cysteine ligase modulatory subunit (GCLm), glutathione reductase (GSR), gluthathione synthetase (GS) and NAD(P)H:quinone oxidoreductases (NQO)[82]. A generally accepted mechanism for Nrf2 mediated cytoprotection is well described in the literature, and illustrated in Figure 1.3. Keap1 functions as a negative regulator of Nrf2 by serving as an adapter for cullin3/ring box1 (Cul3/Rbx1) E3 ubiquitin ligase complex; under basal physiological conditions, Keap1 continuously drives Nrf2 degradation via ubiquitin dependent proteasome degradation in the cytoplasm; in response to oxidative or chemical stress, modifications to the cysteine residues in Keap1 and/or modifications to Nrf2 protein liberates Nrf2 from Keap1 and prevents continued Nrf2 degradation; Nrf2 stabilization and accumulation in the cytoplasm leads to its translocation to the nucleus where it heterodimerizes with small masculoaponeurotic fibrosarcoma (Maf) protein that enhances the binding of Nrf2 to antioxidant response elements (ARE) in the promoter region of Nrf2-regulated

cytoprotective genes; Nrf2 also has ARE sequences within its own promoter and autoactivates its own transcription furthering the antioxidant defence response[82,84-86].

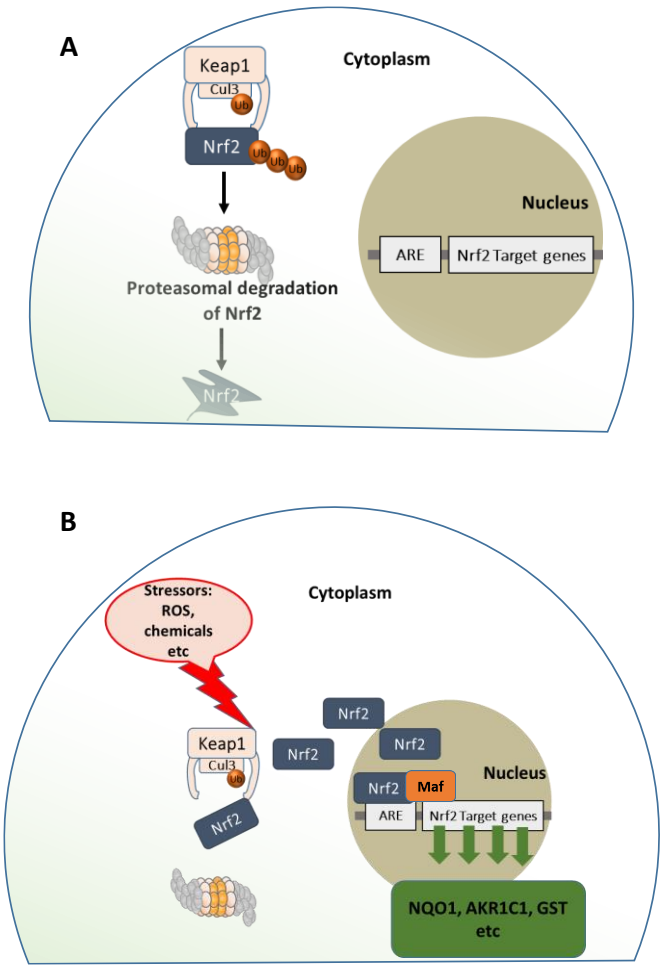

Figure 1.3. Keap1-dependent regulation of Nrf2. (A) Under basal and unstressed conditions, Keap1 anchors Nrf2 for ubiquitination and subsequent degradation by the proteasome. **(B)** When the cell is stressed from endogenous or exogenous factors the interaction between Keap1 and Nrf2 is partial and in this state, Keap1 is no longer able to fully anchor Nrf2 for ubiquitination and subsequent degradation by proteasome. As a result Nrf2 accumulates in the cytoplasm and then in the nucleus where with the cooperation of masculoaponeurotic fibrosarcoma (Maf) protein binds antioxidant response elements (ARE) present in the promoter region of Nrf2 target genes where it drives their transcription.

Another level to Keap1-Nrf2 regulation has been shown to be mediated by p62 also known as sequestosome 1 (SQSTM1)[87]. p62/SQSTM1 functions as a scaffold protein by directing polyubiquinated proteins for autophagy[88]. In a study by Copple *et al.*,

ectopic expression of p62 in several cell lines resulted in downregulation of Keap1 protein while p62 depletion led to an upregulation in Keap1 protein and a concomitant downregulation of Nrf2 proteins as well as a decrease in mRNA and protein levels of Nrf2-regulated genes but without changes to Keap1 or Nrf2 mRNA levels; in addition, in the absence of p62, the half-life of Keap1 almost doubled[87]. Other Keap1-independent Nrf2 regulatory mechanisms have been reported[84].

Oxidative stress is exerted by reactive oxygen species (ROS – such as hydroxyl, $^{\cdot}OH$; superoxide, $^{\cdot}O_2^-$; are free radical ROS while hydrogen peroxide H_2O_2 is a non-radical ROS) which are continuously produced by enzymatic and non-enzymatic reactions[89]. Oxidative stress can contribute to the process of tumour development caused by oxidative damage to macromolecules such as DNA, protein and lipids from ROS overproduction and/or defective antioxidant and/or DNA repair mechanisms Figure 1.4[90,91]. Nrf2 is a master regulator of proteins with antioxidant function. Glutathione (GSH) is the most abundant non-enzymatic antioxidant cofactor in cells and Nrf2 contributes to the regulation of enzymes involved in the synthesis of GSH; Nrf2 also plays a major role in GSH regeneration through its action on increasing the synthesis of NADPH-generating enzymes; NADPH serves as a reducing agent for the regeneration of reduced glutathione (GSH) from oxidized glutathione (GSSG)[89]. Nrf2 can be activated by stressors such as ROS, RNS (reactive nitrogen species) as well as small molecules of endogenous and exogenous origin[90].

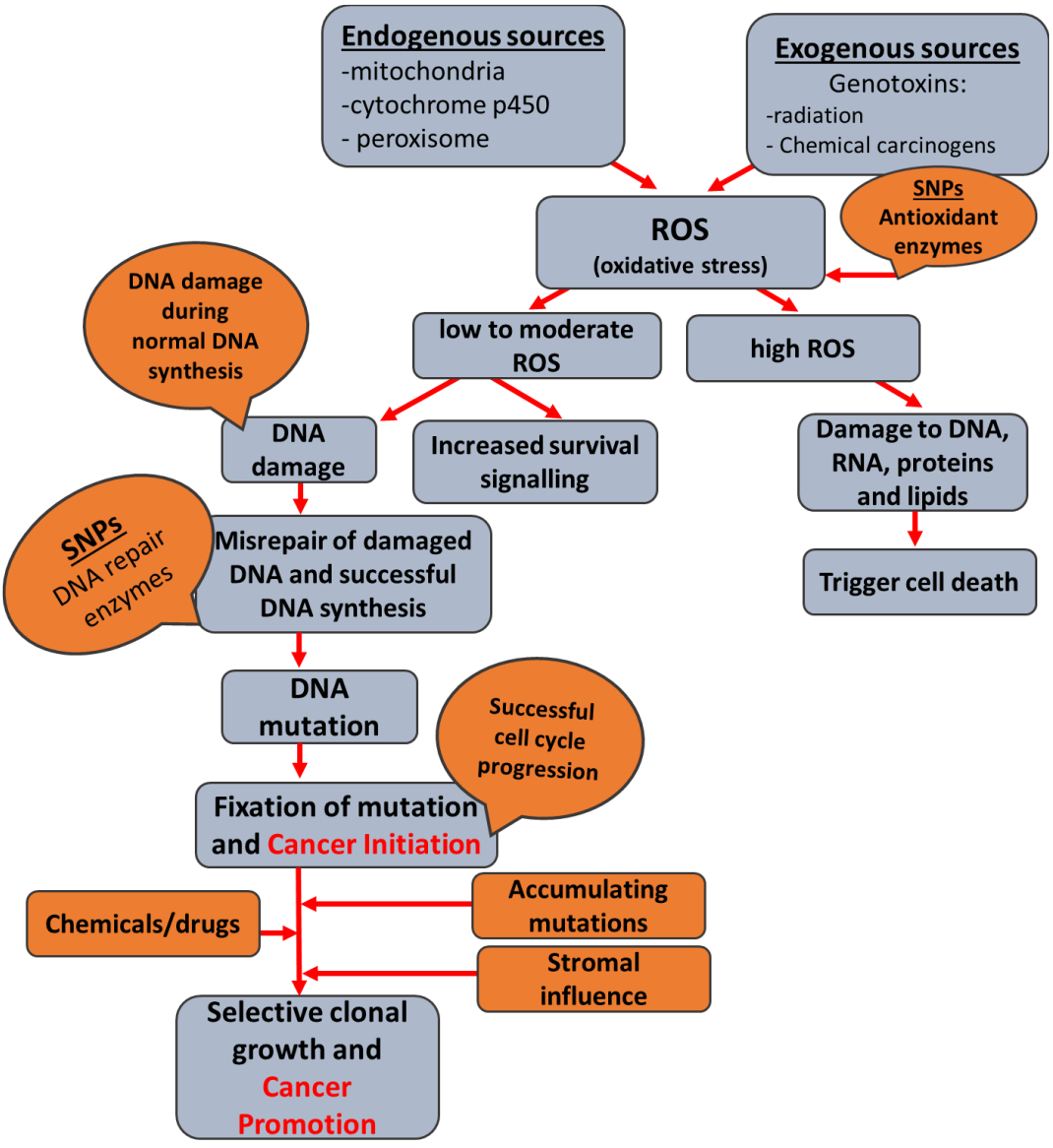

Figure 1.4. Role of reactive oxygen species (ROS) in tumour initiation. Functional single nucleotide polymorphism (SNP) involving antioxidant genes can also contribute to increased ROS levels.

Maintaining low intracellular ROS levels is important for normal homeostasis and protective against cancer as studies have demonstrated a role for ROS in degenerative disease and tumour development[92,93]. Nrf2 studies in mice showed that all aged Nrf2 null mice developed vacuolar leukoencephalopathy[92] while Nrf2-null mice chronically exposed to carcinogenic agents had a significantly higher incidence

of hepatocellular carcinomas compared to their wild-type counterparts[93]. In addition, chronic oxidative stress from chronic inflammatory conditions such as ulcerative colitis[94] and chronic pancreatitis[95] have also been associated with increased incidence of tumour development. ROS, initially considered detrimental to cells, are now being appreciated as contributing to the regulation of redox signalling and may therefore play a role in both normal homeostasis and disease development[90,96,97]. While high ROS levels may induce apoptosis and severe cell damage, low to moderate levels may activate proliferation, differentiation and survival[97]. It therefore appears that the cellular levels of ROS may determine cell fate for either proliferation or death.

Once regarded as primarily beneficial to maintaining normal cellular homeostasis, Nrf2 is increasingly being appreciated as promoting tumourigenesis by protecting cancer cells from oxidative stress as well as chemotherapy and radiotherapy[98,99]. The increase in basal Nrf2 activation seen in cancers may be due to different mechanisms acting alone or in combination to disrupt Keap1-Nrf2 interaction or by other Keap1 independent dysregulation of Nrf2. Some emerging mechanisms for the perturbation leading to increased Nrf2 activity in cancers include *KEAP1* gene promoter methylation[80,100-102], hyper-phosphorylation of SQSTM1[103], somatic mutations in *KEAP1* and *NRF2* genes[104] and oncogene induced Nrf2 transcription independent of Keap1[98]. In pancreatic cancer, two independent research studies have shown that Nrf2 is elevated and promotes cancer cell proliferation[98,99].

In investigating the integrity of Keap1/Nrf2 system in pancreatic cancer, Lister *et al.*[99] examined a panel of pancreatic cancer lines and pancreatic cancer tissue and found

no mutation in Nrf2 exon 2 and only synonymous mutations in Keap1 exons 2 – 6 which in other cancer types have been shown to harbour functionally relevant SNP (single nucleotide polymorphism). In addition, while correlations between basal Keap1 and Nrf2 protein levels were observed in all cell lines (high Keap1 protein levels associated with lower Nrf2 levels or low Keap1 with higher Nrf2 protein levels), there was no uniform correlation between basal Keap1 mRNA and Keap1 protein in the cells relative to each other (FAMPAC cells had high Keap1 mRNA and protein; Suit-2 cells had low Keap1 mRNA and protein and MiaPaCa-2 cells had low Keap1 mRNA and high Keap1 protein) but the classical mechanism of Nrf2 degradation via the proteasome appeared to be in existence as all cell lines showed Nrf2 stabilization following treatment with the proteasome inhibitor, MG132. These observations suggest posttranslational mechanisms play a role in the dysregulation of Keap1/Nrf2 pathway in some pancreatic cancer cell lines. Functional studies in two of the cell lines examined (FAMPAC and MiaPaCa-2) showed that siRNA mediated depletion of Keap1 was accompanied by increased Nrf2 and Nrf2 target proteins suggesting that despite perturbations to the Keap1/Nrf2 pathway, some functional integrity of the pathway is still preserved. Nrf2 siRNA depletion impaired the proliferation of pancreatic cancer cells while depletion of Keap1 reversed and increase proliferation in these cells. Furthermore, Nrf2 depletion in combination with chemotherapy or radiotherapy increased treatment response by decreasing cell viability although the response to different chemotherapeutic agents varied between cells. In summary, Nrf2 appears to play a role in resistance to chemotherapy and radiotherapy. Most

importantly, Lister *et al.* reported a significantly higher Nrf2 immunoreactivity in the cytoplasm of PDAC tumours than in benign duct[99].

In a seminal study by Denicola *et al*., it was demonstrated that oncogenes can induce Nrf2 activity to maintain low ROS levels and reduced intracellular environment in $KRas^{G12D/+}$ MEFs[98]. In that study, Denicola *et al.* first showed that endogenous oncogenes KRas and Myc could both decrease intracellular ROS, 7,8-dihydro-8-oxo-2' –deoxyguanosine (8-oxo-dGuo, a marker of DNA oxidation product) and increase total GSH and GSH/GSSG ratio. They next demonstrated that the increased antioxidant effect observed from endogenous oncogene activation was driven by Nrf2 induction and showed an approximately two-fold increase in Nrf2 protein, Nrf2 mRNA, Nrf2 downstream target proteins and increased binding to Nrf2 downstream target promoters upon endogenous oncogene $KRas^{G12D/+}$ expression. More importantly, at this level of Nrf2 induction, they demonstrated two points: firstly, the induction of Nrf2 activity was independent of Keap1 and secondly in Nrf2 deficient MEFs, $KRas^{G12D/+}$ could not elevate both total GSH and the GSH/GSSG ratio.

In defining the pathway of $KRas^{G12D/+}$ mediated Nrf2 activation, they used a potent and specific inhibitor of MEK, AZD6244 (ARRY – 142886) and this restored the ROS levels almost to that of control $KRas^{LSL/+}$ MEF cells and this treatment was also accompanied by downregulation of Nrf2 downstream target genes. Translating their *in vitro* findings to *in vivo*, they examined the pancreas of KRas mutant mice, human PanINs and PDAC tumours and reported an increased Nrf2 downstream target (NQO1) and decreased 8-oxo-dGuo in cancer cells compared to adjacent normal

ducts. While investigating the involvement of somatic *KEAP1* and *NRF2* mutations in PDAC, Denicola *et al*. sequenced over 100 pancreatic cancers and found only 1 concomitant case of KEAP1 and KRAS mutation. These findings further support an oncogenic KRas mediated Nrf2 activation in effect in human PDAC. To further establish the activity of Nrf2 in promoting $KRas^{G12D/+}$–initiated cancers, the effect of Nrf2 knockout was examined in mouse models of PDAC. Interestingly, the pancreas of Nrf2 knockout mice demonstrated fewer PanINs and lower proliferative activity than Nrf2 wild-type PDAC mouse models[98]. The work by Denicola *et al.* demonstrates an oncogene-mediated Nrf2 signalling in pancreatic cancer that is independent of Keap1 that maintains a reduced intracellular environment. The implication is that high ROS levels could be lethal to cancer cells while low ROS levels may in fact be driving proliferative and survival signalling pathways[89,90].

1.3 Desmoplastic stroma in pancreatic cancer

The importance of cancer-stromal interaction has been of scientific interest for many decades[105,106], and recently research into the stromal content, function and interplay with tumour has gained significant attention. The increasing awareness of this tumour-stromal cross-talk has increased our understanding of the biologic behaviour of solid tumours. However, despite the growing knowledge of stromal interaction, more research is needed to explain the precise cooperation between tumour and stromal elements and to solve ongoing debates[9,107-109].

In solid tumours, there are two distinct yet interdependent compartments; the tumour cells and the surrounding stroma[110]. The tumour microenvironment tumour stroma or desmoplastic reaction is "all components of the tumour other than cancer cells"[111] and includes a complex network of non-neoplastic cells present within a tumour and the proteins and molecules produced including but not limited to extracellular matrix (ECM) components, soluble factors and signalling molecules which influence tumour behaviour[112,113].

Fibroblasts are a resilient group of cells that can withstand extreme stress that will normally be detrimental to other cells; they have been isolated and established in cultures from post-mortem tissue[111,114-116]. Fibroblasts play a crucial role in tissue homeostasis, wound healing, fibrosis and tumour desmoplasia[111,117,118]. Earlier studies investigating the contractile properties of granulation tissue in wound healing, found that fibroblast where responsible for the wound contraction and this was achieved by trans-differentiation into cells with structural and functional

similarities to smooth muscle cells (characterized by extensive cytoplasmic fibrillar system, nuclei indentations and selective cytoplasmic localization of smooth muscle serum-a cytoskeletal protein associated with smooth muscle cells) and the name myofibroblast was proposed by Gabbiani *et al.* to describe such cells[117]. This description of myofibroblast cells in normal wound healing was followed in subsequent years by the observation that myofibroblast cells inhabit tumour stroma. Tremblay *et al.* demonstrated using electron microscopy the ultrastructural features of the stromal aspects of breast cancer and ductal carcinoma of the pancreas and found that a large population of stromal cells in both cancers displayed features that were intermediate between fibroblasts and smooth muscle cells (myofibroblasts); in addition, collagen fibrils were found in the extracellular space[110]. Because of the evidence in support of the similarities between normal wound healing and tumour stroma, Dvorak in 1986 hypothesized that "a tumour is a wound that never heals completely"[105].

An understanding of the physiological role of fibroblasts is important in order to appreciate the wider contribution of fibroblasts in tumours. Fibroblasts are fusiform or spindle like elongated cells of mesodermal origin found in the extracellular matrix (ECM). They are considered to be the primary producers of the ECM and the predominant cells in the connective tissue. The fibrillary collagen, fibronectins, proteoglycans and hyaluronic acid make up the ECM and provide the structural support for tissue homeostasis and serve as a reservoir for growth factors, cytokines and soluble factors [108,111]. Following tissue injury, an initial provisional stroma of clot forms which is later replaced by new blood capillaries and proliferating and

differentiated fibroblasts (myofibroblasts) characterized by α-smooth muscle actin (α-SMA) expression[105]. These myofibroblasts increase their synthesis of ECM production which results in a richly vascular and oedematous tissue called granulation tissue[117]. The myofibroblasts contract to bring the wound edges together and the granulation tissue is subsequently and finally remodelled into a scar tissue characterized by dense collagen and sparse blood vessels and fibrocytes[105]. Once the tissue damage has been restored, the myofibroblast undergo apoptosis[119] or programmed necrosis[120].

1.3.1 Cancer Associated Fibroblast

In much of the published literature, the phrase cancer associated fibroblast (CAF) is often used to refer to fibroblasts in tumours. More importantly, CAFs and the accompanying desmoplastic stroma have been shown to impact on the biological behaviour of tumours[2,108,109,111]. CAFs are one of the most predominant stromal cell types in solid tumours including pancreatic and breast cancers. A cellular definition of CAFs is that "they are all the fibroblastic, nonneoplastic, nonvascular, nonepithelial and noninflammatory cells found in the stroma"[108]. A consensus has not been reached regarding the molecular definition of CAFs[108]. CAFs are activated fibroblasts and in many ways share similarities with fibroblast induced during wound healing and in inflammatory conditions. In their activated states, CAFs produce a host of factors such as α-smooth muscle actin (α-SMA, a typical CAF marker), fibroblast specific protein-1 (FSP-1, also called S100A), fibroblast activation protein (FAP) and vimentin. Others factors include cytokines, chemokines and growth factors[107]. Some of these

molecular markers have been proposed to define CAFs but it is now being acknowledged that these markers are not entirely unique to CAFs[107,108]. Numerous cellular origins of CAF, the tumour-stroma derived factors and tissue type from which the tumour developed are believed to underlie CAF heterogeneity and hence their molecular characteristics. It is important to mention that other than CAFs in the tumour stroma, there are other non-neoplastic cells that also contribute to influencing tumour behaviour such as the immune cells, neural cells and endothelial cells[9].

1.3.2 Origin of CAFs

CAFS are derived from several local and distant cellular sources and include resident fibroblasts, stellate cells and mesenchymal cells; bone marrow derived cells, epithelial to mesenchymal transition (EMT) and endothelial to mesenchymal transition (EndMT) are additional sources that have been proposed[9,108].

1.3.3 Pancreatic stellate cells

Pancreatic stellate cells (PSCs) are the key players responsible for the stromal reaction (desmoplasia) observed in chronic pancreatitis and pancreatic cancer (the two common pancreatic diseases)[121]. They share similarities with hepatic stellate cells (HSCs) in their stellate cell morphology and vitamin A storing lipid droplets. PSC research came into the lime light when they were isolated and cultured by Apte *et al.* and Bachem *et al.* in 1998[122,123]. In a healthy pancreas, PSCs exist in a quiescent phenotype (qPSCs) located in the periacinar spaces and characterized by abundant

vitamin A containing lipid cytoplasmic droplets. qPSCs constitute about 4 – 7 % of all parenchymal tissue in a normal rat pancreas[122,123].

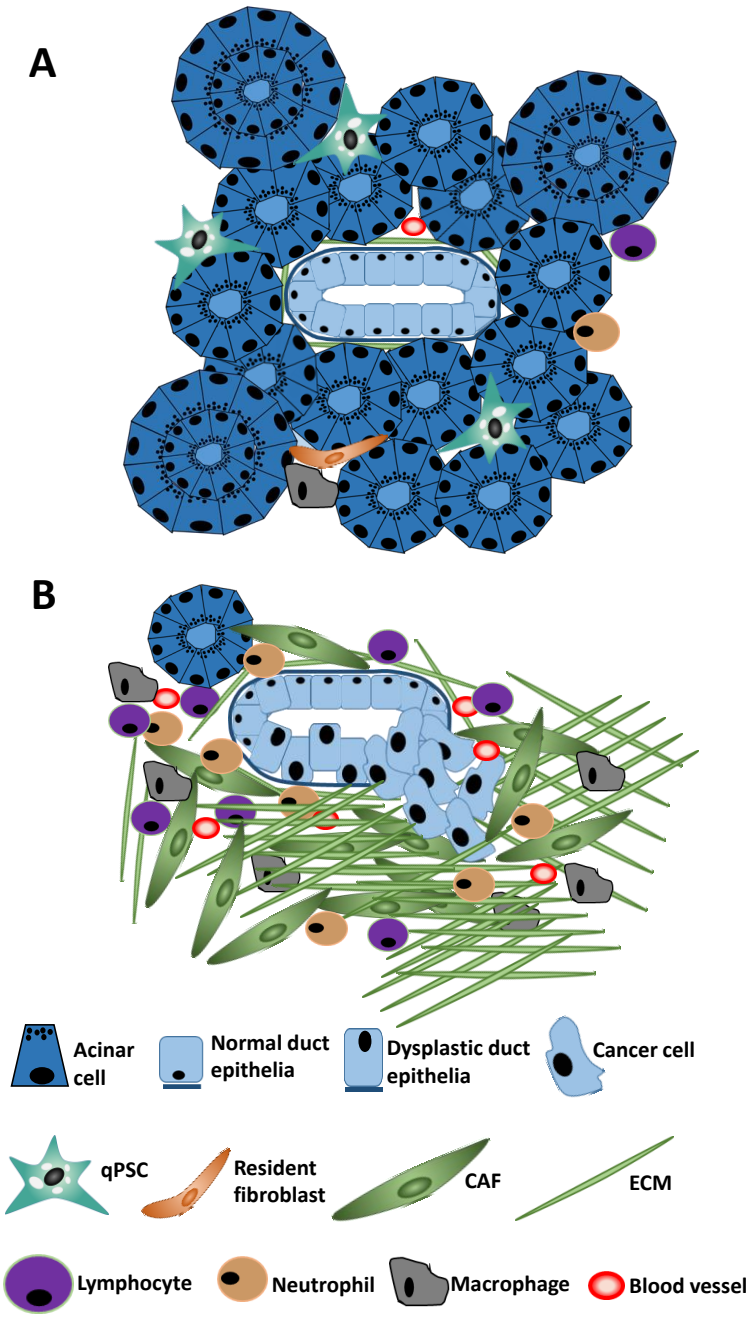

Figure 1.5. The architectural stroma in pancreatic ductal adenocarcinoma (PDAC). (A) The normal exocrine pancreas is largely populated by acini with acinar cells. The normal cuboidal ductal epithelial cells are uniformly arranged and surrounded by intact basement membrane; the normal ductal epithelial cells have their nuclei basally located. Few quiescent pancreatic stellate cells (qPSCs) with perinuclear lipid droplets (white) and resident fibroblast are present and located in the periacinar space. The extracellular matrix (ECM) is thin and limited to periductal areas. Very few immune/inflammatory cells (lymphocyte, neutrophil, macrophage) are seen. **(B)** In

PDAC the normal architecture is distorted and cancer cells breach the basement membrane to invade adjacent stroma. Preceding the PDAC stage are precursor lesions (pancreatic intraepithelial neoplasia – PanIN) which have not breached the basement membrane but have a more elongated ductal epithelial cells and non-basal location of nuclei. A stromal reaction (desmoplasia) is characterized largely by ECM, increased inflammatory/immune cell infiltration and diminished acini tissue. Increase vessel infiltration is also seen in PDAC.

Similar to fibroblasts, qPSCs are activated during tissue injury or carcinogenesis and acquire an activated phenotype (aPSCs or pancreatic CAFs) characterized by α-SMA production[122]. In addition, aPSCs develop a myofibroblast-like morphology, lose their vitamin A lipid containing cytoplasmic droplets and secrete excessive amounts of ECM proteins and other soluble factors (Figure 1.5)[122]. When found in cancer tissue, PSCs are categorized as CAFs[108,111].

Pancreatic cancer is characterized by an intense stromal/ desmoplastic reaction that surrounds cancer cells and comprises 50 – 80 % of the tumour volume [124]. PSCs are the major source of CAFs in pancreatic cancer and are largely responsible for the deposition of collagenous stroma[109]. PSCs have for the most part been shown to have a tumour promoting function but recent studies have suggested a tumour inhibitory role[125,126]. Several *in vitro* and *in vivo* studies have demonstrated a role for PSCs in pancreatic carcinogenesis. *In vitro* conditioned media or co-culture experiments between pancreatic cancer cells and PSCs have demonstrated that pancreatic cancer cell proliferation, survival and migration are enhanced in response to PSCs, while PSC proliferation and ECM synthesis are stimulated upon exposure to pancreatic cancer cells[127-129].

Using mouse xenograft models, Bachem *et al.* demonstrated that co-injection of pancreatic cancer cells and PSCs led to increased cell proliferation, larger tumour, increased stromal content[128]. Orthotopic mouse models have also shown that co-injection of human PSCs and human pancreatic cancer cells directly into mouse pancreas resulted in higher local pancreatic tumour growth and distant metastases with histological evidence of these tumours also showing greater tumour cell density, increased fibrotic content and increased aPSC numbers than tumours formed by pancreatic cancer alone[127,129].

Additional xenograft studies by Xu *et al.* also showed evidence in support of the concept that pancreatic cancer can recruit neighbouring PSCs to favour their survival, growth and distant metastasis[130]. The authors further demonstrated using gender mismatch approach to show that PSCs from primary pancreatic cancer sites were able to establish themselves at distant metastatic sites together with cancer cells. This latter observation was supported by *in vitro* studies demonstrating that the migration of PSCs through a single layer of endothelial cells was in response to platelet derived growth factor (PDGF) secreted by pancreatic cancer cells[130].

Most therapies for treating pancreatic cancer have only targeted cancer cells. In view of the observations that the pancreatic tumour microenvironment influences and promotes cancer growth and metastasis, attempts have been made at targeting different aspects of the tumour stroma with the ultimate aim of improving clinical outcomes. The hedgehog (Hh) signalling pathway mediates cross-talk between PSCs and pancreatic cancer cells[131]. Inhibition of Hh signalling by IPI-926, a smoothened

(Smo) inhibitor in a genetically engineered mouse model (GEMM) of pancreatic cancer, depleted the stroma, increased intratumoural vascular perfusion, vascular density and improved survival when used in combination with gemcitabine chemotherapy[132]. Similarly, hyaluronic acid (HA) targeted degradation of the tumour stroma in a KPC mouse model of pancreatic cancer demonstrated increased vascular perfusion associated with an increase in intratumoural concentration of chemotherapeutic agents and increased survival[133,134]. These above observations were encouraging but a randomized phase II clinical trial of IPI-926 + gemcitabine had to be aborted due to poor survival of patients on this treatment arm.

In a recent study by Rhim *et al.*, genetic ablation of Hh in GEMM of pancreatic cancer resulted in a decrease in intratumoural stroma, increase vascularity, increase over all cancer aggressiveness and decreased survival[125]. In a separate study using drug inducible α-SMA deletion of α-SMA positive myofibroblasts in a transgenic mouse model of pancreatic cancer, similar results were observed characterized by immune suppression (increased infiltrating Tregs), more aggressive and invasive tumours with associated reduced survival[126]. These observations suggest the possible role of the stroma in restricting carcinogenesis contrary to earlier observations suggesting a tumour promoting function and therefore emphasize the need for further understanding of the functions of the stromal elements.

Stromal modulation rather than depletion is another therapeutic approach at targeting the stroma. Sherman *et al*. demonstrated using an orthotopic model of pancreatic cancer that targeting vitamin D receptor on human cancer associated PSCs

with vitamin D receptor ligand, calcipotriol, induced a quiescent PSC phenotype (characterized by increased lipid droplet and decreased α-SMA expression) resulting in stromal remodelling and improved survival[135]. Chemokine ligand 12- chemokine receptor 4 (CXCL12-CXCR4) ligand-receptor pathway has been shown to be active in pancreatic cancer[136]. A study by Ene-Obong *et al.*, demonstrated that in pancreatic cancer, CD 8 positive T cells were sequestered by chemokine CXCL12 secreted by PSCs [137]. In a mouse model of pancreatic cancer, Feig *et al.* showed that CXCR4 inhibition together with immune checkpoint antagonist α-programmed cell death–ligand 1 (α-PD-L1) enhanced tumoural T-cell accumulation and increased cancer cell death[136].

1.3.4 Prognostic value of stromal activity

The precise role of the stroma in pancreatic cancer is still an issue of ongoing concern. Erkan *et al.* investigated the expression of α-SMA and collagen from 233 pancreatic cancer resected specimens and found that patients with higher collagen had a modest survival benefit but no significant association between α-SMA expression and overall survival[138]. When these patients were further classified by stromal activity index (ratio of α-SMA expression to collagen density), a higher stromal activity index was associated with poorer prognosis[138]. In a recent study, Özdemir *et al.* reported a poorer survival in patients with low α-SMA expression[126]. Similarly, Bever *et al.* examined the stromal density (ratio of collagen positive stroma to area of tumour mass) and found a positive association with overall survival in patients with high stromal density[139]. These varied conclusions on the prognostic value of stromal activity may be due to differences in methods of measuring stromal activity but

importantly, brings to light the possible protective role of the desmoplastic stroma in pancreatic cancer. One clear message is that the stroma is not just a bystander but either works in favour of or against pancreatic cancer probably in a context defined manner and more understanding is required to develop effective strategies of targeting both tumour cells and the accompanying stromal elements.

1.3.5 CAF polarization

Recently, the concept of CAF polarization was proposed to reflect functional heterogeneity of CAFs[107,111]. F1 CAFs are suggested to have tumour inhibitory properties, F2 as exhibiting tumour promoting properties, F3 subtypes are proposed to influence tumour immunity and angiogenesis and F4 subtypes are proposed to define ECM production and remodelling. In a study by Sugimoto *et al.*, two CAF subtypes were described using pancreatic and breast cancer mouse models[140]. One subtype was characterized by FSP-1 expression and the other subtype was defined by co-expression of α-SMA, PDBFRβ and NG2. In another study Ikenaga *et al.* using human pancreatic cancer specimen, CD10-positive subpopulation of PSCs were identified and patients with CD10-positive PSCs had significantly poorer survival[141]. These findings call for more investigations to identify, understand and characterize the functions of different subtypes of CAFs in pancreatic cancer in order to understand how to therapeutically intervene.

1.3.6 Epigenetic regulation of fibroblast activation

Several factors activate qPSCs and resting fibroblasts into aPSCs and myofibroblasts respectively[9,142]. Fibroblast activation in the setting of a transient physiological tissue repair process or from an overwhelming/sustained abnormal tissue injury is characterized by increased proliferation, ECM deposition and α-SMA expression[143]. Emerging data indicate a reversible and irreversible fibroblast activation mechanism mediated in part by epigenetic processes[55,143,144]. Bechtel *et al.* demonstrated using *in vivo* and *in vitro* techniques that hypermethylation of RAS protein activator like 1 (*RASAL1*), encoding an inhibitor of RAS oncoprotein, led to downregulation of RASAL1 protein and activation of RAS in kidney fibrosis associated fibroblasts (FAF) but this was not the case in fibroblasts isolated form normal kidney or acute injury associated kidneys; RAS activation was associated with fibroblast activation[143]. Moreover, treatment of FAFs with the demethylating agaent 5-azacytidine, reduced proliferation, α-SMA expression and collagen I synthesis. Bechtel *et al.* furthermore, showed that TGFβ1, which is known to activate fibroblasts, caused the transcriptional silencing of Rasal1 mRNA in a time dependent manner via two distinct mechanisms; mechanism 1 – short term exposure of normal mouse fibroblasts with TGFβ1 led to a reversible suppression of Rasal1 without *RASAL1* methylation and mechanism 2 – a long term exposure with TGFβ1 caused *RASAL1* promoter methylation accompanied by irreversible transcriptional silencing[143]. Their findings suggest a role for methylation in FAFs in fibrotic kidney lesions and could also be a mechanism in CAFs from different cancer tissues including pancreatic cancer. Interestingly, *RASAL1*

hypermethylation has been reported in hepatic stellate cells in experimental liver fibrosis[55].

1.4 Predictive biomarkers in pancreatic cancer

A biomarker, as defined by the National Institutes of Health Biomarkers Definitions Working Group "is a characteristic that is objectively measured and evaluated as an indicator of normal biological processes, pathogenic processes, or pharmacologic responses to a therapeutic intervention"[145]. An emerging area of research that could potentially improve outcome and overall survival in pancreatic cancer patients is predicting the likelihood of a patients response to chemotherapy based on putative biomarkers such as the levels of cellular defence and/or drug metabolising enzymes and genetic variations (germline or tumour biology)[146].

1.4.1 NADP(H):quinone oxidoreductase 1

NADP(H):quinone oxidoreductase 1 (NQO1) is a protein that protects cells against oxidative stress and carcinogenesis (cytoprotective) and also functions to detoxify and bioactivate quinones or xenobiotics; NQO1 transcription is regulated by Nrf2 via ARE present its promoter[147,148]. NQO1 is a cytosolic enzyme that catalyses the two-electron reduction of quinone compounds to less toxic hydroquinone, preventing the generation of semiquinones (1 electron reduction of quinone) free radicals, ROS and depletion of sulfhydryl groups thereby protecting cells against free radical ROS induced mutagenesis and carcinogens[147,149]. Quinones are abundant in nature and are considered to be cytotoxic because unstable quinone derivatives can undergo

rapid redox cycling by interacting with molecular oxygen to generate ROS; furthermore, quinones are electrophilic and dependent on their reactive states, can alkylate DNA[149]. Quinone based polycyclic aromatic hydrocarbons abound in burnt organic materials such as cigarette smoke, automobile exhaust and industrial air pollutants. Quinones naturally exist in foods and are used as chemical compounds in quinone based anticancer drugs[149].

In addition to its role in quinone reduction and in preventing ROS generation, NQO1 directly scavenges superoxides[150]. NQO1 has been reported to play a role in p53 stabilization. Asher *et al.*[151] reported that NQO1 stabilized p53 by inhibiting the proteasomal degradation of p53 in human colon cancer cell line (HCT116). They demonstrated that treatment of HCT116 cells with NQO1 inhibitor dicumarol led to reduced levels of both endogenous and gamma-irradiation-induced p53. Similarly, in normal thymocytes and myeloid leukemic cells that overexpress wild-type p53, NQO1 inhibition increased p53 degradation and caused a reduction in p53 dependent apoptosis. Conversely, this effect was rescued by proteasome inhibitors lactacystin and MG132[151]. Interestingly, transfection with wild type NQO1 but not C609T NQO1 minor allele led to p53 stabilization[152].

Despite these reports, the modulation of p53 by NQO1 is still controversial[153]. A study by Zeekpudsa *et al.*[153] reported that cholangiocarcinoma cells were more susceptible to chemotherapeutic agents (gemcitabine, 5-FU, and doxorubicin) when NQO1 was depleted from the cells, an effect that was accompanied by increase p53, p21 and Bax protein expression. Furthermore, the increased sensitivity of cholangiocarcinoma

cells to chemotherapy following NQO1 silencing was abrogated by p53 knockdown[153]. This study suggests that NQO1 protects cholangiocarcinoma cells from chemotherapy and that NQO1 may not contribute to the stabilization of p53.

Studies have been undertaken to investigate the effects of differential expression of NQO1 in the bioactivation of anticancer drugs. Siegel *et al.* and Siegel *et al.*[154,155] have demonstrated that in colon cancer cells with high NQO1 expression compared with low protein expressing cells, the two electron bioreductive activation of quinone based anticancer drugs (diaziquone and mitomycin C) by NQO1 may be responsible for mitomycin C and diaziquone induced genotoxicity and cytotoxicity. Conversely, other researchers have reported a lack of correlation between NQO1 levels with sensitivity to mitomycin C[156,157].

NQO1 protein levels have been reported to be overexpressed in several cancers including pancreatic cancer[158-160]. In pancreatic cancer, both the cytoprotective and bioactivation properties of NQO1 are being investigated with regard to optimizing response to chemotherapy. A study by Cullen *et al.* [161] showed that NQO1 inhibition in MiaPaCa-2 cells with a selective NQO1 inhibitor dicumarol increased ROS and inhibited cell growth whereas in the presence of manganese superoxide dismutase, these effects were reversed. Taking advantage of the fact that NQO1 is overexpressed in pancreatic cancer several fold above normal tissue levels and that NQO1 can bioactivate quinone based anticancer drugs, strategies are being undertaken to exploit these tumour specific therapeutic potentials. β-Lapachone (3,4-dihydro-2,2-dimethyl-2*H*-naphtho[1,2-b] pyan-5-6-dione) is a quinone based anticancer drug that

is activated by NQO1 in a 2 electron redox process leading to futile redox cycling and production of massive ROS effectively killing cancer cells overexpressing NQO1 while sparing normal cells that lack or have minimal levels of the enzyme[148,162,163].

Clinical trials in pancreatic cancer are currently underway to evaluate the combination of β-Lapachone (ARQ761) and chemotherapy (gemcitabine plus nab-paclitaxel) in predicting response to treatment based on a cut off histo-score (H-score) level of NQO1 in tumours[163]. The levels of NQO1 in tumours could potentially become an integral biomarker to inform patient stratification for treatment options.

1.4.2 Single nucleotide polymorphisms

The majority of the genetic variation in humans are due to single nucleotide polymorphisms (SNPs) which are defined as variation at a single nucleotide position in a DNA sequence which exists in at least 1 % of the population[164,165]. An estimated 10 million SNPs exist in the human genome[166] and most of the SNPs are synonymous (silent) but a small proportion of SNPs occurring in the coding or regulatory regions of genes may cause functional differences[164].

NQO1 has a characteristic SNP, C to T substitution at nucleotide position 609 (C609T, rs1800566) on exon 6 that results in a proline to serine amino acid change at codon 187 (Pro187Ser)[167,168]. The homozygous TT genotype is essentially an inactive enzyme[169] with a half-life of 1.2 h while the heterozygous CT has an intermediate activity in comparison with the homozygous CC genotype with a half-life of > 18 h[170].

In breast cancer, *NQO1* polymorphism has been shown to be predictive of response to treatment. In a study involving two independent cohort of women with breast cancer, the *NQO1* minor allele TT was shown to be correlate with poor overall survival compared with CT, CC genotypes combined (p=0.0017, n=1,005; p=0.005, n=1,162)[171]. Furthermore, in patients who had received adjuvant anthracycline based chemotherapy with epirubicin, *NQO1* TT genotype was independently predictive of poor overall survival ($p=7.52 \times 10^{-6}$, n=178; hazard ratio [HR]=6.55, 95% confidence interval [CI]=2.54-16.90)[171]. Similarly, in another study, the TT genotype was associated with a poorer outcome (overall survival p=0.003, progression free survival p=0.001) in breast cancer patients who had received chemotherapy[172]. In lung cancer, the TT genotype was associated with increased risk for development of non-small cell lung cancer (NSCLC) (p=0.001) and poor response to chemotherapy (p=0.003)[173]. An European study was undertaken to investigate the risk of pancreatic cancer and functional antioxidant SNPs but no association between C609T rs1800566 *NQO1* SNP and the risk for pancreatic cancer development was found[174].

Single nucleotide polymorphisms of *NRF2* and one of its downstream target sulfiredoxin (*SRXN1*) have been examined with relevance to breast cancer treatment. Peroxiredoxins are cytoprotective enzymes that function as scavengers of hydrogen peroxides[175,176]. Peroxiredoxins can become inactivated by hyperoxidation of their cysteine residues [176,177]. SRXN1 is an antioxidant enzyme that reactivates peroxiredoxins from their hyperoxidative state[177]. SRXN1 is a downstream target of Nrf2 and activator protein 1 (AP-1) and have been reported to be overexpressed in various skin cancers[178,179]. *NRF2* and *SRXN1* SNPs were investigated in 452 breast

cancer patients and 370 controls[180]. The *NRF2* SNP rs2886162 minor allele A was associated with low Nrf2 protein expression in tumour tissues (p=0.01) and in patients who had received adjuvant chemotherapy (n=79), the *NRF2* rare homozygous AA genotype predicted poor survival compared to the more common GG and GA genotypes (p=0.019). This *NRF2* minor allele was not associated with survival among patients who did not receive any adjuvant therapy. Similarly, the *SRXN1* rs6116929 rare homozygous minor allele GG and rs2008022 rare alleles CA and AA were predictive of better outcome (p=0.01 and p=0.02 respectively). *SRXN1* rs6053666 common CC genotype was associated with better survival in patients who received radiotherapy (p=0.017).

Studies in other cancers have shown that functional SNPs involving other antioxidant genes may be predictive of response to certain chemotherapeutic agents[181-183]. These SNPs could potentially become biological markers that will inform decision making on treatment options.

1.4.3 Gemcitabine metabolizing enzymes

Gemcitabine is a commonly used chemotherapeutic agent in pancreatic cancer treatment[16] and enzymes metabolizing gemcitabine may modify response to treatment with gemcitabine in pancreatic cancer patients. Deoxycytidine kinase is responsible for phosphorylating and activating gemcitabine[21]. The tissue protein levels of deoxycytidine kinase was examined in 45 pancreatic cancer patients who had received adjuvant gemcitabine-based therapy following resection of their tumours[184]; deoxycytidine kinase expression score (intensity of staining and number

of cells staining positive for deoxycytidine kinase) was dichotomized and patients with a low score demonstrated a strong and statistically significant correlation with disease-free and overall survival (p=0.001; HR=3.61, 95%CI 1.74 – 7.51 and p=0.0008; HR=3.44, 95% CI 1.66 – 7.44 respectively)[184].

1.4.4 DNA synthesis and repair enzymes

Similarly, the expression levels of DNA repair and synthesis enzymes (excision repair cross complementary 1 [ERCC1] and ribonucleotide reductase subunit M1 [RRM1] respectively) were examined in a study involving 94 pancreatic cancer tissues from patients who had surgery for pancreatic cancer followed by adjuvant gemcitabine therapy for 87% of the cases; both enzymes (RRM1 and ERCC1) were not predictive of response to gemcitabine[185].

1.4.5 MicroRNAs

MicroRNAs (miRNAs or miRs) are also gaining attention as potential markers to be investigated for predicting response to treatment in pancreatic cancer. Giovannetti *et al.*[186] reported that miR-21 levels were approximately 1000-fold lower in normal pancreatic ductal epithelial cells (obtained from normal pancreas tissue organ donor program) compared to levels in tumour cells enriched by microdissection. In addition, in pancreatic cancer patients that received gemcitabine in both adjuvant (n=28) and metastatic setting (n=31) or in combined analysis (n=59), low miR-21 expression group was predictive of better survival than the high expression group[186].

In a cohort of 82 South Korean patients who had undergone resection for pancreatic cancer, low miR-21 expression in tumour samples was predictive of better overall and disease-free survival in patients who subsequently had adjuvant chemotherapy [gemcitabine or 5-fluorouracil], combined chemoradiotherapy or both (n=52) whereas in patients who did not receive adjuvant therapy post-surgical resection (n=27), no association between miR-21 tumour tissue levels and outcome was found[187]. Similarly, in a validation cohort of 45 Italian pancreatic cancer cases who had adjuvant therapy (gemcitabine-based treatment), low miR-21 was associated with longer overall survival[187].

While no established biomarker(s) currently exists to predict pancreatic cancer patients' response to treatment[16], these studies put together, provide a role for the development and routine use of predictive biomarkers for current and future therapies.

1.5 Hypotheses

1. UHRF1 contributes to oncogenesis in pancreatic cancer by regulating Keap1-Nrf2 pathway.
2. That single nucleotide polymorphisms (SNPs) and proteins involving the Nrf2 and Nrf2 downstream target genes can predict survival in pancreatic cancer patients.

1.6 Aims and objectives

1. To investigate the functional effects of UHRF1 on Keap1-Nrf2 pathway in pancreatic cancer cells.

   a. Examine the effects of UHRF1 on Keap1-Nrf2 mRNA and protein expression, cell cycle regulation, oxidative stress response and chemosensitivity.

2. To develop a method for analysis of *KEAP1* promoter methylation in PDAC tissues.

   a. Quantify DNA isolated from laser microdissected PDAC tissues and determine the suitability of the isolated DNA for pyrosequencing analysis.

3. To determine the functional effects of UHRF1 on Keap1-Nrf2 pathway from isolated mouse and human primary pancreatic stellate cells.

   a. Investigate the function of UHRF1 on oxidative stress response and cell proliferation and to examine the tissue stromal expression of UHRF1.

4. To investigate the predictive effect of UHRF1 protein and SNPs of *NRF2*, *NQO1*, and *SRXN1* and their corresponding protein expression on overall survival in pancreatic cancer patients from retrospective randomised control clinical trials data.

   a. Determine germline SNPs in patients with advanced PDAC.

   b. Quantify protein expression in PDAC tissue specimens from an independent cohort of patients who had surgical resection for locally resectable PDAC.

2 MATERIALS AND METHODS

2.1 Materials and Reagents

All reagents were supplied by Sigma-Aldrich, UK or Thermo Fisher Scientific, UK unless otherwise stated. Details of the primary and secondary antibodies used for immunoblotting are detailed in Table 2.5. Pancreatic cell lines, MiaPaCa-2 and Panc1, were purchased from American Type Tissue Culture and Suit 2 cells from[188]. Mouse pancreatic cells from KPC mice were kindly isolated by Dr Michael Schmid, University of Liverpool.

2.1.1 Sigma Aldrich

The following were purchased from Sigma-Aldrich, UK with codes indicated in parentheses. RPMI medium (R0883, Sigma Aldrich), Penicillin/Streptomycin (P0781), L-glutamine (G7513), Dulbecco's Modified Eagles Medium (DMEM, D6429), Iscove's Modified Dulbecco's Medium (IMDM, I3390), Dimethyl sulfoxide (DMSO, 276855), Mr Frosty (C1562-1EA), Diethyl maleate (DEM, D97703), Developer solution (P7042-5GA), Fixer solution (P7167-5GA), Gemcitabine (Y0000675), RNAse A (R5125), Trypsin (T3924), HCl (320331), DPX mountant (06522), L-Ascorbic acid (A4403), 10% neutral buffered formalin (HT501128), Glycerol (G5516), Bromophenol blue (B5525), Dithiothreitol (DTT, D9779), Reference dye (R4526), SYBR green jumpstart ready mix (S4438) and Brustal (SML 1868).

2.1.2 Thermo Fisher Scientific

The following were purchased from Thermo Fisher Scientific, UK with codes indicated in parentheses. Pierce bicinchoninic acid (BCA) assay (23225), Microplate reader (Multiskan FC), BCA protein standards (23208), SDS (BP1311-1), Protein ladder (26616), Glycine (BP381-5) and SDS (BP1311-1), NanoDrop spectrophotometer (NanoDrop 2000C), Quant-iT Broad-Range DNA assay kit (Q33130), Histological glass slides (1014356190), Xylene (X/0250/17), Oil Red O (15244664), T75 cell culture flask (10364131).

2.2 Cell line maintenance

2.2.1 Human pancreatic cancer cell lines

The following pancreatic cancer cell lines, MiaPaCa-2, Panc-1 and Suit-2 were used in this study. Cell line characteristics are defined in Table 2.1. Cells were maintained in vented T75 cell culture flask containing RPMI medium, supplemented with 10% fetal bovine serum (FBS, 10500056, Life Technologies, UK) and 2 mM L-glutamine, and with 100 U/mL penicillin and 100 µg/mL streptomycin antibiotics. Cells were grown in a humidified 5 % CO_2 incubator at 37^{o}C and subcultured when approximately 80% confluent. Cells were genotyped prior to and during this thesis by amplifying isolated genomic DNA using the PowerPlex-16 HS system (Promega, USA) according to manufacturer's protocol. Amplified fragments were analysed using Genetic Analyser (3130, Applied Biosystem, USA) and GeneMapper software (version 4.0, Applied Biosystem) as described previously[99].

Table 2.1: Origin of established pancreatic cancer cell lines [189,190].

Cell line	Author and year	Age (years)	Sex	Origin of tumour cells	Common mutations	Reference
MiaPaCa-2	Yunis et al.., 1977	65	Male	Primary tumour	KRAS, TP53, p16INK4a,	[191]
Panc-1	Lieber et al.., 1975	56	Male	Primary tumour	KRAS, TP53, p16INK4a,	[192]
Suit-2	Iwamura et al.., 1987	73	Male	Liver metastasis	KRAS, TP53, p16INK4a,	[188]

2.2.2 Primary mouse pancreatic cancer cells

Primary mouse pancreatic cancer cells were isolated from tumours arising in K-Ras$^{LSL-G12D/+}$, p53$^{R172H/+}$ and Pdx1-Cre (KPC) mice see Table 2.2. Cells were maintained in humidified 5 % CO_2 incubator at 37^{o}C in Dulbecco's Modified Eagles Medium (DMEM) supplemented with 10% FBS), 100 U/mL penicillin and 100 µg/mL streptomycin. Incubation and subculturing was as described earlier for human pancreatic cancer cell lines. Low passage KPC cells (<10) were used in this thesis.

2.2.3 Pancreatic cancer associated primary fibroblast - R2875

Primary pancreatic cancer associated primary (CAF) R2875 cells (Table 2.2) were isolated from the tumours of surgically resected pancreatic cancer patients by Dr Lawrence Barrera (University of Liverpool) as described previously[122]. Cells were maintained in humidified 5 % CO_2 incubator at 37^{o}C in Iscove's Modified Dulbecco's

Medium supplemented with 10% FBS, 4mM L-glutamine, 100 U/mL penicillin and 100 µg/mL streptomycin. Incubation and subculturing was as described earlier for human pancreatic cancer cell lines. CAF and normal activated fibroblasts (NAF) primary cells with a low passage number (<10) were used in this thesis.

Table 2.2: Origin of primary cells.

Primary cells	Isolated by	Origin of cells	References
KPC (mouse cancer cell)	Dr Michael Schmid	GEMM of pancreatic cancer	[193]
CAF-R2875 (pancreatic stellate cell)	Dr Lawrence Barrera	Human pancreatic cancer (stromal) tissue section	
CAF-R2910 (pancreatic stellate cell)	Dr Lawrence Barrera	Human pancreatic cancer (stromal) tissue section	
NAF-R2797 (pancreatic stellate cell)	Dr Lawrence Barrera	Adjacent normal human pancreatic cancer (stromal) tissue section	
NAF-R2796 (pancreatic stellate cell)	Dr Lawrence Barrera	Adjacent normal human pancreatic cancer (stromal) tissue section	

2.3 Cell counting

Cell numbers were determined by using counting slides (145-0011, Bio-Rad, UK) and an automated cell counter (TC10, Bio-Rad) according to manufacturers' instruction. Cells were uniformly resuspended in media and 10 µL of suspended cells were transferred to a counting slide chamber and then inserted into the automated cell counter. An average of 2 cell counts was used to determine cell numbers in subsequent experiments.

2.4 Freezing of cell stocks

Generally, 1mL of freezing media (70% RPMI, 20% FBS and 10% dimethyl sulfoxide containing approximately 2 x 10^6 pancreatic cancer cells uniformly resuspended were transferred to a 1.8mL screw caped cryovial (E3090-6222, Starlab, UK). The cryovials were subsequently transferred to a Mr Frosty and stored at -80^{o}C for 24 hours and then transferred to liquid nitrogen storage tank.

2.5 Culturing cells from frozen stocks

Generally, frozen cells in cryovials were rapidly thawed in a 37^{o}C water bath and transferred to a fresh warm 5mL RPMI medium for centrifugation in 15mL Falcon tubes (188271, Greiner Bio-One, Austria). Centrifugation was performed at 100 x g for 5 minutes and the supernatant obtained was discarded and the pellets were then resuspended in an appropriate volume of warm media and subsequently transferred to a vented T75 flask for culturing as described in section 2.2.1.

The same process of freezing (Section 2.2.3) and culturing as described above, applies to both KPC and CAF-2875 cells. However, for KPC and CAF-2875, DMEM was used in place of RPMI and for CAF-2875, the freezing medium was (75% DMEM, 20% FBS and 5% DMSO).

2.6 siRNA transfection

2.6.1 siRNA stock preparation

All siRNA were supplied lyophilized and then reconstituted in a class II biological safety cabinet with distilled water (B-003000-WB-100, Dharmacon, USA) and 5x siRNA buffer (B-002000-UB-100, Dharmacon, USA). 1x siRNA buffer was used to reconstitute lyophilized siRNAs to a final concentration of 20µM according to manufacturer's instructions. Reconstituted siRNAs were aliquoted and stored at -20^{o}C until needed.

2.6.2 Optimization of siRNA transfection for UHRF1 Knockdown

All siRNAs used in this thesis were supplied by Dharmacon, USA. Optimum siRNA concentration and volume of lipofectamine 2000 (11668-500, Life Technologies)/well of a 6-well plate was determined using Suit-2 pancreatic cell line. A final siRNA concentration of 10 nM and 2 µL lipofectamine/well of a 6-well plate in a final volume of 3 mL was determined to be the optimum and used hereafter for subsequent transfections.

2.6.3 siRNA transfection

Cells were plated in 6 well plates at seeding densities listed in Table 2.3 and placed for 24 hours in an incubator at 37^{o}C with 5% CO_2. After 24 hours media was removed and replaced with antibiotic free media to a final volume of 2.6 mLs. Two hundred microliters (200 µL) of Opti-MEM I 1x, (11058-021, Life Technologies), was incubated with 2µL of Lipofectamine 2000 for 5 minutes before combining with 200µL of Opti-MEM I containing the required concentration of target siRNA Table 2.4 and incubating for a further 30 minutes. Four hundred microliters (400 µL) of combined solution was added to each well in a drop-wise fashion and placed in the incubator for 72 hours. Cells were then harvested and prepared as required for subsequent experiments. At least 2 control or targeting siRNAs are required to control for off target effects. In this thesis however, the siRNAs used have been previously validated for off target effects and specificity[80], and except otherwise stated, single targeting siRNAs where used for each experiment.

For experiments involving 96-well plates seeding densities and transfection reagents were scaled down accordingly to a final volume of 100µl and concentration used previously in 6 well experiments (see Table 2.3 and Table 2.4).

Table 2.3: Seeding densities used for siRNA experiments.

Cell line	Seeding density (per 6 well plate)	Seeding density (per 96 well plate)	
		72hr treatment	120hr treatment
Suit-2	3×10^4	1.0×10^3	0.5×10^3
MiaPaCa-2	5×10^4	1.5×10^3	1.0×10^3

Table 2.4: siRNAs used throughout this thesis including catalogue number and concentration used.

Target Groups	siRNA	Catalogue No.	Final Concentration
Human anti-UHRF1 siRNA	Human UHRF1 targeting siRNA-3	D-006977-03	10nM
	Human UHRF1 targeting siRNA SMARTpool	M-006977-01	10nM
Human anti-Nrf2 siRNAs	Human Nrf2 targeting siRNA-4	D-003755-04	10nM
Human anti-Keap1 siRNA	Human Keap1 targeting siRNA-4	D-012453-04	10nM
Human anti-NQO1 siRNA	Human NQO1 targeting siRNA SMARTpool	M-005133-02	10nM
Human anti-Srxn1 siRNA	Human Srxn1 targeting siRNA SMARTpool	M-015263-00	10nM
Mouse targeting siRNA	Mouse UHRF1 targeting siRNA SMARTpool	D-055507-03	10nM
Control siRNAs	ON-TARGETplus Non-targeting siRNA-1	D-001810-01	10nM
	ON-TARGETplus Non-targeting siRNA-3	D-001810-03	10nM
	ON-TARGETplus Non-targeting pool	D-001810-10	10nM
	RISC-free siRNA	D-001220-01	10nM

2.7 Harvesting cells

Media was discarded from wells and cells were rinsed with phosphate buffered saline (PBS: 0.01M Phosphate buffer, 0.027M KCl, 0.137M NaCl, 20012019, Life Technologies). Cells were then detached with 1x trypsin-EDTA, suspended in PBS and transferred to 15mL Falcon tubes. Cells were centrifuged at 100 x g for 5 minutes and the supernatant discarded from the cell pellet. Forty microliters (40 µL) of ice-cold radioimmunoprecipitation assay (RIPA) buffer (150 mM NaCl, 0.1 % (v/v) Triton X-100, 0.5 % (w/v) sodium deoxycholate, 0.1% (v/v) SDS, 50 mM Tris-HCl, pH 8.0) containing freshly added protease inhibitor cocktail tablet (11836170001, Roche, USA) was added to the cell pellet and stored at -20^{o}C.

2.8 Western blot analysis

2.8.1 Preparation of protein lysate

Cell pellets were lysed in RIPA buffer using a sonicator (Branson digital sonifier 250, Branson Ultrasonics, Shanghai, China) for 4 seconds. Protein lysate was then centrifuged at 10,000 x g for 10 minutes at 4^{o}C. Protein lysates were quantified using a bichinchonic acid assay and stored at -20^{o}C for short term (< 1 month) or long term at -80^{o}C.

2.8.2 Protein quantification

Pierce bicinchoninic acid (BCA) assay (23225, Thermo Scientific, Rockford, USA) was used to quantify the total protein concentration in each lysate according to manufacturer's instruction. Briefly, a 1:10 dilution of sample lysate was prepared to a final volume of 25 µL and 200 µL of BCA assay working solution was added in 96-well plates. Plates were incubated at 37^{o}C for 30 minutes. Protein concentration was determined using a Multiskan FC microplate reader by measuring the absorbance at 562 nm; comparison with standard curve from known protein standards was made to calculate the concentration in each sample.

2.8.3 Protein sample preparation for SDS-PAGE

A 20 µg protein lysate was diluted 4:1 with 5x loading buffer (10 % (v/v) SDS, glycerol 50 % (v/v), 300 mM Tris-HCl pH 6.8, 0.05 % (w/v) bromophenol blue and 0.5 M dithiothreitol (DTT). Samples were vortexed, centrifuged briefly and denatured at 92^{o}C for 10 minutes.

2.8.4 Gel electrophoresis and protein transfer

Equal volumes of denatured protein containing 20 µg of protein/sample and 3 µL of protein standard were separated by SDS polyacrylamide gel electrophoresis (SDS-PAGE). Samples were loaded into an Any KD Mini-PROTEAN TGX precast gel (456-9034, Bio-Rad) and separated at an initial constant voltage of 100 volts for 10 minutes then at 200 volts for 25 minutes in an SDS-PAGE running buffer (0.025 M Tris base (648311, Calbiochem, USA), 0.192 M glycine and 0.1 % (w/v) SDS). The resolved

proteins on the precast gels were transferred onto polyvinylidene difluoride (PVDF) membrane (170-4156, Bio-Rad) using a semi-dry electroblotting system (Trans-Blot Turbo Transfer System, Bio-Rad); transfer was undertaken using the turbo blot programme and mixed molecular weight setting at 25 volts for 7 min.

2.8.5 Blocking and protein detection

For all western blotting experiments undertaken during this thesis, 5 % non-fat dry milk (170-6404, Bio-Rad) in PBS + 0.1 % Tween 20 (PBST) was used for both blocking and primary and secondary antibody dilutions. Successful transfer of proteins onto PVDF membrane was followed by blocking at room temperature on an oscillator. After 1 hour of blocking, the 5 % milk was discarded and membranes were probed with appropriate primary antibody (Table 2.5) overnight at 4^{o}C on an oscillator. Next, the membranes were washed with PBST 3 x 5 min washes and probed with appropriate horseradish peroxidase (HRP) conjugated secondary antibody (Table 2.5) for 1 hour at room temperature and then washed with PBST 3 x 5 min washes. Protein bands were visualized with enhanced chemiluminescence reagent (ECL, NEL105001EA PerkinElmer, USA) and signals were either detected on light sensitive radiographic film (47410 19289, Fuji Medical X-Ray Film, Japan) in a dark room using a developer and fixer or in a ChemiDoc imaging system (1708371, Bio-Rad) according to manufacturer's guidelines.

Table 2.5: Primary and secondary antibodies used for immunoblotting, immunocytochemistry and immunohistochemistry. The dilutions for IHC and ICC are shown in bold.

Antibody	Molecular weight	Dilution for immunoblotting	Catalogue number and Supplier
UHRF1	90 kDa	1:1000 **(1:100 for IHC)** **(1:250 for ICC)**	sc-136264, Santa Cruz
UHRF1	90 kDa	1:1000	sc-98817, Santa Cruz **(KPC - mouse only)**
Keap1	69 kDa	1:1000	sc-15246, Santa Cruz
Nrf2	68/100 kDa	1:1000	ab62352, Abcam
NQO1	31 kDa	1:1000 **(1:20,000 for IHC)** **(1:500 for ICC)**	MA1-16672, Thermo Scientific
Srxn1	13 kDa	1:1000	sc-373829, Santa Cruz
α-SMA	42 kDa	1:500 **(1:50 for IHC)**	ab-7817, Abcam
GAPDH	38 kDa	1:1000	sc-25778, Santa Cruz
β-actin	42 kDa	1:20,000	A5441, Sigma-Aldrich
Anti-mouse HRP		1:2000	P0447, Dako
Anti-rabbit HRP		1:2000	P0448, Dako
Anti-goat HRP		1:2000	P0449, Dako
Mouse Ig G2a isotype control		**1:100 for IHC**	sc-3878, Santa Cruz
Mouse Ig G1 isotype control		**1:20,000 for IHC**	X0931, Dako

2.9 Cell viability and proliferation assay

Cells were seeded (Table 2.3) and transfected in 96-well (655180, Greiner Bio-One) plates as described earlier (Section 2.6.3). Cells were transfected with control, UHRF1 and Nrf2 siRNA (10nM each). Proliferation was determined either at 72 h or 96 h by MTS EZ4U kit (BI-5000, Biomedica, Vienna, Austria) as described in Tonack *et al.*, 2011.[194]. Briefly, at indicated time points, media in cells were replaced with 100 µL of fresh medium containing substrate (SUB) and activator (ACT) solution (1:10) and absorbance was measured hourly for 4 hrs using Multiskan EX plate reader (Thermo Scientific) at 450nm and then at 650nm to adjust for background.

2.10 Cytotoxicity test

Cells were seeded (Table 2.3) in 96-well plates and treated for a total of 120 hours. In the first 48 hours, cells were transfected with either 10nM control or UHRF1 siRNA as described earlier (Section 2.6.3). Media was then replaced with fresh antibiotic free media containing varying concentrations of gemcitabine ranging from 0.1 µM to 100 µM for a further 72 hours. Proliferation was determined as described earlier (Section 2.9) and sigmoidal dose response curves constructed using GraphPad Prism version 5.00 for Windows, GraphPad Software, San Diego California USA.

2.11 Cell cycle analysis

MiaPaCa-2 and Suit-2 cells were seeded at 5 x 10^4 and 3 x 10^4 cells/well respectively in 6-well plates. Cells were transfected with 10 nM siRNA (control, Nrf2, UHRF1 and Keap1) as described earlier (Section 2.6.3). After 72 h, cells were harvested, washed in PBS and centrifuged at 130 x g for 5 min. The resulting cell pellet was suspended in 50 µL of PBS and then fixed in 1 mL ice-cold 70 % ethanol added drop-wise with cells continuously agitated during ethanol addition. Cells were incubated at 4^{o}C for 24 h and then pelleted at 130 x g for 5 min. Cells were then washed twice in PBS and centrifuged as before. Pelleted cells were resuspended in 25 µL of RNAse A and incubated at 37^{o}C. After 15 min, 300 µL of 2 µg/mL of propidium iodide (PI, P3566, Invitrogen, USA) solution was added to RNAse A-cell pellet mix and incubated at room temperature for 15 min in the dark. Cells were then subjected to flow cytometry analysis using BD FACS Canto II (BD Biosciences, USA). PI solution (PI in PBS+ 0.1 % Triton X-100) was prepared fresh for each experiment.

2.12 Analysis of oxidative stress

2.12.1 Reactive oxygen species assay

Measurement of reactive oxygen species generation was determined by incubating cells with 2',7'-dichlorodihydroflourescein diacetate (H_2DCFDA - D399, Life Technologies, UK). Briefly, after seeding and transfecting cells (10 nM control, Nrf2,

UHRF1, Keap1 siRNAs) as described earlier (Section 2.6.3) for 72 hours in 6-well plates, media was discarded and cells were rinsed with PBS. Cells were then detached by adding trypsin which was subsequently quenched by adding fresh culture media (trypsin: culture media, 1:4). Detached cells were centrifuged at 130 x g for 5 minutes and the supernatant was discarded. The resulting cell pellets were resuspended in 5 µM H_2DCFDA working solution (5 µM H_2DCFDA final concentration in pre-warmed PBS) and incubated for 30 minutes at 37^{o}C with intermittent agitation. Next, cells were centrifuged at 130 x g for 5 minutes and the H_2DCFDA working solution supernatant was discarded. The cell pellet obtained was washed with fresh pre-warmed PBS, centrifuged at 130 x g for 5 minutes and the supernatant discarded. The cell pellet was finally suspended in 500 µL of fresh pre-warmed PBS and subjected to flow cytometry (BD LSRFortessa) for ROS detection using laser excitation at 488 nm (495 nm) and detection at 535 nm (525 nm). Data was analysed with FlowJo v 10.0.8.

2.12.2 Glutathione assay

MiaPaCa-2 cells were seeded at a density of 5 x 10^4 cells/well in 6-well plates. Transfection (Control, Nrf2 and UHRF1 siRNA) was undertaken as described earlier in section 2.6.3 for 72 h. Diethyl maleate (DEM) at 1 mM final concentration in RPMI was added to one set of control siRNA treated wells for 1 h. Cells were lysed in 350 µL of 10mM HCl and 70 µL lysate was transferred to a 0.5 mL microcentrifuge (S1605-0000, Starlab, UK) for Bradford assay and the rest to a separate 0.5 mL microcentrifuge for glutathione (GSH) assay. Lysates were stored immediately at -80^{o}C and both assays were performed the following day. Dr Adedamola Olayanju,

(University of Liverpool, UK) assisted by performing both Bradford and GSH assays. Total sample GSH content was quantified using 5,5'-dithiobis-2-nitrobenzoic acid-GSH reductase recycling method as previously described[195]. Sample GSH concentrations were calculated with reference to a standard GSH curve and further normalised to total protein content using Bradford assay.

2.13 Dual-Glo Luciferase assay

The conditions for transfecting firefly and renilla luciferase plasmids were optimized by varying the concentrations of firefly and renilla plasmids and the ratio of firefly to renilla plasmids. A plasmid DNA to lipofectamine 2000 of 1 µg DNA : 2 µL of lipofectamine ratio was used. For all reporter transfections, pGL4.74 renilla luciferase reporter was used as an internal control. pGL4.11 firefly luciferase reporter plasmid containing eight antioxidant response elements (8xAREs), was a kind gift from Dr Jo Walsh and Professor Chris Goldring (University of Liverpool, UK).

1 x 10^3 MiaPaca-2 and Suit-2 cells/well were each seeded into white 96-well plates (655083, Greiner Bio-One) and transfected with 10 nM control, UHRF1 and Nrf2 siRNA as described earlier (Section 2.6.3) for 48 h at 37°C in humidified 5% CO_2. Media was replaced and cells were transfected with pGL4.11 firefly luciferase reporter plasmid (Promega) containing 8xAREs as described previously [196] in a final concentration of 150 ng/100 µL/well and pGL4.74 renilla luciferase reporter plasmid (E6921, Promega) both in a final volume of 100 µL/well for 24 h. A ratio of 100:1 for

firefly : renilla plasmid was used in this thesis for both MiaPaCa-2 and Suit-2 cells. Luciferase activity was measured 24 h later using Dual-Glo luciferase assay system (E2920, Promega) according to manufacturer's instructions. Briefly, following firefly and renilla plasmids transfection, media was replaced with 50 µL of serum free RPMI and an equal volume of Dual-Glo luciferase reagent was added and mixed on a shaker (400 rpm) for 15-20 min. Firefly luminescence was then quantified using a luminometer (Modulus microplate reader, Turner BioSystems, USA). Dual-Glo Stop and Glo reagent 50 µL/well was next added and mixed on a shaker (400 rpm) for 15-20 min and renilla luminescence was measured using the same luminometer.

2.14 Culturing cancer associated fibroblast with conditioned media from cancer cells

Cancer associated fibroblasts R2875 were seeded at 20,000 cells/well in a 24-well plate (662160, Greiner Bio-One) for at least 72h in IMDM as described earlier (Section 2.2.3) before culturing in conditioned media from MiaPaCa-2 cells. MiaPaCa-2 cells were grown in a vented T75 flask and at 80 % confluence, the media was discarded and cells were rinsed twice in warm PBS before further culturing in serum free RPMI media. After 36 h, conditioned media was harvested and centrifuged at 300 x g for 10 min and the supernatant obtained was filtered through 0.22 µm sterile filter (SLGP033RS, Merck Millipore, Ireland). The filtrate was then used to culture and transfect CAF-2875 with pGL4.11 firefly luciferase reporter plasmid in a final concentration of 60 ng/100 µL and a final volume of 1200 µL/well of a 24 well plate with pGL4.74 renilla luciferase reporter plasmid as described in section 2.13 for

MiaPaCa-2 and Suit-2 plasmid transfection. A ratio of 10:1 for firefly to renilla was used in this thesis for CAF-2875. After 36 h, Dual-Glo Luciferase assay was performed. Briefly, media was discarded from the 24-well plate and 75 µL of serum free RPMI and an equal volume of Dual-Glo luciferase reagent was added and mixed on a shaker (400 rpm) for 15-20 min. The contents of each well were then transferred into a 0.5 mL microcentrifuge and centrifuged at 10, 000 x g for 5 min. Next, 100 µL of the supernatant was carefully pipetted into each well of a white 96-well plates and subsequent steps were as described above for MiaPaCa-2 and Suit-2 Dual-Glo luciferase assay.

2.15 RNA isolation

Total RNA was isolated from cultured cells using RNeasy kit (74104, Qiagen, UK) according to manufacturer's instructions and as described previously[80]. Briefly, cells were harvested using cell scrapper (541 070, Greiner Bio-One) and transferred into 1.5 µL microcentrifuge tubes (S1615-5500, Starlab, UK). Cells were pelleted at 300 x g for 5 min and then disrupted with 350 µL of buffer RLT by repeated pipetting. Disrupted cells were then centrifuged at 10,000 x g for 3 min and 350 µL of 70 % ethanol was added to the homogenized lysate and mixed by repeated pipetting. The entire 700 µL sample lysate were transferred to an RNeasy spin column placed in a 2 mL collection tube and centrifuged for 15 sec at 10,000 x g. The spin column was placed in a clean empty 2 mL collection tube and 350 µL of buffer RW1 was added and centrifuged for 15 sec at 10,000 x g. DNase I incubation mix (cat. no. 79254), was

added directly to the spin column membrane, incubated at room temperature for 15 min and washed twice with 500 µL of buffer RPE at 10,000 x g for 15 sec and 2 min respectively. With the spin column empty and a new 2 mL collection tube, another centrifugation at 10,000 x g for 1 min was performed. The spin column was then transferred to a new 1.5 mL microcentrifuge tube and 40 µL of RNase free water was added directly to the spin column, incubated for 1 min at room temperature and eluted at 10,000 x g for 1 min. The quantity and quality of eluted DNA was determined by NanoDrop spectrophotometer (ND-1000, NanoDrop Technology, Wilmington, USA) and stored at -80^{o}C.

2.16 cDNA synthesis

cDNA was synthesized from RNA using ImProm-II reverse transcription system (A3800, Promega) according to manufacturer's instructions and as described previously[80]. Approximately 2 µg of RNA + 1 µL of random primers scaled up to a final volume of 20 µL with dH_2O was reverse transcribed by incubating for 5 min at 70^{o}C followed by rapid cooling on ice. Reverse transcriptase master mix, 20 µL (8 µL of ImProm-II 5 x reaction buffer, 6.4 µL 25 mM $MgCl_2$, 1 µL 0.5 mM dNTP mix and 2 µL ImProm-II reverse transcriptase and 2.6 µL of PCR water) was added to each sample, briefly mixed and incubated under the following thermal cycling conditions: 25^{o}C for 5 min, 42^{o}C for 1 h and 70^{o}C for 15 min. Samples without random primers, dNTPs and reverse transcriptase were used as controls. The quantity and quality of synthesized cDNA was determined by NanoDrop spectrophotometer and then stored at -80^{o}C.

2.17 Quantitative real-time PCR

Quantitative real-time PCR (qRT-PCR) was performed for *UHRF1*, *NRF2*, *KEAP1* and housekeeping gene *GAPDH* using SYBR green jumpstart ready mix according to manufacturer's instructions. Primers (Table 2.6) were designed using Primer Express Software (Applied Biosystem, UK) and synthesized by Eurofins Genomics, Ebersberg, Germany. Briefly, qRT-PCR was performed in a white 96-well PCR plate (I1402-9909-BC, STARLAB, UK) in a final volume of 20 µL/reaction. Twenty nanogram of cDNA/reaction was mixed with 2x SYBR green jumpstart ready mix, forward and reverse primers (each primer 400 nM/reaction final concentration) and reference dye 0.4 µL/reaction, see Table 2.7. Samples without cDNA were used as no-template negative control. PCR was performed using Light Cycler machine (ABI PRISM, 7000 sequence detection system, Applied Biosystem) under the following thermal cycling parameters: Reactions were denatured initially at 95^{o}C for 10 min, then cycled at 95^{o}C for 15 sec and annealing/extension at 60^{o}C for 1 min for 40 cycles. mRNA quantification was analysed using ABI PRISM 7000 SDS software SYBR green template mode and fold change was calculated by Δ (ΔC_T) method. Experiments were performed in triplicate (biological and technical) and normalized to *GAPDH*.

Table 2.6: Primer sequences used for qRT-PCR

Gene	Primer sequence	
UHRF1	Forward	5'- ATG CTC AAC TAC AAC CCC GA - 3'
	Reverse	5'- CTC TTC CGT CTC ATG GGG TT - 3'
NRF2	Forward	5'- AAA CCA GTG GAT CTG CCA AC - 3'
	Reverse	5'- GAC CGG GAA TAT CAG GAA CA - 3'
KEAP1	Forward	5'- CAG ATT GGC TGT GTG GAG TT - 3'
	Reverse	5'- GCT GTT CGC AGT CGT ACT TG - 3'
GAPDH	Forward	5'- GGC CTC CAA GGA GTA AGA CC - 3'
	Reverse	5'- AGG GGT CTA CAT GGC AAC TG - 3'

Table 2.7: Reagents for SYBR Green JumpStart ready mix

Reagent	Volume (µL)
2x SYBR Green JumpStart ready mix	10
Forward primer	0.8 (400 nM final concentration)
Reverse primer	0.8 (400 nM final concentration)
Water	4
Reference dye	0.4
cDNA template	4 (20 ng/reaction)
Total	20

2.18 Method development for investigating DNA methylation in pancreatic cancer tissues

Dylan Williams kindly assisted with the following experiments. DNA methylation analysis including CT conversion, PCR amplification and pyrosequencing is as described previously[197].

2.18.1 Laser capture microdissection

Five formalin-fixed and paraffin embedded (FFPE) pancreatic cancer tumour blocks were selected by a specialist pancreas histopathologist, Professor Fiona Campbell. Five sections, 10 µm thick from each block were cut onto microdissection frame slides (11505151, PET-Membrane, Leica), incubated at 40^{o}C overnight and hematoxylin and eosin (H & E) staining was then performed. The protocol for H & E is as described below in section 2.20 with the immersion time in haematoxylin restricted to 30 sec only and no requirement for cover slips. Pancreatic cancer cells and adjacent stromal cells were separately laser captured using Leica LMD7000 (Leica Microsystems).

2.18.2 Isolation of genomic DNA from pancreatic cancer tissues

DNA was isolated using the QIAamp DNA FFPE Tissue kit (56404, Qiagen). The manufacturer's protocol was varied as part of the optimization (varying reagent volume, incubation time, temperature and excluding or including initial treatment with xylene). The following 3 protocols were used:

Protocol I: adhering to manufacturer's protocol. Briefly, 180 µL of buffer ATL plus 20 µL of proteinase K, were added to sample pellet in 1.5 mL microcentrifuge tubes and agitated briefly. Samples were incubated for 1 h each at 56^{o}C and 90^{o}C. RNAse A, 2 µL was added to each sample and incubated for 2 min at room temperature followed by the addition of 200 µL of buffer AL and then 200 µL of 100 % ethanol with agitation between additions. Entire lysates were transferred into QIAamp MinElute columns in 2 mL collection tubes. Columns were centrifuged at 6000 x g for 1 min and filtrate was discarded. The columns were washed twice sequentially with 500 µL of buffer AW1 and AW2 by centrifugation at 6000 x g for 1 min each. The columns were then centrifuged dry at 17,000 x g for 3 min and transferred to a new 1.5 mL microcentrifuge tube followed by the addition of 30 µL of elution buffer ATE to the center of the membrane and incubation at room temperature. After 1 min of incubation samples were eluted at 17,000 x g for 1 min.

To improve DNA yield, protocol II was developed. Briefly, the initial incubation at 56^{o}C lasted 24 h in contrast to 1 h for protocol I and the second incubation was set at 70^{o}C in contrast to 90^{o}C for protocol I. Proteinase K, 20 µL (not used at this step in protocol I) was added to 200 µL of buffer AL. Ethanol (100 %), 230 µL rather than 200 µL was used at this step. Centrifugation was performed at 2000 x g for 4 min rather than at 6000 x g for 1 min and 700 µL of buffer AW1 and AW2 were used instead with an additional wash with 700 µL of buffer AW2 by centrifugation at 6000 x g for 1 min each. Columns were transferred to a new 1.5 mL microcentrifuge tube and incubated with 30 µL of elution buffer ATE for 30 min in comparison to protocol I and centrifugation performed at 17,000 x g for 3 min rather than 1 min.

Protocol III, was an alteration of protocol II. Protocol III required the agitation of laser dissected tissues in xylene briefly, followed by centrifugation to obtain a pellet and subsequent washing with 100 % ethanol. After washing with ethanol, samples were pelleted and subsequent steps were the same as for protocol II.

After elution in buffer ATE, DNA quality and quantity was determined with NanoDrop 2000 and Quant-iT Broad-Range DNA assay kit (Q33130, Thermo Scientific) and samples were stored at -20^{o}C. Dr Michael Davies, University of Liverpool kindly performed the broad range assay.

2.18.3 CT conversion

Bisulfite conversion (CT conversion) was performed on extracted genomic DNA using EZ DNA Methylation-Gold kit (5005, Zymo Research) according to manufacturer's instructions. Briefly, 130 µL of CT conversion reagent was added to 20 µL of DNA sample in a PCR tube, agitated briefly and incubated using the following thermal cycling steps: 98^{o}C for 10 min, 64^{o}C for 2.5 h and at 4^{o}C for 30 min x 1 cycle. A mixture of M-Binding buffer and 1 µL of 500 ng/µL of tRNA was prepared in a 1.5 mL and bisulfite treated DNA was added and agitated. The entire mixture was next transferred to Zymo-spin IC column in collection tubes. Columns were centrifuged at 10,000 x g for 30 sec and the filtrate discarded followed by a column wash with 500 µL M-Wash buffer with centrifugation at 10, 000 x g for 30 sec. To each column 200 µl of M-Desulphonation buffer was added and incubated at room temperature. After 20 min samples were centrifuged at 10,000 x g for 30 sec followed by 2 washing steps with 500 µL and 200 µL of M-Wash buffer with centrifugation at 10,000 x g for 30 sec

and 4 min respectively. Columns were transferred to a new 1.5 mL microcentrifuge tube and 10 µL of M-Elution buffer was added directly to column matrix, incubated for 2 min at room temperature and centrifuged at 10,000 x g for 1 min. Eluted/bisulfite treated DNA was stored at -20^{o}C and used for downstream analysis the next day.

2.18.4 *KEAP1* pyrosequencing primer design

KEAP1 primers Table 2.8 were designed by Pyromark Assay Design Software, Qiagen and synthesized by Eurofins Genomics, Ebersberg, Germany.

Table 2.8: PCR amplification and pyrosequencing primer sequences

Region	Primer	Primer sequence 5'-> 3'	Size (bp)	CpGs
KEAP1a	Forward	**BIO**-AAAGGAGAATAGTAGATGGTGG	**87**	**6**
	Reverse	CCCCTTCTCACTATCCCT		
	Pyrosequencing	TTCTCACTATCCCTTCC		
KEAP1b	Forward	GGGTAGGTTATTATGATTAAGTAGA	**77**	**5**
	Reverse	**BIO**-CTCCTAAAACCAAAACCC		
	Pyrosequencing	ATTATGATTAAGTAGAGT		

2.18.5 PCR amplifications

PCR was performed using PyroMark PCR kit (978703, Qiagen) according to manufacturer's instructions. PCR optimization was performed with bisulfite treated lymphocyte DNA. Briefly, a 1:2 (final concentration of 3.75 µM:7.5 µM) mixture of biotin-tagged to non-tagged primer mix each for *KEAP1a* and *KEAP1b* primers were prepared. A total volume of 20 µL/PCR reaction was prepared, Table 2.9 + 1 µL (10ng) of bisulfite treated lymphocyte DNA or no-template negative control.

Table 2.9: Reagents for PCR PyroMark kit optimization

COMPONENT	Volume (µL)
PCR grade water	5.6
Pyromark Master mix, 2x	10
25 Mm $MgCl_2$	0.4
CoralLoad Concentrate, 10x	2
Biotin-tagged to non-tagged primer mix (1:2)	1
Total	19

Thermal cycling parameters were set at an initial denaturation of 95°C for 15 min, then at 94°C for 30 sec, annealing at 51°C to 56°C for 30 sec, extension at 72°C for 30 sec and final extension for 10 min at 72°C for 45 cycles. Annealing at 6 temperature points (51°C to 56°C) as stated above, was performed for each biotin-tagged/non-tagged primer mix. After optimization of PCR amplification with bisulfite treated lymphocyte DNA, subsequent PCR was performed using bisulfite treated tumour and stromal DNA. A total volume of 30 µL/PCR reaction was prepared (see Table 2.10) + 4 µL of bisulfite treated tumour or stromal DNA or no-template negative control.

Table 2.10: Reagents for PCR PyroMark kit final optimised reaction

COMPONENT	Volume (µL)
PCR grade water	6.2
Pyromark Master mix, 2x	15
25 Mm $MgCl_2$	0.6
CoralLoad Concentrate, 10x	3
Biotin-tagged to non-tagged primer mix (1:2)	1.2
Total	26

Thermal cycling parameters were as described for bisulfite treated lymphocyte DNA with the annealing temperature set at 51^{o}C. The quality and quantity of PCR products were determined by resolving 4 µL of amplicons in a mixture of 2 % (w/v) agarose gel with 0.5X Tris/Borate/EDTA (TBE: tris 0.11M, borate 90 mM, EDTA 2.5 mM; pH 8.3) and Safe View DNA binding dye 1:20,000 (NBS-SV1, NBS Biologicals, Cambridgeshire, UK). Resolved DNA was visualized with a UVP VisionWorks LS instrument.

2.18.6 Pyrosequencing

Pyrosequencing was performed using streptavidin sepharose high performance kit (17-5113-01, GE Healthcare Life Sciences) according to manufacturer's instructions. Briefly, 75 µL of binding premix (50 µL of binding buffer + 2 µL of beads + 48 µL of dH_2O) was added to 25 µL of PCR amplicon and transferred into a round bottom 96-well plate. Plates were temporarily sealed and agitated for 10 min and transferred to a PyroMark vacuum station (PyroMark Q96 Workstation, Qiagen). With the suction-filter probes of the PyroMark station on, the probes were placed in sterile water for 30 sec and then into the round bottom 96-well plate containing the PCR amplicon-streptavidin mixture for binding double stranded DNA, followed by washing in 70 % ethanol for 10 sec, denaturation in 0.2 M NaOH for 20 sec and neutralization in 1 % Tris acetate, pH 9 for 10 sec. The single stranded biotin-tagged templates were released into a new PyroMark Q96-well plates containing 45 µL annealing mix (annealing buffer 43.5 µL of + 1.5 µL of sequencing primer)/well followed by continuous agitation and incubation at 80^{o}C for 2 min. The plates were then cooled for 2 min and placed in a pyrosequencer (PyroMark Q96ID, Qiagen).

Pyrosequencing assays were undertaken using PyroMark Gold Q96 SQA reagents (972812, Qiagen) according to manufacturer's instructions. Briefly, PyroMark Gold Q96 SQA reagents were loaded into PyroMark Q96 cartridge and placed in the pyrosequencer and pyrosequencing performed. Each run contained at least 1 internal bisulfite control and a no-template control. CpG site methylation was automatically determined by PSQ^{TM} 96 MA software and given as a percentage.

2.19 Animals

In this study, mice were bred according to the regulations contained in the Animals and Scientific Procedure Act (1986) of the United Kingdom and University of Liverpool local guidelines. Homozygous *Nrf2* null ($^{-/-}$) and *Nrf2* wild-type ($^{+/+}$) mice (C57BL/6J strain) utilised in this study have been described elsewhere[198,199]. Nrf2$^{+/+}$ and Nrf2$^{-/-}$ mice of approximately 10 weeks of age were used for isolating quiescent pancreatic stellate cells and mice of approximately 10 months of age for H & E stain. Both *Nrf2*$^{+/+}$ and *Nrf2*$^{-/-}$ *mice* were housed at temperatures between 19°C –23°C under a 12 hour light/dark cycle and had free access to food and water. Mice were sacrificed by exposure to a rising CO_2 concentration and then sustained until death was confirmed. Pancreata harvested from non-fasted male mice were used throughout the present study. The mice used in this study were kindly donated by Professor Chris Goldring (MRC Centre for Drug Safety Science, University of Liverpool).

2.20 Haematoxylin and Eosin stain

Harvested pancreata were immediately fixed in 10% neutral buffered formalin for 24 hours at room temperature before paraffin embedding. The entire pancreas harvested from each mouse was sectioned at 5 µm thickness and mounted onto histological glass slides. They were dried at 40^{o}C and subjected to H & E staining as follows; mice pancreatic tissue sections were deparaffinised in xylene (X/0250/17, Fisher Scientific, UK) for 5 minutes and subsequently agitated in fresh xylene for 1 minute. Next, sections were rehydrated through decreasing concentration of ethanol (100%, 90% and 70% for a min each) and then rinsed under running tap water. Tissues were next immersed in haematoxylin for 5 minutes and subsequently rinsed under running tap water until clear. The sections were agitated for 30 seconds each in acid water (0.25% HCl/dH_2O), Scott's tap water (1g potassium hydrogen carbonate, 10g magnesium sulphate in 500mL dH_2O) and 100% ethanol with a rinse under running tap water after each agitation. Tissues were placed in eosin Y (3801600E, Leica Microsystems, UK) for 2 minutes, then ethanol for 2 minutes and finally in xylene for 90 seconds. Cover slips were mounted on tissues using DPX mountant for microscopic examination and scoring when dry. All sections were reviewed by specialist pancreatic histopathologist, Professor Fiona Campbell.

2.21 Isolating quiescent pancreatic stellate cells

The isolation of quiescent pancreatic stellate cells (PSCs) were as described previously using density gradient centrifugation[122]. Briefly, harvested pancreas were immediately placed into a 50 mL Falcon tube containing ice-cold 0.9% NaCl solution and further isolation steps were undertaken in a class II biological safety cabinet. The pancreas was digested with a mixture of collagenase P, protease and Dnase in Gey's balanced salt solution (GBSS) by injection into the pancreatic tissue until all pancreatic lobules were clearly separated. The digested tissues were washed and subsequently suspended in a solution of 11.4 % (w/v) Nycodenz in GBSS which was then layered underneath a solution of 0.3 % (w/v) bovine serum albumin in GBSS in a round-bottom centrifuge tube. This was centrifuged at 1400 x g for 20 min at 4^{o} C. Mouse PSCs separated into a hazy band just above the interface of Nycodenz and bovine serum albumin aqueous solution. Quiescent PSCs cells were harvested, washed and maintained in a humidified 5 % CO_2 incubator at 37^{o}C in Iscove's Modified Dulbecco's Medium supplemented with 10% FBS, 4mM L-glutamine, 100 U/mL penicillin and 100 µg/mL Streptomycin. Culture medium was changed at 24 hours post isolation and every other day subsequently.

Purity of freshly isolated PSCs was assessed at 24 h hours post-isolation by fluorescence microscopy for cytoplasmic lipid droplets using Oil Red O staining as described previously [200]. Briefly, freshly isolated quiescent PSCs were cultured on sterile cover slips in 24 well plates for 24 hours. Media was discarded from the wells, rinsed twice with PBS pH 7.2 (20012019, Life Technologies, UK) and cells were fixed

by adding 10% neutral buffered formalin for 60 minutes. All procedures involving formalin were conducted in a fume hood and subsequent steps after cell fixation were performed at room temperature. Formalin was discarded appropriately and the wells were rinsed twice with distilled water and 60% isopropanol was next added for 5 minutes and discarded. A fresh working solution of Oil Red O was next added and incubated for 10 minutes after which wells were rinsed with tap water until clear. Cells were next incubated with DAPI (1: 2000) for 1 minute and cells on cover slips were mounted onto histological glass slides with Prolong Gold Antifade reagent (P36930, Invitrogen) and subjected to fluorescent microscopic examination.

2.22 Rescue of pancreatic stellate cells

L-Ascorbic acid (vitamin C) stock solution was prepared by dissolving L-ascorbic acid in water; immediately aliquots were made and quickly wrapped in foil paper, as ascorbic acid is light sensitive, and stored promptly at - 80^{o}C. Single use aliquots of freshly thawed ascorbic acid were added to Nrf2 null PSCs IMDM culture media in increasing doses of 10 µM, 25 µM, 100 µM and 200 µM final concentration in IMDM.

2.23 Antibody validation

Antibody validation was first undertaken using western blotting prior to performing immunocytochemistry or immunohistochemistry for a selected antibody. siRNA

mediated depletion and western blotting is as described previously in section 2.6.3, 2.7 and 2.8. Dr Claire Jenkinson kindly performed NQO1 antibody validation.

2.24 Processing and paraffin embedding of MiaPaCa-2 cell pellet

As described in section 2.6.3, siRNA mediated depletion of proteins of interests was performed but with a scale up using T75 flasks for each treatment. MiaPaCa-2 cells were harvested at 72 h using Trypsin followed by the addition of 10 mL PBS, pH 7.2 and the subsequent transfer of the entire T75 flasks content into a 15 mL Falcon tube. Cell pellet was obtained by centrifuging Falcon tubes at 75 x g for 5 mins and discarding the supernatant. Cell pellets were resuspended and fixed in 10 mL of 10% neutral buffered formalin and left incubating overnight at 4^{o}C on a roller. Procedures involving formalin were conducted in a fume hood. Following the overnight incubation, the Falcon tubes where left to stand for 3 - 5 hours at 4^{o}C and the resulting supernatant was appropriately discarded. A 2% molten agar was maintained in a 60^{o}C water bath.

Two hundred and fifty microliters (250 µL) of the molten agar was used to resuspend the cell pellet which was subsequently transferred into a hollow and narrow cylindrical base and left to cast on ice. Portions of the casted agar containing the cell pellet were visibly identified and cut out of the remaining cast. The cell pellet cast was placed in 10% neutral buffered formalin and sent for paraffin embedding.

2.25 Immunocytochemistry for UHRF1 detection in MiaPaCa-2 and pancreatic fibroblast cell pellets

Pancreatic fibroblasts cell pellets were prepared by Dr Lawrence Barrera and the sections were cut by Drs Claire Jenkinson, Karen Aughton and Anthony Evans. Freshly cut 5µm sections of paraffin embedded cell pellets were dried overnight at 40^{o}C. The conditions for the immunocytochemistry (ICC) were optimized for antigen retrieval buffer and anti-UHRF1 antibody (sc-136264, Santa Cruz Biotechnology) concentration. Target retrieval solution pH 9.0 (K8004 [high pH], Dako, Denmark) and anti-UHRF1 antibody (sc-136264) 1:250 concentration were determined to be the optimum and used hereafter for subsequent ICC. Step-wise, antigen retrieval was performed using a PT Link (PT10126, Dako). Tris buffered saline (TBS, 2.4g Tris base, 8.8g NaCl in 1L of dH_2O, pH7.6) was used to make a 0.1% Tween 20 solution in TBS (TBS+T). After antigen retrieval, sections were rested in TBS+T for approximately 10 minutes and subsequently washed using TBS+T. After each washing step, excess TBS+T on the slides was removed by tilting and drying the edges with tissue. Further steps after antigen retrieval were performed at room temperature. Sections were next blocked for 10 minutes with peroxidase blocking reagent (4007, Dako) and then washed with TBS+T 3 x 5 min washes. Primary anti-UHRF1 antibody was diluted (1:250) in antibody diluent (S2022, Dako) and incubated for 1 hour and then washed with TBS+T 3 x 5 min washes. Labelled polymer anti-mouse secondary antibody (4007, Dako, UK) was applied to the sections for 1 hour and then washed. Sections were next incubated with DiAminoBenzidine (DAB) reagent for 10 minutes and washed with TBS+T followed by a resting step in TBS+T for 5 minutes. Sections were

then counterstained for 45 seconds in Gill III haematoxylin (3801540BBE, Leica Microsystems, UK) and subsequently washed under tap water for 1 minute. Sections were rinsed in 0.25% hydrochloric acid water for 5 seconds and then placed in Scott's tap water (as mentioned previously) for a further 30 seconds. Sections were next dehydrated through 90% and 100% ethanol for 1 minute and 2 minutes respectively. Finally, sections were placed in xylene for two 1 minute incubations and mounted with cover slips using DPX mountant for microscopic examination and scoring.

2.26 Statistical Analysis

Data analysis was performed using GraphPad Prism version 6.00 for Windows, GraphPad Software, La Jolla California USA.

2.27 Samples and Methods for single nucleotide polymorphism and tumour tissue protein expression

2.27.1 Single nucleotide polymorphism - study population

Blood samples obtained with informed consent and ethical approval (11/NW/0083) were taken from patients with advanced pancreatic cancer (n = 149), enrolled in the TeloVac (telomerase vaccine) and ViP (vandetanib in pancreatic cancer) clinical trials. Patients in both trials received gemcitabine therapy (either alone or in combination with other drugs). The TeloVac trial was a phase III open-label randomized trial assessing the efficacy and safety of gemcitabine plus capecitabine with or without telomerase peptide vaccine in patients with advanced pancreatic cancer (locally

advanced and metastatic pancreatic cancer)[29]. The ViP trial was a randomized phase II trial investigating the addition of the tyrosine kinase inhibitor Vandetanib to gemcitabine chemotherapy[30].

2.27.2 Gene and single nuclueotide polymorphism selection

An extensive literature search was undertaken to select candidate genes and SNPs. PubMed/ (http://www.ncbi.nlm.nih.gov/pubmed) was used as the search platform for published literature related to the subject of interest. Keywords used in the search were 'redox gene polymorphism and cancer', 'antioxidant gene polymorphism and cancer', 'Nrf2 polymorphism and cancer'. Three genes were selected based on their putative function in antioxidant and xenobiotic metabolism: *NRF2* and two of its downstream target genes *NQO1* and *SRXN1* involved in cellular redox homeostasis.

A SNP search was further performed on the selected candidate genes using the NCBI SNP database (http://www.ncbi.nlm.nih.gov/snp/). Additional sources linked to the NCBI database[201] were also consulted. The following criteria were applied to select candidate SNPs from each of the selected genes: firstly SNPs for each gene were identified that had the highest number of PubMed publications related to cancer survival or risk, and secondly these must have been validated in humans. After applying these criteria, three SNPs were chosen for allelic discrimination and further analysis in our patient cohorts, one for *NRF2, SRXN1* and *NQO1.*

2.27.3 DNA isolation for single nucleotide polymorphism study

Genomic DNA was isolated from anticoagulated whole blood obtained from two clinical trial (TeloVac and ViP trial) samples using MagNa Pure Compact Nucleic Acid Isolation Kit I (Roche Diagnostics 03730964001) according to manufacturer's instructions. DNA quality and quantity was evaluated using a NanoDrop spectrophotometer (NanoDrop 200C). Isolated genomic DNA was diluted to a final volume and concentration of 50µL and 25ng/µL respectively.

TaqMan SNP Genotyping Assays for each SNP (C___2091255_30: rs1800566,

C_316023_10:rs2886162, C_29328574_30:rs6053666, Thermo Fisher Scientific) were supplied at 40x and 20x concentration and diluted 1:3 or 1:1 respectively to 10x concentration before use in a PCR mix. LightCycler 480 Probe PCR Master mix (4707494001 Roche Diagnostics) and TaqMan SNP Genotyping Assay mix were prepared as shown (Table 2.11) to make up the final mix for the PCR.

Table 2.11: Reagents for genotyping assay PCR mix

Reagent	Volume (µL)
DNase free water	3
Light Cycler 480 PCR Master Mix	10
TaqMan SNP genotyping assay mix	2
Total	15

To each well of a white 96-well PCR plate (STARLAB, UK), 15µL of PCR master mix was added followed by 5µL of 25ng/µL patient genomic DNA or no-template negative

control in triplicate. PCR was performed with LightCycler 480 PCR machine (Roche Diagnostics GmbH, Germany) under the following thermal cycling parameters: reactions were denatured initially at 95^{o}C for 5 min, then cycled at 95^{o}C for 10 sec, 57^{o}C for 30 sec, 50^{o}C for 30 sec and 72^{o}C for 3 sec for 45 cycles, followed by a final cooling step at 40^{o}C for 10 sec. The end-point genotyping software in the LightCycler 480 PCR machine, made the call for allelic discrimination for individual genes tested. This work was undertaken alongside Dr Claire Jenkinson, with each of us contributing to 50% of the effort.

2.27.4 Tissue microarray construction

Permission was obtained from the ESPAC-Tplus Trial Steering Committee (ET011-16) to examine for potential stratification of chemotherapeutic response in pancreatic cancer patients based on tissue levels of cytoprotective biomarkers.

Formalin-fixed paraffin-embedded pancreatic cancer tissue sections were qualitatively reviewed by an experienced specialist pancreas histopathologist (Professor Fiona Campbell).

Tissue microarrays (TMAs) were kindly constructed by Mr Leigh Shannon. Cores were taken from tumour regions within tissue blocks that had been identified and marked by Professor Campbell using haematoxylin and eosin stained sections. TMAs were prepared with two or more cores (0.6mm in diameter) for each patient from the treatment and observation only groups. Control cores from colon, liver, kidney,

normal pancreas and chronic pancreatitis were used on all arrays constructed to serve as orientation cores. Sections of 5µm thickness were cut and mounted onto histological glass slides by Mr Leigh Shannon. After drying overnight at 40^{o}C, IHC was undertaken within 24 h.

2.27.5 Immunohistochemical staining of TMA sections for NQO1 and UHRF1

The steps for optimization and subsequent IHC are as described in chapter 2.25 for ICC using the following antibody concentrations: anti-UHRF1 antibody (sc-136264, Santa Cruz Biotechnology), 1:100 and anti-NQO1 antibody (MA1-16672, Thermo Scientific) 1:20,000. Dr Claire Jenkinson kindly performed NQO1 antibody validation; work on Nrf2 and Srxn1 antibody validation and optimization was shared equally with Dr Jenkinson while optimization of the UHRF1 antibody and IHC for NQO1 and UHRF1 on the ESPAC TMAs were performed by myself.

2.27.6 Scoring

2.27.6.1 Manual scoring

TMAs stained for NQO1 and UHRF1 were scored independently and blindly alongside Professor F. Campbell. Where there was a disagreement, both investigators re-scored until a consensus was reached.

2.27.6.2 Definiens software scoring

In addition to the manual scoring of cores, computer aided scoring was undertaken using Definiens software (Definiens Tissue Studio version 3.51, Germany). TMA core images were acquired using Aperio ScanScope^{TM} (Leica Microsystems, UK). The Definiens settings for IHC analyses for both NQO1 and UHRF1 is documented in Appendix 15 and Appendix 16. UHRF1 Positive index (PI) = number of UHRF1-stainied positive (brown) cancer cells (highlighted as yellow by Definiens) ÷ sum of purple staining (haematoxilin) cancer cells (highlighted as blue) plus brown staining(yellow marked) cancer cells. Definiens software computes a histological score (HS) NQO1 value after analysis of the region of interest (ROI, cancer cell cytoplasm); HS = (proportion of weak staining x 1) + (proportion of moderate staining x 2) + (proportion of strong staining x 3).

2.27.7 Statistical analysis

Chi-square (χ^2) analysis was undertaken to test the concordance of the genotypes with Hardy-Weinberg equilibrium (HWE), using SPSS for Windows software version 14.0. Overall survival (OS) was estimated with the Kaplan-Meier (KM) method. Cox Proportional Hazard models were used to assess the univariate association between *NRF2/NQO1/SRXN1* and overall survival for combined data and by trial and treatment arm. Cox models by arm and *NRF2/NQO1/SRXN1* with a treatment interaction terms were analysed. Multivariate models were fitted for prognostic variables but excluding *NRF2/NQO1/SRXN1.* Prognostic variables for ViP patients included age, sex, treatment arm, Eastern Oncology Cooperative Group (ECOG) performance status,

differentiation status, histology, stage, tumour type and log CA19-9; for Telovac patients sex, treatment arm, stratum, log CA19-9; and for combined ViP and TeloVac analysis, prognostic variables were sex and log CA19-9.

Significant variables were included in these multivariate models. *NRF2/NQO1/SRXN1* as prognostic variables were fitted into a univariate model for the combined ViP and TeloVac data. *NRF2/NQO1/SRXN1* were added to the multivariate models (for ViP, TeloVac and combined data) and significant prognostic variables selected. Data analysis was performed using Stata (version 14) by Dr Richard Jackson and Mr James Dodd of the Liverpool Clinical Trials Unit, University of Liverpool.

Statistical analysis for UHRF1 and NQO1 protein expression including survival analysis for ESPAC-1 and ESPAC-3 data were undertaken using MedCalc Statistical Software version 17.6 (MedCalc Software bvba, Ostend, Belgium, 2017).

3 INVESTIGATING THE FUNCTION OF UHRF1 ON THE KEAP1-NRF2 PATHWAY IN PANCREATIC CANCER CELLS

3.1 Introduction

We have previously reported that UHRF1 is overexpressed in pancreatic cancer[79], whereas Keap1, the main negative regulator of transcription factor Nrf2 was not expressed in approximately 70% of PDAC cases[99]. Following-up on these findings, Abu-Alainin *et al*. showed that methylation of Keap1 promoter in pancreatic cancer cell lines was possibly a contributing factor to the reduced expression of Keap1. Moreover, an inverse correlation between Keap1 and UHRF1 expression in PDAC tissues was observed and Abu-Alainin *et al*. found that Keap1 protein levels were increased when UHRF1 was depleted from pancreatic cancer cell lines. Accompanying the increase in Keap1, Nrf2 protein and several target genes (HO, CYP2A6) were also downregulated[80].

The conclusion from the study by Abu-Alainin and colleagues was that UHFR1 expression maintains Keap1 promoter methylation and this contributes to keeping Keap1 levels low, which in turn allows Nrf2 levels to remain elevated and corresponding Nrf2 downstream proteins to be expressed in pancreatic cancer. The conclusion although interesting and novel, needed to be strengthened. In order to support their initial findings and to further demonstrate the regulatory function of UHRF1, additional functional studies were necessary.

To achieve these, functional examination of the consequences of Keap1 knockdown and simultaneous depletion of both Keap1 and UHRF1 were undertaken. Additionally, Nrf2 downstream target genes monitored to show loss of Nrf2 activity

namely aldo-keto reductase 1C1 (AKR1C1) and NAD(P)H:quinone oxidoreductase 1 (NQO1), were also examined.

On the basis that the Nrf2 activity is usually manifest by alterations in intracellular reactive oxygen species (ROS) and free GSH[98,99,202], these parameters were additionally evaluated. Furthermore, the expression of an ARE-driven luciferase reporter gene in the context of UHRF1 mediated regulation of Nrf2 was also examined. ARE is commonly found in the promoter region of genes encoding various antioxidant and cytoprotective detoxifying proteins and enzymes. Nuclear transcription factor Nrf2 binds to the ARE in the promoter region and mediates ARE-regulated induction of these genes such as NQO1, AKR1C1 and CYP2A6[203-205].

The aims of this chapter were: (I) to examine the effects of UHRF1 on Keap1-Nrf2 mRNA and protein expression, cell cycle regulation, oxidative stress response (II) to determine whether UHRF1 activity alters response to gemcitabine chemotherapy and (III) to develop a method for analysis of Keap1 promoter methylation in pancreatic cancer tissues.

3.2 Results

3.2.1 Optimization for transfection

A number of transfection conditions were tested in order to determine the optimum concentration of control siRNA in combination with the volume of lipofectamine that least affected the target protein level and cell viability, whilst achieving the maximum depletion of the target protein with the indicated target siRNA. The level of UHRF1 protein and the corresponding cell viability was highest in cells that were not transfected with either siRNA or incubated with lipofectamine (Figure 3.1 A, lane 1, Figure 3.1 B) and this was used as a reference to compare changes to protein level and viability in the transfected cells. All treatments (lipofectamine alone or lipofectamine plus siRNA) decreased UHRF1 protein level (Figure 3.1 A, lanes 2 to 13) or cell viability (Figure 3.1 B).

Lipofectamine treatment alone or in combination with 10 nM control siRNA diminished cell viability but the impact was greatest and significantly different ($p < 0.001$) between 2 µL and 4 µL (Figure 3.1 B) based treatments with 4 µL treatments more severely impairing cell proliferation than 2 µL treatments. A similar trend in cell viability was seen between 2 µL and 4 µL based treatments with 20 nM control siRNA and 2 µL and 4 µL treatments with 30 nM control siRNA (Figure 3.1 B).

UHRF1 was depleted to undetectable levels at all UHRF1 siRNA concentrations used (10, 20 and 30 nM, Figure 3.1 A, lanes 6, 7, 12 and 13). Given that 4 µL based lipofectamine treatments with control siRNA decreased cell viability significantly more than with 2 µL (Figure 3.1 B), all 4 µL based treatments were considered not suitable. Furthermore, the lack of significant difference in cell viability between 2 µL lipofectamine plus 30 nM control siRNA and 2 µL lipofectamine plus 30 nM UHRF1 siRNA (Figure 3.1 B) suggested higher siRNA in particular, control siRNA was detrimental to cells and the 30 nM based siRNA treatment was also considered unsuitable. The treatment response profile with 2 µL lipofectamine plus either 10 nM or 20 nM siRNA (Figure 3.1 B) were similar and therefore 10 nM based siRNA concentration was carried forward for use in subsequent experiments.

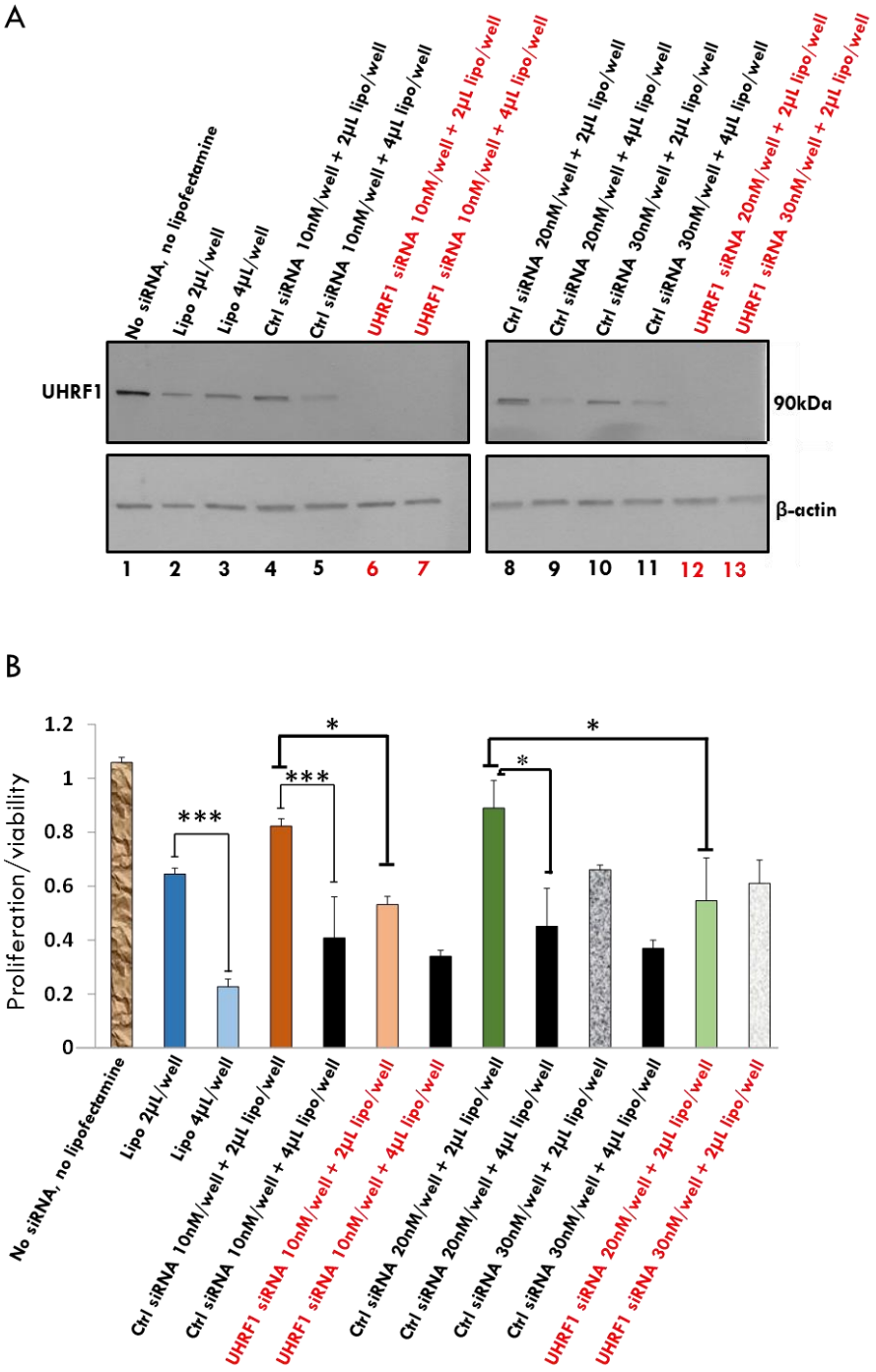

Figure 3.1. Transfection optimization. Suit-2 cells were transfected with varying concentrations and volumes of control and UHRF1 siRNAs and Lipofectamine respectively. (A) Western blot images and (B) MTS assay for corresponding transfection conditions. Lipofectamine 2 µL and 4 µL is indicative of the volume of lipofectamine per well of a 6-well plate that was required to make up a predetermined siRNA concentration in a final volume of 3000 µL of transfection mixture (lipofectamine alone or in combination with siRNA plus culture media); the same siRNA concentration was used in both 6-well and 96-well plates as indicated. * $P < 0.05$, *** $p < 0.001$

3.2.2 UHRF1 depletion is associated with Keap1-Nrf2 pathway deactivation

Dr Wafa Abu-Alainin (then a PhD student within our research laboratory) found that depletion of UHRF1 protein in human pancreatic cancer cell lines, led to an upregulation of Keap1 and a downregulation of Nrf2 proteins[80]. To expand on her findings, I depleted either Nrf2, Keap1 or UHRF1 in human pancreatic cancer cell lines and a primary mouse pancreatic cancer cell line (KPC) and observed the effect on Keap1, Nrf2, and Nrf2 downstream target genes. Depletion of UHRF1 and Nrf2 in Suit-2 cells resulted in downregulation of Nrf2 and Nrf2 downstream targets NQO1 (NAD(P)H:quinone oxidoreductase 1 and AKR1C1 (aldo-keto reductases 1C1) (Figure 3.2A). Similarly, knockdown of UHRF1 and Nrf2 in MiaPaCa-2 cells led to a downregulation of Nrf2 protein (Figure 3.2B). Furthermore, Keap1 depletion was undertaken to determine if this would reverse the effect of UHRF1 depletion on Nrf2. Although, Keap1 knockdown alone led to only a modest increase in Nrf2 protein (Figure 3.2B), it substantially increased the growth of pancreatic cancer cells [80]. Simultaneous depletion of both UHRF1 and Keap1 abrogated the inhibitory effect of UHRF1 depletion alone on Nrf2 in MiaPaCa-2 cells (Figure 3.2B). In primary KPC cells, UHRF1 depletion was also accompanied by upregulation of Keap1 and a concomitant downregulation of Nrf2 (Figure 3.2C). The effect of a time-dependent UHRF1 depletion on mRNA was next investigated. In Suit-2 cells, knockdown of UHRF1 (Figure 3.2D), led to enhanced *KEAP1* transcript levels at 24h but decreased at 48h and 72h to control mRNA level post-UHRF1 depletion (Figure 3.2E), whereas, *NRF2* transcripts initially increased at 24h and 48h to finally decline to its lowest level below

control mRNA level at 72h post-UHRF1 depletion; of note, Nrf2 depletion itself caused *NRF2* transcript downregulation at 24h declining further at 48h before beginning to recover albeit below control mRNA at 72h (Figure 3.2F). These data suggest that Keap1-Nrf2 pathway is active in pancreatic cancer and that UHRF1 contributes to the regulation of this pathway.

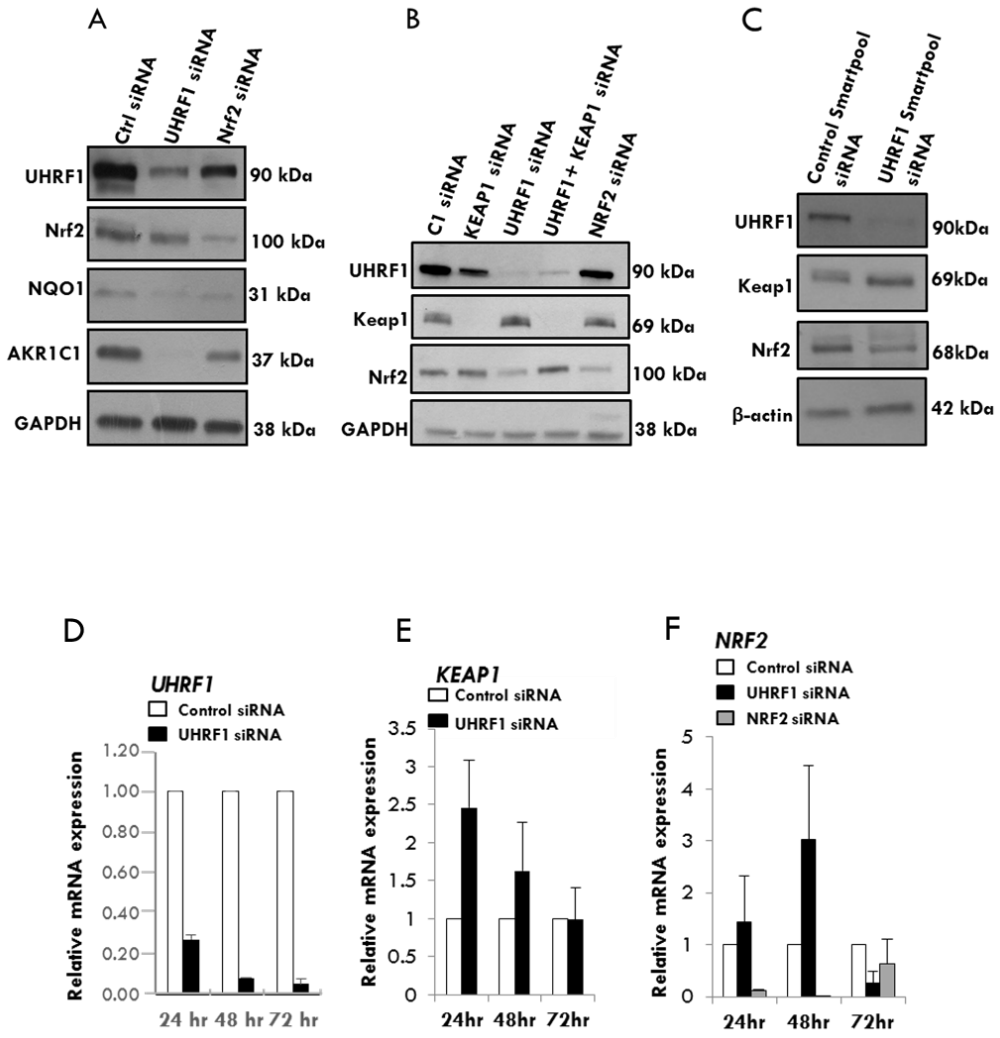

Figure 3.2. UHRF1 regulates Nrf2-Keap1 pathway by inactivating Keap1. Western blot images of indicated proteins following 72h UHRF1, Nrf2, Keap1, UHRF1 + Keap1-targeting siRNAs treatment in (A) Suit-2, (B) MiaPaCa-2 cells and (C) primary PDAC cells from KPC mouse, SMARTpool siRNA 10 nM **Table 2.4**; n=2 for MiaPaCa-2 and Suit-2, n=3 for KPC. GAPDH and β-actin are used as loading controls. (D, E, F) RT-PCR for *UHRF1, KEAP1* and *NRF2* transcripts relative to *GAPDH* in control and UHRF1 or Nrf2 depleted Suit-2 cells n=3.

3.2.3 Suppression of Keap1 by UHRF1 is required for the maintenance of low oxidative states

In order to determine if modulation of the Keap1-Nrf2 pathway impacted on the intracellular redox status of pancreatic cancer cells, reactive oxygen species (ROS) and glutathione (GSH) levels were measured following the indicated treatments in (Figure 3.3). Treatment of MiaPaCa-2 cells with GSH depleter diethyl maleate (DEM) and Nrf2 targeting siRNA (both as positive controls) caused a significant depletion of total GSH. UHRF1 depletion also led to a modest albeit significant depletion of GSH (Figure 3.3 E). Both UHRF1 and Nrf2 depletion significantly increased ROS levels in MiaPaCa-2 cells and the rise in ROS levels was reversed with simultaneous Keap1 and UHRF1 depletion. Keap1 depletion alone did not have significant effect on ROS levels (Figure 3.3 A and B). Since Nrf2 antioxidant effect is mediated through the antioxidant response element (ARE) present in the promoter region of its downstream target genes, I sought to determine if this was the mechanism of UHRF1-mediated effects on Nrf2 targets. Using Nrf2 targeting siRNA as positive control, depletion of UHRF1 resulted in a significant decrease in ARE-luciferase reporter activity (Figure 3.4 A). In Suit-2 cells, similar results were also observed (Figure 3.4 B). Put together, UHRF1 through the suppression of Keap1 is able to activate Nrf2 which drives the maintenance of a low intracellular oxidative status in pancreatic cancer cells to promote their proliferation.

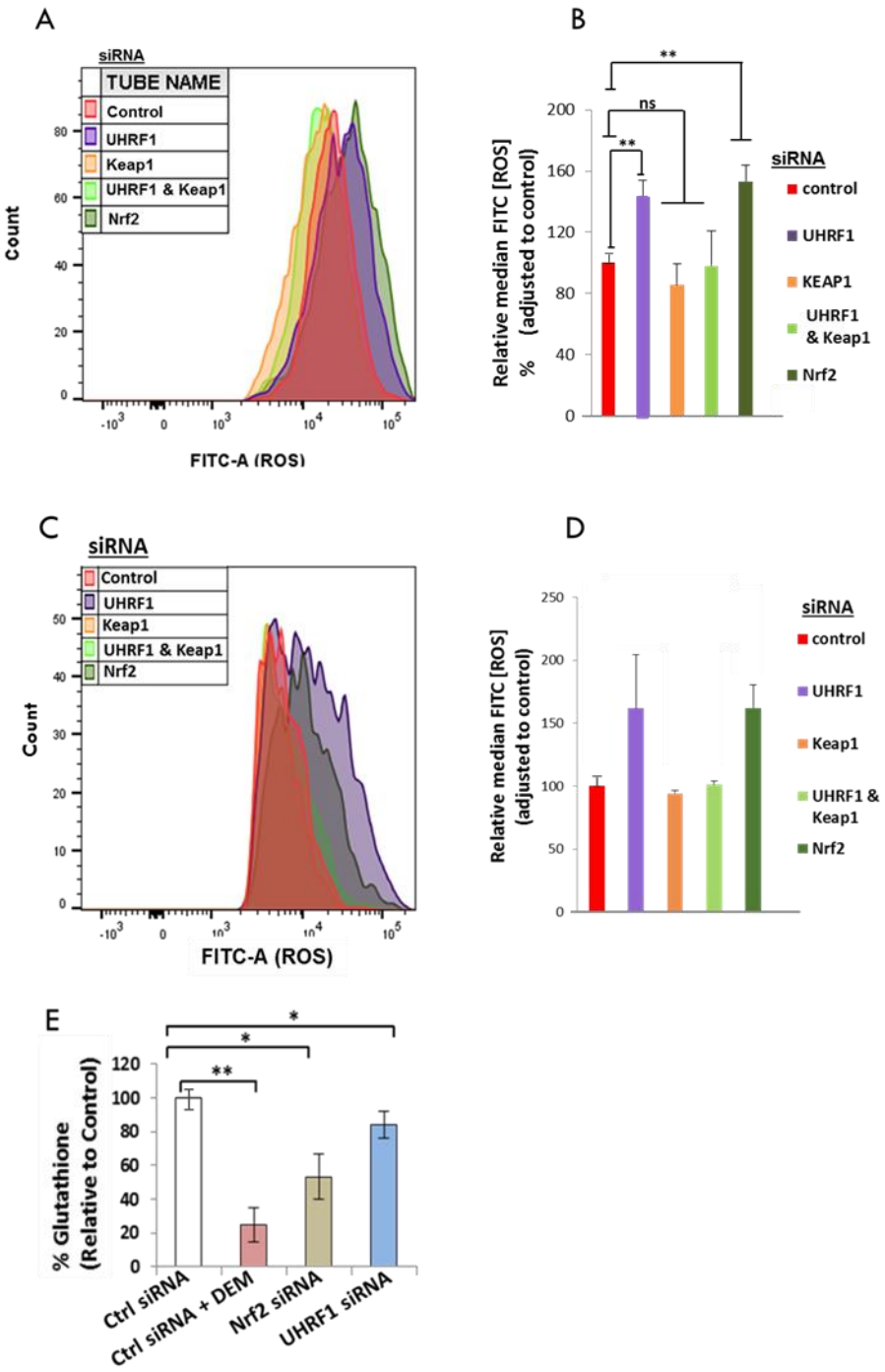

Figure 3.3. UHRF1 contributes to the regulation of oxidative stress through activation of Nrf2. (A, C) Flow cytometry profiles of reactive oxygen species following 72 h of the indicated treatments in MiaPaCa-2 and Suit-2 cells respectively. (B, D) Corresponding mean ± SEM plots for MiaPaCa-2 (n=3). In Suit-2 cells, n=2 hence statistical analysis not undertaken as data obtained from 2 experiments is not sufficient enough to draw a significant conclusion from.(E) Glutathione (GSH) levels after 72 h of the indicated treatments in MiaPaCa-2 cells. Data represents mean ± SEM from three independent experiments performed in triplicates. *p < 0.05; **p < 0.01; ***p < 0.001, ns, not significant.

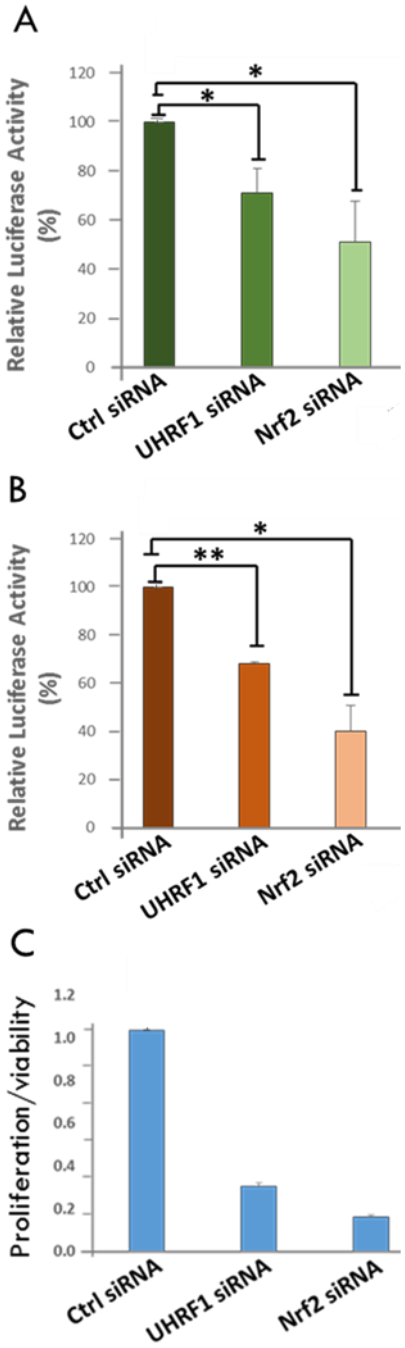

Figure 3.4. Depletion of UHRF1 inhibits Nrf2 pathway and pancreatic cancer cell growth. (A, B) The activation of Nrf2 dependent 8x ARE-reporter was measured following 72 h of the indicated treatments in MiaPaCa-2 and Suit-2 cells respectively. pGL4.74 [*hRluc*/TK] plasmid served as transfection control to normalize luciferase values; n=3 MiaPaCa-2 and Suit-2. . Data represents mean ± SEM from three independent experiments performed in replicates. *$p < 0.05$; **$p < 0.01$. (C) MTS assay following 72 h of the indicated treatments in MiaPaCa-2 cells; n=2 and hence statistical analysis not undertaken as data obtained from 2 experiments is not sufficient enough to draw a significant conclusion from.

3.2.4 UHRF1 depletion causes G_2-M cell cycle arrest

To determine the effect of UHRF1 on cell cycle in pancreatic cancer, cells were depleted of UHRF1 and FACS analysis undertaken. In MiaPaCa-2 cells, a greater proportion of cells were arrested in G_2-M phase of the cell cycle after UHRF1 depletion (Figure 3.5 A and B) while a more prominent G_2-M block was observed following Nrf2 knockdown. This similar cell cycle profile between UHRF1 and Nrf2 depletion may be linked to the fact that both UHRF1 and Nrf2 knockdown led to Nrf2 downregulation (Figure 3.2B). Moreover, depletion of Keap1 caused a greater G_1 cell proportion indicative of a speedy progression though the cell cycle. Interestingly, simultaneous knockdown of both Keap1 and UHRF1 restored cell cycle to that of control siRNA cell cycle profile. Cell cycle profiles did not change to any significant degree with UHRF1 or Nrf2 knockdown in Suit-2 cells (Figure 3.6A and B).

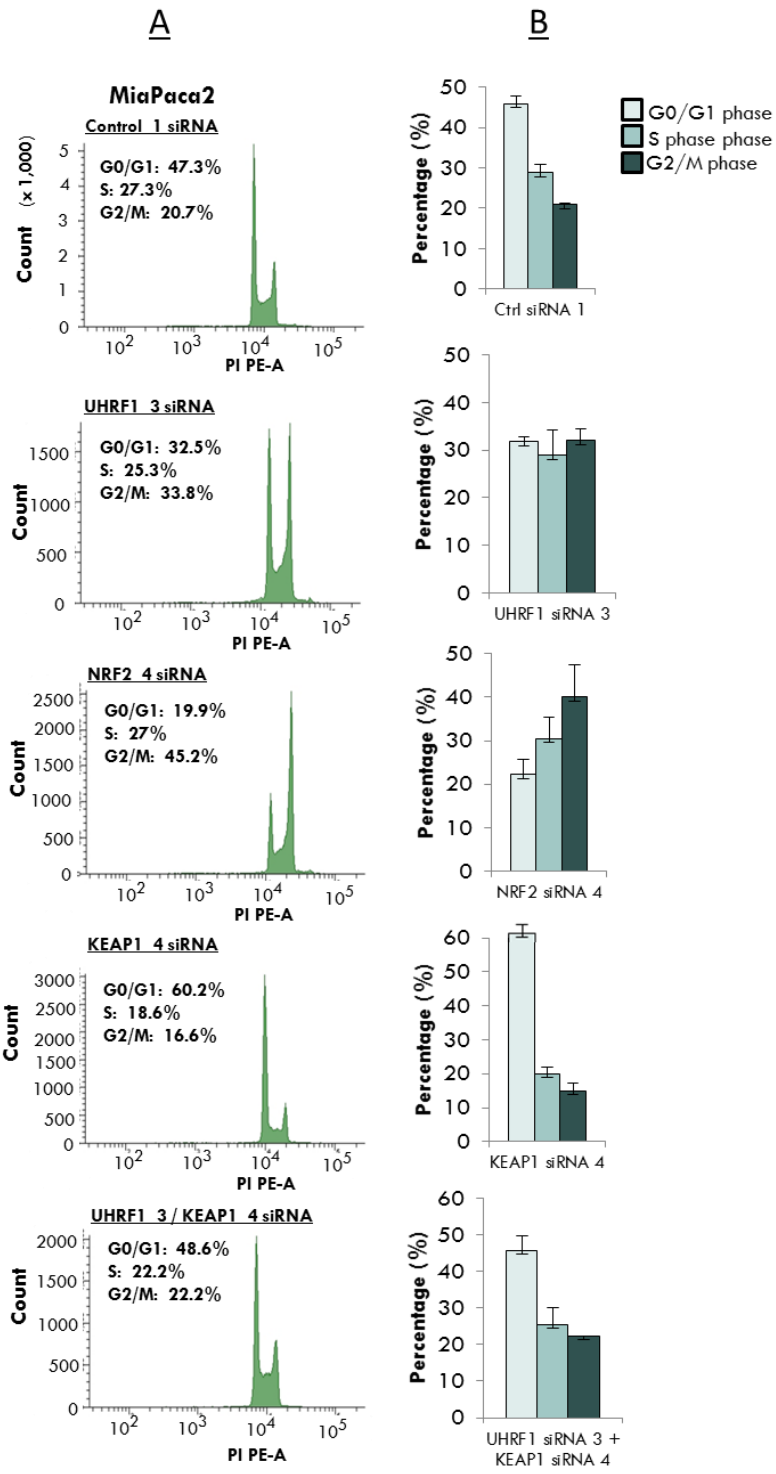

Figure 3.5. Suppression of Keap1 by UHRF1 is required for cell cycle progression in MiaPaCa-2 cells. (A) Flow cytometry profiles of PI-stained MiaPaCa-2 cells after 72 h of the indicated treatments. (B) Corresponding mean ± SEM plots for 3 independent experiments.

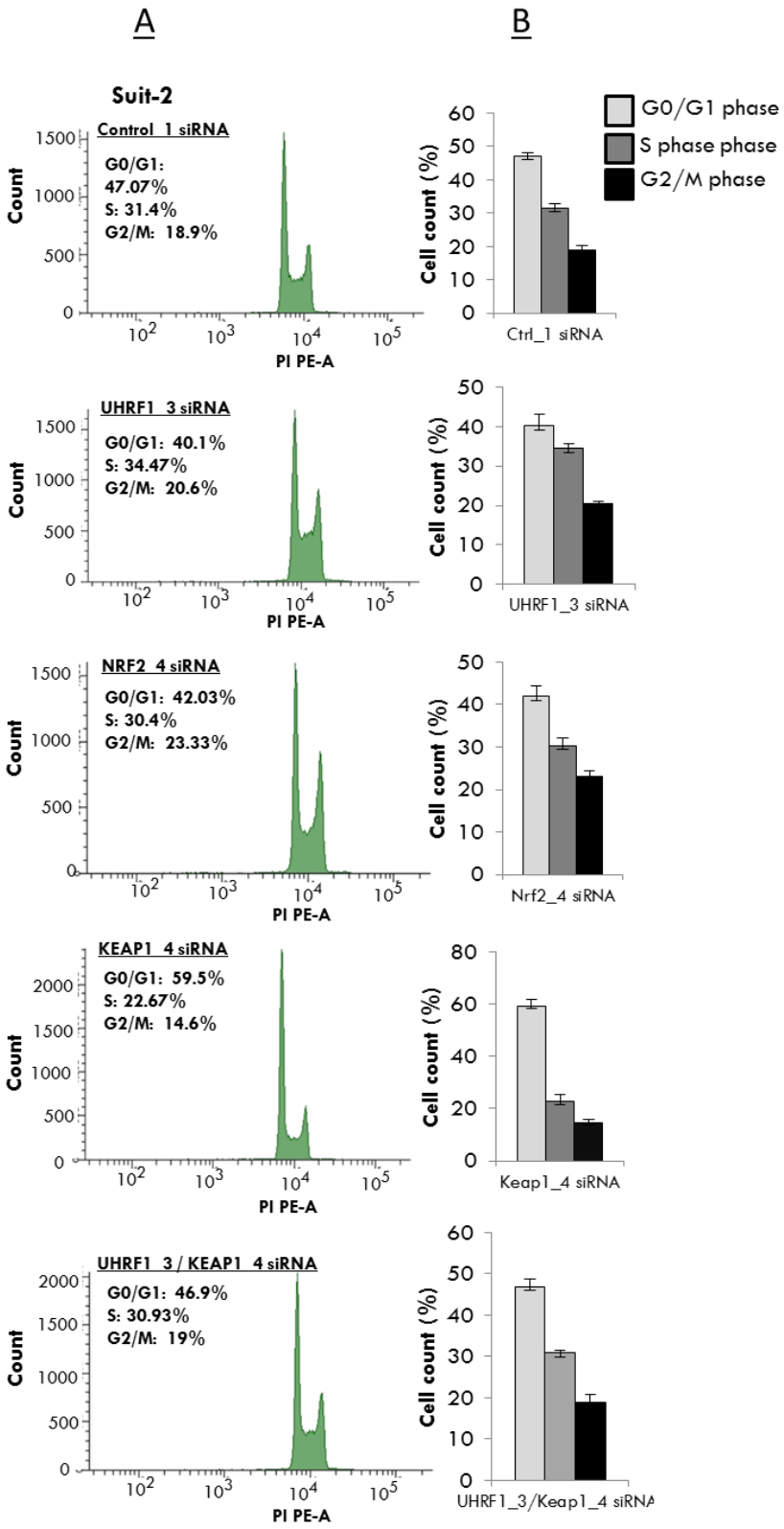

Figure 3.6. Suppression of Keap1 by UHRF1 is required for cell cycle progression in Suit-2 cells. (A) Flow cytometry profiles of PI-stained Suit-2 cells after 72 h of the indicated treatments. (B) Corresponding mean ± SEM plots for 2 independent experiments.

3.2.5 UHRF1 depletion does not confer increased sensitivity to gemcitabine

Since (I) gemcitabine treatment has been the common chemotherapeutic agent of choice for pancreatic cancer, (II) approximately 86% of PDAC tissues overexpress UHRF1[80] and (III) UHRF1 knockdown showed a significant decrease in cell proliferation (Figure 3.4 C), examination of the potential benefit of a combined UHRF1 knockdown and gemcitabine treatment was undertaken. Knockdown of UHRF1 is demonstrated in Figure 3.7 B and D for MiaPaCa-2 and Suit-2 respectively. However, UHRF1 knockdown followed by gemcitabine treatment had no additive or synergistic benefit in both MiaPaCa-2 (IC50, $p = 0.53$, Figure 3.7 A) and Suit-2 cells (IC50, $p = 0.51$ Figure 3.7 C).

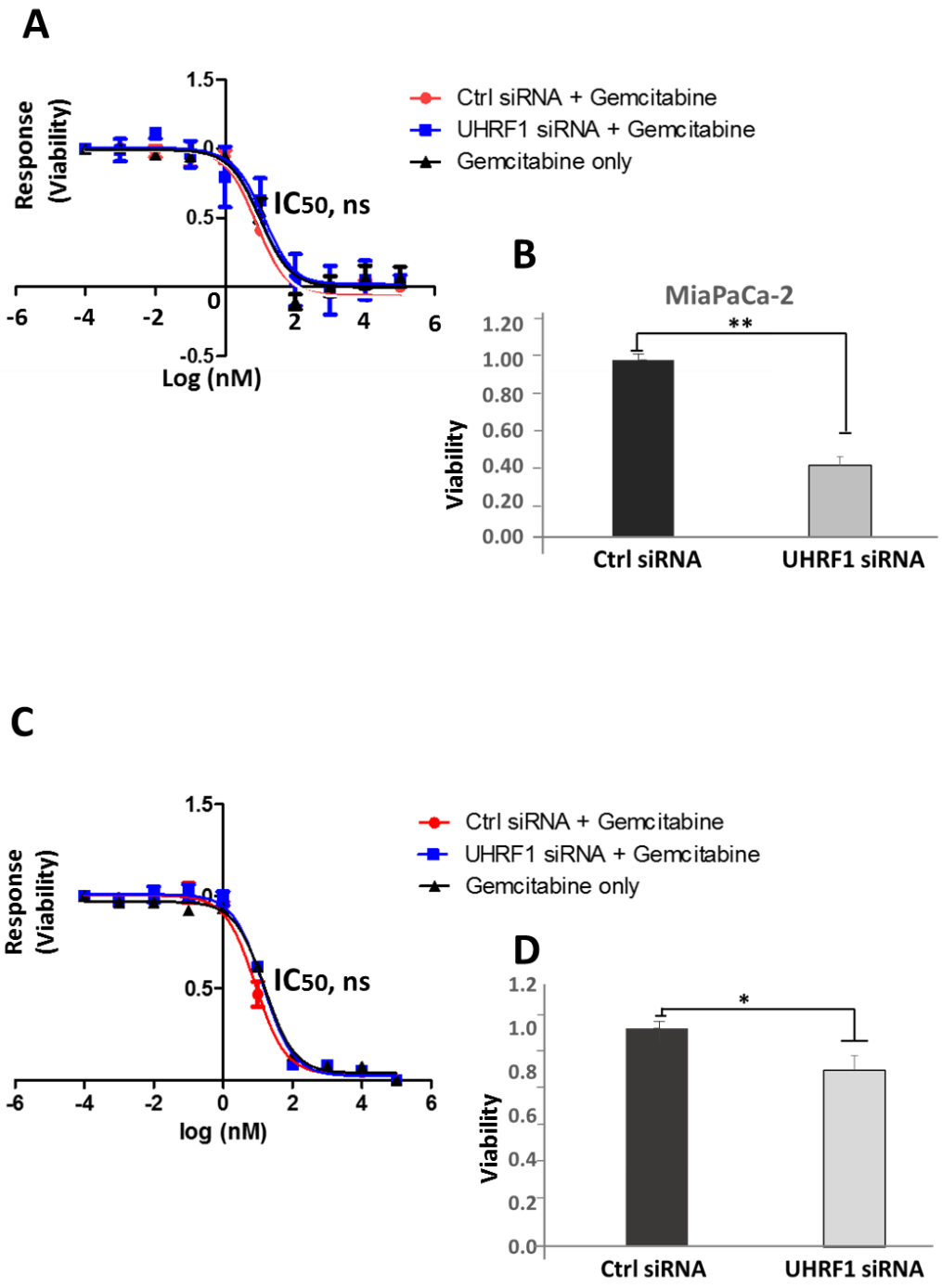

Figure 3.7. Depletion of UHRF1 in pancreatic cancer cells does not increase sensitivity to gemcitabine. (A, C) Dose response curve for MiaPaCa-2 and Suit-2 respectively; cells were treated for an initial 48 h with either Ctrl, UHRF1 siRNA or no siRNA followed by 72 h gemcitabine treatment. (B, D) MTS assay for MiaPaCa-2 and Suit-2 respectively; after an initial 48 h treatment with the indicated siRNAs, cells were cultured for a further 72 h in antibiotic free FBS supplemented RPMI. Data represents mean ± SEM from 3 independent experiments performed in at least 4 replicates. *$p < 0.05$; **$p < 0.01$; ns, not significant.

3.2.6 Method development for *KEAP1* gene promoter analysis

Given that (I) Keap1 expression has been shown to be absent in approximately 70% of PDAC tissues[99], (II) *KEAP1* promoter has been reported by others to be methylated in other cancers[100,101] as well as by our group in pancreatic cancer cell lines[80] and (III) *KEAP1* promoter methylation may explain the absence of Keap1 protein in PDAC, examination of the methylation status of KEAP1 gene promoter in PDAC was necessary. Laser capture microdissection (LCM) is a useful technique for isolating homogenous cell populations from a heterogenous specimen. The aim here was to develop a method to isolate pancreatic cancer cells by LCM from FFPE tissues (Figure 3.8), extract genomic DNA and determine if the extracted genomic DNA was sufficient and suitable for downstream DNA analysis.

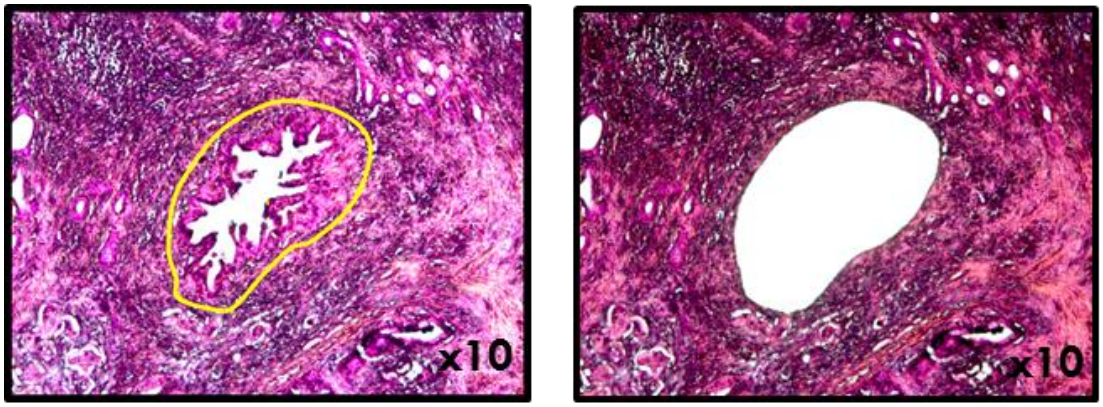

Figure 3.8. Representative images from laser captured microdissection. (A) Cancerous duct highlighted in yellow before laser capture. (B) After laser capture.

3.2.6.1 DNA isolation, quantification and annealing temperature determination

Following cancer cell isolation by laser capture microdissection, different DNA extraction protocols were employed to determine the best yielding DNA extraction method. As described in the method section (2.18.2), three different optimization protocols were evaluated. We found that protocol III with an initial xylene pre-treatment step gave the highest yield of genomic DNA and the DNA obtained was carried forward for pyrosequencing analysis (Table 3.1 A). However, given the low 260/230 ratio absorbance reading, which could have been the result of contaminants and probably contributed to DNA estimation, a more accurate DNA measurement with dsDNA Broad Range Assay kit was used (Table 3.1 B). DNA estimation with Broad Range Assay yielded lower DNA concentration than with the spectrophotometer, reflecting the specificity of the broad range assay for double stranded DNA. A PCR annealing temperature of 51^{o}C was determined to be optimal for both *KEAP1a* and *KEAP1b* primers (Figure 3.9).

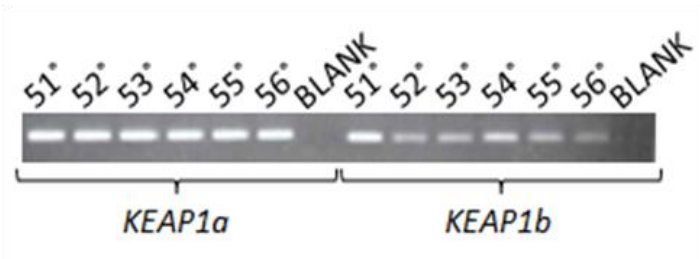

Figure 3.9. Amplification products for *KEAP1a* and *KEAP1b* primers. A, Annealing temperature optimization for *KEAP1a* and *KEAP1b* primers using bisulphite treated lymphocyte derived DNA; optimal annealing temperature = 51^{O}C for both primers based on the abundance of amplicons (thickest white band).

Table 3.1. DNA yield from different extraction protocols.

A. Genomic DNA measurement with NanoDrop Spectrophotometer from 30 µL eluted DNA sample before bisulphite treatment

Extraction protocol	Sample	DNA concentration (ng/µL)	Absorbance (nm) 260/280	Absorbance (nm) 260/230
I	Tumour-1	25.7	1.93	3.84
	Stroma-1	9.4	2.34	1.29
II	Tumour-2	40.5	2.56	1.02
	Tumour-3	86.0	2.70	1.07
III	Tumour-4	46.4	2.41	1.01
	Stroma-4	15.2	2.21	1.04
	Tumour-5	101.5	2.66	1.13
	Stroma-5	26.9	2.58	0.97

B. Genomic DNA measurement with dsDNA Broad Range Assay from 30 µL eluted DNA sample before bisulphite treatment

Sample	DNA concentration (ng/µL)
Tumour-4	7.7
Stroma-4	3.2
Tumour-5	11.8
Stroma-5	3.5

3.2.6.2 Probing KEAP1 methylation from laser captured microdissected samples

Pyrosequencing was used to quantitatively determine the methylation levels of *KEAP1* promoter in PDAC tissues. The pyrosequencing data showed no differential CpG promoter hypermethylation in the 2 promoter regions analysed between the tumour and stromal DNA (Table 3.2 and Appendix 1-4). Two patients DNA were analysed (patient 4 and 5); for each patient, DNA from tumour cells were analysed separately from DNA isolated from adjacent stromal cells. Tumour DNA from patient 4 did not have any *KEAP1* promoter methylation for the region probed by *KEAP1a* primer and with *KEAP1b* primer only 11% promoter methylation was detected at one of the CpG sites while the rest of the CpG sites were negative for *KEAP1* methylation. Stromal DNA from patient 4 with tumour and stromal DNA from patient 5 had less than 7% promoter methylation at the CpG sites examined. Overall, except at 1 CpG site, the rest of the CpG sites had very low to no methylation.

Table 3.2. Percentage methylation for *KEAP1* promoter. The table shows the degree of methylation at CpG sites within *KEAP1* promoter region spanned by *KEAP1a and KEAP1b* primers.

Sample	***KEAP1a* (% methylation)**						***KEAP1b* (% methylation)**				
Tumour-4	0	0	0	0	0	0	0	0	11	0	0
Stroma-4	2	0	6	4	5	4	0	0	4	0	0
Tumour-5	2	0	6	3	5	0	0	3	5	3	4
Stroma-5	2	2	6	3	4	0	0	0	5	0	0

3.3 Discussion

Cell transfection such as with nucleic acids and/or transfection reagents could have untoward effects that blurs the understanding of cellular processes[206]. Optimizing the transfection protocol used in this thesis helped determine the optimum reagent volume and concentration to use and more importantly, to observe how transfection reagents can interfere with cell processes such as proliferation and as observed, higher volume of lipofectamine and higher concentration of siRNAs (both control and targeting siRNA) were associated with increased lethality to cells. As one of the proteins under investigation in this thesis is a stress related protein (Nrf2), achieving a transfection protocol that interfered minimally with the cell function was required in order to determine a clear difference between control and targeted treatment. Having established an optimum transfection protocol that was reasonably possible, undertaking subsequent transfection based cell experiments was reassuring of the experimental cell response outcome to either control or targeted treatment.

Given that both UHRF1 and Nrf2 proteins have been reported to be overexpressed in pancreatic cancer and that Keap1 protein, the negative repressor of Nrf2 was found not to be expressed in approximately 70% of pancreatic cancers[99], it was justified to further investigate the functional role of UHRF1 in the regulation of Nrf2 via Keap1-Nrf2 pathway. UHRF1 is an epigenetic regulator that has DNA methylation and histone modification functions[69]. Here, evidence is provided at the transcript and protein level that UHRF1 regulates the Keap1-Nrf2 pathway and we propose a model (Figure 3.10). In MiaPaCa-2 and primary mouse KPC cell line, siRNA depletion of

UHRF1 was accompanied by upregulation of Keap1 and downregulation of Nrf2 and in Suit-2 cells, depletion of UHRF1 was also followed by a decrease in Nrf2 and Nrf2 downstream targets, NQO1 and AKR1C1. Of note, concomitant depletion of UHRF1 and Keap1 in MiaPaCa-2 cells restored Nrf2 protein to control levels. The mRNA transcript profile was however variable following UHRF1 depletion in Suit-2 cells. *UHRF1* transcripts decreased steadily over the time course of the 24h, 48h and 72h as expected but *KEAP1* transcripts upregulation was not sustained following UHRF1 knockdown. The reason for this *KEAP1* mRNA response could not be established but suggests Keap1 protein upregulation is an early event during UHRF1 depletion. Although Copple *et al.*[87] reported the half-life of Keap1 in murine hepatoma cell lines (Hepa-1c1c7) was 11.3h, further investigation such as measuring Keap1 protein half-life in PDAC cells may help clarify the discrepancy between upregulated Keap1 proteins and low Keap1 mRNA at 72h following UHRF1 depletion. But there also remains the possibility that the functional significance of UHRF1 depletion may be due to epigenetic silencing of other (than *KEAP1*) targets. To provide evidence in support of whether or not *KEAP1* promoter is methylated, the methylation status of the *KEAP1* gene promoter in PDAC tissues needed to be investigated. Towards this end, a method for analysing *KEAP1* gene promoter was developed to make way for future studies that will study *KEAP1* promoter in PDAC samples. The lack of *KEAP1* promoter hypermethylation in the two tumour DNA samples investigated could suggest the possibility that in these patient samples Keap1 protein was expressed as a previous study reported that 30% of PDAC specimens examined expressed Keap1[99]; however, I did not establish the Keap1 protein expression status of these patients

tumours. In addition, although no KEAP1 methylation was found in the stroma DNA, future experiments with normal pancreatic ducts as controls will be most ideal. This was only a method development and meaningful conclusion cannot be obtained from 2 sample analysis. More importantly, this study demonstrates that sufficient DNA from five sections of FFPE tissue, each 10 µm thick can be isolated for downstream DNA analysis. Further research with a larger patient number will be required before conclusions can be reliably made.

I did not test for Keap1 protein levels in Suit-2 cells in my experiments as a colleague had previously demonstrated upregulation of Keap1 proteins at 72h following UHRF1 knockdown. siRNA mediated Nrf2 depletion resulted in *NRF2* transcript downregulation as expected. Depletion of UHRF1 led to a demonstrable *NRF2* transcript mRNA suppression at 72h after an initial *NRF2* transcript upregulation at 24h and 48h. The reason for this initial *NRF2* transcript upregulation following UHRF1 depletion could possibly be explained by an initial protective stress response mechanism by Suit-2 cells to UHRF1 knockdown. Nevertheless, a consistent finding and agreement between the Nrf2 mRNA and protein of Suit-2 cells after 72h of UHRF1 depletion is suppression Nrf2 mRNA and protein. These findings taken together demonstrate that UHRF1 may contribute to the regulation of Nrf2 at the mRNA and protein levels but importantly brings to focus the fact that UHRF1 may also be regulating *NRF2* transcription in addition to silencing *KEAP1* transcription. With this, a possible mechanism emerges, where UHRF1 regulates Nrf2 levels independent of Keap1. To test this model, further analysis such as examination of the effects of UHRF1 knockdown on Nrf2-null cells, chromatin immunoprecipitation

(ChIP) experiments and examination of the effects of UHRF1 depletion or overexpression on Nrf2 in Keap1-null cells will be required.

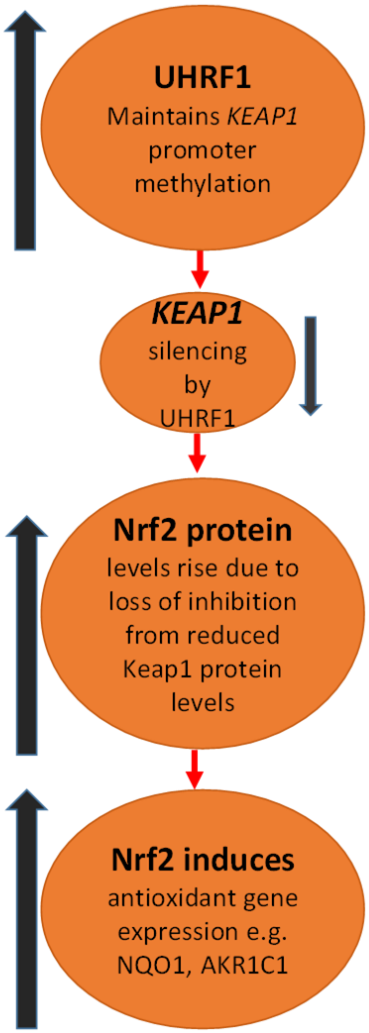

Figure 3.10. An illustration of the working model of UHRF1 in pancreatic cancer. Working model for UHRF1 mediated regulation of Nrf2 via Keap1 silencing; UHRF1 indirectly stabilises Nrf2 protein levels by repressing *KEAP1* transcription which is a negative regulator of Nrf2.

Nrf2 protects pancreatic cancer cells from oxidative stress[98]. Depletion of UHRF1 and Nrf2 independently, in both MiaPaCa-2 and Suit-2 cells increased the level of oxidative stress as determined by ROS in both cells whereas Keap1 knockdown and concomitant Keap1 and UHRF1 knockdown restored ROS to basal control levels. Additionally, ARE-driven luciferase reporter and GSH measurements both showed a significant decrease in ARE activity and GSH levels with independent siRNA mediated UHRF1 and Nrf2 knockdown. These findings further demonstrate that UHRF1 through deactivation of Keap1-Nrf2 pathway protects cells from cellular stress.

UHRF1 may play an important role in regulating PDAC growth. Independent depletion of UHRF1 and Nrf2 caused both MiaPaCa-2 and Suit-2 cells to arrest in G_2-M phase of the cell cycle although this effect appeared to be cell specific as the G_2-M arrest was more prominent in MiaPaCa-2 than Suit-2 cells. It has been previously reported that Nrf2-null alveolar endothelial cells also arrested in G_2-M[207] and in other cancers UHRF1 depletion has led to G_2-M arrest[64]. These findings further corroborate the cell cycle findings in this thesis and altogether, the findings of this chapter reinforce the role of UHRF1 in the regulation of Keap1-Nrf2 pathway in pancreatic cancer. Although, more mechanistic evidence of UHRF1 regulation of Keap1-Nrf2 pathway will be valuable in understanding this interaction.

The lack of increased pancreatic cancer cell sensitivity to gemcitabine following UHRF1 depletion in this study could have been related to the activation of other survival response or regulatory pathways. Similarly, as presented in chapter 5.2.16 of this thesis, UHRF1 protein expression was not associated with survival in patients

who received gemcitabine chemotherapy. Gemcitabine induced-ROS and growth inhibition in pancreatic cancer has been reported previously[208]. A study by Yin *et al.*[209] demonstrated that Bmi1 (B-cell-specific Moloney murine leukemia virus insertion site 1) promoted pancreatic cancer cell resistance to gemcitabine chemotherapy, an effect that was conferred by the antioxidant role of Bmi1 in regulating antioxidant genes and stimulation of NF-Kb signalling; importantly, they showed that certain doses of gemcitabine induced Bmi1 expression in pancreatic cancer cell lines and further demonstrated that Bmi1 depletion enhanced ROS production and enhanced pancreatic cancer cell sensitivity to gemcitabine cytotoxic effects [209]. Bmi1 has been shown to be overexpressed in PanIN, pancreatic cancer tissues and pancreatic cancer cell lines where it is implicated in the growth and invasiveness of pancreatic cancer and in the regulation of pancreatic cancer stem cells[210]. It is tempting to speculate that combined depletion of UHRF1 and other protein targets in pancreatic cancer together with chemotherapy may effectively increase response to treatment.

4 INVESTIGATING THE FUNCTION OF UHRF1 ON THE NRF2 PATHWAY IN PANCREATIC STELLATE CELLS

4.1 Introduction

In chapter 3, having investigated the role of UHRF1 in contributing to the Keap1/Nrf2 pathway in pancreatic cancer cells, I sought to investigate the function of UHRF1 in pancreatic stellate cells (PSCs), one of the prominent cellular elements in pancreatic cancer[211]. Pancreatic cancer stroma is very heterogeneous and comprises of pancreatic stellate cells, immune cells, endothelial cells and extracellular matrix (desmoplasia), which have been attributed to contributing to pancreatic cancer's immune escape, resistance to chemotherapy, proliferation and metastasis[212-216]. The desmoplasia seen in pancreatic cancer is thought primarily to be due to PSC activation[212] and they play a prominent role in the tumour microenvironment[217,218] .

Owing to the growing interest in understanding the role of PSCs in pancreatic cancer progression and in developing potential targets for pancreatic cancer treatment, it was of interest to investigate the role of UHRF1 in PSCs. PSCs share similarities with fibroblasts[108,121] and given that fibroblast activation can be mediated in part by epigenetic mechanisms like DNA methylation in kidney fibroblasts[143], it was reasonable to conceive that UHRF1 which plays a key role in maintenance of DNA methylation[65] might also be crucial to epigenetic processes in pancreatic stellate cells. Given the role myself and others in the group elucidated for UHRF1 in regulating Nrf2 in pancreatic cancer cells[80], I sought to test the hypothesis that UHRF1 also controlled the growth rates and redox status in PSCs through Nrf2. To address this, quiescent mouse PSCs were isolated by myself and Dr Lawrence B. Barrera (University of Liverpool) from the pancreas of both Nrf2-null ($Nrf2^{-/-}$) and Nrf2-wild type ($Nrf2^{+/+}$)

mice. I also used human PSCs that were isolated by Dr Lawrence B. Barrera from pancreatic cancer patient tumours. The mice used in this study were kindly donated by Professor Chris Goldring (MRC Centre for Drug Safety Science, University of Liverpool).

The aim of the study described in this chapter was therefore to (I) investigate the function of UHRF1 on Keap1/Nrf2 antioxidant pathway in PSCs (II) investigate the role and mechanism of UHRF1 in PSC activation (III) investigate the effect of conditioned media from pancreatic cancer cells on PSCs oxidative status and (IV) to examine the pancreas of Nrf2-null mice for pathological abnormalities.

4.2 Results

4.2.1 Isolated stellate cells from the pancreas of both Nrf2 wild-type and Nrf2 null mice exhibit a quiescent phenotype

In order to investigate the role of UHRF1 in pancreatic stellate cells, it was first important to characterize their phenotype. Pancreatic stellate cells were isolated from the pancreas of 10 week old Nrf2 wild-type and Nrf2 null mice. Immunofluorescence imaging of pancreatic stellate cells isolated from both mice revealed the presence of cytoplasmic vitamin A-containing lipid droplets (Figure 4.1) which is a marker of quiescent (inactivated) stellate cells[122]. Over the course of stellate cell expansion in culture, the amount of lipid droplets decreased progressively as the cells assumed an activated phenotype (Figure 4.2).

4.2.2 Pancreatic stellate cell rescue

Pancreatic stellate cells from both $Nrf2^{+/+}$ and $Nrf2^{-/-}$ mice expanded well in culture in the first few days post-isolation (Figure 4.2 – top row). At 10 days post-isolation however, $Nrf2^{-/-}$ cell expansion decreased and cell death began to be observed (Figure 4.2 – bottom right). Attempts were made to prevent these cells from dying.

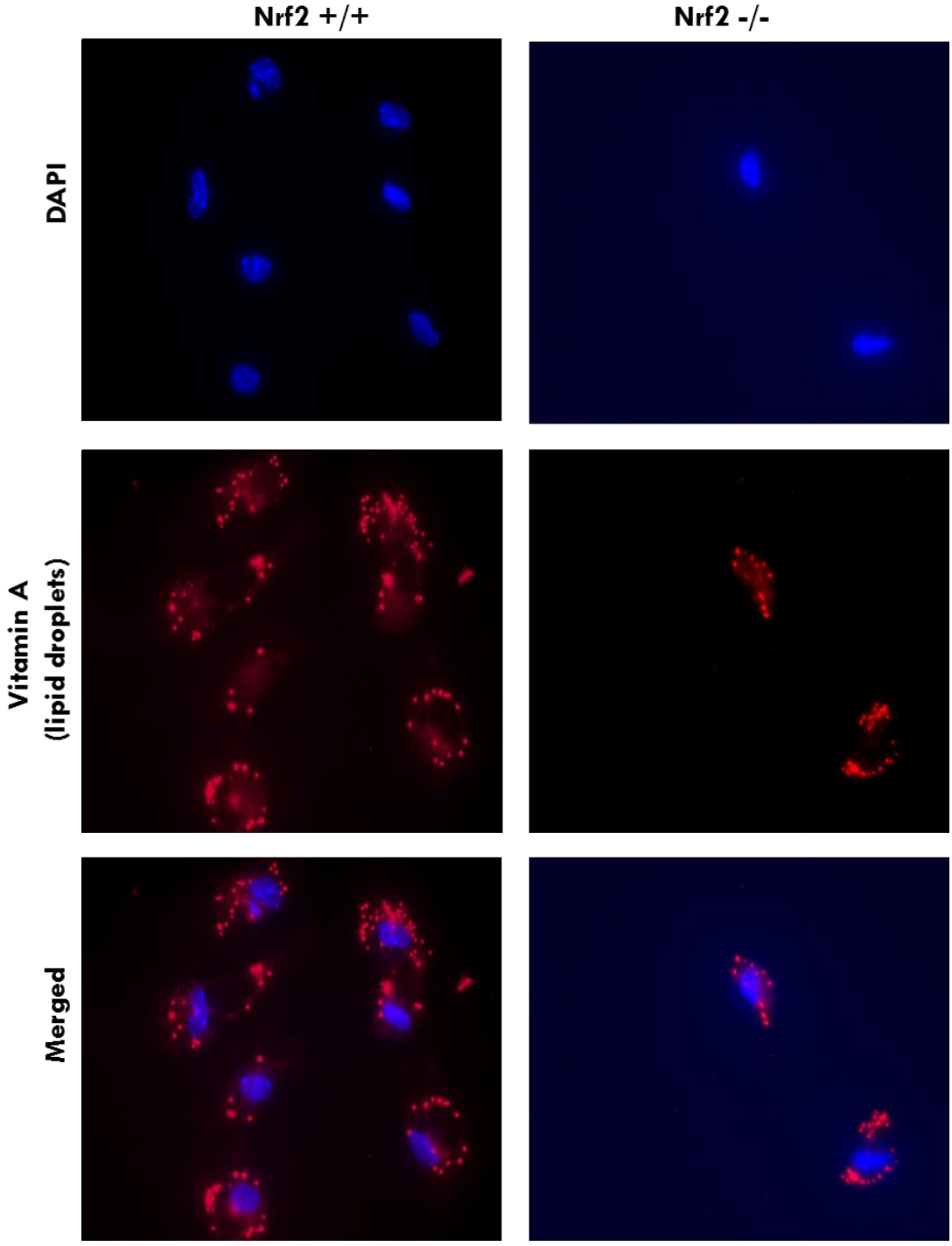

Figure 4.1. Immunofluorescence images of Nrf2$^{+/+}$ stellate cells (left column) and Nrf2$^{-/-}$ stellate cells (right column) 24 h post-isolation from the pancreas of Nrf2$^{+/+}$ and Nrf2$^{-/-}$ mouse respectively. Blue - DAPI, Red – lipid droplets. Magnification x 63 (oil immersion).

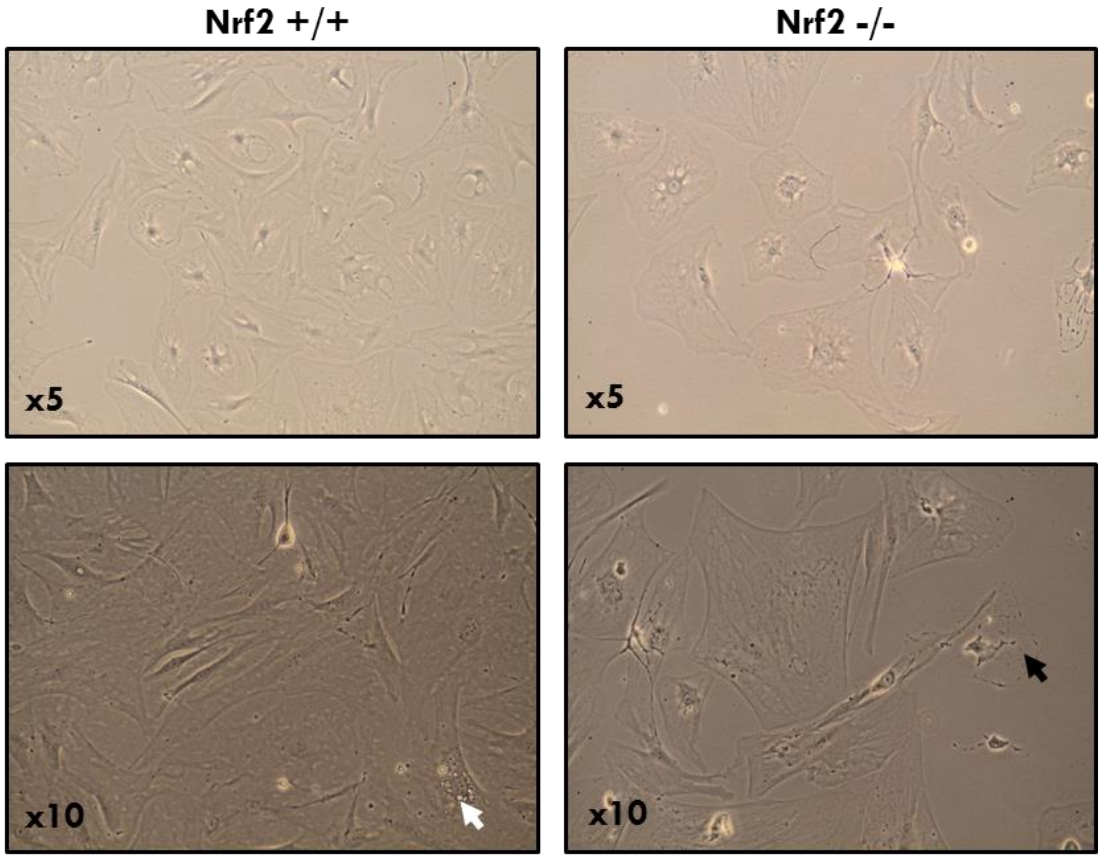

Figure 4.2. Pancreatic stellate cells in culture. Phase contrast microscopy of isolated Nrf2$^{+/+}$ (left column) and Nrf2$^{-/-}$ (right column) stellate cells in culture at 5 days post-isolation (top row) and 10 days post-isolation (bottom row). There is a lower cell density in Nrf2$^{-/-}$ PSCs culture compared to that of Nrf2$^{+/+}$ PSCs. White arrow-head indicates a stellate cell with residual lipid droplets (white dots) surrounding the nucleus; black arrow-head indicates a necrosing/apoptosing Nrf2$^{-/-}$ PSC.

Nrf2 null PSCs were treated with L-ascorbic acid (vitamin C) in increasing concentrations of 10 µM, 25 µM, 100 µM and 200 µM in IMDM (as vitamin C has been reported to provide a survival advantage in cells exposed to oxidative stress[219]. This was unsuccessful and the Nrf2$^{-/-}$ stellate cells could not be rescued (Figure 4.3).

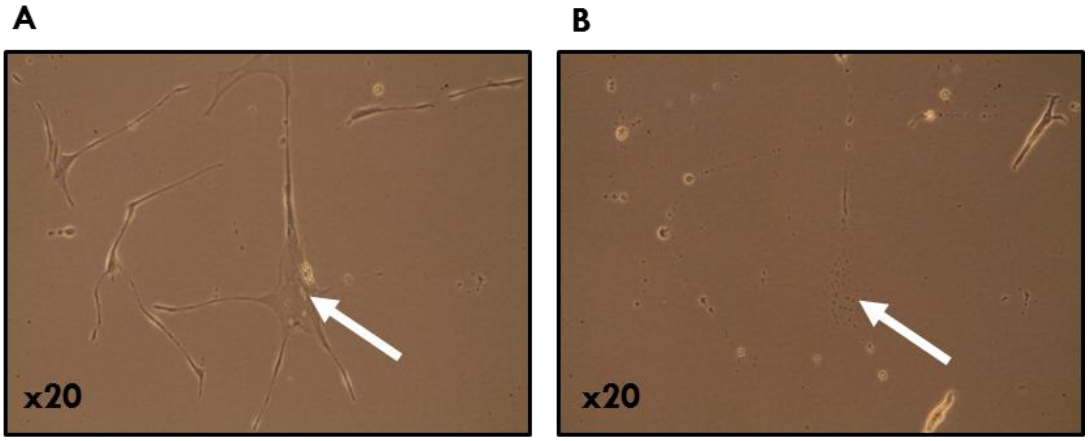

Figure 4.3. Nrf2 -/- stellate cells rescue in culture. Phase contrast microscopy of isolated Nrf2$^{-/-}$ PSCs (A) at day 9 and (B) at day 13 after initiating L-ascorbic acid (vitamin C) treatment. White arrows indicate positions of tracked stellate cell during rescue effort.

4.2.3 Differential expression of UHRF1 and α-SMA in PDAC cell lines and primary pancreatic stellate cell lines

As the attempt to investigate the role of UHRF1 in the regulation of Nrf2 in PSCs derived from Nrf2$^{-/-}$ mice was unsuccessful, I now sought to investigate the function of UHRF1 in the regulation of Nrf2 in primary human pancreatic stellate cells (cancer associated fibroblasts, **CAFs** – pancreatic stellate cells isolated from within human pancreatic cancer tissue; normal activated fibroblasts, **NAFs** - pancreatic stellate cells isolated from adjacent normal pancreatic tissue derived from human pancreatic cancer tissue) isolated from human pancreatic tissues. To achieve this, the expression of UHRF1 in primary CAFs was first examined. Despite previous reports of UHRF1 expression in fibroblasts[61,62], UHRF1 protein was undetectable in primary pancreatic CAFs (Figure 4.4). As this was unexpected, additional primary isolated PSCs were examined. The result interestingly still confirmed the initial finding, which is a lack of

UHRF1 expression in all five PSCs examined while PDAC cell lines expressed UHRF1 (Figure 4.5).

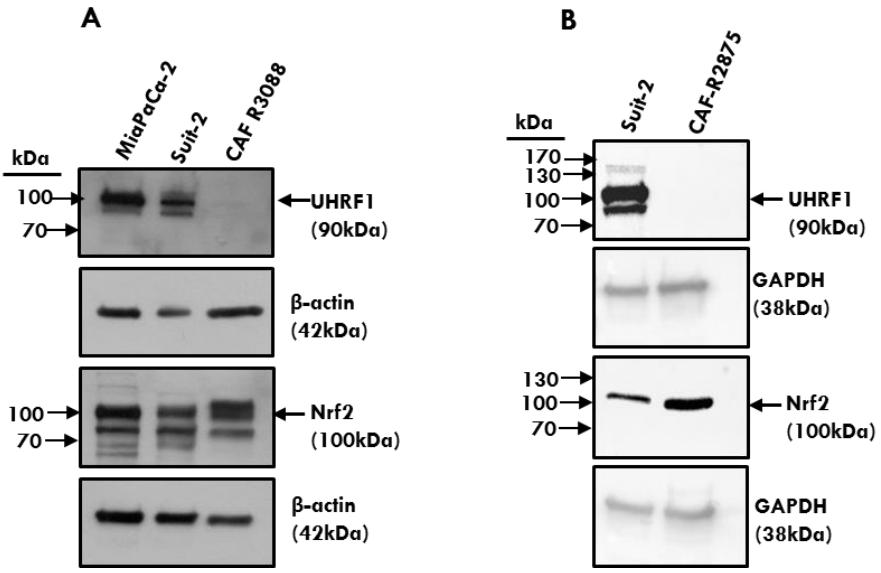

Figure 4.4. Basal expression of UHRF1 and Nrf2. (A, B) Representative western blot images of indicated proteins from whole cell lysates of PDAC cell lines (MiaPaCa-2 and Suit-2) and primary pancreatic CAFs (CAF-R3088, CAF-R2875). UHRF1 1:1000, Nrf2 1:1000; β-actin and GAPDH were used as loading controls. n=2.

To confirm that the primary PSCs cell lines used where myofibroblast-like (aPSCs), the expression of α-SMA a marker of aPSC[122] was investigated. Characteristically, only PSCs expressed α-SMA while its expression was undetectable in PDAC cell lines despite over exposing the membranes (Figure 4.6).

Given that one of the aims of this chapter was to investigate the role of UHRF1 in the regulation of Nrf2 in PSCs, the expression of Nrf2 was examined despite the lack of UHRF1 expression in PSCs. Notably, PSCs expressed Nrf2 in comparable and possibly higher levels to PDAC cells (Figure 4.4).

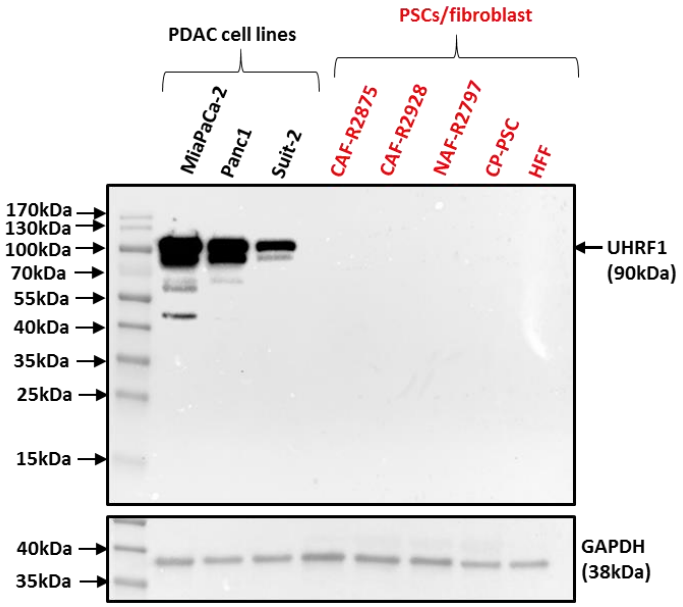

Figure 4.5. Basal expression of UHRF1. Representative western blot image of the indicated protein from whole cell lysates of PDAC cell lines and primary PSCs and fibroblasts. CP – chronic pancreatitis, HFF - (Human foreskin fibroblast) cell line. UHRF1 expression was overexposed. UHRF1 1:1000; GAPDH was used as loading control. n=2.

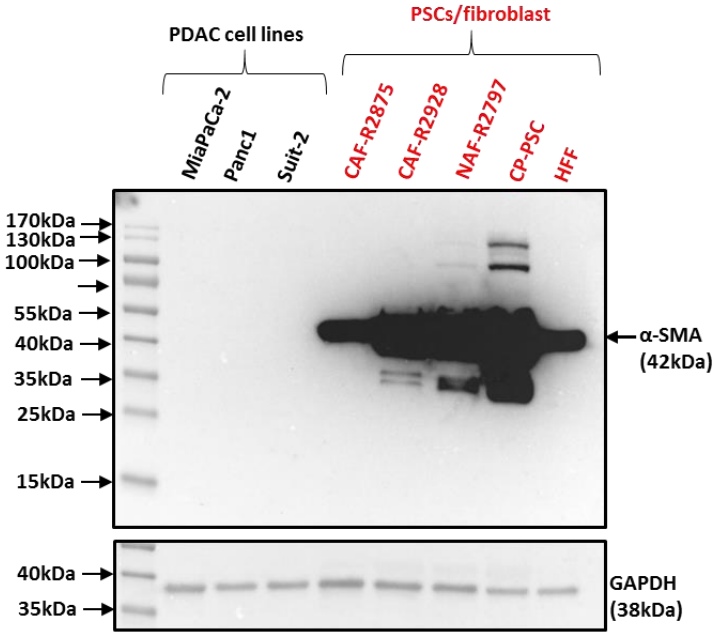

Figure 4.6. Basal expression of α-SMA and UHRF1. Representative western blot image of the indicated protein for PDAC cell lines and primary PSCs and fibroblast cells. The membrane in Figure 4.5 above was stripped and used to probe α-SMA. HFF - (Human foreskin fibroblast) cell line. α-SMA expression were overexposed. α-SMA 1:500; GAPDH was used as loading control. n=2.

As part of the antibody validation and optimization for IHC, both western blotting and ICC were undertaken. UHRF1 antibody specificity was confirmed by western blotting which showed a single predominant 90kDa UHRF1 band following control and UHRF1-targeted siRNA depletion of UHRF1 in MiaPaCa-2 cells (Figure 4.7 A). UHRF1 cell localization was determined by ICC in MiaPaCa-2 cells which detected brown nuclear staining in control treated cells (Figure 4.7 B – I) and predominantly blue nuclear cells in UHRF1 depleted cells (Figure 4.7 B – II). Using MiaPaCa-2 cells as positive controls, ICC was simultaneously undertaken for pancreatic CAFs and NAFs. As observed previously by western blotting CAFs lacked UHRF1 immunoreactivity but interestingly, only a few NAF cells in each of the 2 primary NAF cell lines examined expressed nuclear UHRF1. (Figure 4.8).

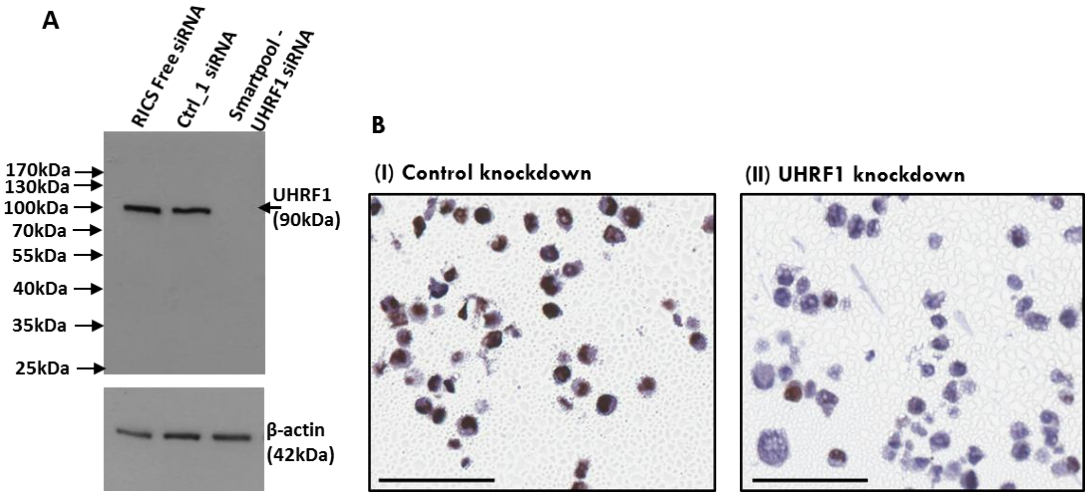

Figure 4.7. Specificity of UHRF1 antibody used for immunocytochemistry and immunohistochemistry. (A) Western blot image of UHRF1 expression following siRNA mediated depletion in MiaPaCa-2 cells. UHRF1 1:1000; β-actin was used as loading control. (B) Immunocytochemistry for UHRF1 expression after (I) control siRNA and (II) UHRF1 targeting siRNA depletion in MiaPaCa-2 cell line. Brown nuclei immunoreactivity indicates positive UHRF1 staining. UHRF1 1:250 dilution; Scale bar = 100 µm.

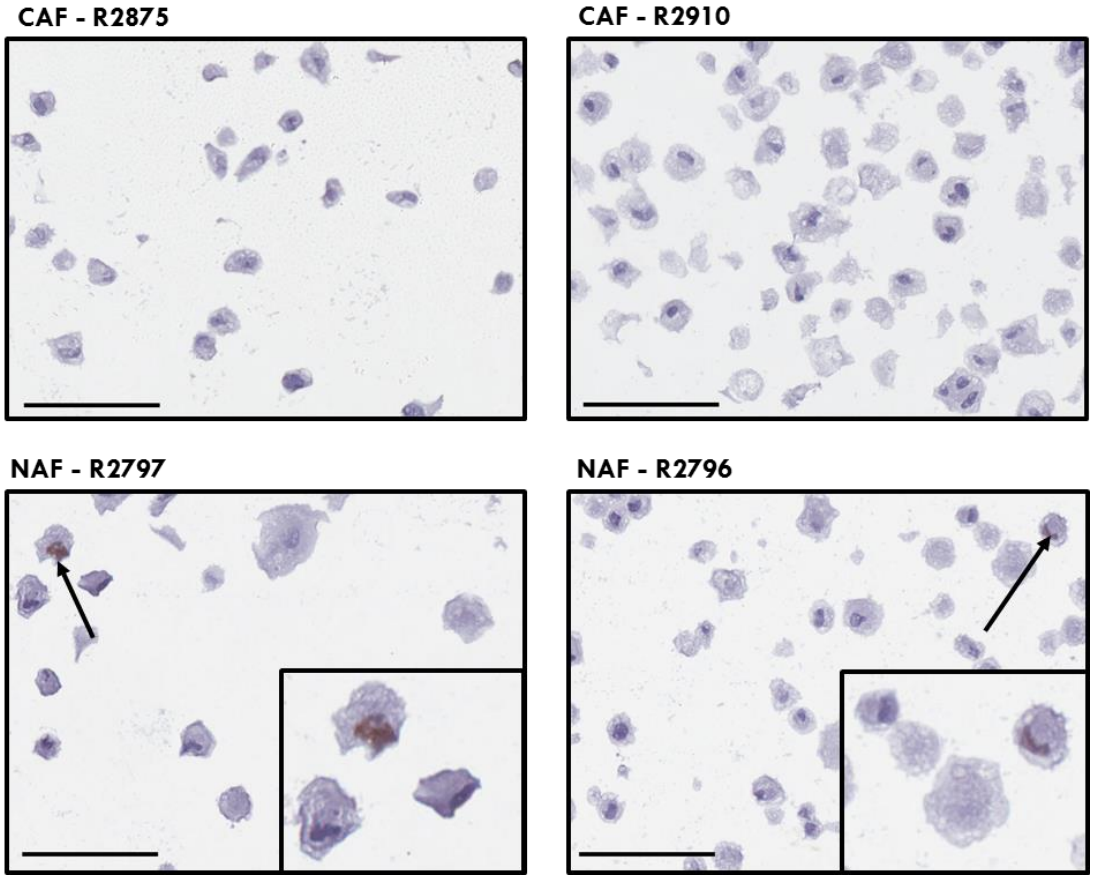

Figure 4.8. Basal UHRF1 expression in primary PSCs. Immunocytochemistry showing basal UHRF1 expression in CAFs (top row) and NAFs (bottom row). Black arrows indicates cells positive for nuclear UHRF1 within the field of view shown for NAF-R2797 and NAF-2796. CAF-R2875, CAF-R2910, NAF-R2797 and NAF-R2796 have passage numbers 9, 6, 8 and 6 respectively. UHRF1 1:250 dilution; isolated primary human pancreatic fibroblasts courtesy of Dr Lawrence B. Barrera. Scale bar = 100 µm.

4.2.4 Differential expression of UHRF1 and α-SMA in PDAC tissues

Expanding on the above observations, TMA sections containing tissues from patients with PDAC were stained for UHRF1 and α-SMA. α-SMA stained tissues were undertaken by Ms Frances Atherton and Dr Anthony Evans in a previous study and we all used TMA sections obtained from the same TMA block; the difference being only in the depth at which the TMA sections were cut out from the block. Uniquely,

in all cores examined α-SMA was exclusively localized to the stromal compartment of the tumour microenvironment as have been previously reported[220,221] whereas UHRF1 was detected as nuclear brown staining in cancer cells (Figure 4.9) with some occasional spindle shaped UHRF1 positive cells in the stroma (Figure 4.10). These observations correlated perfectly well with the readouts from western blotting and ICC.

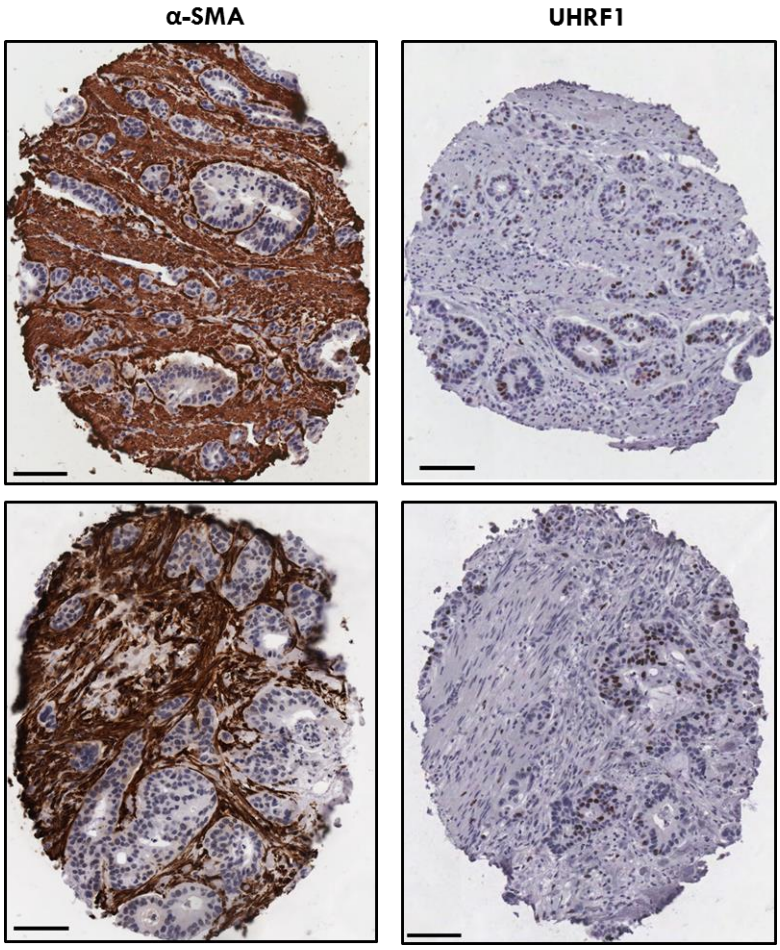

Figure 4.9. Examples of IHC TMA cores containing PDAC tissues stained for α-SMA (left column) and corresponding UHRF1 stained cores (right column). The corresponding cores for α-SMA and UHRF1 were taken at different depths (106 and 134 respectively) from the same TMA block hence the slight variation in core appearance. Stromal brown immunoreactivity indicates positive α-SMA staining in CAFs (myofibroblast-like, spindle shaped) (left column) and nuclei brown staining indicates positive UHRF1 immunoreactivity in cancer cells (right column). UHRF1 1:100, α-SMA 1:50; α-SMA stained cores courtesy Ms Frances Atherton and Dr Anthony Evans. Scale bar = 100 µm.

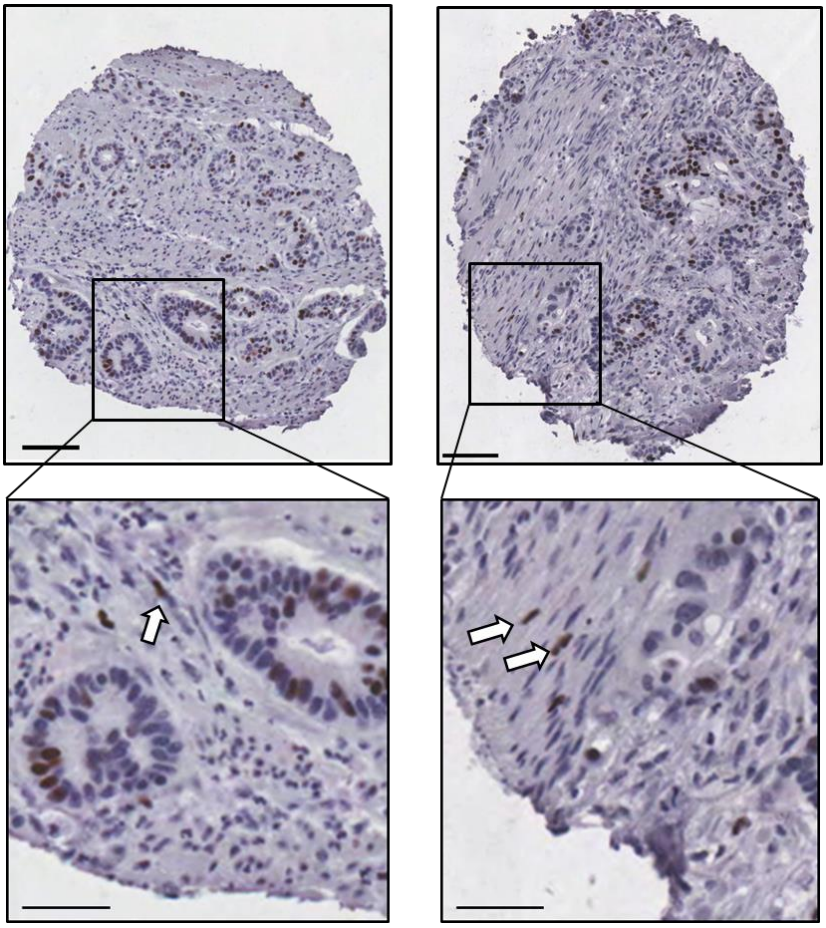

Figure 4.10. Examples of stromal UHRF1 staining. Occasional spindle shaped UHRF1 positive staining cells (white arrows) were seen in PDAC stroma. Scale bar original image = 100 µm and magnified inset = 50 µm

4.2.5 UHRF1 stromal expression in normal gastrointestinal tissues

Most of the tissues examined so far were pathologically derived. Given PSCs share similarities with fibroblasts and myofibroblasts[108,121], it was necessary to investigate these cells in other tissues. Fibroblasts and myofibroblasts have been shown to be present in normal intestinal stroma[222]. To determine if the absence of UHRF1 in other tissue fibroblast and myofibroblast was a recurring theme, the stroma of

normal tissues of the pancreas, liver, duodenum and colon were examined for UHRF1 expression. Rarely was UHRF1 expression observed in the stroma of normal liver (Figure 4.11), pancreas (Figure 4.12), duodenal and colonic tissues (Figure 4.13). Interestingly, UHRF1 nuclei expression was observed in a distinct histological pattern in normal duodenal and colonic crypts (Figure 4.13,

Figure 4.14).

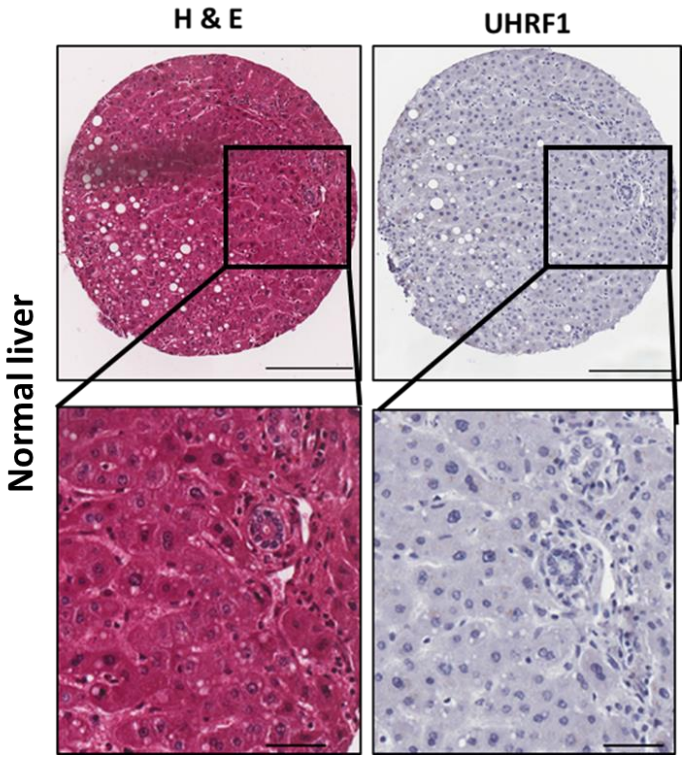

Figure 4.11. Representative images of a normal liver. H & E and UHRF1 stained sections of a normal liver showing hepatocytes and bile duct at 3 o'clock position negative for UHRF1 expression. UHRF1 1:100; scale bar = 200 µm (top row) and bottom row = 50 µm.

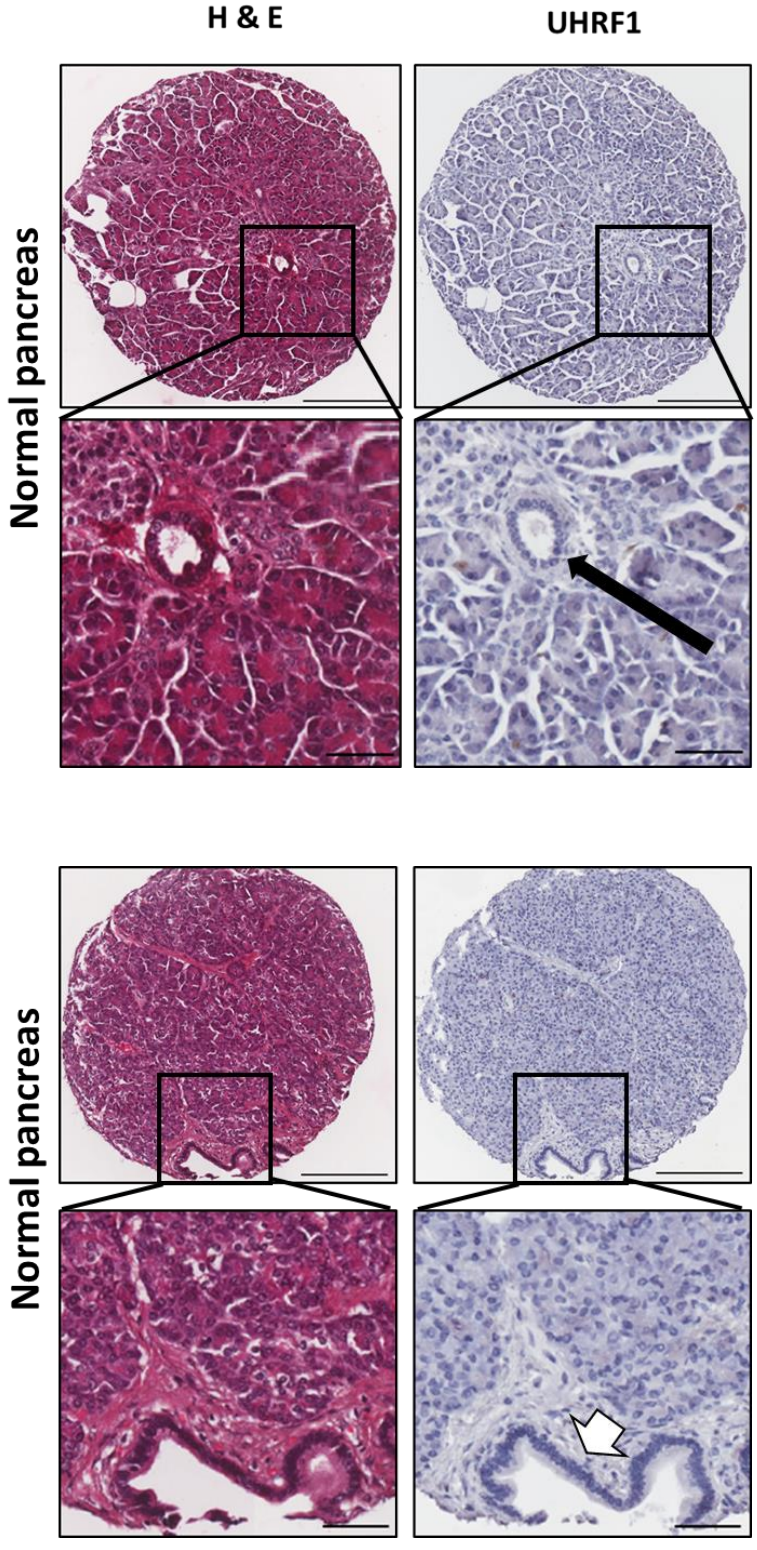

Figure 4.12. Representative images of a normal pancreas. H & E and UHRF1 stained sections of normal pancreatic sections negative for UHRF1 expression. Note the intralobular duct black arrow. The interlobular duct white arrow head surrounded by a thick fibrous layer. UHRF1 1:100; Scale bar = 200 µm (full core image) and magnified segment = 50 µm.

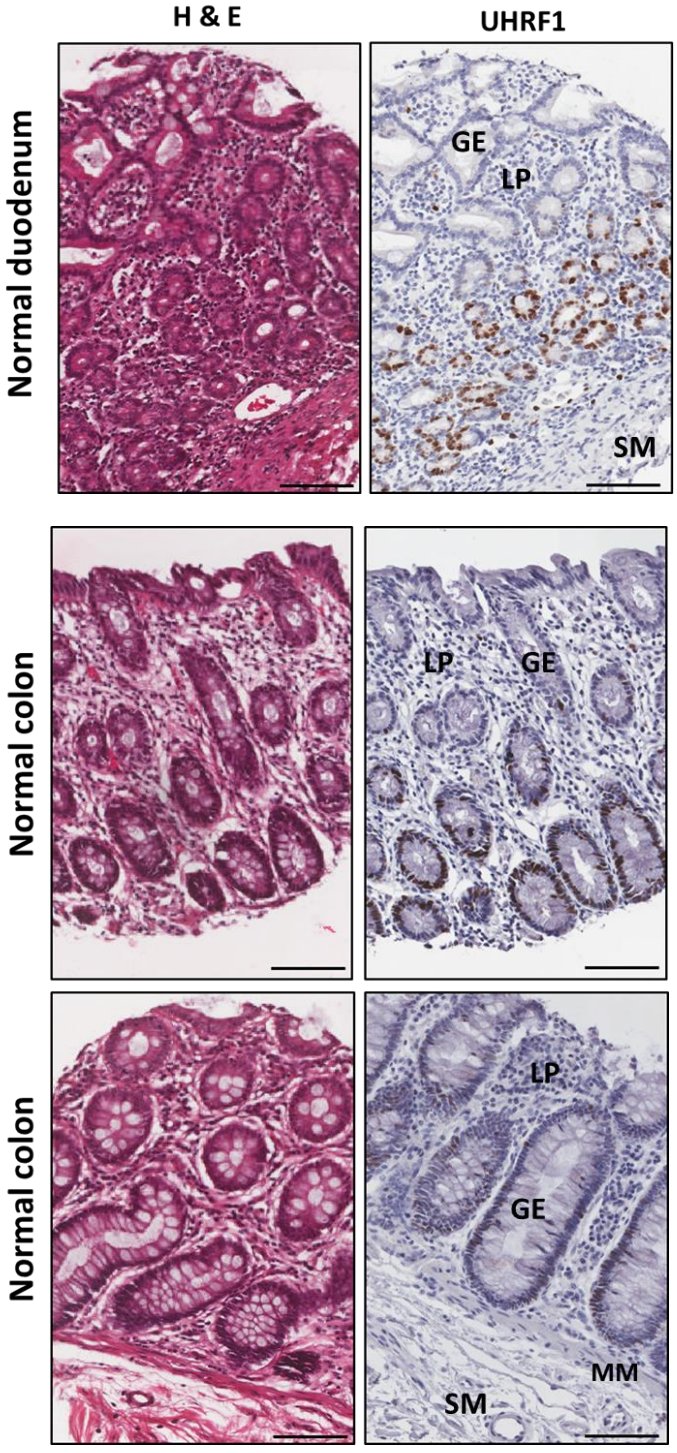

Figure 4.13. Representative images of normal duodenum and colon. H & E and UHRF1 stained sections of normal duodenum and colon sections. The mucosa is the innermost layer of duodenum and colon comprising of the glandular epithelium (GE), lamina propria (LP) and muscularis mucosae (MM). The submucosa (SM) is the next layer to the mucosa. The glandular epithelium, GE, forms crypts which are cylindrical structures. UHRF1 1:100; scale bar = 100 µm.

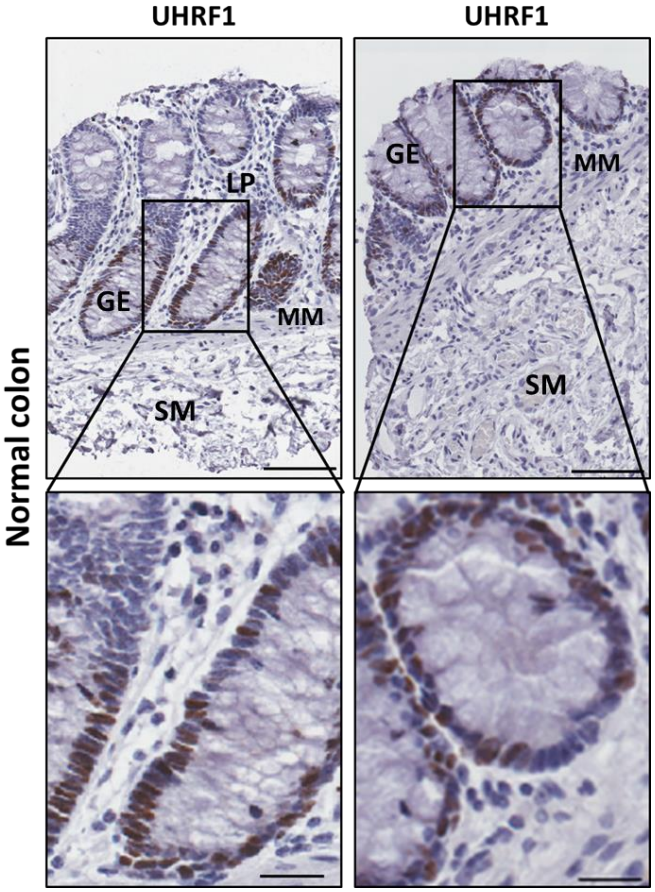

Figure 4.14. Representative image of a normal colon. UHRF1 stained sections of a normal colon. In the magnified image, UHRF1 staining is observed in some but not all of the basal crypt cells. The GE comprises of several cell types: stem cells, undifferentiated crypt cells, goblet cells, Paneth cells, absorptive cells and M cells. The LP provides connective stroma tissue support for the glandular GE. **Note UHRF1 expression at the base of the crypts**. Stem cells and other undifferentiated cells are located at the base of intestinal crypts. UHRF1 1:100; Scale bar = 100 µm and magnified segment = 25 µm.

4.2.6 Conditioned media from cancer cells induces Nrf2 in pancreatic stellate cells

To understand part of the functional interaction between pancreatic CAFs and pancreatic cancer, the effect of conditioned media from MiaPaCa-2 cell lines on primary CAF-R2875 was investigated using 8x ARE driven luciferase assay. An induction in Nrf2 activity was observed in CAF-R2875 following culture of CAF-R2875 with conditioned media from MiaPaCa-2 cells (Figure 4.15).

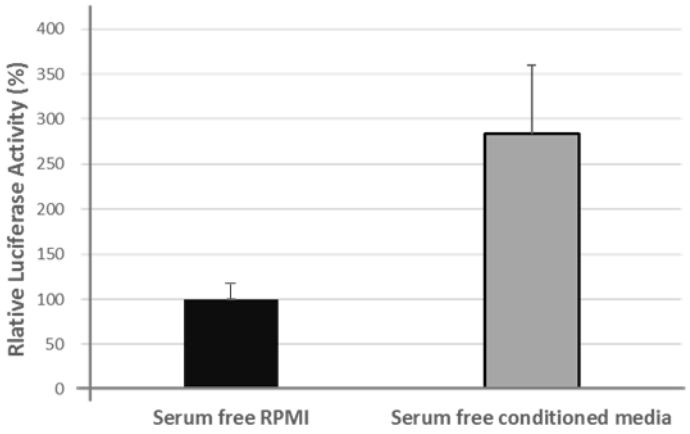

Figure 4.15. Induction of Nrf2 in CAF-R2875 primary cells with conditioned media from PDAC cell line dual-glo luciferase assay. The activity of Nrf2 dependent 8x ARE-reporter was measured after 36 h of culturing CAF-R2875 cells in conditioned from MiaPaCa-2 cells. pGL4.74 [*hRluc*/TK] plasmid served as transfection control to normalize luciferase values. N=2, hence statistical analysis not undertaken as data obtained from 2 experiments is not sufficient enough to draw a significant conclusion from.

4.2.7 Nrf2 null mice show differential weight gain and develop early signs of pancreatitis

To investigate the effect of genetic deletion of Nrf2 on mice growth and pancreatic tissue morphology, four 10 month old mice (two $Nrf2^{+/+}$ and two $Nrf2^{-/-}$) were examined. Ten month old mice were chosen for this study to permit the detection of subtle changes over a longer period of observation in comparison to the 10 week old mice that were used for PSC isolation (Chapter 4.2.1) were the mean weight ± SD of both Nrf2+/+ and Nrf2 -/- mice was 21.1 ± 1.56g.

There was a differential weight gain between the two 10 month old $Nrf2^{+/+}$ mice compared with the two 10 month old $Nrf2^{-/-}$ mice; the mean weight of the two 10 month old $Nrf2^{+/+}$ mice was 53.2 g compared with the two 10 month old $Nrf2^{-/-}$ mice mean weight 34.45 g . As there were only 2 of each type of mice, no further statistical analysis was undertaken. Additional mice could not be sourced as the few we had were a gift and the mice are expensive. Importantly, acinar cell vacuolisation typical of that seen in early pancreatitis induced mice studies[223,224] were observed and reported here for the first time in the pancreas of $Nrf2^{-/-}$ mice. No preneoplastic lesions, oedema, necrosis or areas of fibrosis where identified in the pancreas of either $Nrf2^{+/+}$ or $Nrf2^{-/-}$ mice (Figure 4.16).

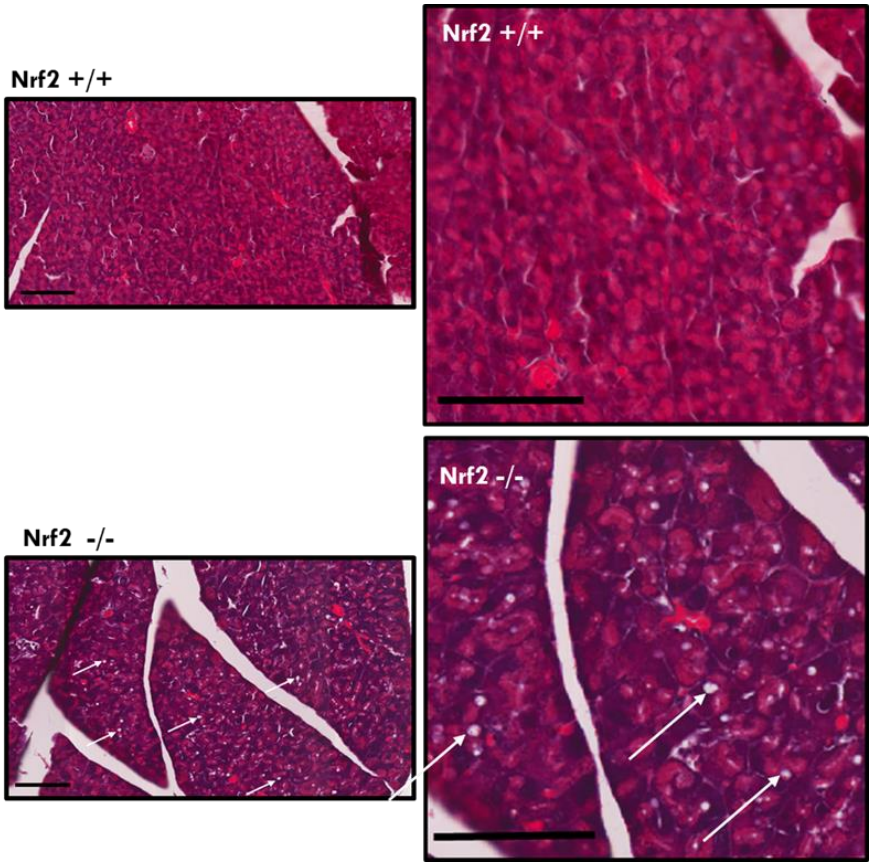

Figure 4.16. H and E sections of pancreatic tissue from Nrf2$^{+/+}$ and Nrf2$^{-/-}$ mice (left column) and corresponding magnified images (right column). White arrows indicate vacuolated lesions in acinar cells from Nrf2 null pancreatic tissues. Scale bar = 100 µm

4.3 Discussion

Pancreatic stellate cells (PSCs) play an important role in pancreatic cancer desmoplasia and in influencing the behaviour pancreatic cancer[211]. Identifying and understanding mechanisms and pathways by which PSCs interact with cancer cells and other stromal elements is crucial to developing strategies to intervene in this malignancy.

Successful isolation of primary qPSCs from the pancreas of $Nrf2^{-/-}$ and $Nrf2^{+/+}$ mice was demonstrated by the presence of vitamin A lipid droplets. Their subsequent activation in culture was also demonstrated by the gradual loss of vitamin A. Although the expression of α-SMA was not examined in the cultured PSCs, the disappearance of the vitamin A lipid droplets is in keeping with PSC activation in culture[122,225]. In culture however, both $Nrf2^{-/-}$ and $Nrf2^{+/+}$ PSCs grew well initially but after an initial rapid expansion, the $Nrf2^{-/-}$ PSCs grew poorly. This observation is not surprising as Nrf2 is known to be vital to cell survival by maintaining the oxidative state of cells within physiological limits during basal and inducible oxidative metabolic states[84]. In an attempt to rescue the $Nrf2^{-/-}$ PSCs, vitamin C a water soluble antioxidant was added to cell culture medium. The rational for the use of vitamin C is based on findings from studies that show vitamin C enhanced the survival of oxidatively stressed cells[219]. However, despite vitamin C treatment, the $Nrf2^{-/-}$ PSCs did not survive in culture. Nrf2 deletion can gravely affect the entire repertoire of antioxidative and xenobiotic response and recovery[219] with a resultant effect that mitigates the ability of the administered vitamin C in buffering the oxidative stress.

Vitamin C and glutathione (GSH) have been shown to cooperate in maintaining a potent antioxidant defence system[219] and Nrf2 is known to induce the transcription of a host of genes that provide antioxidant, cellular defence and xenobiotic functions including enzymes glutamate cysteine ligase (GCL) that are crucial to GSH synthesis[89]. Of note, there was no differential weight gain between the 10 week old $Nrf2^{-/-}$ and $Nrf2^{+/+}$ mice used for PSC isolation which is in keeping with previous reports[226]. This observation suggests that $Nrf2^{-/-}$ mice up to 10 weeks of age have similar growth patterns to their wild-type mice and this led to the gross assumption that when isolated, $Nrf2^{-/-}$ PSCs could survive *in vitro* forming the basis for a testable hypothesis. However, in culture $Nrf2^{-/-}$ PSCs failed to survive suggesting that their isolation and *in vitro* culture caused an inducible stress. The loss of the primary $Nrf2^{-/-}$ mouse PSCs meant the hypothesis relating to whether UHRF1 depletion affected proliferation and oxidative state in $Nrf2^{-/-}$ PSCs could not be tested.

We have previously shown that loss of UHRF1 was followed by downregulation of Nrf2 and increased oxidative stress in pancreatic cancer cell lines and in the same study, we observed cytoplasmic UHRF1 expression in both cancer cells and stromal cells in addition to nuclear UHRF1 expression in cancer cells[80]. Given that a different anti-UHRF1 antibody was used for IHC in that report[80] compared with the anti-UHRF1 used in this thesis and our focus was not on the stroma, it was important to investigate whether UHRF1 was actually expressed in stromal cells. The anti-UHRF1 used in this thesis only detected UHRF1 expression in the nucleus of cells. To demonstrate the role of UHRF1 on Nrf2 regulation and the potential epigenetic activation of primary human PSCs, the basal expression of UHRF1 was first examined.

Surprisingly, UHRF1 was undetectable by western blotting in primary PSCs (CAFs) as previous studies have demonstrated the expression of UHRF1 in fibroblasts[61,62]. However, on immunocytochemistry (ICC) a subset of primary PSCs (NAFs with a positivity of <3%) expressed nuclear UHRF1. Although the few positively staining UHRF1 NAF cells microscopically appeared identical to the rest of the UHRF1 negative NAF cells, it can be argued that they are a nonhomogeneous population of stromal cells as neither the nycodenz density gradient method nor the outgrowth method for PSCs isolation yields completely pure PSC population[121]; both methods were used to isolate PSCs used in this thesis. Despite the potential risk of not obtaining a pure PSC population, it is also possible that the very scanty UHRF1 staining NAF cells are truly PSCs in which case they could represent a subset of PSCs population. Moreover, subsets of fibroblasts population with different protein markers and functions have been proposed[107,111]. Previously, we reported variations in levels of UHRF1 at different stages of cell cycle in PDAC cells; it could be speculated that these UHRF1 positive PSCs are in different stages of cell cycle. Obviously, more work needs to be undertaken before conclusions can be drawn. PSCs (CAFs and NAFs) however expressed α-SMA, a marker of activated PSCs which is absent in quiescent PSCs[122,225]. Conversely, MiaPaCa-2, Suit-2, Panc1 and other pancreatic cancer cell lines[80] express UHRF1 but were negative for α-SMA. Importantly, Nrf2 expression was observed in both pancreatic cancer cell lines and primary pancreatic CAFs. IHC examination of pancreatic cancer tissues further supports the above findings where to a wider extent cancer cells express nuclear UHRF1 with very limited expression of UHRF1 in spindle shaped stromal cells whereas the tumour stroma was characterized by spindle

shaped cells expressing α-SMA. To ensure consistency in probing UHRF1, the same UHRF1 antibody was used throughout in this thesis for all the western blots, ICC and IHC undertaken. What is not yet known is whether qPSCs express UHRF1. Although qPSCs were not specifically stained for UHRF1 in freshly isolated PSCs, UHRF1 expression was not observed in normal pancreas or liver sections. It can be speculated that qPSCs do not express UHRF1. To the best of our knowledge, this is the first report of UHRF1 expression in a subset of PSCs.

Previous studies have documented the expression of UHRF1 in primary human fibroblasts cells[61,62] and mouse embryonic fibroblast (MEFs)[227]. Mousli *et al.* showed UHRF1 expression in foetal primary lung fibroblasts, WI-38 and IMR-90 (derived from human lung foetuses at 12 and 16 weeks of gestation respectively), when grown and harvested under proliferating conditions (60–70% confluence), although UHRF1 expression was lower in comparison to that in cancer cell lines[62]. Hopfner *et al.* also demonstrated UHRF1 expression in primary adult lung fibroblast cells (derived from adjacent normal lung tissue of a resected bronchial carcinoma patient) when grown and harvested under proliferating conditions; in addition, they examined UHRF1 expression from non-growing 100% confluent fibroblasts that had been serum starved for 48 hours and reported a very weak expression of UHRF1[61]. However, I harvested PSCs in culture at approximately 80% confluence as the primary interest was first to determine the basal levels of UHRF1. Nevertheless, pancreatic cancer tissue sections examined for UHRF1 *in situ*, only rarely expressed UHRF1 in tissue stroma. Furthermore, the foetal origin of lung fibroblast and the expression of UHRF1 in adult lung fibroblast and basal crypts of the intestine raises the possibility that

UHRF1 may confer some degree of stemness in a cell type or age (foetal or adult) dependent manner. Based on these observations, it can be suggested that UHRF1 expression in PDAC could be a marker of stemness or proliferative activity.

The phenotypic effect of Nrf2 deletion was not evident at the early age of 10 weeks as both $Nrf2^{-/-}$ and $Nrf2^{+/+}$ mice had similar weights which is in agreement with a previous study showing no early growth or phenotypic consequences in $Nrf2^{-/-}$ mice[226]. However, at 10 months of age, there was a differential weight gain with $Nrf2^{+/+}$ mice weighing significantly more than the $Nrf2^{-/-}$ mice. More importantly, at 10 months of age the pancreas of the $Nrf2^{-/-}$ mice showed early signs of pancreatitis[223,224] as evidenced by the appearance of vacuolated lesions in acinar cells which were absent in $Nrf2^{+/+}$ mice pancreas. Similar vacuolated lesions have been reported in different regions of the brain of $Nrf2^{-/-}$ mice older than 10 months of age[92].The finding of vacuolated lesions in the pancreas of $Nrf2^{-/-}$ mice is novel to the best of our knowledge and further provide evidence in support of the vital function of Nrf2 in maintaining homeostasis at basal conditions. Taking advantage of this observation and looking at the positive side, $Nrf2^{-/-}$ mice or more specifically a targeted pancreas specific Nrf2 knockout could be used to investigate the protective and therapeutic role of Nrf2 in pancreatitis induced mouse models. With such a model, the development of early and florid pancreatitis picture is likely to allow for shortened time of experimentation in pancreatitis induced setting. Microscopic changes in the pancreas of $Nrf2^{-/-}$ and $Nrf2^{+/+}$ mice at an earlier age of 10 weeks was not undertaken.

Several studies have demonstrated a cross-talk between pancreatic cancer cells and PSCs[215,228]. In investigating the mechanism by which pancreatic cancer cells promote PSC activity, conditioned media from MiaPaCa-2 was used to culture and induce Nrf2 activity in PSCs (CAF-R2875). Although the Nrf2 induction in CAF-R2875 did not reach statistical significance, it is proof of principle that Nrf2 can be induced in CAFs. Nevertheless, additional experiments will be required to confirm this finding since it can be argued that conditioned media is spent which in itself could induce Nrf2 activity independent of secreted factors from cancer cells. The significance of Nrf2 induction can be seen from studies that have demonstrated glutathione (GSH) efflux from hepatic cells into the plasma to exert distant antioxidant extracellular effects[229]. Nrf2 contributes to the regulation of GSH synthesis by inducing the transcription of enzymes required for GSH synthesis[89]. It can be speculated that Nrf2 induction in PSCs (CAFs) by cancer cells provides additional drive for GSH synthesis which is subsequently effluxed[229] into the tumour stroma where it can provide GSH substrates to the cancer cells as well as antioxidant and xenobiotic functions within the extracellular space of the tumour stroma. More recently, Martinez-Outschoorn *et al.*[230] showed that H-Ras transformed immortalized keratinocytes (epithelial cancer cells) manifest an increased oxidative stress evidenced by increased ROS production, an effect which was rescued by n-acetyl cysteine (NAC); they further demonstrated that co-culture of epithelial Ras transformed cancer cells with fibroblasts reduced ROS production in these cancer cells suggesting that fibroblasts may protect adjacent cancer cells from oxidative stress by stimulating an antioxidant response in such cancer cells[230]. We speculate from our results that in response to secreted factors

from cancer cells, CAFs (aPSCs) induce their own antioxidant response and secrete antioxidant factors into the stroma to protect cancer cells. PSCs can also induce Nrf2 in cancer cells as demonstrated by Wu *et al.*[215]. This observation suggests the possibility of a feedback loop and a vicious circle where both cancer cells and PSCs promote a potent antioxidant intracellular and extracellular defence environment.

An interesting and new observation was made in normal tissues of intestine (colon and duodenum) which were used as orientation cores in TMA generated for use in this thesis. Briefly, the colonic epithelium makes invaginations called glandular crypts; at the base of the crypts are adult somatic stem cells that are responsible for regenerating the colonic epithelium[231-233]. Pericryptal myofibroblasts located around the colonic crypts form the stem cell niche and provide signalling factors that maintain the stem cells in an undifferentiated state[222,231,233]. The concentration of the signalling factors decrease from the basal crypts further away towards the luminal surface of the colonic epithelium; this creates a signalling gradient that determines cell behaviour at different histological levels of the colonic epithelium[233]. The UHRF1 IHC data of normal duodenum and colonic epithelium from this thesis uniquely showed UHRF1 expression localised to histologically defined intestinal basal crypts areas where intestinal stem cells are known to reside[233]. These findings, although not the primary focus of my thesis are really interesting. UHRF1 expression has been observed in cancer cells and in proliferative areas of human appendix[59,61]. Using IHC, Hopfner *et al.*[61] examined UHRF1 expression in the proliferative areas (glandular crypts) of human appendix and reported nuclei UHRF1 expression localized to the glandular crypts just as observed in this thesis. In addition, normal active tissues

(proliferative tissues) of foetal liver, foetal thymus, adult thymus and bone marrow were found to be tissues richest in UHRF1 mRNA whereas well differentiated tissues of the central nervous system and peripheral leucocytes were free of UHRF1 mRNA[61]. Studies in mouse embryonic stem cells have indicated a role for UHRF1 during embryogenesis and development[227] and may explain UHRF1 expression within this defining proliferative stem cell layer (intestinal crypts) of intestinal epithelium in this case possibly functioning as marker of stemness. In this context, the expression of UHRF1 can be considered to be function specific, organ or tissue specific and when found with in an organ or tissue like the intestine its expression may have to be histologically defined within a normal intestinal mucosa.

Only a few other studies have reported on the expression of UHRF1 in intestinal tissues. Kofunato Y. *et al.*[78] and Wang F. *et al.*[234] examined normal colon and colon cancer tissues and reported the absence of UHRF1 expression in non-neoplastic adjacent normal colonic epithelial cells and UHRF1 overexpression in colorectal cancer tissues[78,234]. None of these studies reported on the pattern of UHRF1 expression in normal colon observed in this thesis. The differences in expression could reasonably be due to different anti-UHRF1 antibodies used in those studies compared to that used in this thesis and by Hopfner *et al*[61].

This is a novel finding of UHRF1 expression in the intestinal mucosa that can be carried forward. Understanding the signals that regulate the tight expression of UHRF1 within basal intestinal crypts and factors that aberrantly induce UHRF1 expression in pancreatic ductal epithelium could provide better understanding of the

function of UHRF1 and in normal and diseased states. Taken together, these data suggest UHRF1 may have no role in the majority of adult human PSCs. The significance of UHRF1 expression in the subset of PSC population is undetermined and the classic histological distribution pattern of UHRF1 in intestinal epithelium may be worth investigating further.

In conclusion, the findings in this chapter further reflect differences between non-malignant stromal PSCs and cancer cells as having different molecular signatures and further suggests that PSCs have a role to play in modulating oxidative stress in PDAC. Deciphering the precise role of PSCs and its subtypes will greatly improve our approach to targeting the stroma as part of a combined therapeutic approach to addressing this disease.

5 EXAMINATION FOR POTENTIAL PREDICTIVE BIOMARKERS FOR PANCREATIC CANCER

5.1 Introduction

The dismal outcome associated with pancreatic cancer[235] needs to be improved. The widening understanding of the molecular and cellular basis of pancreatic cancer may potentially lead to more targeted and novel therapies[16,236] but enhancing the predictability of patient response to both current and novel therapies could potentially change survival for pancreatic cancer patients[146].

Using patients' tissue samples from the European Study Group for Pancreatic Cancer-3 (ESPAC-3) trial, which did not show any significant overall survival benefit with adjuvant 5-fluorouracil (5-FU) plus folinic acid (551 patients) compared to gemcitabine (537 patients) treatment[7], Greenhalf *et al.* showed that high levels of human equilibrative nucleoside transporter 1 (hENT1) was predictive for better survival in patients treated with gemcitabine but not with 5-FU[146]. Recent work within our research group, and presented in this thesis has indicated an important role for both UHRF1 and Nrf2 in contributing to the stabilization of oxidative stress in pancreatic cancer[80,99]. In other cancers, single nucleotide polymorphisms (SNPs) in antioxidant and drug detoxifying genes and tissue levels of putative proteins are emerging as predictive biomarkers[170,171,237,238]. However, in pancreatic cancer, there are currently no biomarkers in routine use that can predict which patients will respond to treatment[16].

The aims of the study described in this chapter were: (I) to investigate whether germline SNPs and tumour protein expression of oxidative stress and drug metabolising enzymes could be prognostic for survival or predict response to

chemotherapy treatment in pancreatic cancer patients and (II) to determine if an automated scoring system using Definiens software could complement manual scoring for the expression levels of proteins in IHC stained tissues. To address these aims, putative germline SNPs of *NRF2, NQO1* and *SRXN1* were analysed from whole blood from two clinical trials of advanced pancreatic cancer patients[29,30]. In addition, the analysis of the respective protein levels in pancreatic cancer tissues from adjuvant clinical trial samples was attempted[146]. Finally, UHRF1 protein expression in pancreatic cancer tissues was also examined and measured.

5.2 Results

5.2.1 SNP genotyping

Three SNPs one each for *NRF2* (rs2886162), *NQO1* (rs1800566) and *SRXN1* (rs6053666) were genotyped (Figure 5.1). Three different genotypes for each gene were observed (major homozygous, minor homozygous and heterozygous, Table 5.1); however, for *NQO1*, there was only one patient with minor homozygous (TT) genotype, so they were grouped with heterozygous (CT) patient for further analysis. The SNP genotypes were tested for concordance with HWE; the observed genotype frequencies did not significantly deviate from the HWE (Table 5.1).

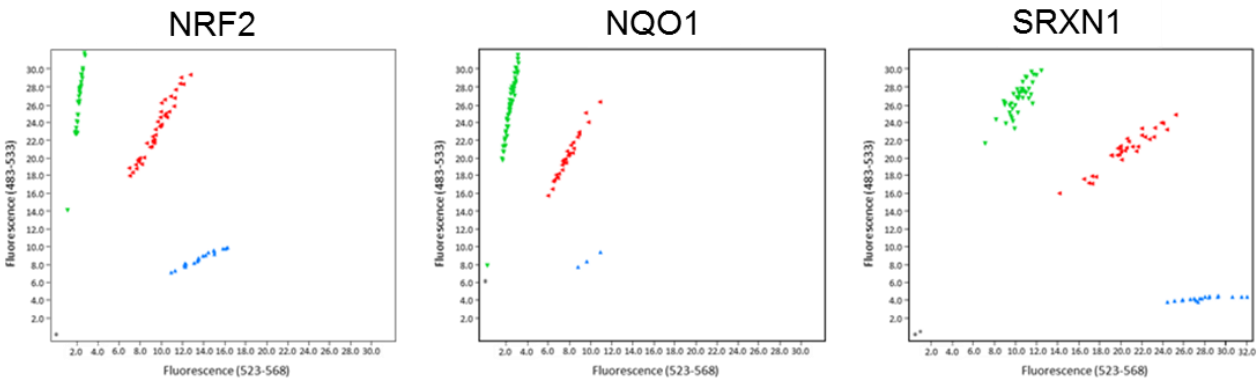

Figure 5.1 Representative allelic discrimination plots for *NRF2, NQO1* and *SRXN1* SNPs. Minor homozygous allele VIC dye-labelled (wavelength 523 – 568) is on the X axis and major homozygous allele FAM dye-labelled (wavelength 483 – 533) is on the Y axis. The heterozygous genotype has a fluorescence intensity that is intermediate between that of homozygous major and minor alleles. Each SNP/patient was genotyped in triplicate and there was 100% concordance. Each patient is represented as three dots on each plot.

Table 5.1. Allelic and genotypic frequency table for 149 patients and genotype concordance with Hardy-Weinberg equilibrium (HWE) based on a European population.

Gene	SNP ID	Allele (minor/major)	Allelic Frequencies (%)	Homozygous minor (n)	Homozygous major (n)	Heterozygous (n)	χ^2 *P* value for HWE
NRF2	rs2886162	A/G	49/51	AA (34)	GG (37)	AG (78)	0.779
NQO1	rs1800566	T/C	19.5/80.5	TT (1)	CC (92)	CT (56)	0.192
SRXN1	rs6053666	C/T	34.9/65.1	CC (13)	TT (58)	CT (78)	0.173

5.2.2 Patient dataset

SNP data was ascertained for 106 ViP and 43 TeloVac patients. Of these, SNP data for 97 (92%) VIP patients were analysed (as 9 of the samples were for patients screened and consented but ultimately not randomised). All 43 TeloVac patients were analysed, making a combined dataset of 140 patients.

5.2.3 Analyses of ViP patients

In ViP patients, univariate analysis for *NRF2/NQ01/SRXN1* SNPs revealed no significant correlation between individual SNPs and overall survival (OS) (Appendix 5, Table A1). Multivariate models without *NRF2/NQO1/SRXN1* SNPs were fitted for log CA19-9, ECOG status and differentiation status which were significantly associated with OS (p=0.008, 0.001 and 0.027 respectively, Appendix 7). *NRF2/NQO1/SRXN1* SNPs were added to the multivariate model with log CA19-9 and ECOG status and no SNP significantly correlated with OS (Appendix 5, Table A2).

5.2.4 Analyses of TeloVac patients

In the univariate analysis for Telovac patients, only the *NQO1* SNP rs1800566 was observed to be significantly associated with OS (p=0.038) with the major homozygous CC correlating with an unfavourable prognosis (Appendix 6, Table A3). Multivariate models without *NRF2/NQO1/SRXN1* SNPs were fitted and log CA19-9 was significantly associated with OS (p=0.007,

Appendix 8). *NRF2/NQO1/SRXN1* SNPs were then added to the multivariate model with log CA19-9 and no SNP significantly correlated with OS although the NQO1 SNP showed a trend for an independent association with survival (p=0.053), (Appendix 6, Table A4).

5.2.5 Overall survival analysis for ViP and TeloVac patients combined

5.2.5.1 NQO1 genotype is an independent prognostic biomarker in advanced pancreatic cancer patients

A Kaplan-Meier (KM) analysis for overall survival by trial (ViP and Telovac trials) and by SNP (both trials combined) is shown in Figure 5.2. There was no significant difference in OS between patients from either trial; the median (95% CI) survival for ViP patients was 9.38 (7.73, 11.48) months compared with 8.98 (4.80, 12.23) months for TeloVac patients (p=0.969, Table 5.2 and Figure 5.2 A). The median (95% CI) survival by SNP for combined ViP and TeloVac patients is shown in Table 5.2. *NQO1* rs1800566 showed a significant correlation with OS; patients with the *NQO1* CC major

genotype had a significantly poorer outcome than patients with CT and TT *NQO1* genotypes combined (p=0.010 Figure 5.2 C). No SNP–related differences in survival for *NRF2* and *SRXN1* SNPs were observed (p=0.405 and p=0.634 respectively, Figure 5.2 B and D). Multivariate models without *NRF2/NQO1/SRXN1* SNPs were fitted and log CA19-9 was significantly associated with OS (p=0.001, Appendix 9, Table A7). *NRF2/NQO1/SRXN1* SNPs were then added to the model with log CA19-9, and only *NQO1* SNP emerged as independently significantly associated with OS (p=0.028, Table 5.2).

Table 5.2. Median overall survival of SNP genotypes for combined ViP and TeloVac data and the univariate and multivariate analysis.

			Univariate		Multivariate*	
Prognostic Variable	**No of patients (deaths)**	**Median OS (95% CI)**	**HR**	**p**	**HR**	**p**
NRF2				**0.405**		
AA	30 (23)	8.03 (4.77,17.00)	1.34(0.84, 2.17)	(0.353 AG		**0.511**
AG	75 (62)	8.95 (7.70,11.02)	1.08 (0.63,1.86)	and GG		
GG	35 (31)	9.24 (5.00,13.03)		consolidated)		
NQO1						
TT/CT	55 (40)	11.34 (8.94,12.96)		**0.010**		**0.028**
CC	85 (76)	7.83 (5.19,10.86)	1.66 (1.12,2.46)		1.56(1.04,2.32)	
SRXN1						
CC	12 (10)	11.77 (1.71,18.29)	0.93 (0.43,1.86)	**0.634**		**0.295**
CT	75 (64)	10.86 (7.73,12.43)	0.83 (0.56,1.22)			
TT	53 (42)	8.16 (5.33, 9.67)				
Trial						
ViP	97 (93)	9.38 (7.73, 11.48)		**0.969**		
TeloVac	43 (23)	8.98 (4.80, 12.23)				

**Log CA19-9 included as explanatory variable, Trial as a stratified variable*

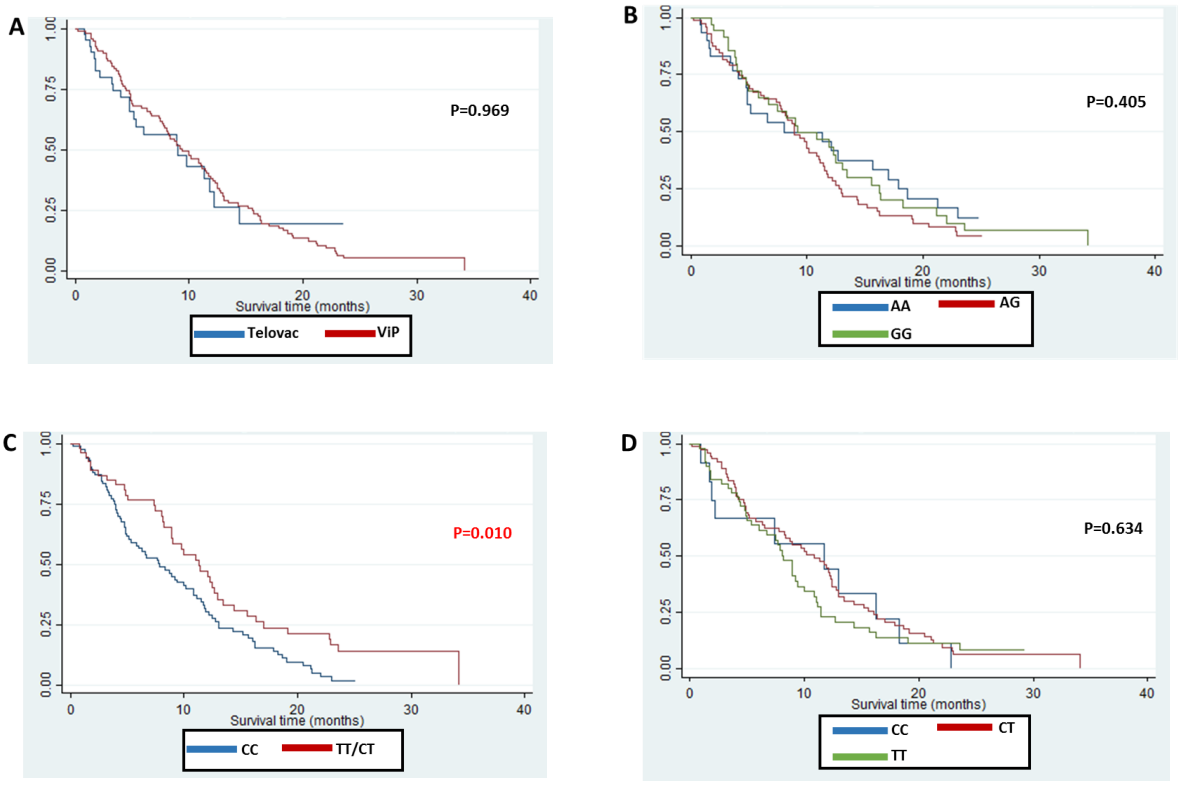

Figure 5.2. Kaplan-Meier analysis of overall survival by trial and by SNP in advanced pancreatic cancer patients for the TeloVac and ViP trials. (A) Survival plot for TeloVac and ViP data. (B, C and D) Survival plot for combined VIP and TeloVac data by *NRF2, NQO1* and *SRXN1* respectively. P values were derived from univariate Cox regression analysis.

5.2.5.2 Combined NQO1 and SRXN1 genotypes are independent prognostic biomarkers in advanced pancreatic cancer.

Given that the median overall survival for heterozygous (CT) and minor homozygous (CC) *SRXN1* genotypes were similar to each other and more importantly that they were different from the major homozygous (TT) SRXN1 genotype, patients with both the CT and the CC genotypes were consolidated and their survival compared against those with major homozygous (TT) *SRXN1* genotypes (Figure 5.3). The median (95% CI) survival for patients with *SRXN1* CC/CT of 10.86 (8.22, 12.8) months was not significantly different in comparison to 8.16 (6.02, 10.86) months for wild-type (TT)

homozygous *SRXN1* (p=0.371). A further consolidation was undertaken between patients with *SRXN1* and *NQO1* SNPs to create new group variables (Table 5.3) given that the median overall survival for heterozygous and minor homozygous genotypes for both *NQO1* and *SRXN1* were similar to each other but different from their corresponding major homozygous genotypes.

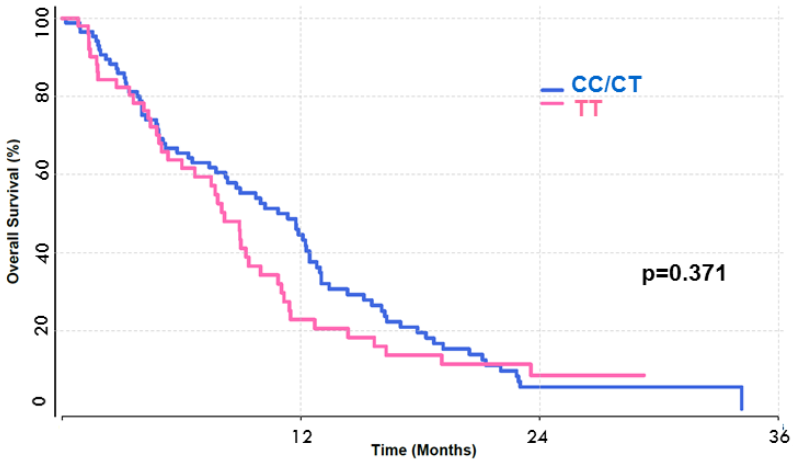

Figure 5.3. VIP and TeloVac data for combined CC and CT versus TT *SRXN1* SNP. P value was derived from univariate Cox regression analysis.

Table 5.3. New variables after *SRXN1* and *NQO1* genotype consolidation; group 1 - pure homozygous major genotypes; group 4 – pure heterozygous/homozygous minor genotypes and groups 2 and 3 together make the 3rd variant.

	SRXN1		
Prognostic variable	**TT** (homozygous major)	**CT/CC** (heterozygous and homozygous minor)	**Total**
CC (homozygous major)	**33 (Group 1)**	**52 (Group 2)**	**85**
CT/TT (heterozygous and homozygous minor)	**20 (Group 3)**	**35 (Group 4)**	**55**
Total	**53**	**87**	**140**

Interestingly, patients with purely heterozygous and homozygous minor genotypes for both *SRXN1* and *NQO1* (group 4) had significantly better survival with a median (95% CI) survival of 12.27 (8.95, 17.01) months than pure homozygous majors for both *SRXN1* and *NQO1* (group 1) with a median survival of 6.68 (4.77, 10.86) months or mixed homozygous major with heterozygous and homozygous minor genotypes for both *SRXN1* and *NQO1* (groups 2 and 3) with a median survival of 8.98 (7.5, 11.88) months (p=0.039, Figure 5.4, Table 5.4). In addition, multivariate analysis using Cox proportional hazard regression identified pure heterozygous and homozygous minor genotypes for both *SRXN1* and *NQO1* (group 4) as independent prognostic factors for overall survival in PDAC patients (hazard ratio = 0.5, 95% CI= 0.29 to 0.88, p=0.016).

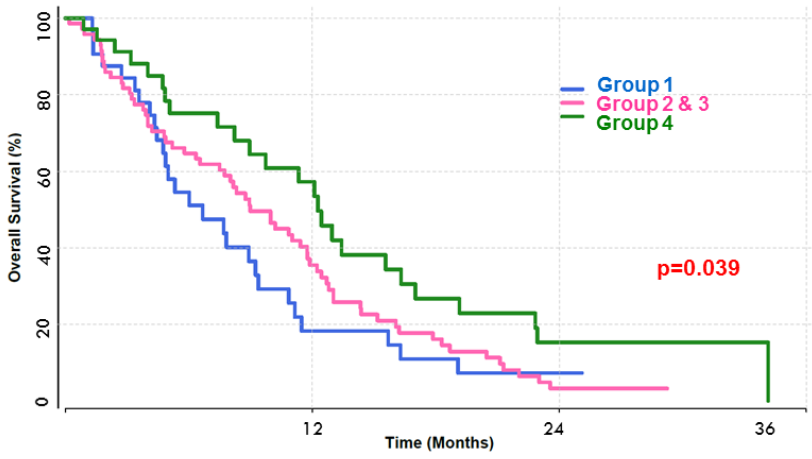

Figure 5.4. Kaplan-Meier survival curves of consolidated *SRXN1* and *NQO1* genotypes. Survival plot for VIP and TeloVac data for combined *NQO1* and *SRXN1* SNPs as shown in Table 5.3. P value was derived from univariate Cox regression analysis.

Table 5.4. Median overall survival of consolidated *SRXN1* and *NQO1* SNP genotypes for combined ViP and TeloVac data and the univariate and multivariate analysis.

			Univariate		Multivariate	
Prognostic Variable	No of patients (deaths)	Median OS (95% CI)	HR	p	HR	p
(Group 1)	33 (27)	6.68 (4.77,10.86)	1.0 (ref)			
(Group 2 and 3)	72 (64)	8.98 (7.5, 11.88)	0.81 (0.52, 1.27)		0.81 (0.51, 1.26)	**0.353**
(Group 4)	35 (25)	12.27 (8.95, 17.01)	0.51 (0.29, 0.88)	**0.039**	0.5 (0.29, 0.88)	**0.016**

5.2.6 Evaluating the predictive effect of SNP on treatment

Only patients from the ViP trial were evaluated for the predictive effect of SNP on treatment as patient numbers from the TeloVac trial were small and in addition had different treatments to those in ViP. The differential effect of treatment category for each type of SNP covariates were assessed by fitting multivariate models including treatment as a nested effect within each type of SNP to investigate the effect of gemcitabine alone compared with gemcitabine plus vandetanib for each category of SNP. Each multivariable model also included ECOG status as an independent prognostic variable. No SNP had a predictive effect on treatment in the multivariate models fitted but ECOG status correlated with survival in the multivariate models for *NRF2* (p=0.004), *SRXN1* (p=0.015) and was tending towards significance for *NQO1* *(*p=0.053, Appendix 10 and Appendix 11).

5.2.7 Antibody validation for immunohistochemistry in resected pancreatic cancer patients (ESPAC-1 and ESPAC-3)

Antibodies for NQO1, Srxn1 and Nrf2 were validated using western blotting and were subsequently optimized for immunocytochemistry (ICC) and immunohistochemistry (IHC) with cell pellets and PDAC TMAs respectively. Western blotting for NQO1 revealed a single band that was reduced in intensity following targeted siRNA mediated depletion (Figure 5.5). Nrf2 and Srxn1 immunoblots also revealed bands at the expected molecular weight that decreased in intensity following targeted siRNA-mediated depletion of corresponding proteins, but in addition contained other nonspecific bands which were not affected by the knockdown (Figure 5.5).

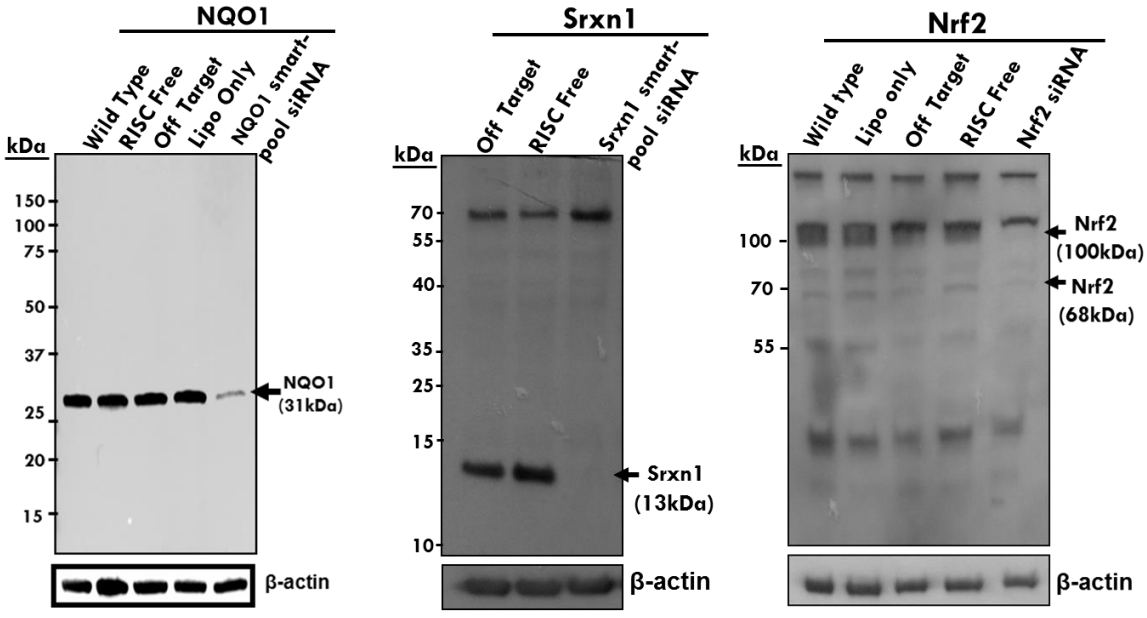

Figure 5.5. Antibody validation for NQO1, Srxn1 and Nrf2 in MiaPaCa-2 cells. Western blot images showing antibody specificity of indicated proteins following NQO1, Srxn1 or Nrf2 depletion by siRNA.

The specificity of all three antibodies for use with ICC was tested using siRNA-mediated depletion of their corresponding proteins. The specificity of the antibodies for Nrf2 and Srxn1 could not be confirmed (Figure 5.6 A-D). Interestingly, Nrf2 depleted cell pellets failed to remain adherent to the glass slides during routine antigen retrieval (heat induced) processing and therefore could not be stained for Nrf2; the reason for the detachment of Nrf2 depleted cells from glass slides during this step could not be ascertained in this study. Attempts were made to treat cells on cover slips and avoided the antigen retrieval steps but these also proved unsuccessful in confirming the specificity of the antibody (Figure 5.6). The NQO1 antibody was successfully optimized (Figure 5.6 E and F); the results differentiated NQO1 depleted cells from control treated cells and as a result, only the NQO1 antibody was carried forward for use on the ESPAC TMAs.

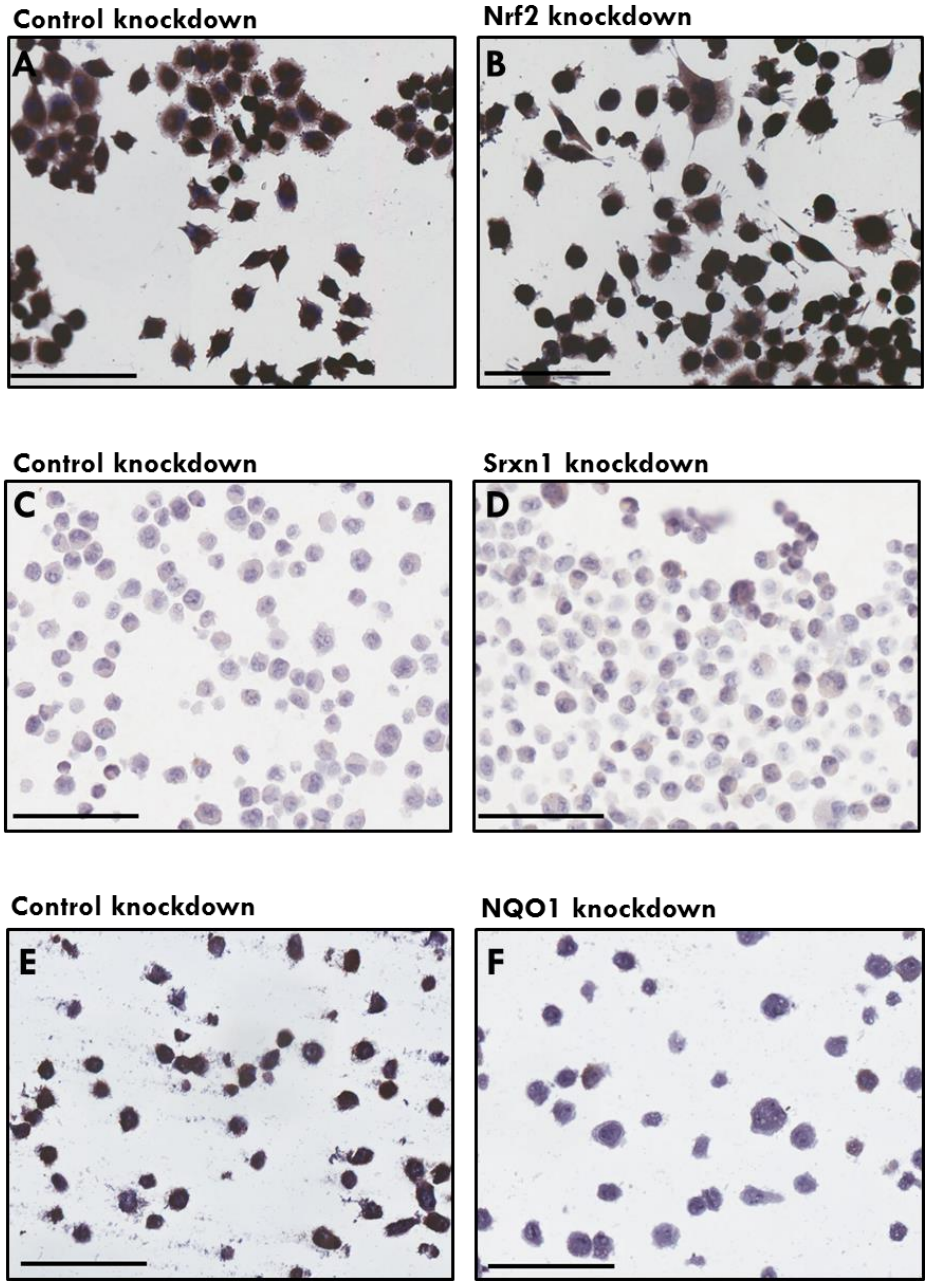

Figure 5.6 Assessment of antibody specificity for immunocytochemistry. MiaPaCa-2 cells treated with control or indicated targeting siRNAs were embedded in paraffin and stained for Srxn1 (C, D) and NQO1 (E, F) while Nrf2 siRNA-treated cells and the corresponding control cells were prepared on cover slips (A, B). In both Nrf2 and Srxn1 depleted cells, no observable differences in staining was seen between control treated and targeted protein depleted cells. NQO1 control treated cells expressed brown positive cytoplasmic staining (E) while no staining is seen in NQO1 depleted cells indicative of antibody specificity. **Scale bar = 100 µm**

5.2.8 UHRF1 and NQO1 immunohistochemistry staining in normal pancreatic tissues

Normal pancreatic tissues were first examined for UHRF1 and NQO1 expression. In normal pancreatic tissues, UHRF1 expression was not observed in intralobular or interlobular ducts or ductules whereas in serial tissue section, NQO1 expression was variable ranging from no expression in intralobular ducts and/or ductules to weak cytoplasmic staining in interlobular ducts (Figure 5.7). No UHRF1 nor NQO1 staining was seen in acinar tissues.

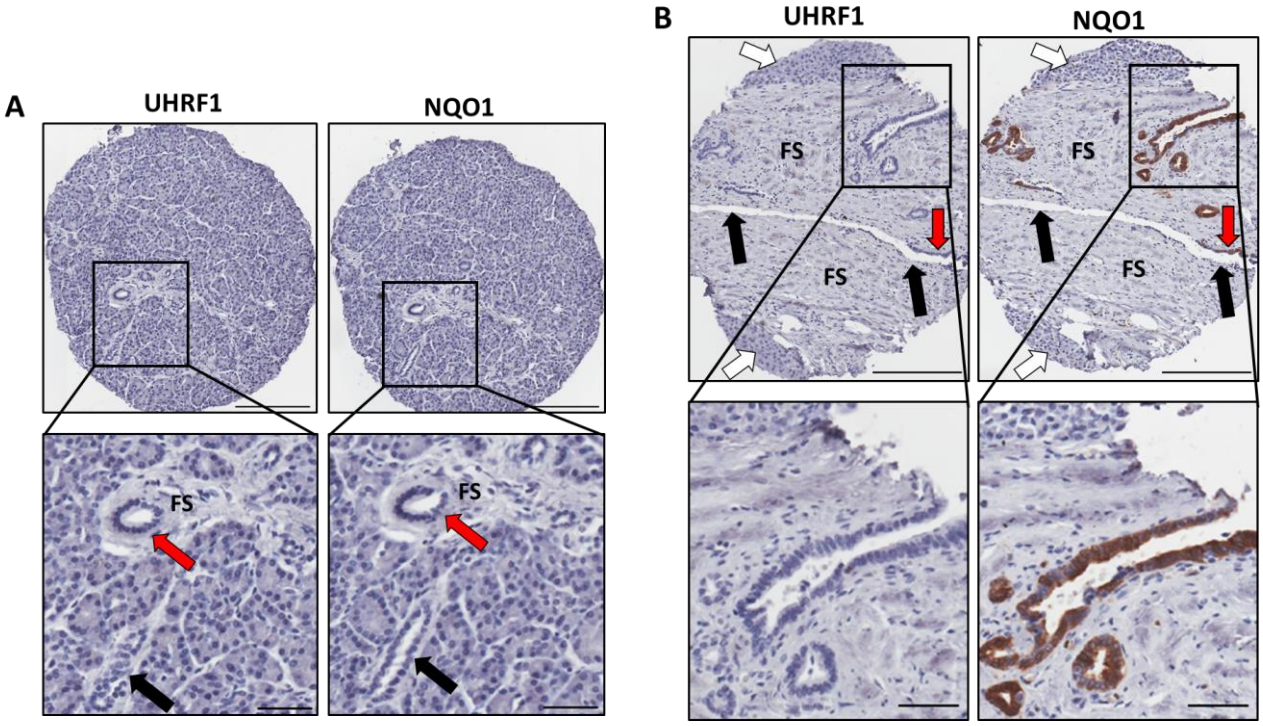

Figure 5.7. Representative micrographs of normal pancreatic tissue. (A) Matched core sections of a normal pancreas with intact acinar and ductal architecture; magnified inset shows normal intralobular duct (red arrow) surrounded by a layer of fibrous sheath (FS) and normal intralobular ductule (black arrow) with no or very scanty fibrous sheath. Tissues were stained for UHRF1 and NQO1 as indicated and both ducts, ductules and acinar tissue did not express UHRF1 or NQO1. **(B)** Matched core sections of a normal pancreas showing one of the main ducts (black arrow) at the centre of the core surrounded by thick fibrous sheath (FS) with red arrows indicating a visible part of the ductal epithelium; normal acinar tissue (white arrows) can be seen at 12 and 7 o'clock positions and NQO1 positively-stained (brown) ducts. Magnified inset shows cytoplasmic NQO1 staining in interlobular ducts but no corresponding UHRF1 immunoreactivity. Scale bar = 200µm and magnified inset 50µm.

5.2.9 UHRF1 and NQO1 immunohistochemistry staining in adjacent normal pancreatic tissues and ducts

Adjacent normal pancreatic tissue with normal appearing pancreatic ducts were also examined and variable UHRF1 expression was observed between patients, ranging from negative expression in some patients to positive nuclei expression in others; NQO1 expression was observed in the cytoplasm of all normal appearing ducts of matched adjacent normal pancreatic tissues (Figure 5.8 and Appendix 12). Within pancreatic cancer cores, adjacent normal-appearing ducts generally had weaker cytoplasmic NQO1 expression than malignant ducts; an example of normal duct transformation (cancerization) further illustrates this differential NQO1 expression where normal ducts stain weakly for cytoplasmic NQO1 and the transformed (cancer) cells stain strongly (Figure 5.9 and Appendix 12). Neither UHRF1 nor NQO1 expression was observed in acinar tissues.

Interestingly, some lymphoid cells within pancreatic lymphoid tissue obtained from adjacent PDAC tissues expressed UHRF1 (Figure 5.10), with some of these also observed in the stroma of some PDAC patients (Figure 5.9 and Appendix 14, image C). NQO1 also stained endothelial cells in pancreatic tissues (lymphoid and malignant tissues, Figure 5.10 and Appendix 14, image B), in keeping with previous studies that reported NQO1 staining in blood vessels[147].

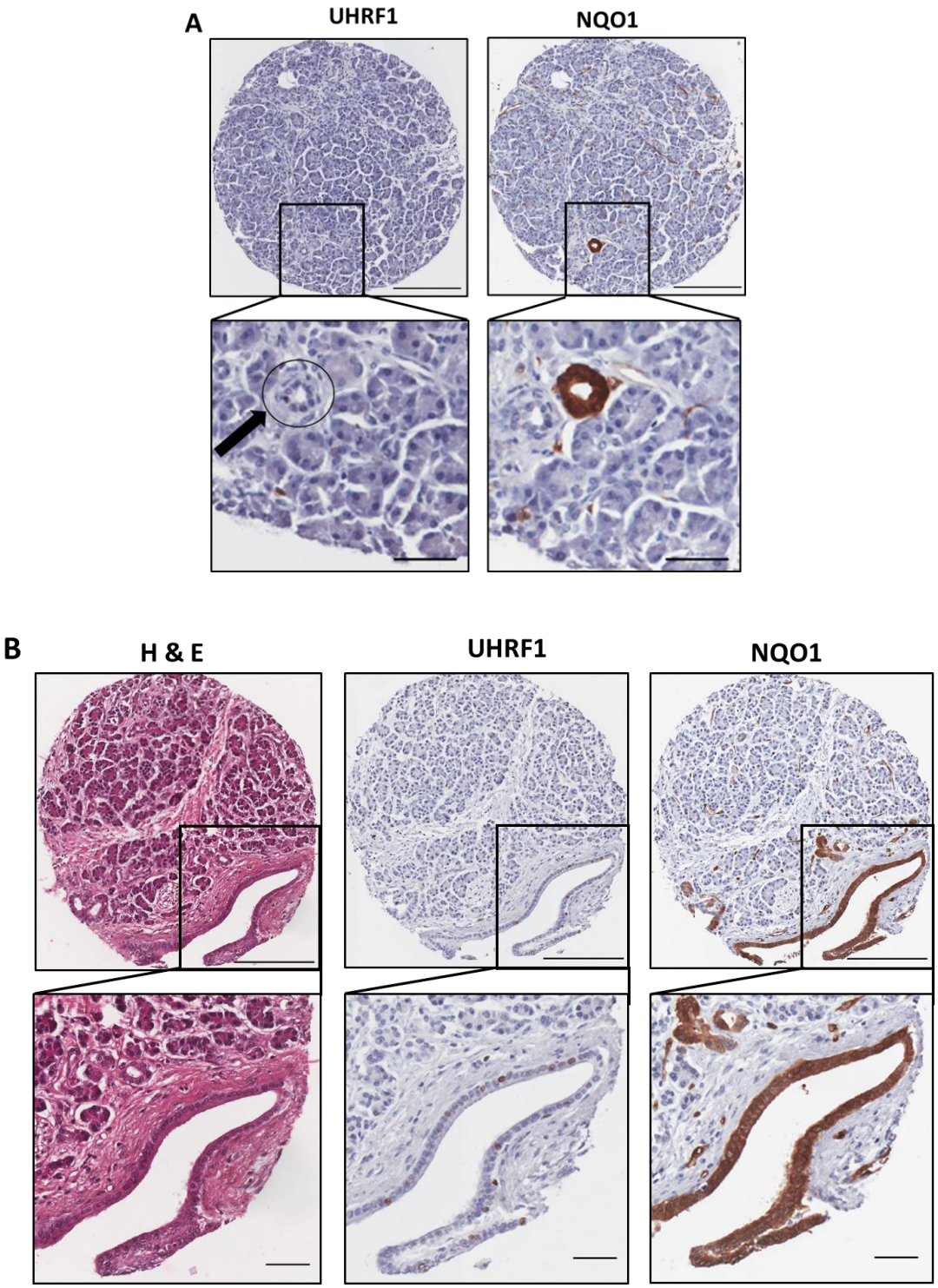

Figure 5.8. Representative micrographs of adjacent normal pancreatic tissues. (A) Matched core sections of **adjacent normal** pancreas from healthy tissue donor with intact acinar and ductal architecture; magnified inset shows normal appearing intralobular duct. No ductal (black arrow with a circle) UHRF1 immunoreactivity is observed but NQO1 has positive cytoplasmic immunoreactivity. **(B)** Matched core sections of **adjacent normal** pancreas from PDAC patient showing normal looking ducts and acinar tissue architecture; magnified inset shows normal appearing interlobular duct with a few brown nuclei staining for UHRF1 and positively-stained brown cytoplasmic NQO1 immunoreactivity. Tissues stained with haematoxylin and eosin, or for UHRF1 and NQO1 as indicated. Scale bar = 200μm and magnified inset 50μm.

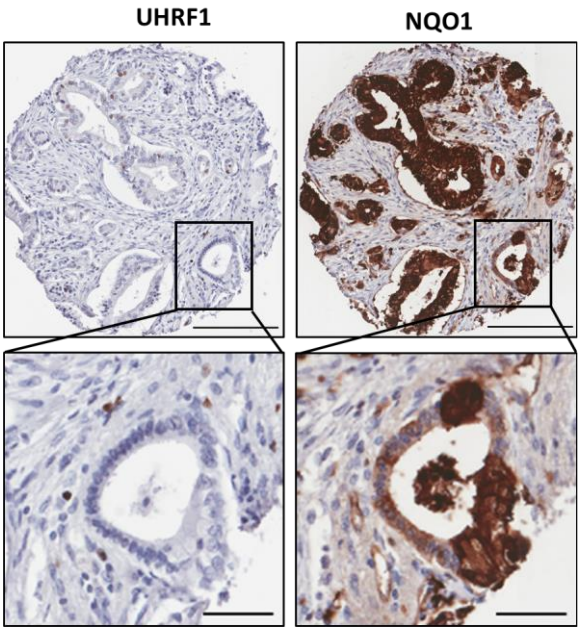

Figure 5.9. Example of normal duct cancerization. Magnified inset of matched cores from a PDAC patient showing normal duct undergoing transformation; cancer cells can be seen arising from 1 o'clock and 3 – 6 o'clock position with a distorted nuclei arrangement whilst the remaining normal ductal epithelia maintained uniform nuclei alignment. Tissues stained for UHRF1 and NQO1 as indicated. No UHRF1 immunoreactivity is observed within the normal and malignant ductal cells but a few cells in the stroma stain positively for UHRF1. Stronger NQO1 expression is seen in the malignant area of the ductal epithelium while a weak cytoplasmic NQO1 staining is observed in the remaining aspect of the normal epithelium. Scale bar = 200µm and magnified inset 50µm

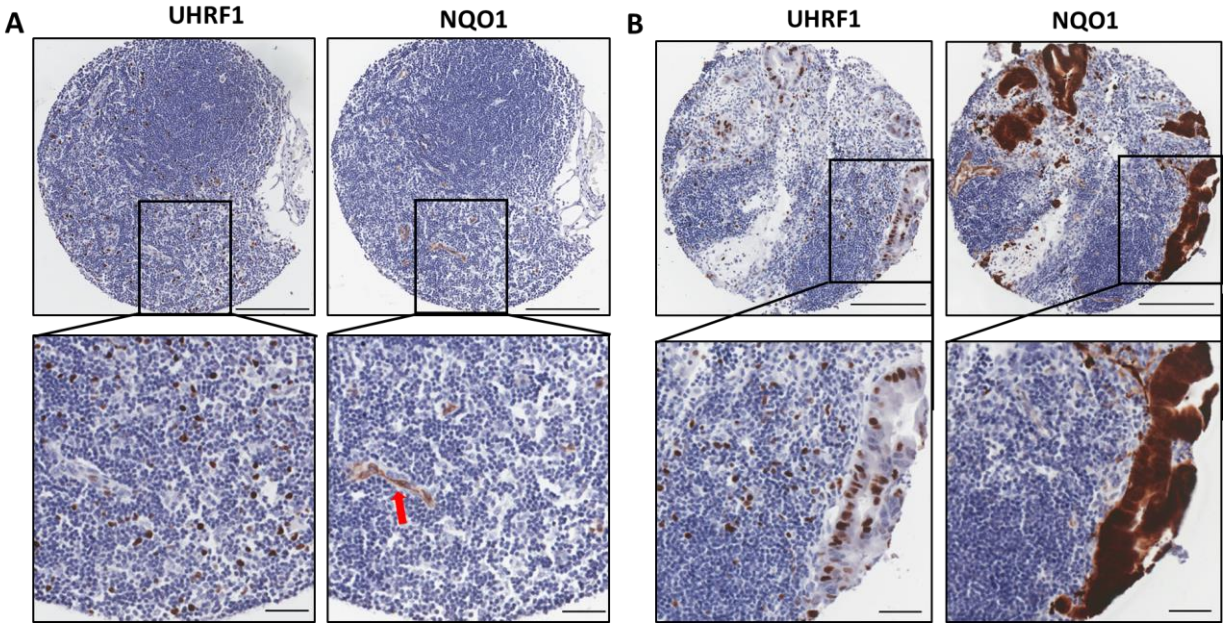

Figure 5.10. Representative micrographs of pancreatic lymphoid tissues from PDAC patients. (A) Matched core sections of a lymphoid tissue. Tissues stained for UHRF1 and NQO1 as indicated and brown positive UHRF1 immunoreactivity of some lymphoid/immune cells can be seen; brown immunoreactivity for NQO1 (red arrow) stains blood vessels but not lymphoid/immune cells. **(B)** Matched core sections of a lymphoid tissue from a PDAC patient. Both lymphoid tissue and pancreatic ducts can be seen in this core. Magnified inset – smaller positively staining brown UHRF1 lymphoid/immune cells can be seen whilst larger positive UHRF1 staining pancreatic duct nuclei can be seen to the right extending from 2 to 5 O'clock position. NQO1 vividly stains pancreatic ducts. Scale bar = 200µm and magnified inset 50µm.

5.2.10 UHRF1 and NQO1 immunohistochemistry staining in normal colon and duodenum

Normal tissue cores of duodenum and colon which were present on the PDAC TMAs as orientation cores were also examined for UHRF1 and NQO1 expression. UHRF1 uniquely stained glandular epithelial cells limited to the basal crypts with no immunoreactivity in the glandular epithelia located proximal to the luminal part of the intestinal epithelium in both colon and duodenum (Figure 5.11). NQO1 expression was inversely related to UHRF1 expression; in areas where UHRF1 was expressed, NQO1 was negligibly or weakly expressed. Similarly, in areas of the intestinal epithelium were UHRF1 was not expressed, NQO1 was strongly expressed resulting in a gradient of NQO1 expression across the entire intestinal epithelium (Figure 5.11).

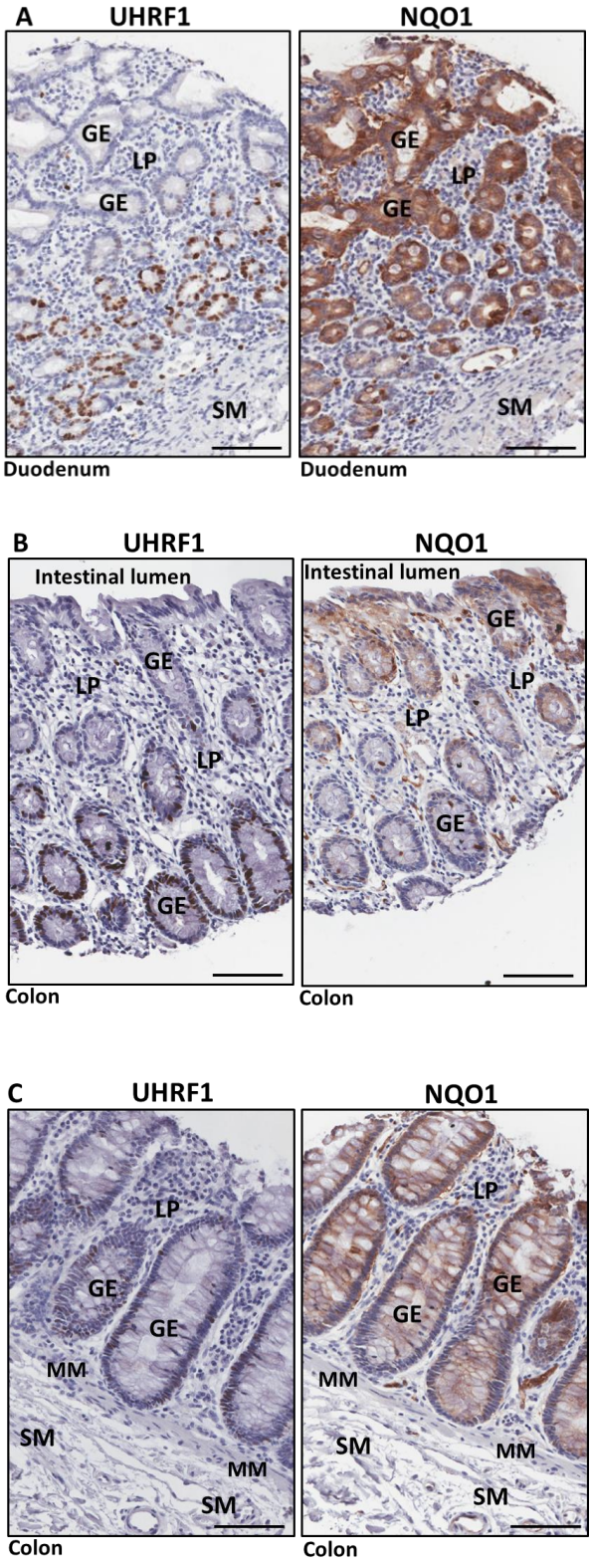

Figure 5.11. Example micrographs of UHRF1 and NQO1 expression in matched normal duodenum and colon from donor tissues. (A) Duodenum **(B)** Colon **(C)** Colon**.** In both colon and duodenum, UHRF1 nuclei expression is seen within the basal part of the **glandular epithelial (GE)** cells with an abrupt loss of UHRF1 beyond this zone towards the luminal layer of the GE. A gradient of NQO1 expression is seen in both colon and duodenum with weak cytoplasmic expression in GE cells in the basal aspect of the GE and stronger expression towards the luminal surface. **LP, lamina propria; MM, muscularis mucosae; SM, submucosa.** Scale bar = 100µm

5.2.11 UHRF1 and NQO1 immunohistochemistry staining and manual scoring in PDAC

UHRF1 expression was confined to the nuclei and tumour in cores were scored as either abundant (≥ 75 %), moderate (25 % to < 75 %), scanty (5 % to < 25 %) or negative (< 5 %) based on the proportion of the tumour cells expressing UHRF1 (Figure 5.12 and Appendix 13), whilst NQO1 cores were scored as: (I) strong, moderate, weak or negative for cytoplasmic immunoreactivity, (II) positive or negative for nuclei expression and (III) positive or negative stromal expression (Figure 5.13 and Appendix 13).

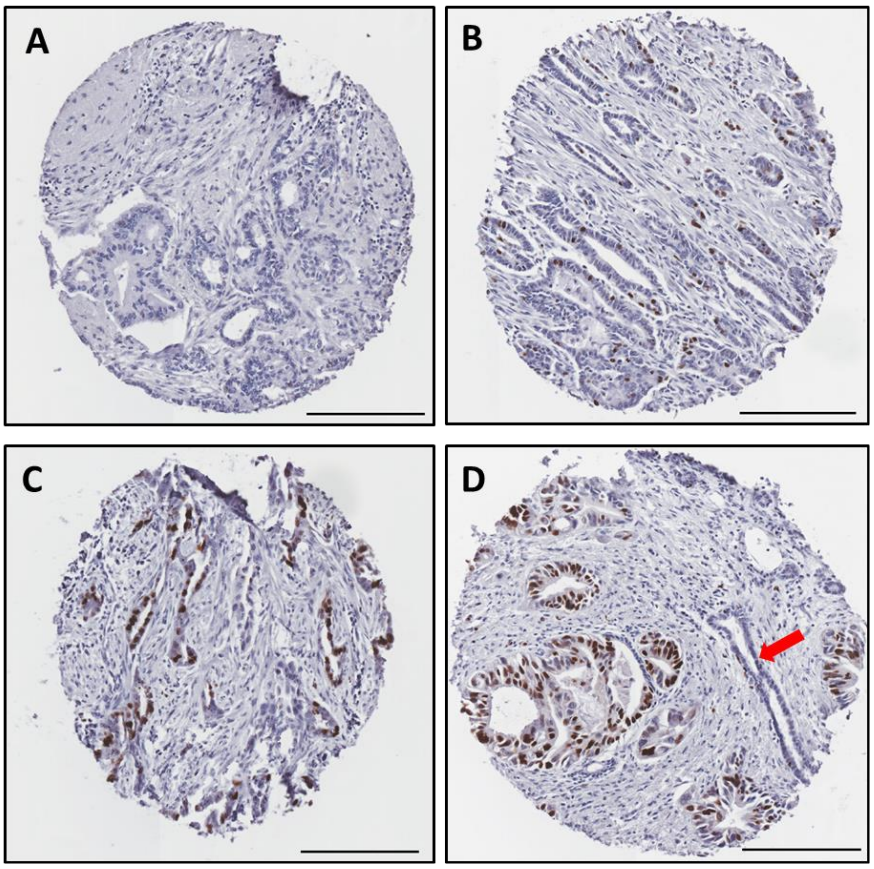

Figure 5.12. Example micrographs of UHRF1 expression in PDAC samples and cells. (A) Negative expression **(B)** Scanty nuclei expression **(C)** Moderate nuclei expression **(D)** Abundant nuclei expression**.** Red arrow - normal appearing adjacent duct negative for UHRF1 expression. Note the distorted pancreatic architecture with loss of acinar tissue in PDAC. Scale bar 200µm

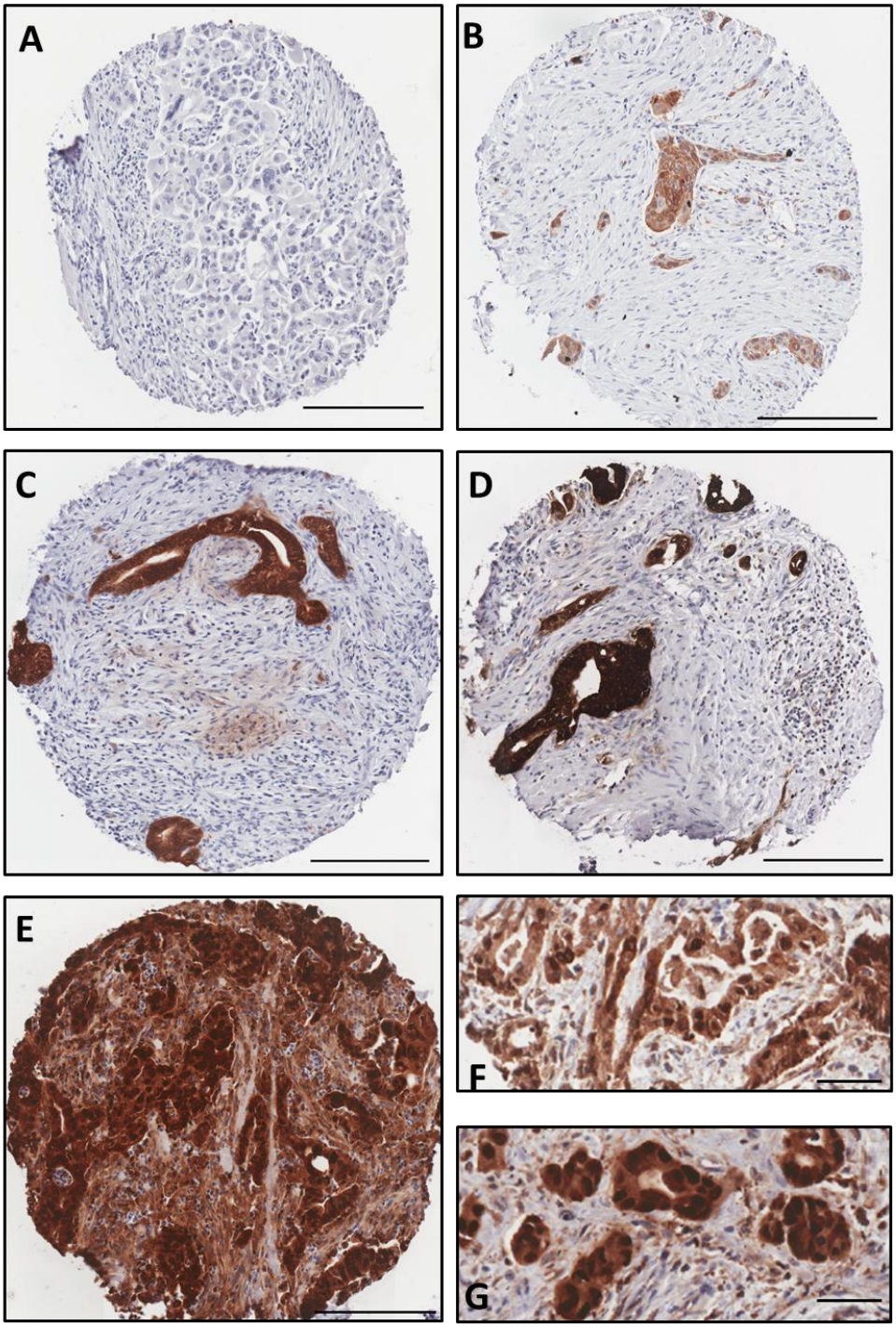

Figure 5.13. Example micrographs of NQO1 expression in PDAC samples and cells. (A) Negative tumour expression **(B)** Weak cytoplasmic tumour expression **(C)** Moderate cytoplasmic tumour expression **(D)** Strong cytoplasmic tumour expression **(E)** Moderate cytoplasmic tumour expression with positive nuclei staining and stromal expression of NQO1**. Scale bar = 200µm. (F)** Weak cytoplasmic and (G) Moderate cytoplasmic tumour expression of NQO1 with positive nuclei expression. Scale bar = 50µm.

5.2.12 UHRF1 and NQO1 immunohistochemistry staining and Definiens (software) scoring in PDAC

Given that automation can be time saving, robust and can yield reproducible high-throughput data, an attempt was made to use Definiens software to complement manual scoring for TMAs stained for UHRF1 and NQO1. Depending on the type of analysis executed, several output data are generated; for UHRF1 'nuclei and marker area' analysis was used which generated, amongst other values, a positive index (PI) (Figure 5.14), whilst for NQO1 a 'marker area' analysis was used which generated a histologic score (H-score) (Figure 5.15). Comparative statistical analyses were undertaken to assess the correlation between manual UHRF1 versus Definiens PI score (Figure 5.16A and B), and manual cytoplasmic NQO1 versus Definiens H-score (Figure 5.16C and D). A statistically significant correlation between manual and Definiens scores was seen for both UHRF1 and NQO1 (Figure 5.16A, B, C and D). With the exception of a nonsignificant difference between NQO1 moderate and strong cytoplasmic scores and Definiens H-score (Figure 5.16C), there is an overlap in assignment of Definiens analysis scores for a corresponding manually scored UHRF1 or NQO1 expression.

In the case of UHRF1 expression analysis by Definiens, both brown UHRF1 nuclear and blue haematoxylin nuclear staining cancer cells were required to compute the PI score as described previously in section 2.27.6.2. An overestimation or underestimation is introduced when blue haematoxylin-stained or the brown UHRF1-stained cells respectively are not captured in the computation of PI (Figure 5.14).

In the case of NQO1 expression analysis by Definiens, cytoplasmic NQO1 expression was of interest. However, some patients displayed nuclear NQO1 in addition to cytoplasmic staining. Their H-scores were falsely higher because nuclear expression, which generally had a stronger NQO1 immunoreactivity, was automatically included in the computation of H-score (Figure 5.15). In summary, use of Definiens led to overestimation or underestimation of PI values for UHRF1 for some patients, and overestimation of H-score values for cytoplasmic NQO1 in some cases (Figure 5.16). Only manual scores were carried forward for subsequent data analysis.

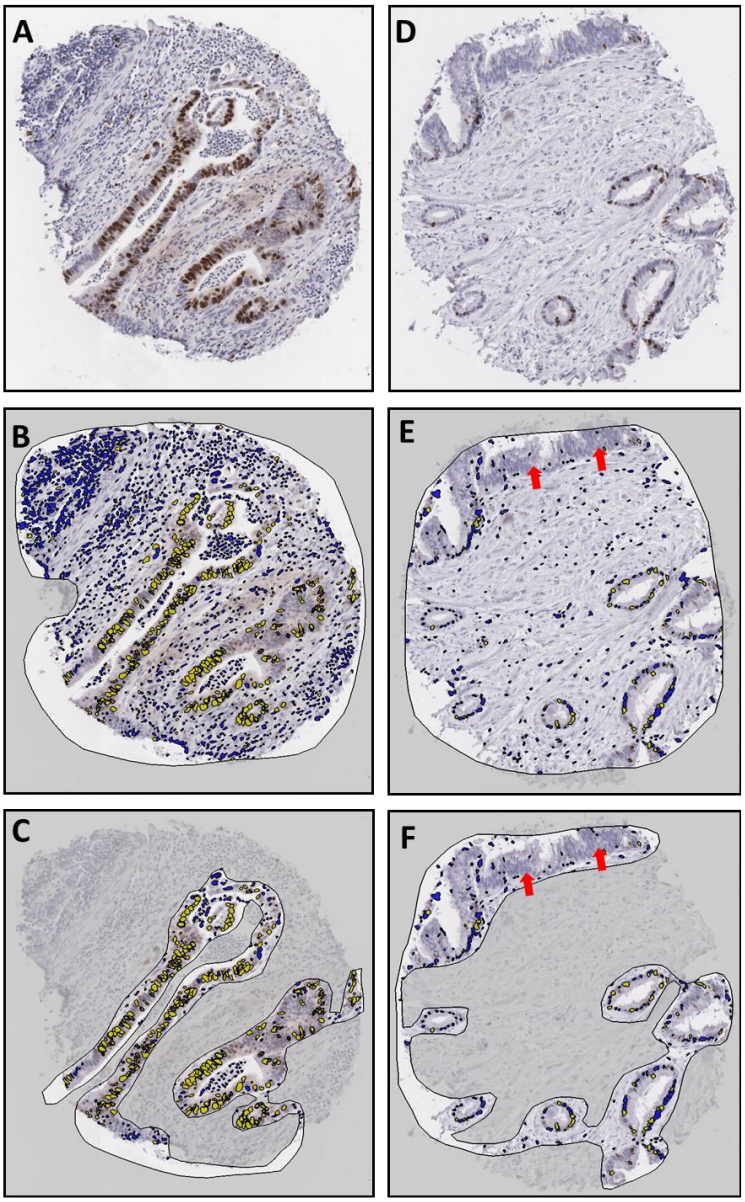

Figure 5.14. Representative images of Definiens software 'NUCLEI and MARKER AREA' analysis for UHRF1. (A and D) are two original IHC images before Definiens analysis. Definiens software computes a positive index (PI) % value after analysis of the region of interest (ROI, cancer cell nuclei); **(B and E)** Initial Definiens analysis with a PI of 15% and 12% for patients **(B)** and **(E**) respectively. After correcting for the ROI, the PI increased markedly for **(B)** from 15 to 53% **(C)** and increased slightly for **(E)** from 12 to 17% **(F).** However, there are numerous cancer nuclei (red arrows) not included in the PI analysis as they have remained purple during the analysis (not highlighted blue).

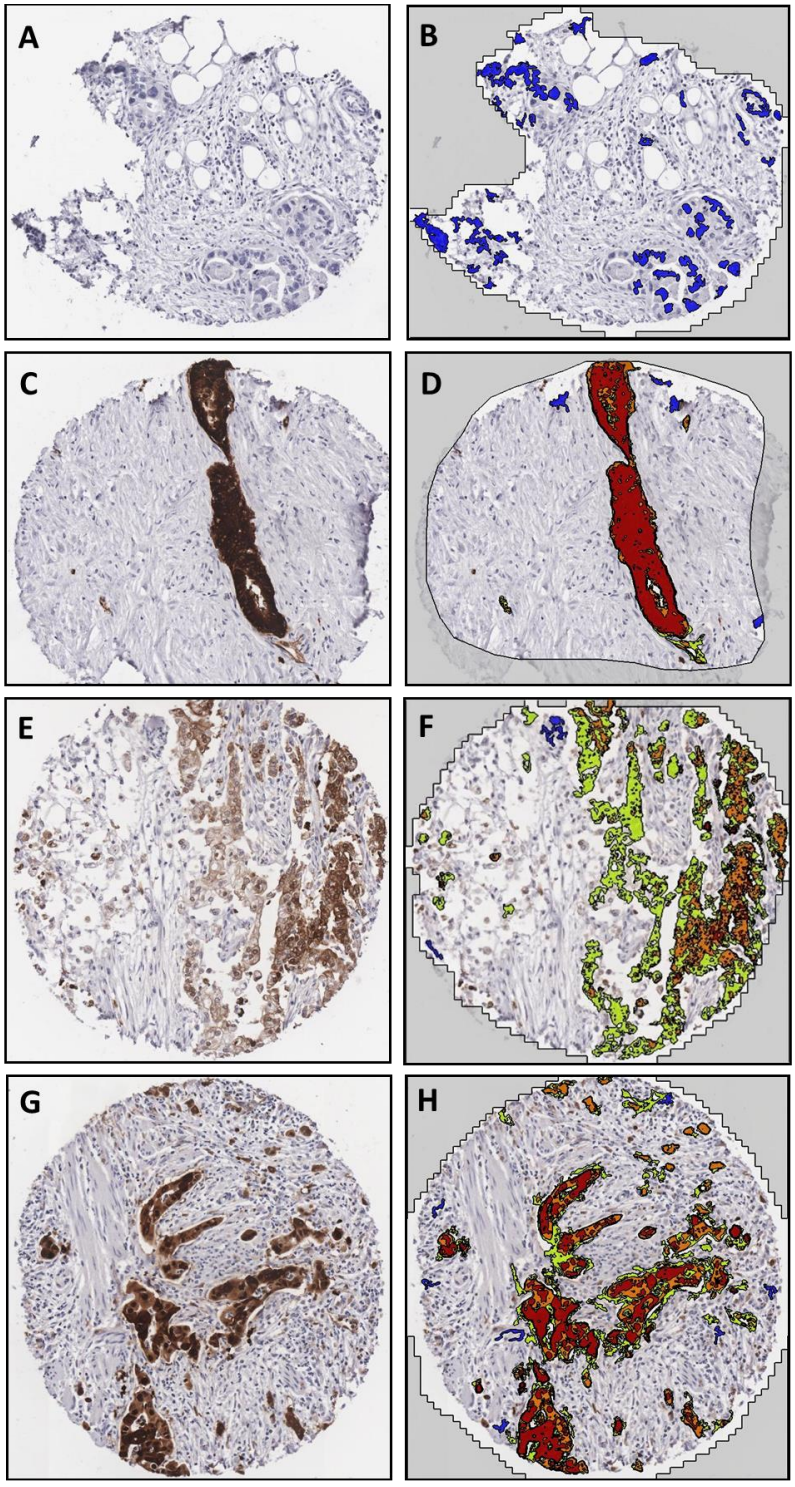

Figure 5.15. Representative images of Definiens software '<u>MARKER AREA</u>' analysis for cytoplasmic NQO1. (A, no NQO1 expression**; C,** strong NQO1 expression**; E,** weak with some moderate expression and **G,** moderate cytoplasm with positive nuclei) are four original IHC images before Definiens analysis. **(B, D, F and H)** Images after Definiens analysis of the corresponding images to the left; Green corresponds to weak, orange corresponds to moderate and red corresponds to strong NQO1 expression. H-scores B = 0; D = 255.63; F= 134; H = 192. Note, positive nuclei staining in (G) appearing as red in (H) has skewed the H-score towards higher values.

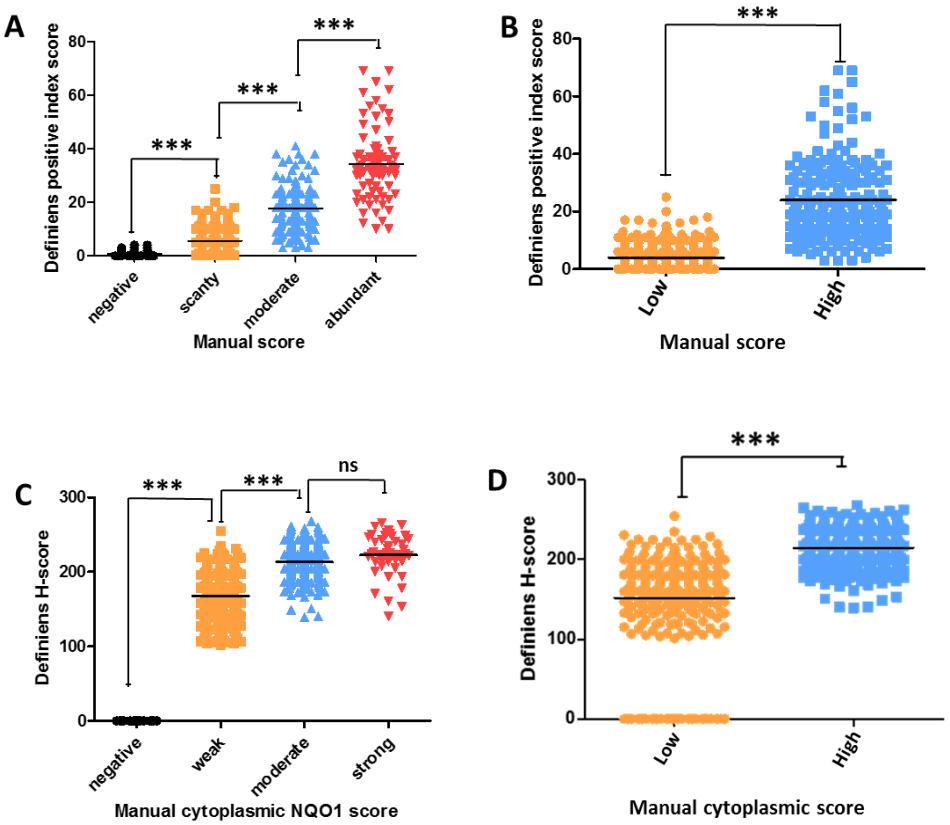

Figure 5.16. Comparison of manual UHRF1 and NQO1 scores with Definiens positive index (PI) for UHRF1 and H-score for NQO1. (A and B = UHRF1), (C and D = NQO1). (A) Four group manual UHRF1 scores vs PI values. **(B)** Consolidated UHRF1 manual - low (negative plus scanty) and high (moderate plus abundant). **(C)** Four group manual NQO1 scores vs H-score values. **(D)** Consolidated NQO1 manual - low (negative plus weak) and high (moderate plus strong). Two tailed t-test, (B and D), ANOVA, (A and C). ns, not significant; ***, p<0.001

5.2.13 UHRF1 and NQO1 immunohistochemistry data analysis

Nine tissue microarrays representing 349 patients, 318 adjuvant chemotherapy-treated (gemcitabine or 5FU/folinic acid) patients plus 31 observation only (true resection only) patients, were each analyzed for UHRF1 and NQO1 expression. Of the chemotherapy treated, 181 (56.9%) patients with 362 cores together with 18 observation only patients (58.1%) with 74 cores for UHRF1 and 187 (58.8%) chemotherapy-treated patients with 374 cores together with 20 (64.5%) observation only patients with 81 cores for NQO1 were suitable and included in the final analysis. To be included in the final analysis, patients must have 2 or more eligible cores. Reasons for ineligibility included patients with one single representative core, completely missing cores, folded cores or no histological evidence of cancer cells on the core.

5.2.14 UHRF1 and NQO1 are overexpressed in pancreatic cancer

Although only a few normal pancreatic specimen were available to be examined and compared with resected pancreatic cancer tissues, both UHRF1 and NQO1 were observed to be overexpressed in comparison to adjacent normal pancreatic ducts within the same tumour cores (Figure 5.7 and Figure 5.9), as expected[80,160]. Eighteen (9.1%) patient tumours scored negative for UHRF1 and 181 (90.9%) scored positive; of those who scored positive for UHRF1, 80 (40.2%) scored scanty, 57 (28.6%) scored moderate and 44 (22.1%) scored abundant. NQO1 staining was also variable between patients.

Ten (4.8%) patients scored negative for NQO1 whilst 197 (95.2%) patients' tumours were positive cytoplasmic NQO1; in patients who were positive for cytoplasmic NQO1, 62 (30%) scored weak, 109 (52.7%) scored moderate and 26 patients (12.6%) scored strong. Nuclei and stromal expression were also observed for NQO1 with 124 (59.9%) and 19 (9.2%) of the patients scoring positive for nuclei and stromal NQO1 respectively. There was a bias in the classification of nuclei NQO1 scores in patients who had moderate to strong cytoplasmic NQO1 as it was difficult to identify their nuclear expression; as a result further NQO1 nuclei analysis was not undertaken. Patients who scored negative for cytoplasmic NQO1 were also negative for nuclear and stromal NQO1 immunoreactivity.

5.2.15 Clinicopathological correlation of UHRF1 and NQO1 in pancreatic cancer

The association between UHRF1 and NQO1 with clinical and tumour characteristics was investigated. UHRF1 levels were dichotomized into low (negative and scanty) and high (moderate and abundant). UHRF1 expression was significantly associated with tumour staging (p=0.048) and diabetic status (p=0.029, Table 5.5). Statistical significance was lost after retesting using negative, scanty, moderate and abundant UHRF1 levels versus tumour staging (p=0.374, Table 5.6) whilst for diabetic status, statistical significance further improved (p=0.005, Table 5.6). A trend emerged where an inverse relationship between UHRF1 level and diabetic status was observed; patients with diabetes are less likely to express high UHRF1 (Figure 5.17).

NQO1 cytoplasmic protein levels were also dichotomized into low (negative and weak) and high (moderate and strong) but no statistically significant association with clinicopathological parameters was observed (Table 5.7).

The association between UHRF1 and cytoplasmic NQO1 was also investigated; high UHRF1 expression correlated significantly with high cytoplasmic NQO1 ($p=0.003$) and stromal positivity ($p=0.009$, Table 5.8). Patients with high cytoplasmic NQO1 were significantly associated with a positive NQO1 stromal expression ($p=0.022$, Table 5.9).

Table 5.5. Relationship between UHRF1 protein levels and clinicopathological parameters.

Characteristic	Number	Low UHRF1	High UHRF1	P
Stage				
1	11	9	2	0.048 †
2	43	19	24	
3	106	48	58	
4	8	6	2	
Lymph node status				
Negative	38	23	15	0.128 †
Positive	150	70	80	
Tumour grade				
Well	14	8	6	0.641 †
Moderate	113	57	56	
Poor	56	25	31	
Maximum tumour diameter				
<30 mm	79	42	37	0.538 †
≥30 mm	103	50	53	
Diabetes				
No	138	60	78	0.029 †
Yes	45	28	17	
Sex				
Male	106	51	55	0.674 †
Female	82	42	40	
Age, y				
<60	71	35	36	0.971 †
≥60	117	58	59	

†, χ_2 test two-tailed

Table 5.6. Relationship between tumour stage and diabetes versus UHRF1 protein levels (negative, scanty, moderate and abundant)

		UHRF1				
Characteristic	Number	Negative	Scanty	Moderate	Abundant	P
Stage						
1	11	2	7	2	0	0.374 †
2	43	3	16	11	13	
3	106	7	41	32	26	
4	8	1	5	1	1	
Diabetes						
No	138	7	53	40	38	0.005 †
Yes	45	9	19	12	5	

†, χ_2 test two-tailed

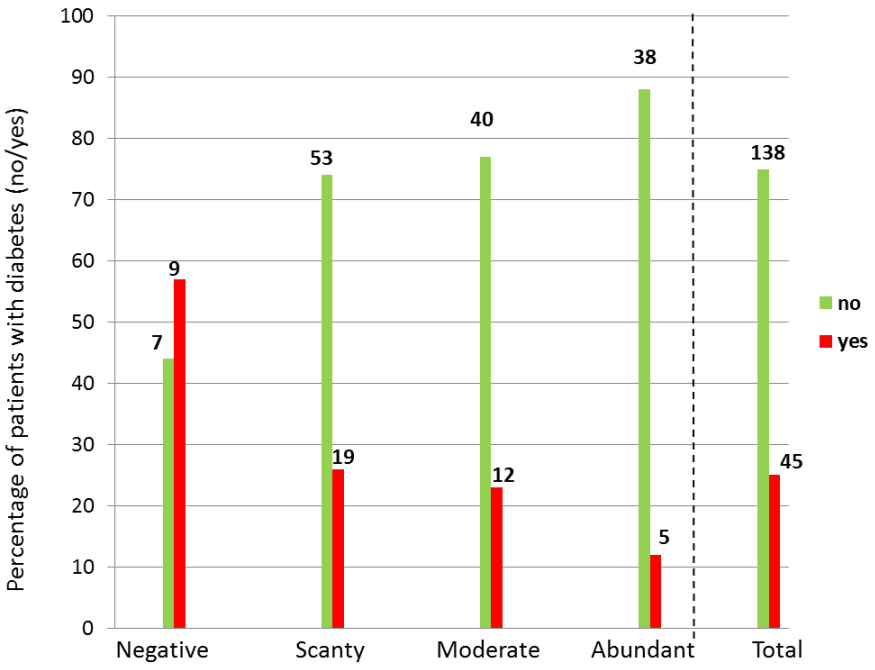

Figure 5.17. Relationship between UHRF1 and diabetes. Bar chart showing the inverse relationship between UHRF1 protein levels and diabetic status. Patient numbers are indicated at the top of each bar. no = no diabetes; yes = diabetes.

Table 5.7. Relationship between NQO1 protein levels and clinicopathological parameters.

Characteristic	Number	Low NQO1	High NQO1	P
Stage				
1	13	5	8	0.569 †
2	49	14	35	
3	105	42	63	
4	7	3	4	
Lymph node status				
Negative	45	15	30	0.683 †
Positive	150	55	95	
Tumour grade				
Well	12	4	8	0.406 †
Moderate	116	37	79	
Poor	62	26	36	
Maximum tumour diameter				
<30 mm	92	33	59	0.923 †
≥30 mm	93	34	59	
Diabetes				
No	146	49	97	0.185 †
Yes	45	20	25	
Sex				
Male	82	33	49	0.282 †
Female	113	37	76	
Age, y				
<60	77	27	50	0.845 †
≥60	118	43	75	

†, χ^2 test two-tailed; Low and High NQO1 = Low and High cytoplasmic NQO1 expression

Table 5.8. Relationship between UHRF1 and NQO1 protein levels

Protein expression	Number	Low UHRF1	High UHRF1	P
Cytoplasmic NQO1				
Low	56	36	20	0.003 †
High	104	41	63	
Stromal NQO1				
Negative	143	74	69	0.009 *
Positive	17	3	14	

†, χ_2 test two-tailed; * Fischer's exact test two-tailed

Table 5.9. Relationship between cytoplasmic and stromal NQO1 protein levels

Protein expression	Number	Low NQO1	High NQO1	P
Stromal NQO1				
Negative	188	70	118	0.022 *
Positive	19	2	17	

†, χ_2 test two-tailed; * Fischer's exact test two-tailed Low and High NQO1, Low and High cytoplasmic NQO1 expression

5.2.16 Overall survival analysis

5.2.16.1 NQO1 protein levels but not UHRF1 protein levels are associated with survival in pancreatic cancer

Overall survival was estimated using Kaplan-Meier survival curves and compared using log-rank tests. Available retrospective data from ESPAC-1 and ESPAC-3 trials were used to test for differences in survival between adjuvant chemotherapy treated patients and resection only (observation only) patients. The median overall survival for adjuvant chemotherapy treated patients was 20.2 (95% CI=16.7 to 22.7) months compared with 8.6 (95% CI=6.1 to 15.2) months for observation only patients (p=0.021, Figure 5.18) and in agreement with the results from ESPAC-1 and -3 (v1) trial with a statistically significant difference between adjuvant chemotherapy (5-FU) versus resection only[19].

There was no difference in survival for patients treated with gemcitabine, median survival 21.0 months (95% CI=16.3 to 24.8) months versus 5FU/folinic acid treated patients, median survival 18.5 (95% CI=15.3 to 22.3) months (p=0.997, Figure 5.18 B) and consistent with the previous report from ESPAC-3 (v2) trial where adjuvant 5-FU/folinic acid was not superior to adjuvant gemcitabine[7]. No statistically significant difference in median overall survival was observed for UHRF1 expression.

The median (95% CI) overall survival for negative, scanty, moderate and abundant UHRF1 expression was 16.8 (6.3 to 27.6), 22.1 (16.4 to 26.5), 15.2 (13.7 to 20.12) and 18.5 (14.2 to 29.3) months respectively (p=0.581, Figure 5.18 C). In the dichotomized

plot, median (95% CI) overall survival for low and high UHRF1 protein expression was 21.3 (16.4 to 26.5) and 16.7 (14.3 to 20.6) months respectively (p=0.478, Figure 5.18 C).

In the case of NQO1 protein expression analysis, an increasing trend in median overall survival was observed. The median (95% CI) overall survival for negative, weak, moderate and strong expressers was 10.2 (7.6 to 32.3), 13.4 (10.9 to 15.8), 18.8 (15.5 to 24.5) and 25 (17.3 to 39.1) months respectively (p=0.007, Figure 5.18 D). When patients were dichotomized into high and low expression, the median (95% CI) overall survival for low and high NQO1 protein expressers was 13.4 (10.9 to 15.3) and 20.9 (16.7 to 25.1) months respectively, (p=0.003, Figure 5.18 D).

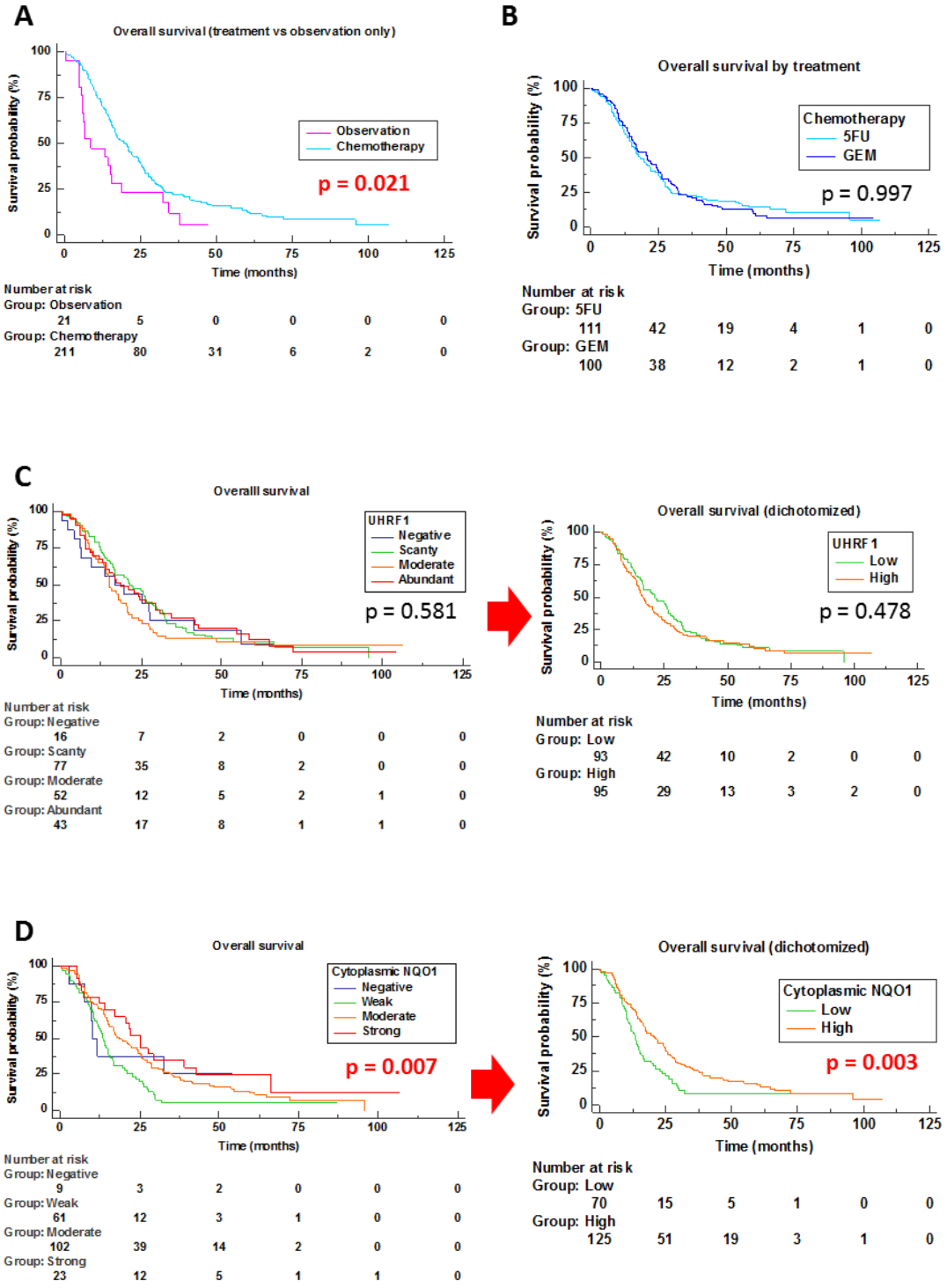

Figure 5.18. Kaplan-Meier overall survival curves stratified by (A) treatment arm- chemotherapy (Gemcitabine and 5Flourouracil/folinic acid versus observation only (resection only); **(B)** treatment arm- Gemcitabine versus 5-Flourouracil/folinic acid; **(C**) UHRF1 and **(D**) by NQO1 protein expression. P values were determined by log-rank testing. All statistical tests were 2-sided. **5FU = 5 Fluorouracil plus folinic acid; GEM = Gemcitabine.**

5.2.16.2 NQO1 protein levels but not UHRF1 protein levels may be associated with response to treatment in pancreatic cancer

To determine if UHRF1 or NQO1 protein levels are predictive of response to treatment in PDAC patients, pairwise comparisons were undertaken for both proteins (Figure 5.19 and Figure 5.20). UHRF1 protein levels were not prognostic in the observation only group [median (95% CI) survival of 15.2 (6.8 to 18.8) months in high UHRF1 group versus 6.5 (5.4 to 32.4) months in low UHRF1 group, p=0.882, Figure 5.19 B], nor were they predictive of response to treatment (p=0.79, Figure 5.19A, C, D, E and F, Table 5.10).

The median survival of patients treated with gemcitabine with low NQO1 levels was 13.7 (95% CI 10.2 to 16.8) versus 24.2 (95% CI 16.3 to 29.5) months in patients with high NQO1 expression (p=0.013, Figure 5.20 D). In 5FU/folinic acid treated patients, the median survival difference was tending towards significance with 13.4 (95% CI 10.9 to 19.6) months for low NQO1 levels compared with 21.8 (95 % CI 16.9 to 25.7) months for patients with high NQO1 levels (p=0.083, Figure 5.20 C). Although NQO1 levels were significantly associated with response to treatment in the gemcitabine group, there is no sufficient evidence to suggest its levels are predictive of response to treatment. NQO1 levels were not prognostic of survival for the observation only group [median (95% CI) survival of 6.8 (6.0 to 18.8) months in high NQO1 group versus 5.4 (4.8 to 14.3 months in low NQO1 group, p=0.301, Figure 5.20 D). Other pairwise comparisons were not found to be significant (Figure 5.20 E and F, Table 5.11).

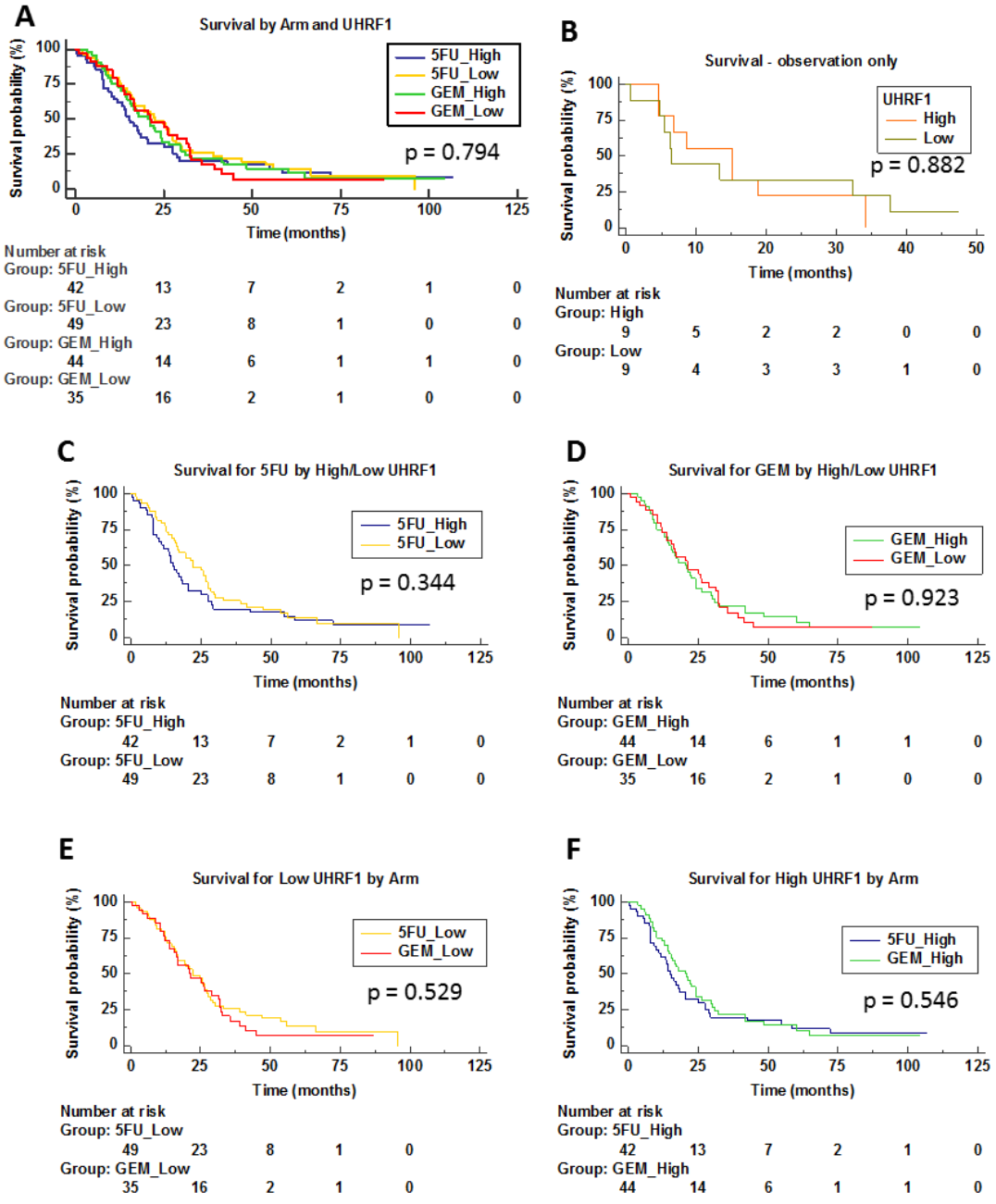

Figure 5.19. Kaplan-Meier overall survival curves stratified by (A) chemotherapy and UHRF1 protein expression **(B)** observation only (resection only) and UHRF1 protein expression**; (C)** 5-Flourouracil/folinic acid and UHRF1 protein expression**; (D)** Gemcitabine and UHRF1 protein expression **(E)** Gemcitabine or 5FU/folinic acid treated patients expressing low UHRF1 **(F)** Gemcitabine or 5FU/folinic acid treated patients expressing high UHRF1. P values were determined by log-rank test. All statistical tests were 2-sided**. 5FU = 5 Fluorouracil plus folinic acid; GEM = Gemcitabine**

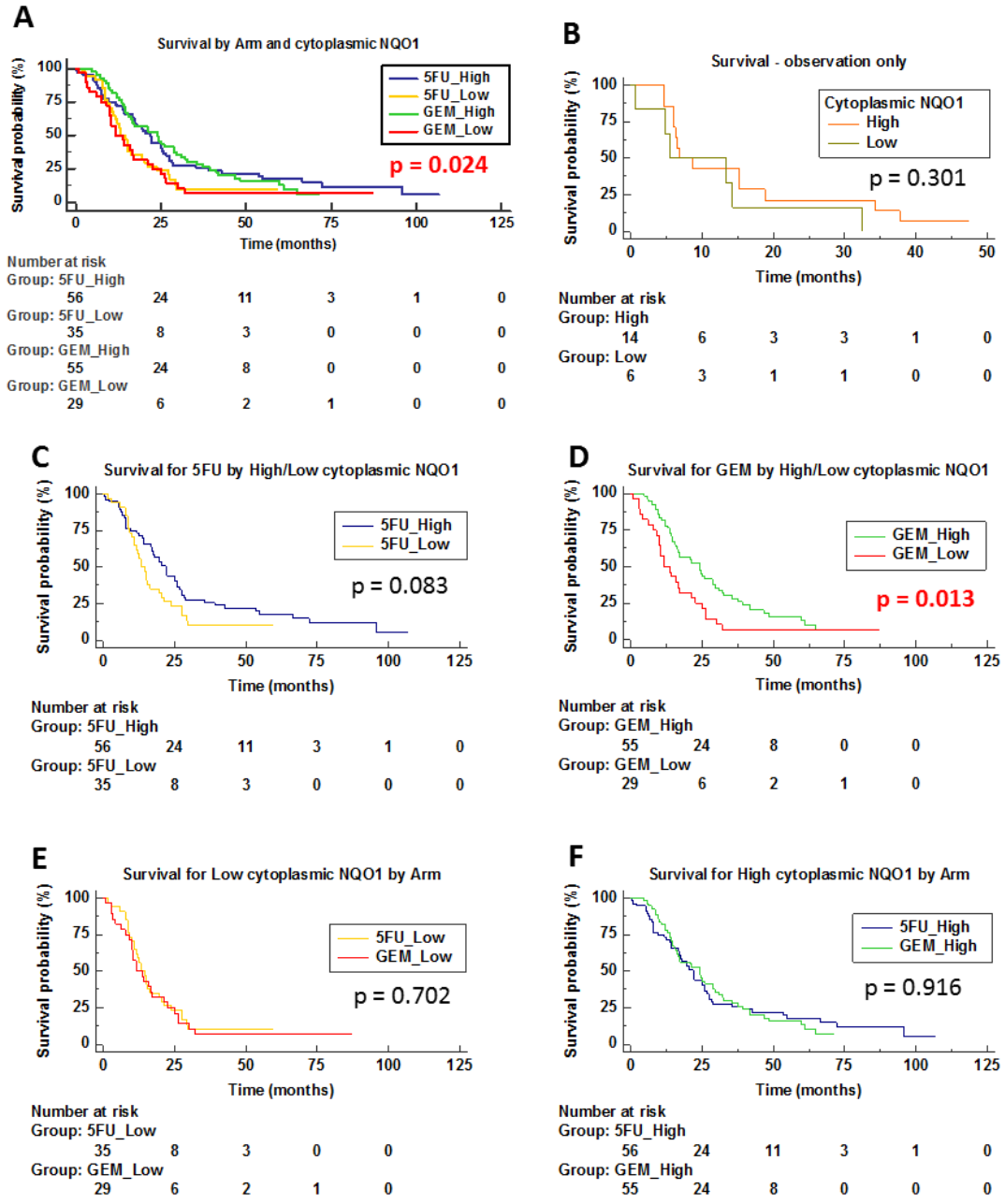

Figure 5.20. Kaplan-Meier overall survival curves stratified by (A) chemotherapy and NQO1 protein expression **(B)** observation only (resection only) and UHRF1 protein expression**; (C) 5**-Flourouracil/folinic acid and NQO1 protein expression; **(D)** Gemcitabine and NQO1 protein expression **(E)** Gemcitabine or 5FU/folinic acid treated patients expressing low NQO1 **(F)** Gemcitabine or 5FU/folinic acid treated patients expressing high NQO1. P values were determined by log-rank test. All statistical tests were 2-sided. **5FU = 5 Fluorouracil plus folinic acid; GEM = Gemcitabine.**

Table 5.10. Median survival for UHRF1 levels by treatment group. Differences between groups was determined by Kaplan-Meier curves and Log-rank test. 5FU = 5 Fluorouracil/folinic acid, GEM = Gemcitabine; CI = confidence interval Multivariate Cox proportional hazard regression analysis stratified by chemotherapy

Variable	No of patients (deaths)	Median OS (95% CI)	p
5FU_High	42 (37)	15.0 (10.9, 20.2)	0.794
5FU_Low	49 (43)	22.3 (16.4, 27.3)	
GEM_High	44 (39)	20.6 (14.6, 24.5)	
GEM_Low	35 (31)	21.3 (15.4, 31.4)	

Table 5.11. Median0 survival for NQO1 levels by treatment group. Differences between groups was determined by Kaplan-Meier curves and Log-rank test. 5FU = 5 Fluorouracil/folinic acid, GEM = Gemcitabine; CI = confidence interval Multivariate Cox proportional hazard regression analysis stratified by chemotherapy

Variable	No of patients (deaths)	Median OS (95% CI)	p
5FU_High	56 (48)	21.8 (16.9, 25.7)	0.024
5FU_Low	35 (30)	13.4 (10.9, 19.6)	
GEM_High	55 (48)	24.2 (16.3, 29.5)	
GEM_Low	29 (26)	13.7 (10.2, 16.8)	

5.2.16.3 NQO1 protein expression is not an independent predictive biomarker of response to adjuvant gemcitabine treatment.

Univariate Cox proportional hazard analysis (Table 5.12) revealed that gemcitabine treated PDAC patients with high cytoplasmic NQO1 exhibited higher overall survival with a hazard ratio (HR) of 0.55 (95% CI=0.34 to 0.89, p=0.018) compared with patients with low NQO1 cytoplasmic expression. In the case of 5FU/folinic acid treated PDAC patients, NQO1 levels were not significantly associated with better survival (HR=0.66, 95% CI=0.42 to 1.06, p=0.09) for high cytoplasmic NQO1 expressers compared with low expressers. When gemcitabine and 5FU/folinic acid treated patients were combined, NQO1 was significantly associated with survival (HR=0.59, 95% CI=0.43 to 0.84, p=0.003). Additionally, tumour stage, lymph node status, tumour grade, maximum tumour diameter and resection margin were significantly associated with overall survival (Table 5.12).

To explore the effects of several covariates on survival, a multivariable Cox proportional hazard regression model was fitted for variables that were significant ($p<0.1$ for gemcitabine treatment arm) in the univariate analysis. NQO1 protein levels did not emerge as an independent predictive factor (HR=0.69, 95% CI=0.39 to 1.2, p=0.19, for high NQO1 levels compared with low NQO1) in adjuvant gemcitabine treated patients (Table 5.13). NQO1 as a covariate in 5FU/folinic acid treated patients remained nonsignificant in the multivariate analysis (HR=0.86, 95% CI=0.51 to 1.43, p=0.56, Table 5.13).

Table 5.12. Univariate Cox proportional hazard analysis of survival factors stratified by chemotherapy*

	HR (95%) CI		
	Chemotherapy		
Characteristic	**5-FU/folinic acid**	**Gemcitabine**	**Total**
Stage	n = 110	n = 99	n = 209
1	1.00 (ref) **p=0.119**	1.00 (ref) **p=0.223**	1.00 (ref) **p=0.018**
2	1.42 (0.63 to 3.20)	1.55 (0.37 to 6.57)	1.45 (0.73 to 2.89)
3	2.07 (0.98 to 4.40)	2.35 (0.57 to 9.70)	2.15 (1.12 to 4.13)
4	1.22 (0.36 to 4.06)	1.96 (0.36 to 10.81)	1.48 (0.58 to 3.75)
Lymph node status	n = 111	n = 100	n = 211
Negative	1.00 (ref) **p=0.0003**	1.00 (ref) **p=0.085**	1.00 (ref) **p=0.0001**
Positive	2.61 (1.48 to 4.60)	1.55 (0.92 to 2.61)	2.02 (1.39 to 2.95)
Tumour grade	n = 108	n = 98	n = 206
Well	1.00 (ref) **p=0.82**	1.00 (ref) **p=0.04**	1.00 (ref) **p=0.21**
Moderate	0.76 (0.30 to 1.90)	1.07 (0.46 to 2.51)	0.92 (0.50 to 1.72)
Poor	0.83 (0.31 to 2.19)	1.97 (0.81 to 4.80)	1.25 (0.65 to 2.39)
Maximum tumour Diameter	n = 108	n = 92	n = 200
<30 mm	1.00 (ref) **p=0.250**	1.00 (ref) **p=0.014**	1.00 (ref) **p=0.016**
≥30 mm	1.27 (0.84 to 1.93)	1.78 (1.11 to 2.86)	1.46 (1.07 to 1.98)
Resection margin	n = 111	n = 100	n = 211
Negative	1.00 (ref) **p=0.068**	1.00 (ref) **p=0.153**	1.00 (ref) **p=0.019**
Positive	1.46 (0.97 to 2.20)	1.37 (0.89 to 2.10)	1.06 (1.05 to 1.91)
Diabetes	n = 107	n = 98	n = 205
No	1.00 (ref) **p=0.95**	1.00 (ref) **p=0.48**	1.00 (ref) **p=0.64**
Yes	1.02 (0.60 to 1.73)	1.21 (0.72 to 2.02)	1.09 (0.76 to 1.58)
Sex	n = 111	n = 100	n = 211
Female	1.00 (ref) **p=0.79**	1.00 (ref) **p=0.31**	1.00 (ref) **p=0.65**
Male	1.06 (0.71 to 1.58)	0.80 (0.53 to 1.23)	0.93 (0.70 to 1.25)
Age, y	n = 111	n = 100	n = 211
<60	1.00 (ref) **p=0.75**	1.00 (ref) **p=0.19**	1.00 (ref) **p=0.31**
≥60	0.94 (0.62 to 1.41)	0.74 (0.48 to 1.15)	0.86 (0.64 to 1.15)
Smoking	n = 102	n = 95	n = 197
Never	1.00 (ref) p=0.89	1.00 (ref) p=0.14	1.00 (ref) **p=0.71**
Past	0.98 (0.62 to 1.56)	1.30 (0.81 to 2.07)	1.11 (0.80 to 1.54)
Present	0.88 (0.49 to 1.57)	2.00 (1.03 to 3.90)	1.18 (0.76 to 1.82)
NQO1	n = 91	n = 84	n = 175
Low	1.00 (ref) **p=0.09**	1.00 (ref) **p=0.018**	1.00 (ref) **p=0.003**
High	0.66 (0.42 to 1.06)	0.55 (0.34 to 0.89)	0.59 (0.43 to 0.84)
UHRF1	n = 91	n = 79	n = 170
Low	1.00 (ref) **p=0.35**	1.00 (ref) **p=0.92**	1.00 (ref) **p=0.48**
High	1.24 (0.79 to 1.93)	0.98 (0.61 to 1.57)	1.12 (0.82 to 1.55)

* All statistical test were two-tailed. 5-FU = 5-Fluorouracil; CI = confidence interval; HR = hazard ratio; ref = reference

Table 5.13. Multivariable Cox proportional hazard regression analysis stratified by chemotherapy*

	HR (95%) CI		
	Chemotherapy		
Characteristic	**5-FU/folinic acid (n=85)**	**Gemcitabine (n=75)**	**Total (n=160)**
Lymph node status			
Negative	1.00 (ref)	1.00 (ref)	1.00 (ref)
Positive	3.75 (1.74 to 8.09)	2.18 (1.21 to 3.94)	2.73 (1.73 to 4.31)
	p=0.0008	**p=0.0095**	**p<0.0001**
Maximum tumour Diameter			
<30 mm	1.00 (ref)	1.00 (ref)	1.00 (ref)
≥30 mm	1.22 (0.76 to 1.95)	1.99 (1.16 to 3.42)	1.47 (1.04 to 2.08)
	p=0.41	**p=0.01**	**p=0.03**
Tumour grade			
Well	1.00 (ref)	1.00 (ref)	1.00 (ref)
Moderate	0.47 (0.11 to 2.04)	1.23 (0.50 to 3.01)	0.91 (0.44 to 1.91)
	p=0.32	**p=0.65**	**p=0.81**
Poor	0.67 (0.15 to 3.01)	2.46 (0.94 to 6.43)	1.44 (0.66 to 3.11)
	p=0.60	**p=0.07**	**p=0.36**
NQO1			
Low	1.00 (ref)	1.00 (ref)	1.00 (ref)
High	0.86 (0.51 to 1.43)	0.69 (0.39 to 1.2)	0.73 (0.50 to 1.05)
	p=0.56	**p=0.19**	**p=0.09**

* All statistical test were two-tailed. 5-FU = 5-Fluorouracil; CI = confidence interval; HR = hazard ratio; ref = reference

5.3 Discussion

This study is the first analysis in advanced pancreatic cancer patients to show an interesting link between an *NQO1* C609T (rs1800566) germline polymorphism and survival. Of the three SNPs investigated (one each for *NRF2* (rs2886162), *NQO1* (rs1800566) and *SRXN1* (rs6053666) only the *NQO1* SNP was associated with survival. Patients with the *NQO1* CC major homozygous genotype had a significantly unfavourable outcome compared to patients with TT and CT *NQO1* genotypes combined. Individuals with homozygous *NQO1* TT express little or no active enzyme, the heterozygous CT express intermediate activity with a half-life of 1.2 h and homozygous major CC have a half-life of over 18 h[169]. Although, *NQO1* (rs1800566) SNP was the only individual SNP associated with survival, our analysis indicates that combining pure heterozygous and homozygous minor genotypes for both *NQO1* and *SRXN1* SNPs gave a better survival difference. This suggests that combining biomarkers may be a better strategy for prognosticating patient subgroups. In this study, we could not establish an association between any SNP and a particular type of treatment.

To the best of our knowledge, there are no published reports on the prognostic or predictive effects of the germline *NQO1* C609T polymorphism in advanced pancreatic cancer. The *NQO1* SNP has been studied in other cancers where Fagerholm *et al.*[171] and Kolesar *et al.*[170] reported a poor OS for homozygous minor TT *NQO1* C609T in breast and lung cancer respectively. Fagerholm *et al*. was a Finnish study undertaken in breast cancer patients [n=2,167 with 71 (3.3%) homozygous TT minor] who had

surgery followed by adjuvant anthracycline-based chemotherapy with epirubicin[171]. Similarly, the study by Kolesar *et al.* [n=152 with 24 (16%) homozygous TT minor] involved non-small cell lung cancer (NSCLC) patients (where 85% of the patients were Caucasians) who had surgical resection for stages II and IIIa NSCLC followed with radiotherapy or combined radiotherapy plus chemotherapy cisplatin and etoposide[170]. In both studies, major and heterozygous (CC and CT) genotypes were grouped as one category (as the survival curves of NQO1 heterozygotes resembled that of homozygous wild-types[171]) and compared against TT; CC/CT genotypes had a better OS than homozygous minor TT. In our study however (n=140), the comparison was between *NQO1* homozygous major CC and heterozygous and homozygous minor CT/TT as there was just one TT patient. Nevertheless, a significant difference in survival between CC and CT/TT was observed in our study (*UK based study*) and it is possible that the differences between these studies and ours may be related to disease-specific or treatment-specific effects since *NQO1* C609T polymorphism was investigated in patients with different cancers[170,171] who had surgical resection followed by adjuvant chemotherapy with different treatment agents compared to patients in our dataset who had advanced pancreatic cancer (and were therefore not suitable for surgical resection) and received systemic gemcitabine based regimens[29,30].

This study had some limitations. Analysis, particularly for the TeloVac patients, was confined to the small number of patients available for this study. It was not possible to meaningfully investigate whether the minor homozygote TT for *NQO1* was prognostic for OS as only one patient with *NQO1* TT was observed in this study.

Furthermore, the lack of a treatment naïve (observation only) group in this study limits our conclusion on whether this *NQO1* polymorphism is only prognostic of survival or is also predictive of response to treatment. Analysis of this *NQO1* SNP in the context of chemotherapy and in an observation only arm will permit the assessment of this SNP as a prognostic only survival variable or a predictive treatment specific response variable. However, observation only without any form of intervention would be unethical. A predictive biomarker is more useful clinically than a prognostic biomarker, as it relates to treatment.

In our study, the nuclear expression of UHRF1 is as previously reported[80] and the pattern of NQO1 expression (cytoplasmic and nuclear) is also consistent with previous studies[160,239]. However, the stromal expression of NQO1 in PDAC reported in our study is a new observation.

In the context of normal intralobular and interlobular ducts and ductules, we went further to examine the expression of UHRF1 and NQO1. UHRF1 was not detected in intralobular ductules and ducts nor in interlobular ducts of normal pancreas consistent with our previous observation that UHRF1 is infrequently detected in normal pancreatic ductal cells[80]. In matched tissue sections, NQO1 was also not detectable in intralobular ductules and ducts of normal pancreas. However, in interlobular ducts of normal pancreas, NQO1 was expressed in the cytoplasm. Whether the histological location of a pancreatic duct (intralobular or interlobular) has any implication on the expression of NQO1 in normal pancreas is a question that

will require further investigation. Overall, future studies involving larger numbers of normal pancreas tissue samples will be beneficial in elucidating these findings.

We have previously reported that UHRF1 depletion in pancreatic cancer cell lines was accompanied by down regulation of Nrf2 and of Nrf2 downstream proteins including NQO1[80]. In this study, our finding of a significant association between NQO1 and UHRF1 expression in PDAC tissues is consistent with a regulatory relationship between UHRF1 and antioxidant protein NQO1. In the analysis of tissue levels of UHRF1 and NQO1, manual scoring was used as it was more accurate. Despite attempts, we could not use Definiens software analysis to complement manual scoring because of the propensity of Definiens to computational errors.

This study is the first to report that high tumour NQO1 protein levels in PDAC patients is associated with better survival. There was no sufficient evidence to suggest that in adjuvant gemcitabine treated group, NQO1 protein levels were associated with response to treatment. In order to investigate the prognostic effect of NQO1 expression on overall survival, a limited number of control group (resection only) were examined but no evidence was found that NQO1 protein levels were prognostic.

Our finding that NQO1 expression was not associated with any patient clinicopathological characteristic is in contrast to the findings by Ji *et al.* who found high tumoural levels of NQO1 to be significantly associated with lymph node metastasis and TNM stage in PDAC[160]. Their findings further conflicts ours where they reported a poor overall survival in patients who expressed high levels of NQO1.

Moreover in our study, high NQO1 levels were associated with better survival in gemcitabine treated patients and high levels of NQO1 were also associated with better overall survival when all treatment arms, including gemcitabine, 5FU and observation only were considered. The discrepancy between our findings and Ji *et al.*[160] may be due to differences in patient cohorts; our study evaluated PDAC in patients from 159 pancreatic cancer centers in Europe, Australasia, Japan and Canada[7] while the study by Ji *et al.*[160] was undertaken in a Chinese cohort. Secondly, it was not stated whether their patients received adjuvant treatment.

Multivariable Cox proportional hazard analysis in gemcitabine treated patients, revealed that NQO1 expression was not an independent predictive factor in PDAC, suggesting that in the presence of other covariates, NQO1 protein levels are not significantly associated with survival.

The basis for the increased survival associated with patients receiving gemcitabine requires further investigation. Anticancer agents such as β-Lapachone have been reported to require NQO1 specific activation to kill cancer cells through elevated ROS levels[148]. The conventional mechanism of action of gemcitabine is by interfering with DNA synthesis[22]. More recently, gemcitabine has been reported to induce pancreatic cancer cell death through ROS mediated effects[240]. It is likely that the full spectrum of the mechanisms of action of gemcitabine are not yet fully understood.

In this evaluation of UHRF1 in ESPAC material, UHRF1 expression was upregulated in PDAC tissues, consistent with our previous observation[80]. An association with UHRF1 expression and survival could not be established, in agreement with the study by Abu-

Alainin *et al.*[80] but contrary to the study undertaken by Cui *et al*.[81], where a high UHRF1 expression was associated with poor survival outcome. The difference could be due to patient cohort; the study by Cui *et al.* was undertaken in a Chinese cohort, reflecting a possible difference in genetic background. Furthermore, in Cui *et al*. UHRF1 expression was cytoplasmic. In our study, patients were recruited from 159 pancreatic cancer centers in Europe, Australasia, Japan and Canada[7]. In addition, UHRF1 localization in our study was nuclear. Moreover, UHRF1 has been described to be a nuclear protein[62].

A surprising finding in this study was the inverse relationship between UHRF1 expression and diabetes. Diabetes is an area of intense interest in our research group and this finding will be followed up. Although, we also reported here that UHRF1 expression was significantly associated with tumour staging, this may be due chance association and further evaluation will be required.

Finally, we report an interesting observation of a limited number of PDAC samples on the immunoreactivity of subgroups of lymphoid cells to UHRF1. Obata Y. *et al.* recently reported on the epigenetic function of UHRF1 in promoting the proliferation and maturation of colonic regulatory T (Treg) cells[241]. Treg cells regulate immune responses and prevent autoimmune or severe immune responses[242]. Obata Y. *et al.* showed that UHRF1 was required for the maintenance of gut immunological homeostasis by demonstrating that colonization of germ-free mice with gut microbiota upregulated UHRF1 in intestinal Treg cells and prevented the development of severe colitis an effect that was observed in T cell-specific deficient

UHRF1 mice. They further showed that in T cell-specific deficient UHRF1 mice, p21 (cyclin-dependent kinase inhibitor) promoter was hypomethylated which resulted in Treg cell-cycle arrest[241]. The study by Obata Y. *et al.* brings to focus the subsets of UHRF1 immunoreactive lymphoid cells identified in this thesis as to their possible role in PDAC tissues. Understanding the function of this lymphoid subsets in PDAC tissues may be instrumental to manipulating the immune system in favour of PDAC treatment. NQO1 was not immunoreactive to lymphoid cells.

We have also shown in that UHRF1 was localized to a histologically defined zone within the intestinal epithelium, we sought to determine if this relationship was maintained for NQO1 in matched normal intestinal epithelium of duodenum and colon; interestingly, an inverse relationship was observe but no immediate explanation could be advanced for this difference other than they are not pancreatic in origin. To confirm these observations, larger number of benign samples will be required. As mentioned previously, the duodenum and colon were not the focus of my thesis but I reasoned it was good practice to mention these observations as they were present as orientation cores on the PDAC TMAs stained for UHRF1 and NQO1.

Taken together, the results of this chapter indicate that NQO1 is not an independent predictive biomarker in pancreatic cancer patients receiving adjuvant gemcitabine and may therefore not suitable as a biomarker for guiding patient treatment stratification.

6 OVERALL DISCUSSION

The overall aims of my thesis were to elucidate the role of UHRF1 on Nrf2 function in (I) pancreatic cancer cells (II) pancreatic stellate cells (PSCSs) and (III) to identify potentially predictive antioxidant enzyme biomarkers that can inform patient stratification for personalised pancreatic cancer treatment.

UHRF1 was observed to be expressed in up to 90% of the PDAC tissues examined and contributed to PDAC tumourigenesis since its depletion was associated with pancreatic cancer cell growth inhibition, cell cycle arrest, Nrf2 downregulation and increased oxidative stress[80]. The transcriptional evidence for the regulation of Keap1 mRNA by UHRF1 presented in this thesis suggests the possibility that UHRF1, in cooperation with other factors or regulators, may be required to effectively maintain inhibition of Keap1 transcription. Furthermore, UHRF1 may be involved with transcriptional regulation of Nrf2 but more studies will be helpful to confirm this regulatory pathway.

Our intention to investigate the role of UHRF1 in the redox response in PSCs isolated from Nrf2-null mice was hampered by our finding that Nrf2-null PSCs could not survive in culture. Nevertheless, we successfully examined the expression of UHRF1 in human PDAC cell lines, pancreatic stellate cells (PSCs) and *in situ* in human PDAC tissue samples. Interestingly, UHRF1 was not globally expressed in PSCs but only present in a small subset of PSCs and lymphoid cells indicating the possibility that UHRF1 may be most relevant in these subsets. Further work will be required to delineate the functional role of these subsets of UHRF1 positive cells.

Nrf2 is a master regulator of the antioxidant system that protects cells from oxidative, xenobiotic and electrophilic stress[243]. In cancers, including pancreatic cancer, the Nrf2 cytoprotective function is not only hijacked but it is constitutively expressed at higher levels to favour tumour progression and resistance to chemo-radiotherapy[99]. A greater understanding of how Nrf2 and its downstream targets such as NQO1 are relevant to cancer treatment needs to be explored.

The *NQO1* (rs1800566) SNP may be prognostic of overall survival in advanced pancreatic cancer patients receiving gemcitabine-based therapies but the *SRXN1* (rs6053666) SNP and the *NRF2* (rs2886162) SNP were not associated with overall survival. A combination of *NQO1* (rs1800566) and *SRXN1* (rs6053666) SNPs was however associated with greater overall survival than observed for either *NQO1* or *SRXN1* SNPs alone, suggesting the potential for combining SNPs as prognostic biomarkers.

The effect of single nucleotide polymorphisms (SNPs) involving oxidative stress and drug metabolising enzymes on predicting response to chemotherapy in pancreatic cancer may be achieved by association studies[164,244] (such as genome-wide association studies, GWAS, where candidate SNPs can be interrogated in respect to their association with response to therapy), proteomic and functional studies. It is also important to appreciate that the effect of SNPs on response to therapy in cancers may be the contributing effect of multiple SNPs or environmental factors[164].

The functional effect of *NQO1* rs1800566 SNP are well established[169]; *NQO1* CC wild-type is a functionally active enzyme, CT is only partially functional and TT has very reduced or no activity. In our study, we could not fully understand or explain the reason(s) for the differences in survival between germline (blood cell-derived) NQO1 CC genotype which was found to be associated with poor survival in the combined retrospective ViP and TeloVac trial data and high pancreatic cancer tissue NQO1 protein levels which was found to be associated with better survival in retrospective ESPAC-1 and ESPAC-3 adjuvant trial data. Given that wild-type NQO1 CC genotype is known to be fully functional (active and strongly expressed protein)[171], it was our expectation that the survival outcomes would be identical between CC NQO1 genotypes in the combined ViP and TeloVac trials and high NQO1 protein expression in ESPAC-1 and ESPAC-3 trials. The patient cohorts in the TeloVac and ViP trials had advanced PDAC and were therefore not suitable for surgical resection while the ESPAC patients had surgical resection; we can only speculate that these are possible reasons for the observed differences in survival. Secondly, it has been reported that there is a high degree of concordance between germline (inherited) DNA SNPs and somatic (acquired tumour DNA SNPs) suggesting the same genotype SNPs in germline DNA also exists in tumour DNA[245]. In our study however, germline DNA SNPs and tumour DNA SNPs were not compared. Future studies will be important to determine the concordance between germline DNA SNPs and tumour DNA SNPs in PDAC. Ideally, cancer cells would be separated from stromal cells which may interfere with the interpretation of tumour DNA SNP analysis if homogenous cell populations are not used.

The survival of patients with pancreatic cancer may be improved by using biomarkers capable of predicting response to therapy[146,246]. To conclude, biomarkers are sorely needed to predict (I) patients mostly likely to respond to current therapies and (II) patients that will perform better on novel therapies.

6.1 Future directions

Potentially interesting areas for future research arising from this thesis include the following:

Given the role elucidated for UHRF1 in regulating the Keap1-Nrf2 pathway (Keap1 repression leading to the activation of Nrf2) in pancreatic cancer cell lines, it will be important to determine the methylation status of *KEAP1* promoter in PDAC tissue samples. This will help confirm if this is the mechanism for Keap1 repression in pancreatic cancer.

In this thesis, although there was no strong evidence for a down-regulation of Nrf2 mRNA following 72 h of UHRF1 knockdown, a marginal decrease in Nrf2 mRNA was observed at 72 h time point. In order to investigate this further and exclude a transcriptional regulation of Nrf2 by UHRF1, additional analysis such as examination of the effects of UHRF1 knockdown on Nrf2-null cells, chromatin immunoprecipitation (ChIP) experiments and examination of the effects of UHRF1 depletion or overexpression on Nrf2 in Keap1-null cells will be helpful.

The observation that a subset PSCs and lymphoid cells expressed UHRF1 may indicate a special functional role for these subsets of cells or a cell cycle effect as pancreatic cancer cells have been reported to have a peak in UHRF1 expression at G_2M phase of

the cell cycle[80]. To investigate further, Ki-67 protein expression (a cellular marker of proliferation) and stem cell markers may be assessed in these UHRF1 positive subsets of PSCs and lymphoid cells. Additionally, the cytotoxicity status of UHRF1 positive lymphoid cells may also be assessed for granzyme B or perforin expression.

We also made an interesting observation on a limited number of normal intestinal tissues. The restricted expression of UHRF1 to the basal crypts of the normal duodenum and colonic epithelium suggests the possibility of a stem cell-like role in this basal layer of the intestinal epithelium. To determine if this pattern of expression is a recurring theme in normal colon and duodenum, larger numbers of these normal intestinal tissues will need to be stained and examined for UHRF1.

The observation that Nrf2-null mice develop early signs of pancreatitis suggest a protective role for Nrf2 in preventing pancreatitis. This Nrf2-null mice may potentially be used as a model for pancreatitis research.

Finally, the *NQO1* CC genotype has been reported to translate into a functionally active NQO1 protein compared with CT with reduced activity and TT with little or no activity[169]. We reported that patients with germline CC *NQO1* SNP C609T polymorphism were associated with poor survival in advanced pancreatic cancer patients whereas in adjuvant chemotherapy treated pancreatic cancer patients, we reported that high tumour tissue NQO1 protein expression was associated with better survival. Determining the genotype status between *NQO1* germline SNP and *NQO1* tumour SNP as well as the NQO1 tumour tissue protein expression will further illuminate the concordance between these 3 levels of translational interest.

7 APPENDICES

Appendix 1. Pyrogram report for *KEAP1a* primers

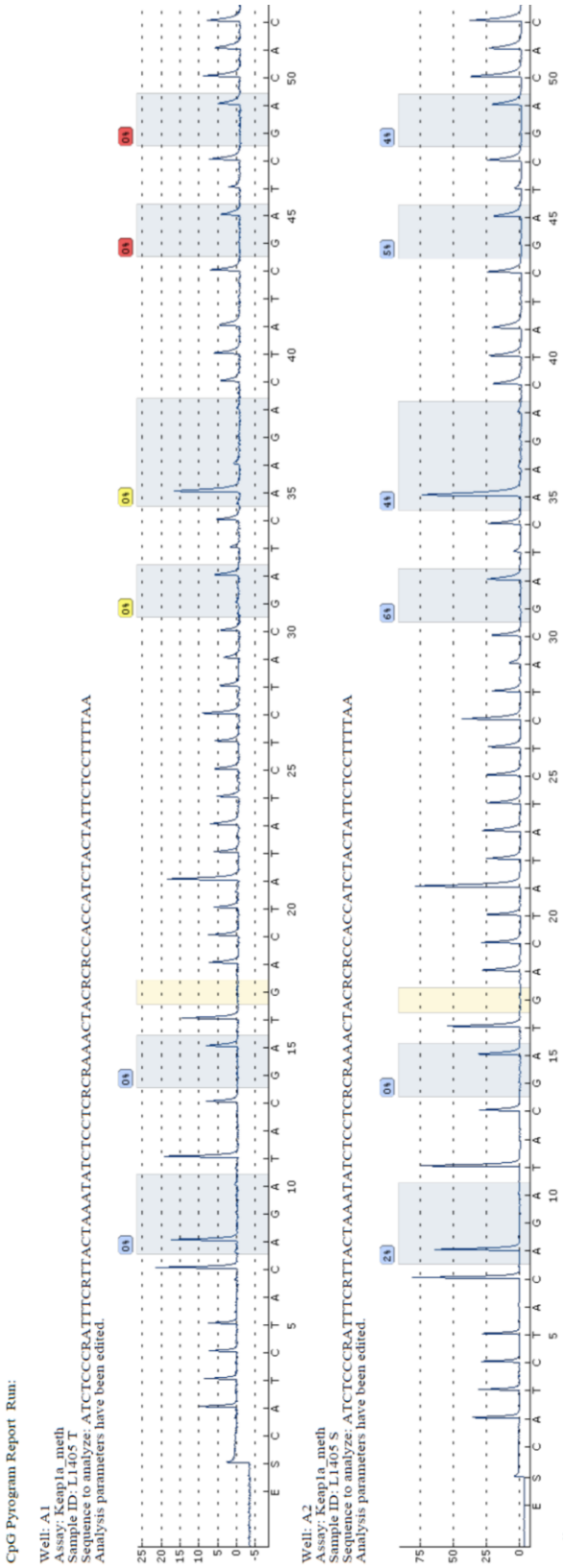

Appendix 2. Pyrogram report for *KEAP1a* primers

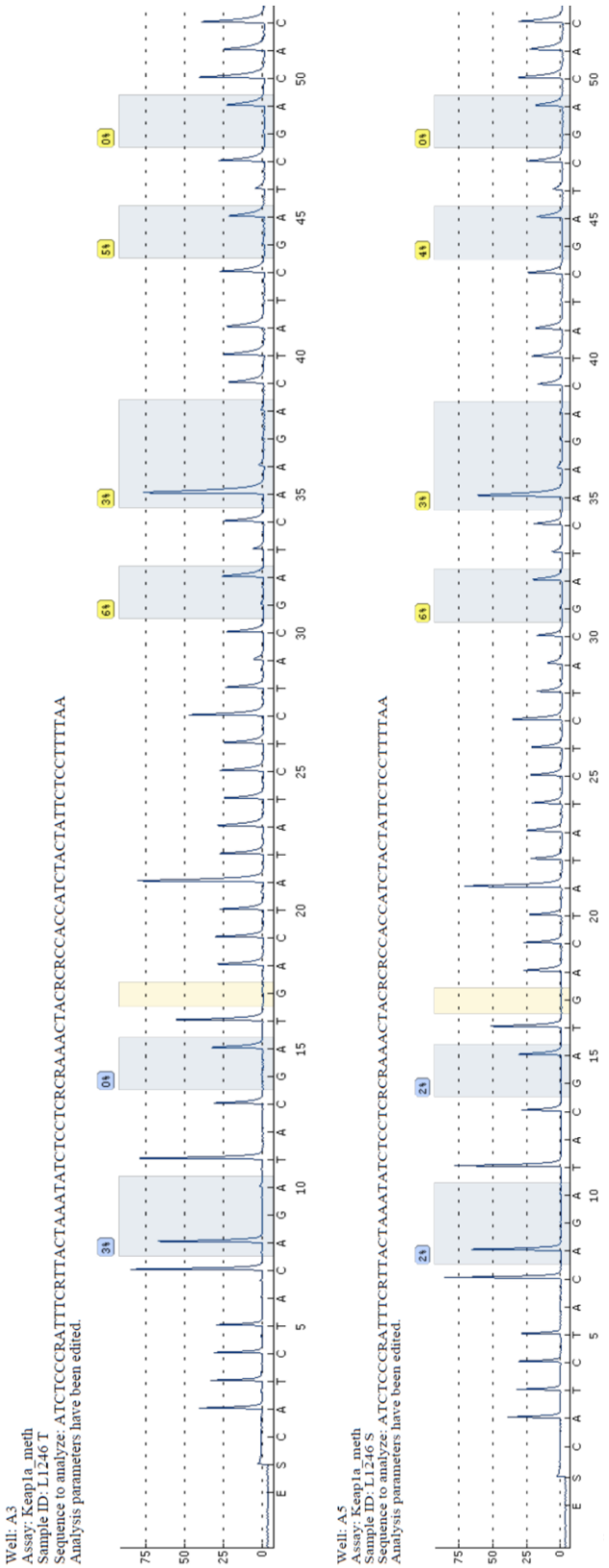

Appendix 3. Pyrogram report for *KEAP1b* primers

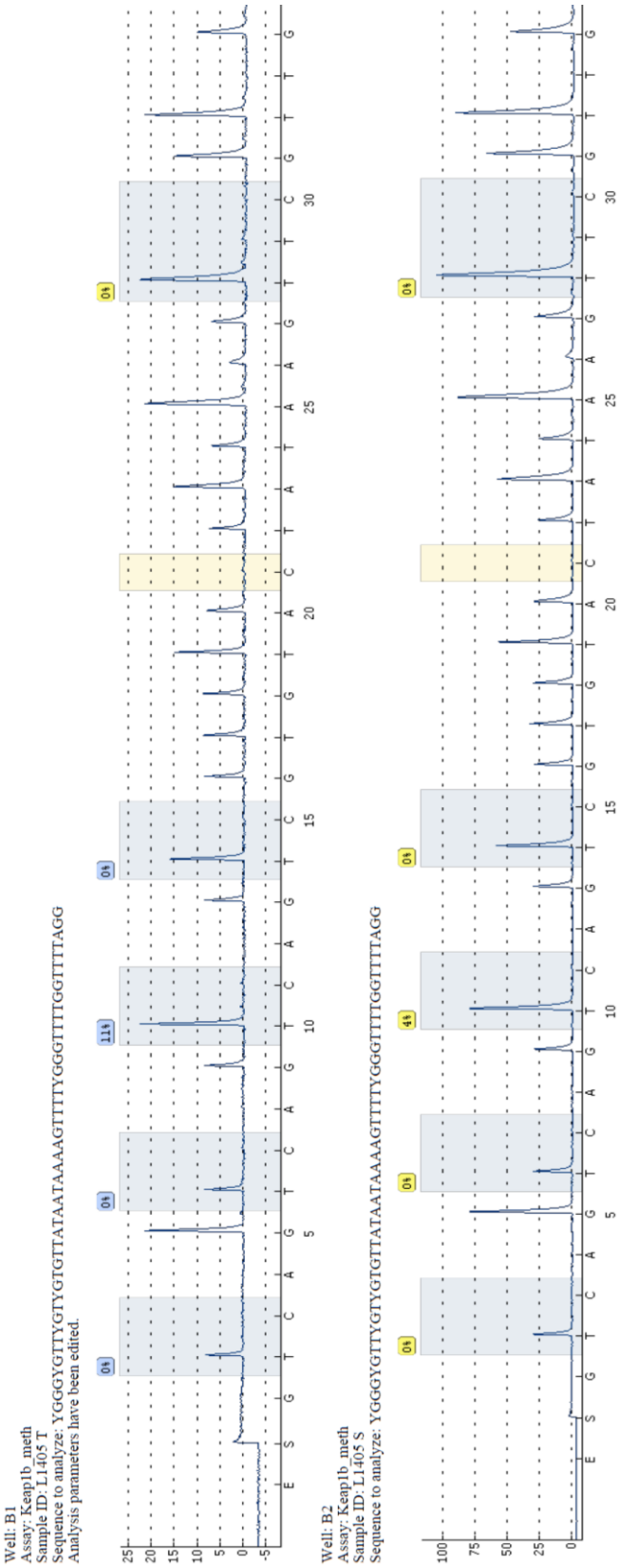

Appendix 4. Pyrogram report for *KEAP1b* primers

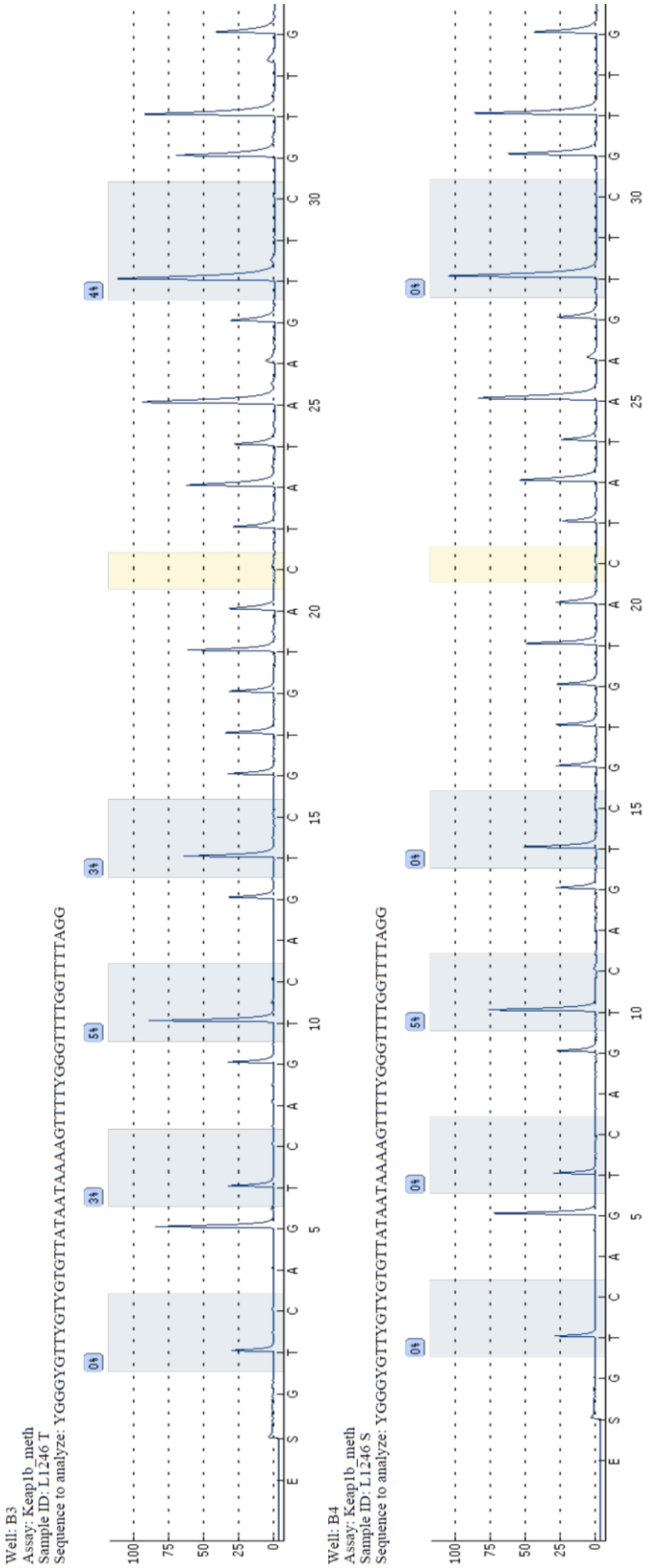

Appendix 5. Table A1 – Summary statistics and results of univariate models for *NRF2/NQO1/SRXN1* ViP data

	Overall				Gemcitabine				Gemcitabine + Vandetanib			
Prognostic Variable	**No patients (deaths)**	**Median OS (95% CI)**	**HR**	**P**	**No patients (deaths)**	**Median OS (95% CI)**	**HR**	**P**	**No patients (deaths)**	**Median OS (95% CI)**	**HR**	**P**
NRF2				**0.174**				**0.258**				**0.747**
AA	18(16)	12.11(4.84,		(0.144 AG	8(7)	12.70(3.59,23.02)		(0.218 AG	10(9)	4.87(1.55,17.86)		(0.470 AG
AG	49(48)	17.86)	1.66(0.93,2.95)	and GG	21(20)	8.16(4.01,10.86)	1.96(0.82,4.68)	and GG	28(28)	9.97(7.70,11.48)	1.34(0.63,2.85)	and GG
GG	30(29)	8.95 (7.70,11.02)	1.26(0.68,2.33)	consolidated)	17(16)	10.86(4.74-16.32)	1.36(0.56,3.30)	consolidated)	13(13)	8.22(3.19,13.03)	1.22(0.51,2.92)	consolidated)
		9.24 (7.73,11.48)										
NQO1				**0.084**				**0.465**				**0.105**
CT&TT	36(33)	11.02(6.35,11.15)	0.68(0.44,1.06)		17(15)	8.95(4.74,16.32)	0.79(0.42,1.49)		19(18)	8.32(4.21,12.43)	0.60(0.32,1.13)	
CC	61(60)	8.91(6.35,11.15)			29(28)	9.37(5.00,11.87)			32(32)	11.41(7.73,11.48)		
SRXN1				**0.583**				**0.965**				**0.091**
CC	6(6)	13.03(1.87,NK)			2(2)	1.87(1.87,NK)			4(4)	13.03(7.40,NK)		
CT	58(56)	10.20(6.55,12.80)	1.20(0.51,2.78)		25(24)	10.86(6.35,15.56)	0.84(0.20,3.59)		33(32)	10.20(4.84,12.80)	1.42(0.50,4.05)	
TT	33(31)	8.16(5.00,11.48)	1.45(0.60,3.51)		19(17)	8.16(4.87,12.7)	0.81(0.18,3.58)		14(14)	7.82(3.39,11.15)	2.86(0.90,9.05)	

Table A2 – *p*-values for *NRF2/NQO1/SRXN1* when fitted to multivariate model for ViP patients

	Multivariate model		
Prognostic Variable	**No patients (deaths)**	**HR**	**p**
NRF2			**0.117**
AA	18(16)		
AG	49(48)		
GG	30(29)		
NQO1			**0.294**
CT&TT	36(33)		
CC	61(60)		
SRXN1			**0.723**
CC	6(6)		
CT	58(56)		
TT	33(31)		

Appendix 6. Table A3– Summary statistics and results of univariate models for NRF2/NQO1/SRXN1 TeloVac data

	Overall				Arm 1				Arm 2				Arm 3			
Prognostic Variable	**No patients (deaths)**	**Median OS (95% CI)**	**HR (95% CI)**	**P**	**No patients (deaths)**	**Median OS (95% CI)**	**HR (95% CI)**	**P**	**No patients (deaths)**	**Median OS (95% CI)**	**HR**	**P**	**No patients (deaths)**	**Median OS (95% CI)**	**HR**	**P**
Nrf2																
AA	12 (7)	5.19(0.92,NK)			8(4)	4.77(0.92,NK)			4(3)	5.19(0.82,NK)			0(0)	-	-	
AG	26 (14)	9.73(4.01,14.37)	0.69(0.28,1.72)		12(7)	6.01(1.81,NK)	0.55(0.14,2.11)		5(2)	11.77(2.20,NK)	0.53(0.09,3.23)		9(5)	8.94(1.32,NK)	**NA**	
GG	5 (2)	8.98(3.22,NK)	0.54(0.11,2.61)	**0.648** (0.294 AG and GG consolidated)	4(1)	NK(3.22,NK)	0.31(0.04,2.92)	**0.504** (0.294 AG and GG consolidated)	1(1)	NK	1.53(0.14,16.52)	**0.667** (0.641 AG and GG consolidated)	0(0)	-	-	**NA**
NQO1																
TT	0(0)	-			0(0)	-			0(0)	-			0(0)			
CT	19(7)	11.34(8.94,NK)			8 (2)	14.37(1.74,NK)			7(3)	11.34(0.82,NK)			4(2)	8.94(8.94,NK)		
CC	24(16)	5.19(3.22,11.77)	2.49(1.01,6.15)	**0.038**	16 (10)	4.80(1.71, NK)	6.41(0.82,50.2)	**0.025**	3(3)	5.19(2.20,NK)	2.48(0.49,12.48)	**0.278**	5(3)	5.33(1.32,NK)	1.27(0.20,8.02)	**0.798**
SRXN1																
CC	6(4)	2.20(0.92,NK)	1.45(0.45,4.64)		4(2)	1.71(0.92,NK)	1.27(0.24,6.77)		2(2)	2.20(2.20,NK)	1.61 (0.22,11.69)		0(0)	-		
CT	17(8)	11.34(4.01,NK)	0.71(0.28,1.77)		9(4)	12.23(3.22,NK)	0.71(0.19,2.65)		4(2)	11.34(5.19,NK)	0.90(0.13,6.44)		4(2)	9.73(4.01,NK)	0.82 (0.14,5.00)	
TT	20(11)	8.94(1.81,NK)		**0.498**	11(6)	6.01(1.35,NK)		**0.775**	4(2)	8.98(0.82,NK)		**0.838**	5(3)	5.33(1.32,NK)		**0.832**

Arm1-Gemcitabine + Capecitabine alone (chemotherapy); Arm2-Chemotherapy + sequential immunotherapy; Arm3-Chemotherapy + concurrent immunotherapy

Table A4 – p-values for *NRF2/NQO1/SRXN1* when fitted to multivariate model – TeloVac patients

	Multivariate Model		
Prognostic Variable	**No patients (deaths)**	**HR (95% CI)**	**P**
NRF2			**0.385**
AA	12 (7)		
AG	26 (14)		
GG	5 (2)		
NQO1			**0.053**
TT	0(0)		
CT	19(7)		
CC	24(16)	2.46 (0.99,6.10)	
SRXN1			**0.490**
CC	6(4)		
CT	17(8)		
TT	20(11)		

Appendix 7. Table A5. ViP data patient demographics and multivariate models without *NRF2/NQO1/SRXN1*

Prognostic Variable	No patients (deaths)	Median (IQR)	HR	P (multivariate model)
Treatment				**0.263**
Gem+Vandetanib	51(5)			
Gem+Placebo	46(43)			
Histology				**0.269**
Pancreatic ductal adenocarcinoma	85(81)			
Undifferentiated carcinoma of the pancreas	12(12)			
ECOG				**<0.001**
Fully active	28(26)		0.29 (0.13,0.67)	
Ambulatory (work able)	58(56)		0.46 (0.21,0.96)	
Ambulatory (not work able)	11(11)			
Stage				**0.233**
Locally advanced	31(29)			
Metastatic	66(64)			
Tumour Site				**0.170**
Pancreas – head	51(48)			
Pancreas – tail	13(13)			
Pancreas – uncinate	7(7)			
Pancreas - body	26(25)			
Differentiation Status				**0.027** (but excluded from AIC model)
Undifferentiated	3 (3)		7.14 (1.59,32.07)	
Poor	17 (16)		2.99 (1.14,7.83)	
Moderate	17 (16)		1.83 (0.70,4.77)	
Well	8 (8)			
Not Known	52 (51)		2.88 (1.22,6.83)	
Sex				**0.240**
Female	43 (42)			
Male	54 (51)			
Age	97(93)	67(61,73)		**0.358**
Log CA19-9	93(89)	6.9(5.4,8.5)	1.18 (1.07,1.30)	**0.008**

Appendix 8. Table A6. TeloVac data patient demographics and multivariate models without NRF2/NQO1/SRXN1

Prognostic Variable	No patients (deaths)	Median (IQR)	HR	P (multivariate model)
Treatment				
Gem+Vandetanib				
Gem+Placebo				
Histology				
Pancreatic ductal adenocarcinoma				
Undifferentiated carcinoma of the pancreas				
ECOG				
Fully active				
Ambulatory (work able)				
Ambulatory (not work able)				
Stage				
Locally advanced				
Metastatic				
Tumour Site				
Pancreas – head				
Pancreas – tail				
Pancreas – uncinate				
Pancreas - body				
Differentiation Status				
Undifferentiated				
Poor				
Moderate				
Well				
Not Known				
Sex				**0.471**
Female	23(11)			
Male	20(12)			
Age				
Log CA19-9	42(23)	6.90(5.16,8.92)	1.25(1.05,1.47)	**0.007**
Stratum *(consolidation of Stage and ECOG)*				**0.320**
1	5(4)			
2	7(4)			
3	1(0)			
4	8(4)			
5	18(7)			
6	4(4)			
Arm				**0.353**
Arm 1	24(12)			
Arm 2	10(6)			
Arm 3	9(5)			

Appendix 9. Table A7. Combined data patient demographics and multivariate models without *NRF2/NQO1/SRXN1*

Prognostic Variable	No patients (deaths)	Median (IQR)	HR	P (multivariate model)
Treatment				
Gem+Vandetanib				
Gem+Placebo				
Histology				
Pancreatic ductal adenocarcinoma				
Undifferentiated carcinoma of the pancreas				
ECOG				
Fully active				
Ambulatory (work able)				
Ambulatory (not work able)				
Stage				
Locally advanced				
Metastatic				
Tumour Site				
Pancreas – head				
Pancreas – tail				
Pancreas – uncinate				
Pancreas - body				
Differentiation Status				
Undifferentiated				
Poor				
Moderate				
Well				
Not Known				
Sex				**0.871**
Female	66(53)			
Male	74(63)			
Age				
Log CA19-9	135(112)	6.91(5.31,8.67)	1.23(1.12,1.34)	**<0.001**
Stratum *(consolidation of Stage and ECOG)*				
1				
2				
3				
4				
5				
6				
Arm				
Arm 1				
Arm 2				
Arm 3				

Table A8 – p-values for treatment interactions by trial

Study	p-value for treatment interaction
VIP	
NRF2	0.702 (0.634 AG and GG consolidated)
NQO1	0.614
SRXN1	0.296
TeloVac	
NRF2	0.584 (0.690 AG and GG consolidated)
NQO1	0.371
SRXN1	0.913

Appendix 10. Predictive effect of individual SNPs on treatment

Effects of *NRF2* SNPs on treatment

Covariates	HR (95% CI)	P
ECOG	1.75 (1.195, 2.571)	0.004
NRF2 AG	2.29 (0.957, 5.474)	0.063
NRF2 GG	1.14 (0.463, 2.789)	0.781
NRF2 AA: Arm Vandetanib	1.07 (0.389, 2.949)	0.894
NRF2 AG: Arm Vandetanib	0.78 (0.434, 1.408)	0.413
NRF2 GG: Arm Vandetanib	1.46 (0.683, 3.105)	0.33

Effects of *NQO1* SNPs on treatment

Covariates	HR (95% CI)	P
ECOG	1.45 (0.996, 2.116)	0.053
NQO1 TT/CT	0.75 (0.399, 1.416)	0.378
NQO1 CC: Arm Vandetanib	1.11 (0.653, 1.879)	0.704
NQO1 TT/CT: Arm Vandetanib	1.1 (0.548, 2.224)	0.782

Effects of *SRXN1* SNPs on treatment

Covariates	HR (95% CI)	P
ECOG	1.55 (1.091, 2.214)	0.015
SRXN1 TT	0.87 (0.468, 1.619)	0.661
SRXN1 CC/CT: Arm Vandetanib	0.89 (0.534, 1.493)	0.665
SRXN1 TT: Arm Vandetanib	2.02 (0.97, 4.206)	0.06

Appendix 11. Predictive effect of combined *SRXN1* and *NQO1* SNPs on treatment

Effects of combined *SRXN1* and *NQO1* SNPs on treatment

Covariates	HR (95% CI)	P
SRXN1_NQO1 group 2 &3	0.83 (0.403, 1.701)	0.607
SRXN1_NQO1 group 4	0.80 (0.331, 1.933)	0.62
SRXN1_NQO1 group 1: Arm Vandetanib	1.69 (0.711, 4.038)	0.234
SRXN1_NQO1 group 2& 3: Arm Vandetanib	1.36 (0.77, 2.408)	0.288
SRXN1_NQO1 group 4: Arm Vandetanib	0.79 (0.335, 1.851)	0.584

Appendix 12. Matched UHRF1 and NQO1 expression in PDAC

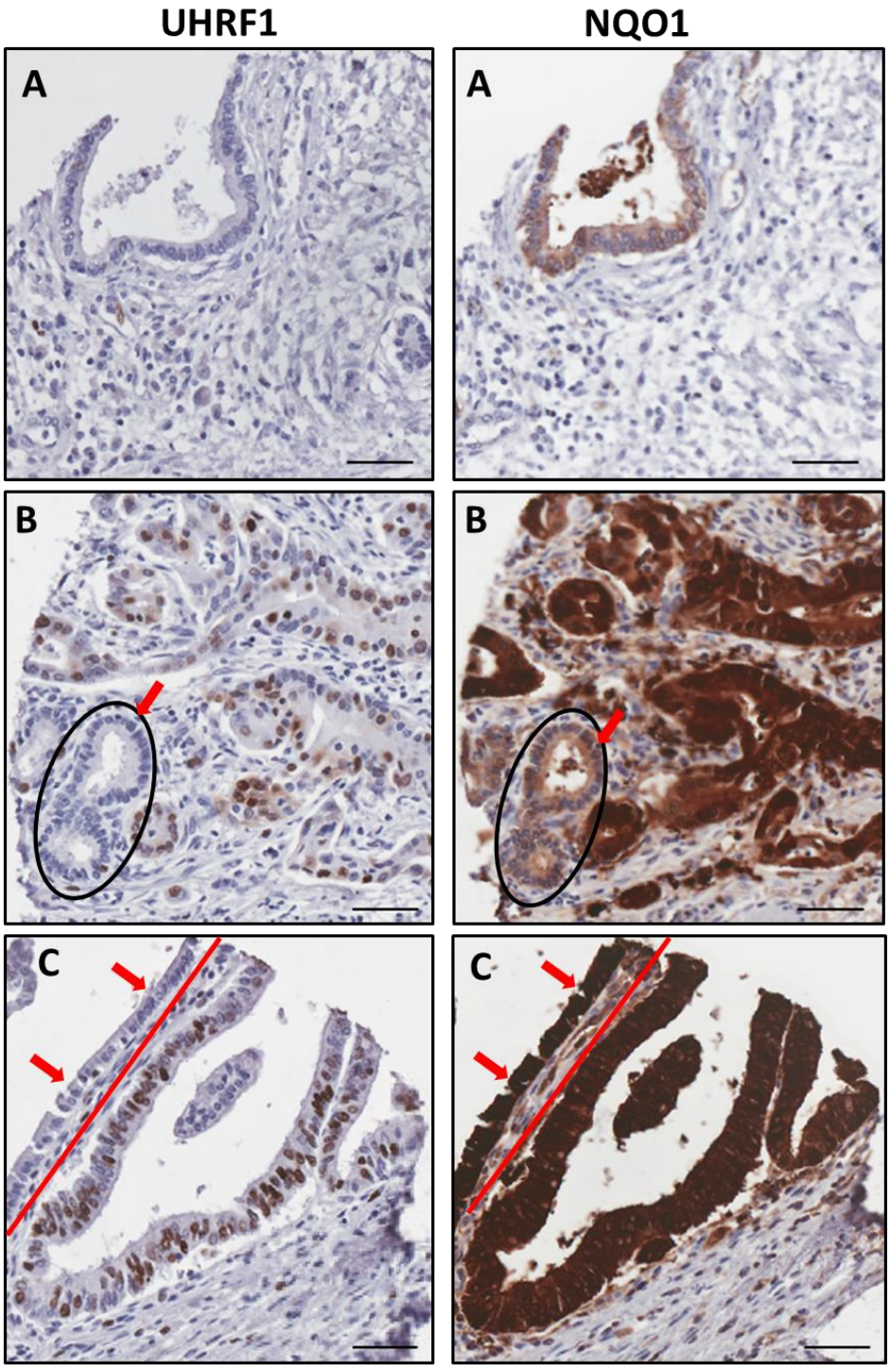

Micrograph of adjacent normal ducts from PDAC patients. In the left column, normal adjacent ducts (A, B and C – red arrows) do not express UHRF1. Matched adjacent normal ducts for NQO1 (A and B [red arrow and black circle]) stain weakly and (C) strongly for NQO1. Scale bar = 50 µm

Appendix 13. Matched UHRF1 and variants NQO1 expression in PDAC

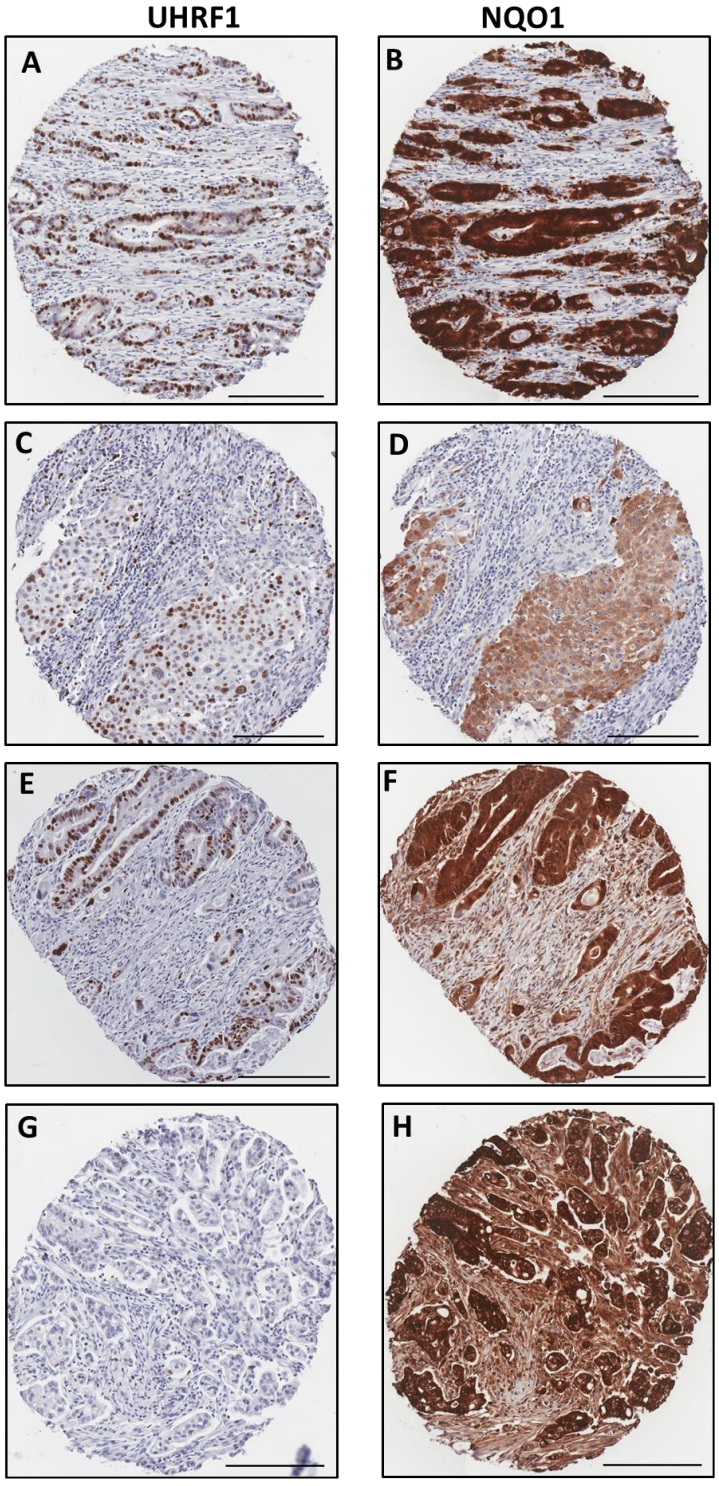

Micrograph of matched UHRF1 and NQO1 expression in PDAC patients. With patient stratification into high and low for UHRF1 and NQO1, A and B are both high-high for UHRF1 and NQO1; C and D are high-low for UHRF1 and NQO1 respectively; E and F are both high-high for UHRF1 and NQO1 and G and H are low-high for UHRF1 and NQO1 respectively. Scale bar = 200 µm

Appendix 14. Matched UHRF1 and NQO1 expression in PDAC continued

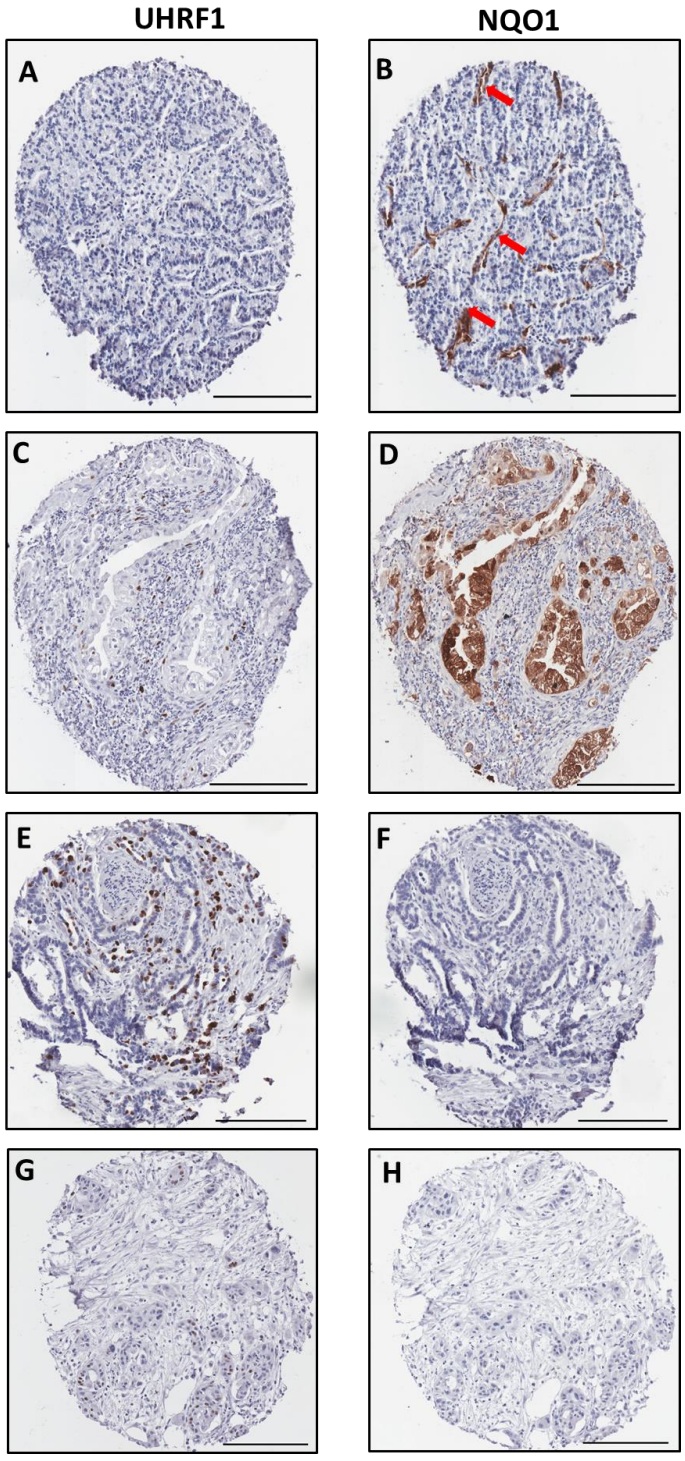

Micrograph of matched UHRF1 and NQO1 expression in PDAC patients. For matched comparison, patients are stratified into high or low for either UHRF1 or NQO1: (A) and (B) are both low-low for UHRF1 and NQO1; (C) and (D) are low-low for UHRF1 and NQO1; E and F are high-low for UHRF1 and NQO1 respectively and (G) and (H) are both low-low for UHRF1 and NQO1. Endothelial cells (blood vessels) are immunoreactive for NQO1, red arrows in (B) and in (C) some inflammatory/immune cells in the stroma are UHRF1 positive. Scale bar = 200 µm.

Appendix 15. Definiens analysis UHRF1 setting

Parameter	Value
Action	General Settings
Magnification	20
µm/pixel	0.504
Use metadata from file	TRUE
Stain Combination	IHC Brown chromogen (e.g. DAB)
IHC Marker	Nuclear
Production Mode	FALSE
Action	Initialize Cellular Analysis
Activate Random Sampling	FALSE
Magnification	10
Action	Nucleus Detection
Hematoxylin Threshold	0.2
IHC Threshold	0.5
Typical Nucleus Size (µm²)	75
Action	Marker Area Detection
Threshold Marker	0.48
Minimum Area (µm²)	40
Action	Marker Area Classification
Select Feature	IHC Marker Intensity
Threshold Low/Medium	0.6
Threshold Medium/High	1.1
Use Condition	FALSE
Remove Excluded Areas	FALSE
Action	Default Export
ROI Statistics	TRUE
Cellular Analysis: Screenshot 1	Original
Cellular Analysis: Screenshot 2	Overlay with Outlines
Cellular Analysis Statistics	TRUE

Appendix 16. Definiens analysis NQO1 setting

Parameter	Value
Action	General Settings
Magnification	20
µm/pixel	0.504
Use metadata from file	TRUE
Stain Combination	IHC Brown chromogen (e.g. DAB)
IHC Marker	Cytoplasm
Production Mode	FALSE
Action	Initialize Cellular Analysis
Activate Random Sampling	FALSE
Magnification	10
Action	Marker Area Detection
Threshold Hematoxylin	0.2
Threshold Marker	0.25
Minimum Area (µm²)	200
Action	Marker Area Classification
Select Feature	IHC Marker Intensity
Threshold Low/Medium	0.6
Threshold Medium/High	1.1
Use Condition	FALSE
Remove Excluded Areas	FALSE
Action	Default Export
ROI Statistics	TRUE
Cellular Analysis: Screenshot 1	Original
Cellular Analysis: Screenshot 2	Overlay with Outlines
Cellular Analysis Statistics	TRUE

8 REFERENCES

1 Longnecker, D. *Anatomy and Histology of the Pancreas*, <https://www.pancreapedia.org/reviews/anatomy-and-histology-of-pancreas> (2014).

2 Hanahan, D. & Weinberg, R. A. Hallmarks of Cancer: The Next Generation. *Cell* **144**, 646-674, doi:10.1016/j.cell.2011.02.013 (2011).

3 Torre, L. A. *et al.* Global cancer statistics, 2012. *CA Cancer J Clin* **65**, 87-108, doi:10.3322/caac.21262 (2015).

4 Ferlay, J. *et al.* Cancer incidence and mortality patterns in Europe: estimates for 40 countries in 2012. *Eur J Cancer* **49**, 1374-1403, doi:10.1016/j.ejca.2012.12.027 (2013).

5 Siegel, R. L., Miller, K. D. & Jemal, A. Cancer Statistics, 2017. *CA Cancer J Clin* **67**, 7-30, doi:10.3322/caac.21387 (2017).

6 Vincent, A., Herman, J., Schulick, R., Hruban, R. H. & Goggins, M. Pancreatic cancer. *Lancet* **378**, 607-620, doi:10.1016/S0140-6736(10)62307-0 (2011).

7 Neoptolemos, J. P. *et al.* Adjuvant chemotherapy with fluorouracil plus folinic acid vs gemcitabine following pancreatic cancer resection: a randomized controlled trial. *JAMA* **304**, 1073-1081, doi:10.1001/jama.2010.1275 (2010).

8 Neoptolemos, J. P. *et al.* Comparison of adjuvant gemcitabine and capecitabine with gemcitabine monotherapy in patients with resected pancreatic cancer (ESPAC-4): a multicentre, open-label, randomised, phase 3 trial. *Lancet* **389**, 1011-1024, doi:10.1016/S0140-6736(16)32409-6 (2017).

9 Nielsen, M. F., Mortensen, M. B. & Detlefsen, S. Key players in pancreatic cancer-stroma interaction: Cancer-associated fibroblasts, endothelial and inflammatory cells. *World J Gastroenterol* **22**, 2678-2700, doi:10.3748/wjg.v22.i9.2678 (2016).

10 Porta, M. *et al.* Exocrine pancreatic cancer: symptoms at presentation and their relation to tumour site and stage. *Clin Transl Oncol* **7**, 189-197 (2005).

11 Ryan, D. P., Hong, T. S. & Bardeesy, N. Pancreatic adenocarcinoma. *N Engl J Med* **371**, 2140-2141, doi:10.1056/NEJMc1412266 (2014).

12 Quaresma, M., Coleman, M. P. & Rachet, B. 40-year trends in an index of survival for all cancers combined and survival adjusted for age and sex for each cancer in England and Wales, 1971-2011: a population-based study. *Lancet* **385**, 1206-1218, doi:10.1016/S0140-6736(14)61396-9 (2015).

13 Rahib, L. *et al.* Projecting cancer incidence and deaths to 2030: the unexpected burden of thyroid, liver, and pancreas cancers in the United States. *Cancer Res* **74**, 2913-2921, doi:10.1158/0008-5472.CAN-14-0155 (2014).

14 Willett, C. G., Czito, B. G., Bendell, J. C. & Ryan, D. P. Locally advanced pancreatic cancer. *J Clin Oncol* **23**, 4538-4544, doi:10.1200/JCO.2005.23.911 (2005).

15 Jones, S. *et al.* Core signaling pathways in human pancreatic cancers revealed by global genomic analyses. *Science* **321**, 1801-1806, doi:10.1126/science.1164368 (2008).

16 Costello, E., Greenhalf, W. & Neoptolemos, J. P. New biomarkers and targets in pancreatic cancer and their application to treatment. *Nat Rev Gastroenterol Hepatol* **9**, 435-444, doi:10.1038/nrgastro.2012.119 (2012).

17 Sultana, A. *et al.* Meta-analyses of chemotherapy for locally advanced and metastatic pancreatic cancer. *J Clin Oncol* **25**, 2607-2615, doi:10.1200/JCO.2006.09.2551 (2007).

18 Neoptolemos, J. P. *et al.* A randomized trial of chemoradiotherapy and chemotherapy after resection of pancreatic cancer. *N Engl J Med* **350**, 1200-1210, doi:10.1056/NEJMoa032295 (2004).
19 Neoptolemos, J. P. *et al.* Adjuvant 5-fluorouracil and folinic acid vs observation for pancreatic cancer: composite data from the ESPAC-1 and -3(v1) trials. *Br J Cancer* **100**, 246-250, doi:10.1038/sj.bjc.6604838 (2009).
20 Burris, H. A., 3rd *et al.* Improvements in survival and clinical benefit with gemcitabine as first-line therapy for patients with advanced pancreas cancer: a randomized trial. *J Clin Oncol* **15**, 2403-2413 (1997).
21 Plunkett, W. *et al.* Gemcitabine: metabolism, mechanisms of action, and self-potentiation. *Semin Oncol* **22**, 3-10 (1995).
22 Mini, E., Nobili, S., Caciagli, B., Landini, I. & Mazzei, T. Cellular pharmacology of gemcitabine. *Ann Oncol* **17 Suppl 5**, v7-12, doi:10.1093/annonc/mdj941 (2006).
23 Longley, D. B., Harkin, D. P. & Johnston, P. G. 5-fluorouracil: mechanisms of action and clinical strategies. *Nat Rev Cancer* **3**, 330-338, doi:10.1038/nrc1074 (2003).
24 Uesaka, K. *et al.* Adjuvant chemotherapy of S-1 versus gemcitabine for resected pancreatic cancer: a phase 3, open-label, randomised, non-inferiority trial (JASPAC 01). *Lancet* **388**, 248-257, doi:10.1016/S0140-6736(16)30583-9 (2016).
25 Cunningham, D. *et al.* Phase III randomized comparison of gemcitabine versus gemcitabine plus capecitabine in patients with advanced pancreatic cancer. *J Clin Oncol* **27**, 5513-5518, doi:10.1200/JCO.2009.24.2446 (2009).
26 Conroy, T. *et al.* FOLFIRINOX versus gemcitabine for metastatic pancreatic cancer. *N Engl J Med* **364**, 1817-1825, doi:10.1056/NEJMoa1011923 (2011).
27 Von Hoff, D. D. *et al.* Increased survival in pancreatic cancer with nab-paclitaxel plus gemcitabine. *The New England journal of medicine* **369**, 1691-1703, doi:10.1056/NEJMoa1304369 (2013).
28 Bachet, J. B. *et al.* Nab-paclitaxel plus either gemcitabine or simplified leucovorin and fluorouracil as first-line therapy for metastatic pancreatic adenocarcinoma (AFUGEM GERCOR): a non-comparative, multicentre, open-label, randomised phase 2 trial. *Lancet Gastroenterol Hepatol* **2**, 337-346, doi:10.1016/S2468-1253(17)30046-8 (2017).
29 Middleton, G. *et al.* Gemcitabine and capecitabine with or without telomerase peptide vaccine GV1001 in patients with locally advanced or metastatic pancreatic cancer (TeloVac): an open-label, randomised, phase 3 trial. *Lancet Oncol* **15**, 829-840, doi:10.1016/S1470-2045(14)70236-0 (2014).
30 Middleton, G. *et al.* Vandetanib plus gemcitabine versus placebo plus gemcitabine in locally advanced or metastatic pancreatic carcinoma (ViP): a prospective, randomised, double-blind, multicentre phase 2 trial. *Lancet Oncol* **18**, 486-499, doi:10.1016/S1470-2045(17)30084-0 (2017).
31 Sawai, H. *et al.* The G691S RET polymorphism increases glial cell line-derived neurotrophic factor-induced pancreatic cancer cell invasion by amplifying mitogen-activated protein kinase signaling. *Cancer Res* **65**, 11536-11544, doi:10.1158/0008-5472.CAN-05-2843 (2005).
32 Wells, S. A., Jr. *et al.* Vandetanib in patients with locally advanced or metastatic medullary thyroid cancer: a randomized, double-blind phase III trial. *J Clin Oncol* **30**, 134-141, doi:10.1200/JCO.2011.35.5040 (2012).
33 Jenkins, Y. *et al.* Critical role of the ubiquitin ligase activity of UHRF1, a nuclear RING finger protein, in tumor cell growth. *Mol Biol Cell* **16**, 5621-5629, doi:10.1091/mbc.E05-03-0194 (2005).

34 Bird, A. DNA methylation patterns and epigenetic memory. *Genes Dev* **16**, 6-21, doi:10.1101/gad.947102 (2002).
35 Bird, A. Perceptions of epigenetics. *Nature* **447**, 396-398, doi:10.1038/nature05913 (2007).
36 Yachida, S. *et al.* Distant metastasis occurs late during the genetic evolution of pancreatic cancer. *Nature* **467**, 1114-1117, doi:10.1038/nature09515 (2010).
37 Campbell, P. J. *et al.* The patterns and dynamics of genomic instability in metastatic pancreatic cancer. *Nature* **467**, 1109-1113, doi:10.1038/nature09460 (2010).
38 Biankin, A. V. *et al.* Pancreatic cancer genomes reveal aberrations in axon guidance pathway genes. *Nature* **491**, 399-405, doi:10.1038/nature11547 (2012).
39 Waddell, N. *et al.* Whole genomes redefine the mutational landscape of pancreatic cancer. *Nature* **518**, 495-501, doi:10.1038/nature14169 (2015).
40 Winter, J. M. *et al.* 1423 pancreaticoduodenectomies for pancreatic cancer: A single-institution experience. *J Gastrointest Surg* **10**, 1199-1210; discussion 1210-1191, doi:10.1016/j.gassur.2006.08.018 (2006).
41 Aichler, M. *et al.* Origin of pancreatic ductal adenocarcinoma from atypical flat lesions: a comparative study in transgenic mice and human tissues. *J Pathol* **226**, 723-734, doi:10.1002/path.3017 (2012).
42 Hruban, R. H., Goggins, M., Parsons, J. & Kern, S. E. Progression model for pancreatic cancer. *Clin Cancer Res* **6**, 2969-2972 (2000).
43 Murphy, S. J. *et al.* Genetic alterations associated with progression from pancreatic intraepithelial neoplasia to invasive pancreatic tumor. *Gastroenterology* **145**, 1098-1109 e1091, doi:10.1053/j.gastro.2013.07.049 (2013).
44 Cowan, R. W. & Maitra, A. Genetic progression of pancreatic cancer. *Cancer J* **20**, 80-84, doi:10.1097/PPO.0000000000000011 (2014).
45 Rall, C. J. *et al.* Ki-ras and p53 mutations in pancreatic ductal adenocarcinoma. *Pancreas* **12**, 10-17 (1996).
46 Huang, C., Wang, W. M., Gong, J. P. & Yang, K. Oncogenesis and the clinical significance of K-ras in pancreatic adenocarcinoma. *Asian Pac J Cancer Prev* **14**, 2699-2701 (2013).
47 Yan, L. *et al.* Molecular analysis to detect pancreatic ductal adenocarcinoma in high-risk groups. *Gastroenterology* **128**, 2124-2130 (2005).
48 Collins, M. A. *et al.* Oncogenic Kras is required for both the initiation and maintenance of pancreatic cancer in mice. *J Clin Invest* **122**, 639-653, doi:10.1172/JCI59227 (2012).
49 McCleary-Wheeler, A. L. *et al.* Insights into the epigenetic mechanisms controlling pancreatic carcinogenesis. *Cancer Lett* **328**, 212-221, doi:10.1016/j.canlet.2012.10.005

S0304-3835(12)00593-9 [pii] (2013).
50 Sato, N. *et al.* Discovery of novel targets for aberrant methylation in pancreatic carcinoma using high-throughput microarrays. *Cancer Res* **63**, 3735-3742 (2003).
51 Sato, N. *et al.* Frequent hypomethylation of multiple genes overexpressed in pancreatic ductal adenocarcinoma. *Cancer Res* **63**, 4158-4166 (2003).
52 Sato, N., Fukushima, N., Hruban, R. H. & Goggins, M. CpG island methylation profile of pancreatic intraepithelial neoplasia. *Mod Pathol* **21**, 238-244, doi:10.1038/modpathol.3800991 (2008).
53 Schutte, M. *et al.* Abrogation of the Rb/p16 tumor-suppressive pathway in virtually all pancreatic carcinomas. *Cancer Res* **57**, 3126-3130 (1997).

54 Kulis, M. & Esteller, M. DNA methylation and cancer. *Adv Genet* **70**, 27-56, doi:10.1016/B978-0-12-380866-0.60002-2 (2010).
55 Zeisberg, E. M. & Zeisberg, M. The role of promoter hypermethylation in fibroblast activation and fibrogenesis. *J Pathol* **229**, 264-273, doi:10.1002/path.4120 (2013).
56 Smets, M. *et al.* DNMT1 mutations found in HSANIE patients affect interaction with UHRF1 and neuronal differentiation. *Hum Mol Genet* **26**, 1522-1534, doi:10.1093/hmg/ddx057 (2017).
57 Rothbart, S. B. *et al.* Association of UHRF1 with methylated H3K9 directs the maintenance of DNA methylation. *Nat Struct Mol Biol* **19**, 1155-1160, doi:10.1038/nsmb.2391 (2012).
58 Liu, X. *et al.* UHRF1 targets DNMT1 for DNA methylation through cooperative binding of hemi-methylated DNA and methylated H3K9. *Nat Commun* **4**, 1563, doi:10.1038/ncomms2562 (2013).
59 Bronner, C. *et al.* The UHRF family: oncogenes that are drugable targets for cancer therapy in the near future? *Pharmacol Ther* **115**, 419-434, doi:10.1016/j.pharmthera.2007.06.003 (2007).
60 Lu, H. *et al.* Loss of UHRF2 expression is associated with human neoplasia, promoter hypermethylation, decreased 5-hydroxymethylcytosine, and high proliferative activity. *Oncotarget* **7**, 76047-76061, doi:10.18632/oncotarget.12583 (2016).
61 Hopfner, R. *et al.* ICBP90, a novel human CCAAT binding protein, involved in the regulation of topoisomerase IIalpha expression. *Cancer Res* **60**, 121-128 (2000).
62 Mousli, M. *et al.* ICBP90 belongs to a new family of proteins with an expression that is deregulated in cancer cells. *Br J Cancer* **89**, 120-127, doi:10.1038/sj.bjc.6601068 (2003).
63 Arima, Y. *et al.* Down-regulation of nuclear protein ICBP90 by p53/p21Cip1/WAF1-dependent DNA-damage checkpoint signals contributes to cell cycle arrest at G1/S transition. *Genes Cells* **9**, 131-142 (2004).
64 Tien, A. L. *et al.* UHRF1 depletion causes a G2/M arrest, activation of DNA damage response and apoptosis. *Biochem J* **435**, 175-185, doi:10.1042/BJ20100840 (2011).
65 Bostick, M. *et al.* UHRF1 plays a role in maintaining DNA methylation in mammalian cells. *Science* **317**, 1760-1764, doi:10.1126/science.1147939 (2007).
66 Kim, J. K., Esteve, P. O., Jacobsen, S. E. & Pradhan, S. UHRF1 binds G9a and participates in p21 transcriptional regulation in mammalian cells. *Nucleic Acids Res* **37**, 493-505, doi:10.1093/nar/gkn961 (2009).
67 Citterio, E. *et al.* Np95 is a histone-binding protein endowed with ubiquitin ligase activity. *Mol Cell Biol* **24**, 2526-2535 (2004).
68 Unoki, M., Nishidate, T. & Nakamura, Y. ICBP90, an E2F-1 target, recruits HDAC1 and binds to methyl-CpG through its SRA domain. *Oncogene* **23**, 7601-7610, doi:10.1038/sj.onc.1208053 (2004).
69 Rottach, A. *et al.* The multi-domain protein Np95 connects DNA methylation and histone modification. *Nucleic Acids Res* **38**, 1796-1804, doi:10.1093/nar/gkp1152 (2010).
70 Hashimoto, H., Horton, J. R., Zhang, X. & Cheng, X. UHRF1, a modular multi-domain protein, regulates replication-coupled crosstalk between DNA methylation and histone modifications. *Epigenetics* **4**, 8-14 (2009).
71 Arita, K., Ariyoshi, M., Tochio, H., Nakamura, Y. & Shirakawa, M. Recognition of hemi-methylated DNA by the SRA protein UHRF1 by a base-flipping mechanism. *Nature* **455**, 818-821, doi:10.1038/nature07249 (2008).

72 Qin, W., Leonhardt, H. & Spada, F. Usp7 and Uhrf1 control ubiquitination and stability of the maintenance DNA methyltransferase Dnmt1. *J Cell Biochem* **112**, 439-444, doi:10.1002/jcb.22998 (2011).
73 Hickman, E. S., Moroni, M. C. & Helin, K. The role of p53 and pRB in apoptosis and cancer. *Curr Opin Genet Dev* **12**, 60-66 (2002).
74 Jeanblanc, M. *et al.* The retinoblastoma gene and its product are targeted by ICBP90: a key mechanism in the G1/S transition during the cell cycle. *Oncogene* **24**, 7337-7345, doi:10.1038/sj.onc.1208878 (2005).
75 Du, Z. *et al.* DNMT1 stability is regulated by proteins coordinating deubiquitination and acetylation-driven ubiquitination. *Sci Signal* **3**, ra80, doi:10.1126/scisignal.2001462 (2010).
76 Unoki, M. *et al.* UHRF1 is a novel diagnostic marker of lung cancer. *Br J Cancer* **103**, 217-222, doi:10.1038/sj.bjc.6605717 (2010).
77 Unoki, M. *et al.* UHRF1 is a novel molecular marker for diagnosis and the prognosis of bladder cancer. *Br J Cancer* **101**, 98-105, doi:10.1038/sj.bjc.6605123 (2009).
78 Kofunato, Y. *et al.* UHRF1 expression is upregulated and associated with cellular proliferation in colorectal cancer. *Oncol Rep* **28**, 1997-2002, doi:10.3892/or.2012.2064 (2012).
79 Crnogorac-Jurcevic, T. *et al.* Proteomic analysis of chronic pancreatitis and pancreatic adenocarcinoma. *Gastroenterology* **129**, 1454-1463, doi:10.1053/j.gastro.2005.08.012 (2005).
80 Abu-Alainin, W. *et al.* UHRF1 regulation of the Keap1-Nrf2 pathway in pancreatic cancer contributes to oncogenesis. *J Pathol* **238**, 423-433, doi:10.1002/path.4665 (2016).
81 Cui, L. *et al.* Up-regulation of UHRF1 by oncogenic Ras promoted the growth, migration, and metastasis of pancreatic cancer cells. *Mol Cell Biochem* **400**, 223-232, doi:10.1007/s11010-014-2279-9 (2015).
82 Copple, I. M., Goldring, C. E., Kitteringham, N. R. & Park, B. K. The Nrf2-Keap1 defence pathway: role in protection against drug-induced toxicity. *Toxicology* **246**, 24-33, doi:10.1016/j.tox.2007.10.029 (2008).
83 Li, Y., Paonessa, J. D. & Zhang, Y. Mechanism of chemical activation of Nrf2. *PLoS One* **7**, e35122, doi:10.1371/journal.pone.0035122 (2012).
84 Bryan, H. K., Olayanju, A., Goldring, C. E. & Park, B. K. The Nrf2 cell defence pathway: Keap1-dependent and -independent mechanisms of regulation. *Biochem Pharmacol* **85**, 705-717, doi:10.1016/j.bcp.2012.11.016 (2013).
85 Lau, A., Tian, W., Whitman, S. A. & Zhang, D. D. The predicted molecular weight of Nrf2: it is what it is not. *Antioxid Redox Signal* **18**, 91-93, doi:10.1089/ars.2012.4754 (2013).
86 Nguyen, T., Sherratt, P. J. & Pickett, C. B. Regulatory mechanisms controlling gene expression mediated by the antioxidant response element. *Annu Rev Pharmacol Toxicol* **43**, 233-260, doi:10.1146/annurev.pharmtox.43.100901.140229 (2003).
87 Copple, I. M. *et al.* Physical and functional interaction of sequestosome 1 with Keap1 regulates the Keap1-Nrf2 cell defense pathway. *J Biol Chem* **285**, 16782-16788, doi:10.1074/jbc.M109.096545 (2010).
88 Katsuragi, Y., Ichimura, Y. & Komatsu, M. p62/SQSTM1 functions as a signaling hub and an autophagy adaptor. *FEBS J* **282**, 4672-4678, doi:10.1111/febs.13540 (2015).
89 Gorrini, C., Harris, I. S. & Mak, T. W. Modulation of oxidative stress as an anticancer strategy. *Nat Rev Drug Discov* **12**, 931-947, doi:10.1038/nrd4002 (2013).

90 Klaunig, J. E., Kamendulis, L. M. & Hocevar, B. A. Oxidative stress and oxidative damage in carcinogenesis. *Toxicol Pathol* **38**, 96-109, doi:10.1177/0192623309356453 (2010).
91 Shibutani, S., Takeshita, M. & Grollman, A. P. Insertion of specific bases during DNA synthesis past the oxidation-damaged base 8-oxodG. *Nature* **349**, 431-434, doi:10.1038/349431a0 (1991).
92 Hubbs, A. F. *et al.* Vacuolar leukoencephalopathy with widespread astrogliosis in mice lacking transcription factor Nrf2. *Am J Pathol* **170**, 2068-2076, doi:10.2353/ajpath.2007.060898 (2007).
93 Kitamura, Y. *et al.* Increased susceptibility to hepatocarcinogenicity of Nrf2-deficient mice exposed to 2-amino-3-methylimidazo[4,5-f]quinoline. *Cancer Sci* **98**, 19-24, doi:10.1111/j.1349-7006.2006.00352.x (2007).
94 Seril, D. N., Liao, J., Yang, G. Y. & Yang, C. S. Oxidative stress and ulcerative colitis-associated carcinogenesis: studies in humans and animal models. *Carcinogenesis* **24**, 353-362 (2003).
95 Kong, X., Sun, T., Kong, F., Du, Y. & Li, Z. Chronic Pancreatitis and Pancreatic Cancer. *Gastrointest Tumors* **1**, 123-134, doi:10.1159/000365306 (2014).
96 Rhee, S. G. Cell signaling. H2O2, a necessary evil for cell signaling. *Science* **312**, 1882-1883, doi:10.1126/science.1130481 (2006).
97 Sena, L. A. & Chandel, N. S. Physiological roles of mitochondrial reactive oxygen species. *Mol Cell* **48**, 158-167, doi:10.1016/j.molcel.2012.09.025 (2012).
98 DeNicola, G. M. *et al.* Oncogene-induced Nrf2 transcription promotes ROS detoxification and tumorigenesis. *Nature* **475**, 106-109, doi:10.1038/nature10189 (2011).
99 Lister, A. *et al.* Nrf2 is overexpressed in pancreatic cancer: implications for cell proliferation and therapy. *Mol Cancer* **10**, 37, doi:10.1186/1476-4598-10-37 (2011).
100 Hanada, N. *et al.* Methylation of the KEAP1 gene promoter region in human colorectal cancer. *BMC Cancer* **12**, 66, doi:10.1186/1471-2407-12-66 (2012).
101 Barbano, R. *et al.* Aberrant Keap1 methylation in breast cancer and association with clinicopathological features. *Epigenetics* **8**, 105-112, doi:10.4161/epi.23319 (2013).
102 Wang, R. *et al.* Hypermethylation of the Keap1 gene in human lung cancer cell lines and lung cancer tissues. *Biochem Biophys Res Commun* **373**, 151-154, doi:10.1016/j.bbrc.2008.06.004 (2008).
103 Nguyen, E. V. *et al.* Hyper-phosphorylation of Sequestosome-1 distinguishes resistance to cisplatin in patient derived high grade serous ovarian cancer cells. *Mol Cell Proteomics*, doi:10.1074/mcp.M116.058321 (2017).
104 Hayes, J. D. & McMahon, M. NRF2 and KEAP1 mutations: permanent activation of an adaptive response in cancer. *Trends Biochem Sci* **34**, 176-188, doi:10.1016/j.tibs.2008.12.008 (2009).
105 Dvorak, H. F. Tumors: wounds that do not heal. Similarities between tumor stroma generation and wound healing. *N Engl J Med* **315**, 1650-1659, doi:10.1056/NEJM198612253152606 (1986).
106 Jones, F. S. & Rous, P. On the Cause of the Localization of Secondary Tumors at Points of Injury. *J Exp Med* **20**, 404-412 (1914).
107 Augsten, M. Cancer-associated fibroblasts as another polarized cell type of the tumor microenvironment. *Front Oncol* **4**, 62, doi:10.3389/fonc.2014.00062 (2014).
108 Ohlund, D., Elyada, E. & Tuveson, D. Fibroblast heterogeneity in the cancer wound. *J Exp Med* **211**, 1503-1523, doi:10.1084/jem.20140692 (2014).
109 Pothula, S. P. *et al.* Key role of pancreatic stellate cells in pancreatic cancer. *Cancer Lett* **381**, 194-200, doi:10.1016/j.canlet.2015.10.035 (2016).

110 Tremblay, G. Stromal aspects of breast carcinoma. *Exp Mol Pathol* **31**, 248-260 (1979).
111 Kalluri, R. The biology and function of fibroblasts in cancer. *Nat Rev Cancer* **16**, 582-598, doi:10.1038/nrc.2016.73 (2016).
112 Catalano, V. *et al.* Tumor and its microenvironment: a synergistic interplay. *Semin Cancer Biol* **23**, 522-532, doi:10.1016/j.semcancer.2013.08.007 (2013).
113 Quail, D. F. & Joyce, J. A. Microenvironmental regulation of tumor progression and metastasis. *Nat Med* **19**, 1423-1437, doi:10.1038/nm.3394 (2013).
114 Rohde, M. C. *et al.* Characteristics of human infant primary fibroblast cultures from Achilles tendons removed post-mortem. *Forensic Sci Int* **234**, 149-153, doi:10.1016/j.forsciint.2013.11.007 (2014).
115 Uma Mahesh, Y. *et al.* Cell cycle synchronization of bison (Bos gaurus) fibroblasts derived from ear piece collected post-mortem. *Reprod Domest Anim* **47**, 799-805, doi:10.1111/j.1439-0531.2011.01970.x (2012).
116 Meske, V., Albert, F., Wehser, R. & Ohm, T. G. Culture of autopsy-derived fibroblasts as a tool to study systemic alterations in human neurodegenerative disorders such as Alzheimer's disease--methodological investigations. *J Neural Transm (Vienna)* **106**, 537-548, doi:10.1007/s007020050177 (1999).
117 Gabbiani, G., Hirschel, B. J., Ryan, G. B., Statkov, P. R. & Majno, G. Granulation tissue as a contractile organ. A study of structure and function. *J Exp Med* **135**, 719-734 (1972).
118 Gabbiani, G. & Majno, G. Dupuytren's contracture: fibroblast contraction? An ultrastructural study. *Am J Pathol* **66**, 131-146 (1972).
119 Desmouliere, A., Redard, M., Darby, I. & Gabbiani, G. Apoptosis mediates the decrease in cellularity during the transition between granulation tissue and scar. *Am J Pathol* **146**, 56-66 (1995).
120 Bizik, J. *et al.* Cell-cell contacts trigger programmed necrosis and induce cyclooxygenase-2 expression. *Cell Death Differ* **11**, 183-195, doi:10.1038/sj.cdd.4401317 (2004).
121 Erkan, M. *et al.* StellaTUM: current consensus and discussion on pancreatic stellate cell research. *Gut* **61**, 172-178, doi:10.1136/gutjnl-2011-301220 (2012).
122 Apte, M. V. *et al.* Periacinar stellate shaped cells in rat pancreas: identification, isolation, and culture. *Gut* **43**, 128-133 (1998).
123 Bachem, M. G. *et al.* Identification, culture, and characterization of pancreatic stellate cells in rats and humans. *Gastroenterology* **115**, 421-432 (1998).
124 Apte, M. V. *et al.* Pancreatic cancer: The microenvironment needs attention too! *Pancreatology* **15**, S32-38, doi:10.1016/j.pan.2015.02.013 (2015).
125 Rhim, A. D. *et al.* Stromal elements act to restrain, rather than support, pancreatic ductal adenocarcinoma. *Cancer Cell* **25**, 735-747, doi:10.1016/j.ccr.2014.04.021 (2014).
126 Ozdemir, B. C. *et al.* Depletion of carcinoma-associated fibroblasts and fibrosis induces immunosuppression and accelerates pancreas cancer with reduced survival. *Cancer Cell* **25**, 719-734, doi:10.1016/j.ccr.2014.04.005 (2014).
127 Hwang, R. F. *et al.* Cancer-associated stromal fibroblasts promote pancreatic tumor progression. *Cancer Res* **68**, 918-926, doi:10.1158/0008-5472.CAN-07-5714 (2008).
128 Bachem, M. G. *et al.* Pancreatic carcinoma cells induce fibrosis by stimulating proliferation and matrix synthesis of stellate cells. *Gastroenterology* **128**, 907-921 (2005).

129 Vonlaufen, A. *et al.* Pancreatic stellate cells: partners in crime with pancreatic cancer cells. *Cancer Res* **68**, 2085-2093, doi:10.1158/0008-5472.CAN-07-2477 (2008).
130 Xu, Z. *et al.* Role of pancreatic stellate cells in pancreatic cancer metastasis. *Am J Pathol* **177**, 2585-2596, doi:10.2353/ajpath.2010.090899 (2010).
131 Hwang, R. F. *et al.* Inhibition of the hedgehog pathway targets the tumor-associated stroma in pancreatic cancer. *Mol Cancer Res* **10**, 1147-1157, doi:10.1158/1541-7786.MCR-12-0022 (2012).
132 Olive, K. P. *et al.* Inhibition of Hedgehog signaling enhances delivery of chemotherapy in a mouse model of pancreatic cancer. *Science* **324**, 1457-1461, doi:10.1126/science.1171362 (2009).
133 Provenzano, P. P. *et al.* Enzymatic targeting of the stroma ablates physical barriers to treatment of pancreatic ductal adenocarcinoma. *Cancer Cell* **21**, 418-429, doi:10.1016/j.ccr.2012.01.007 (2012).
134 Jacobetz, M. A. *et al.* Hyaluronan impairs vascular function and drug delivery in a mouse model of pancreatic cancer. *Gut* **62**, 112-120, doi:10.1136/gutjnl-2012-302529 (2013).
135 Sherman, M. H. *et al.* Vitamin D receptor-mediated stromal reprogramming suppresses pancreatitis and enhances pancreatic cancer therapy. *Cell* **159**, 80-93, doi:10.1016/j.cell.2014.08.007 (2014).
136 Feig, C. *et al.* Targeting CXCL12 from FAP-expressing carcinoma-associated fibroblasts synergizes with anti-PD-L1 immunotherapy in pancreatic cancer. *Proc Natl Acad Sci U S A* **110**, 20212-20217, doi:10.1073/pnas.1320318110 (2013).
137 Ene-Obong, A. *et al.* Activated pancreatic stellate cells sequester CD8+ T cells to reduce their infiltration of the juxtatumoral compartment of pancreatic ductal adenocarcinoma. *Gastroenterology* **145**, 1121-1132, doi:10.1053/j.gastro.2013.07.025 (2013).
138 Erkan, M. *et al.* The activated stroma index is a novel and independent prognostic marker in pancreatic ductal adenocarcinoma. *Clin Gastroenterol Hepatol* **6**, 1155-1161, doi:10.1016/j.cgh.2008.05.006 (2008).
139 Bever, K. M. *et al.* The prognostic value of stroma in pancreatic cancer in patients receiving adjuvant therapy. *HPB (Oxford)* **17**, 292-298, doi:10.1111/hpb.12334 (2015).
140 Sugimoto, H., Mundel, T. M., Kieran, M. W. & Kalluri, R. Identification of fibroblast heterogeneity in the tumor microenvironment. *Cancer Biol Ther* **5**, 1640-1646 (2006).
141 Ikenaga, N. *et al.* CD10+ pancreatic stellate cells enhance the progression of pancreatic cancer. *Gastroenterology* **139**, 1041-1051, 1051 e1041-1048, doi:10.1053/j.gastro.2010.05.084 (2010).
142 Baum, J. & Duffy, H. S. Fibroblasts and myofibroblasts: what are we talking about? *J Cardiovasc Pharmacol* **57**, 376-379, doi:10.1097/FJC.0b013e3182116e39 (2011).
143 Bechtel, W. *et al.* Methylation determines fibroblast activation and fibrogenesis in the kidney. *Nat Med* **16**, 544-550, doi:10.1038/nm.2135 (2010).
144 Tampe, B. & Zeisberg, M. Contribution of genetics and epigenetics to progression of kidney fibrosis. *Nephrol Dial Transplant* **29 Suppl 4**, iv72-79, doi:10.1093/ndt/gft025 (2014).
145 Strimbu, K. & Tavel, J. A. What are biomarkers? *Curr Opin HIV AIDS* **5**, 463-466, doi:10.1097/COH.0b013e32833ed177 (2010).

146 Greenhalf, W. *et al.* Pancreatic cancer hENT1 expression and survival from gemcitabine in patients from the ESPAC-3 trial. *J Natl Cancer Inst* **106**, djt347, doi:10.1093/jnci/djt347 (2014).
147 Dinkova-Kostova, A. T. & Talalay, P. NAD(P)H:quinone acceptor oxidoreductase 1 (NQO1), a multifunctional antioxidant enzyme and exceptionally versatile cytoprotector. *Arch Biochem Biophys* **501**, 116-123, doi:10.1016/j.abb.2010.03.019 (2010).
148 Li, L. S. *et al.* Modulating endogenous NQO1 levels identifies key regulatory mechanisms of action of beta-lapachone for pancreatic cancer therapy. *Clin Cancer Res* **17**, 275-285, doi:10.1158/1078-0432.CCR-10-1983 (2011).
149 Belinsky, M. & Jaiswal, A. K. NAD(P)H:quinone oxidoreductase1 (DT-diaphorase) expression in normal and tumor tissues. *Cancer Metastasis Rev* **12**, 103-117 (1993).
150 Siegel, D. *et al.* NAD(P)H:quinone oxidoreductase 1: role as a superoxide scavenger. *Mol Pharmacol* **65**, 1238-1247, doi:10.1124/mol.65.5.1238 (2004).
151 Asher, G., Lotem, J., Cohen, B., Sachs, L. & Shaul, Y. Regulation of p53 stability and p53-dependent apoptosis by NADH quinone oxidoreductase 1. *Proc Natl Acad Sci U S A* **98**, 1188-1193, doi:10.1073/pnas.021558898 (2001).
152 Asher, G., Lotem, J., Kama, R., Sachs, L. & Shaul, Y. NQO1 stabilizes p53 through a distinct pathway. *Proc Natl Acad Sci U S A* **99**, 3099-3104, doi:10.1073/pnas.052706799 (2002).
153 Zeekpudsa, P., Kukongviriyapan, V., Senggunprai, L., Sripa, B. & Prawan, A. Suppression of NAD(P)H-quinone oxidoreductase 1 enhanced the susceptibility of cholangiocarcinoma cells to chemotherapeutic agents. *J Exp Clin Cancer Res* **33**, 11, doi:10.1186/1756-9966-33-11 (2014).
154 Siegel, D., Gibson, N. W., Preusch, P. C. & Ross, D. Metabolism of mitomycin C by DT-diaphorase: role in mitomycin C-induced DNA damage and cytotoxicity in human colon carcinoma cells. *Cancer Res* **50**, 7483-7489 (1990).
155 Siegel, D., Gibson, N. W., Preusch, P. C. & Ross, D. Metabolism of diaziquone by NAD(P)H:(quinone acceptor) oxidoreductase (DT-diaphorase): role in diaziquone-induced DNA damage and cytotoxicity in human colon carcinoma cells. *Cancer Res* **50**, 7293-7300 (1990).
156 Robertson, N., Stratford, I. J., Houlbrook, S., Carmichael, J. & Adams, G. E. The sensitivity of human tumour cells to quinone bioreductive drugs: what role for DT-diaphorase? *Biochem Pharmacol* **44**, 409-412 (1992).
157 Phillips, R. M. *et al.* Predicting tumor responses to mitomycin C on the basis of DT-diaphorase activity or drug metabolism by tumor homogenates: implications for enzyme-directed bioreductive drug development. *Cancer Res* **60**, 6384-6390 (2000).
158 Cui, X. *et al.* NAD(P)H:quinone oxidoreductase-1 overexpression predicts poor prognosis in small cell lung cancer. *Oncol Rep* **32**, 2589-2595, doi:10.3892/or.2014.3494 (2014).
159 Cui, X. *et al.* High expression of NQO1 is associated with poor prognosis in serous ovarian carcinoma. *BMC Cancer* **15**, 244, doi:10.1186/s12885-015-1271-4 (2015).
160 Ji, M. *et al.* Clinicopathological implications of NQO1 overexpression in the prognosis of pancreatic adenocarcinoma. *Oncol Lett* **13**, 2996-3002, doi:10.3892/ol.2017.5821 (2017).
161 Cullen, J. J. *et al.* Dicumarol inhibition of NADPH:quinone oxidoreductase induces growth inhibition of pancreatic cancer via a superoxide-mediated mechanism. *Cancer Res* **63**, 5513-5520 (2003).
162 Pardee, A. B., Li, Y. Z. & Li, C. J. Cancer therapy with beta-lapachone. *Curr Cancer Drug Targets* **2**, 227-242 (2002).

163 Beg, M. S. *et al.* Using a novel NQO1 bioactivatable drug, beta-lapachone (ARQ761), to enhance chemotherapeutic effects by metabolic modulation in pancreatic cancer. *J Surg Oncol*, doi:10.1002/jso.24624 (2017).
164 Collins, F. S., Brooks, L. D. & Chakravarti, A. A DNA polymorphism discovery resource for research on human genetic variation. *Genome Res* **8**, 1229-1231 (1998).
165 Brookes, A. J. The essence of SNPs. *Gene* **234**, 177-186 (1999).
166 Kruglyak, L. & Nickerson, D. A. Variation is the spice of life. *Nat Genet* **27**, 234-236, doi:10.1038/85776 (2001).
167 Traver, R. D. *et al.* NAD(P)H:quinone oxidoreductase gene expression in human colon carcinoma cells: characterization of a mutation which modulates DT-diaphorase activity and mitomycin sensitivity. *Cancer Res* **52**, 797-802 (1992).
168 Ross, D. *et al.* A polymorphism in NAD(P)H:quinone oxidoreductase (NQO1): relationship of a homozygous mutation at position 609 of the NQO1 cDNA to NQO1 activity. *Br J Cancer* **74**, 995-996 (1996).
169 Traver, R. D. *et al.* Characterization of a polymorphism in NAD(P)H: quinone oxidoreductase (DT-diaphorase). *Br J Cancer* **75**, 69-75 (1997).
170 Kolesar, J. M. *et al.* The NQO1*2/*2 polymorphism is associated with poor overall survival in patients following resection of stages II and IIIa non-small cell lung cancer. *Oncol Rep* **25**, 1765-1772, doi:10.3892/or.2011.1249 (2011).
171 Fagerholm, R. *et al.* NAD(P)H:quinone oxidoreductase 1 NQO1*2 genotype (P187S) is a strong prognostic and predictive factor in breast cancer. *Nat Genet* **40**, 844-853, doi:10.1038/ng.155 (2008).
172 Jamieson, D. *et al.* Two minor NQO1 and NQO2 alleles predict poor response of breast cancer patients to adjuvant doxorubicin and cyclophosphamide therapy. *Pharmacogenet Genomics* **21**, 808-819, doi:10.1097/FPC.0b013e32834b6918 (2011).
173 Tian, G., Wang, M. & Xu, X. The role of NQO1 polymorphisms in the susceptibility and chemotherapy response of Chinese NSCLC patients. *Cell Biochem Biophys* **69**, 475-479, doi:10.1007/s12013-014-9820-z (2014).
174 Mohelnikova-Duchonova, B. *et al.* Superoxide dismutase and nicotinamide adenine dinucleotide phosphate: quinone oxidoreductase polymorphisms and pancreatic cancer risk. *Pancreas* **40**, 72-78, doi:10.1097/MPA.0b013e3181f74ad7 (2011).
175 Cox, A. G., Winterbourn, C. C. & Hampton, M. B. Mitochondrial peroxiredoxin involvement in antioxidant defence and redox signalling. *Biochem J* **425**, 313-325, doi:10.1042/BJ20091541 (2009).
176 Rhee, S. G., Yang, K. S., Kang, S. W., Woo, H. A. & Chang, T. S. Controlled elimination of intracellular H(2)O(2): regulation of peroxiredoxin, catalase, and glutathione peroxidase via post-translational modification. *Antioxid Redox Signal* **7**, 619-626, doi:10.1089/ars.2005.7.619 (2005).
177 Woo, H. A. *et al.* Reduction of cysteine sulfinic acid by sulfiredoxin is specific to 2-cys peroxiredoxins. *J Biol Chem* **280**, 3125-3128, doi:10.1074/jbc.C400496200 (2005).
178 Soriano, F. X. *et al.* Transcriptional regulation of the AP-1 and Nrf2 target gene sulfiredoxin. *Mol Cells* **27**, 279-282, doi:10.1007/s10059-009-0050-y (2009).
179 Wei, Q., Jiang, H., Matthews, C. P. & Colburn, N. H. Sulfiredoxin is an AP-1 target gene that is required for transformation and shows elevated expression in human skin malignancies. *Proc Natl Acad Sci U S A* **105**, 19738-19743, doi:10.1073/pnas.0810676105 (2008).

180 Hartikainen, J. M. *et al.* Genetic polymorphisms and protein expression of NRF2 and Sulfiredoxin predict survival outcomes in breast cancer. *Cancer Res* **72**, 5537-5546, doi:10.1158/0008-5472.CAN-12-1474 (2012).
181 Glynn, S. A. *et al.* A mitochondrial target sequence polymorphism in manganese superoxide dismutase predicts inferior survival in breast cancer patients treated with cyclophosphamide. *Clin Cancer Res* **15**, 4165-4173, doi:10.1158/1078-0432.CCR-09-0119 (2009).
182 Xu, Z. *et al.* SOD2 rs4880 CT/CC genotype predicts poor survival for Chinese gastric cancer patients received platinum and fluorouracil based adjuvant chemotherapy. *Am J Transl Res* **7**, 401-410 (2015).
183 Deng, X. *et al.* GSTP1 and GSTO1 single nucleotide polymorphisms and the response of bladder cancer patients to intravesical chemotherapy. *Sci Rep* **5**, 14000, doi:10.1038/srep14000 (2015).
184 Marechal, R. *et al.* Deoxycitidine kinase is associated with prolonged survival after adjuvant gemcitabine for resected pancreatic adenocarcinoma. *Cancer* **116**, 5200-5206, doi:10.1002/cncr.25303 (2010).
185 Valsecchi, M. E. *et al.* Is there a role for the quantification of RRM1 and ERCC1 expression in pancreatic ductal adenocarcinoma? *BMC Cancer* **12**, 104, doi:10.1186/1471-2407-12-104 (2012).
186 Giovannetti, E. *et al.* MicroRNA-21 in pancreatic cancer: correlation with clinical outcome and pharmacologic aspects underlying its role in the modulation of gemcitabine activity. *Cancer Res* **70**, 4528-4538, doi:10.1158/0008-5472.CAN-09-4467 (2010).
187 Hwang, J. H. *et al.* Identification of microRNA-21 as a biomarker for chemoresistance and clinical outcome following adjuvant therapy in resectable pancreatic cancer. *PLoS One* **5**, e10630, doi:10.1371/journal.pone.0010630 (2010).
188 Iwamura, T., Katsuki, T. & Ide, K. Establishment and characterization of a human pancreatic cancer cell line (SUIT-2) producing carcinoembryonic antigen and carbohydrate antigen 19-9. *Jpn J Cancer Res* **78**, 54-62 (1987).
189 Deer, E. L. *et al.* Phenotype and genotype of pancreatic cancer cell lines. *Pancreas* **39**, 425-435, doi:10.1097/MPA.0b013e3181c15963 (2010).
190 Gradiz, R., Silva, H. C., Carvalho, L., Botelho, M. F. & Mota-Pinto, A. MIA PaCa-2 and PANC-1 - pancreas ductal adenocarcinoma cell lines with neuroendocrine differentiation and somatostatin receptors. *Sci Rep* **6**, 21648, doi:10.1038/srep21648 (2016).
191 Yunis, A. A., Arimura, G. K. & Russin, D. J. Human pancreatic carcinoma (MIA PaCa-2) in continuous culture: sensitivity to asparaginase. *Int J Cancer* **19**, 128-135 (1977).
192 Lieber, M., Mazzetta, J., Nelson-Rees, W., Kaplan, M. & Todaro, G. Establishment of a continuous tumor-cell line (panc-1) from a human carcinoma of the exocrine pancreas. *Int J Cancer* **15**, 741-747 (1975).
193 Nielsen, S. R. *et al.* Macrophage-secreted granulin supports pancreatic cancer metastasis by inducing liver fibrosis. *Nat Cell Biol* **18**, 549-560, doi:10.1038/ncb3340 (2016).
194 Tonack, S. *et al.* Tetracycline-inducible protein expression in pancreatic cancer cells: effects of CapG overexpression. *World J Gastroenterol* **17**, 1947-1960, doi:10.3748/wjg.v17.i15.1947 (2011).
195 Vandeputte, C., Guizon, I., Genestie-Denis, I., Vannier, B. & Lorenzon, G. A microtiter plate assay for total glutathione and glutathione disulfide contents in

cultured/isolated cells: performance study of a new miniaturized protocol. *Cell Biol Toxicol* **10**, 415-421 (1994).
196 Kratschmar, D. V. *et al.* Suppression of the Nrf2-dependent antioxidant response by glucocorticoids and 11beta-HSD1-mediated glucocorticoid activation in hepatic cells. *PLoS One* **7**, e36774, doi:10.1371/journal.pone.0036774 (2012).
197 Daskalos, A. *et al.* UHRF1-mediated tumor suppressor gene inactivation in nonsmall cell lung cancer. *Cancer* **117**, 1027-1037, doi:10.1002/cncr.25531 (2011).
198 Itoh, K. *et al.* An Nrf2/small Maf heterodimer mediates the induction of phase II detoxifying enzyme genes through antioxidant response elements. *Biochem Biophys Res Commun* **236**, 313-322 (1997).
199 McMahon, M. *et al.* The Cap'n'Collar basic leucine zipper transcription factor Nrf2 (NF-E2 p45-related factor 2) controls both constitutive and inducible expression of intestinal detoxification and glutathione biosynthetic enzymes. *Cancer Res* **61**, 3299-3307 (2001).
200 Ramirez-Zacarias, J. L., Castro-Munozledo, F. & Kuri-Harcuch, W. Quantitation of adipose conversion and triglycerides by staining intracytoplasmic lipids with Oil red O. *Histochemistry* **97**, 493-497 (1992).
201 Genomes Project, C. *et al.* A global reference for human genetic variation. *Nature* **526**, 68-74, doi:10.1038/nature15393 (2015).
202 MacLeod, A. K. *et al.* Characterization of the cancer chemopreventive NRF2-dependent gene battery in human keratinocytes: demonstration that the KEAP1-NRF2 pathway, and not the BACH1-NRF2 pathway, controls cytoprotection against electrophiles as well as redox-cycling compounds. *Carcinogenesis* **30**, 1571-1580, doi:10.1093/carcin/bgp176 (2009).
203 Reddy, S. P. The antioxidant response element and oxidative stress modifiers in airway diseases. *Curr Mol Med* **8**, 376-383 (2008).
204 Vomhof-Dekrey, E. E. & Picklo, M. J., Sr. The Nrf2-antioxidant response element pathway: a target for regulating energy metabolism. *J Nutr Biochem* **23**, 1201-1206, doi:10.1016/j.jnutbio.2012.03.005 (2012).
205 Dhakshinamoorthy, S. & Jaiswal, A. K. Functional characterization and role of INrf2 in antioxidant response element-mediated expression and antioxidant induction of NAD(P)H:quinone oxidoreductase1 gene. *Oncogene* **20**, 3906-3917, doi:10.1038/sj.onc.1204506 (2001).
206 Fiszer-Kierzkowska, A. *et al.* Liposome-based DNA carriers may induce cellular stress response and change gene expression pattern in transfected cells. *BMC Mol Biol* **12**, 27, doi:10.1186/1471-2199-12-27 (2011).
207 Reddy, N. M. *et al.* Genetic disruption of the Nrf2 compromises cell-cycle progression by impairing GSH-induced redox signaling. *Oncogene* **27**, 5821-5832, doi:10.1038/onc.2008.188 (2008).
208 Donadelli, M. *et al.* Synergistic inhibition of pancreatic adenocarcinoma cell growth by trichostatin A and gemcitabine. *Biochim Biophys Acta* **1773**, 1095-1106, doi:10.1016/j.bbamcr.2007.05.002 (2007).
209 Yin, T. *et al.* Bmi1 inhibition enhances the sensitivity of pancreatic cancer cells to gemcitabine. *Oncotarget* **7**, 37192-37204, doi:10.18632/oncotarget.9293 (2016).
210 Proctor, E. *et al.* Bmi1 enhances tumorigenicity and cancer stem cell function in pancreatic adenocarcinoma. *PLoS One* **8**, e55820, doi:10.1371/journal.pone.0055820 (2013).
211 Apte, M. V. *et al.* Desmoplastic reaction in pancreatic cancer: role of pancreatic stellate cells. *Pancreas* **29**, 179-187 (2004).

212 Feig, C. *et al.* The pancreas cancer microenvironment. *Clin Cancer Res* **18**, 4266-4276, doi:10.1158/1078-0432.CCR-11-3114 (2012).
213 Neesse, A., Algul, H., Tuveson, D. A. & Gress, T. M. Stromal biology and therapy in pancreatic cancer: a changing paradigm. *Gut* **64**, 1476-1484, doi:10.1136/gutjnl-2015-309304 (2015).
214 Evans, A. & Costello, E. The role of inflammatory cells in fostering pancreatic cancer cell growth and invasion. *Front Physiol* **3**, 270, doi:10.3389/fphys.2012.00270 (2012).
215 Wu, Y. S., Looi, C. Y., Subramaniam, K. S., Masamune, A. & Chung, I. Soluble factors from stellate cells induce pancreatic cancer cell proliferation via Nrf2-activated metabolic reprogramming and ROS detoxification. *Oncotarget*, doi:10.18632/oncotarget.9165 (2016).
216 Zhang, H. *et al.* Paracrine SDF-1alpha signaling mediates the effects of PSCs on GEM chemoresistance through an IL-6 autocrine loop in pancreatic cancer cells. *Oncotarget* **6**, 3085-3097, doi:10.18632/oncotarget.3099 (2015).
217 Moir, J. A., Mann, J. & White, S. A. The role of pancreatic stellate cells in pancreatic cancer. *Surg Oncol* **24**, 232-238, doi:10.1016/j.suronc.2015.05.002 (2015).
218 McCarroll, J. A. *et al.* Role of pancreatic stellate cells in chemoresistance in pancreatic cancer. *Front Physiol* **5**, 141, doi:10.3389/fphys.2014.00141 (2014).
219 Montecinos, V. *et al.* Vitamin C is an essential antioxidant that enhances survival of oxidatively stressed human vascular endothelial cells in the presence of a vast molar excess of glutathione. *J Biol Chem* **282**, 15506-15515, doi:10.1074/jbc.M608361200 (2007).
220 Sinn, M. *et al.* alpha-Smooth muscle actin expression and desmoplastic stromal reaction in pancreatic cancer: results from the CONKO-001 study. *Br J Cancer* **111**, 1917-1923, doi:10.1038/bjc.2014.495 (2014).
221 Fujita, H. *et al.* alpha-Smooth Muscle Actin Expressing Stroma Promotes an Aggressive Tumor Biology in Pancreatic Ductal Adenocarcinoma. *Pancreas*, doi:10.1097/MPA.0b013e3181dbf647 (2010).
222 Adegboyega, P. A., Mifflin, R. C., DiMari, J. F., Saada, J. I. & Powell, D. W. Immunohistochemical study of myofibroblasts in normal colonic mucosa, hyperplastic polyps, and adenomatous colorectal polyps. *Arch Pathol Lab Med* **126**, 829-836, doi:10.1043/0003-9985(2002)126<0829:ISOMIN>2.0.CO;2 (2002).
223 Athwal, T. *et al.* Expression of human cationic trypsinogen (PRSS1) in murine acinar cells promotes pancreatitis and apoptotic cell death. *Cell Death Dis* **5**, e1165, doi:10.1038/cddis.2014.120 (2014).
224 Frick, T. W., Hailemariam, S., Heitz, P. U., Largiader, F. & Goodale, R. L. Acute hypercalcemia induces acinar cell necrosis and intraductal protein precipitates in the pancreas of cats and guinea pigs. *Gastroenterology* **98**, 1675-1681 (1990).
225 Yoshida, S. *et al.* Pancreatic stellate cells (PSCs) express cyclooxygenase-2 (COX-2) and pancreatic cancer stimulates COX-2 in PSCs. *Mol Cancer* **4**, 27, doi:10.1186/1476-4598-4-27 (2005).
226 Chan, K., Lu, R., Chang, J. C. & Kan, Y. W. NRF2, a member of the NFE2 family of transcription factors, is not essential for murine erythropoiesis, growth, and development. *Proc Natl Acad Sci U S A* **93**, 13943-13948 (1996).
227 Kim, K. B. *et al.* H3K9 methyltransferase G9a negatively regulates UHRF1 transcription during leukemia cell differentiation. *Nucleic Acids Res* **43**, 3509-3523, doi:10.1093/nar/gkv183 (2015).

228 Xu, Z., Pothula, S. P., Wilson, J. S. & Apte, M. V. Pancreatic cancer and its stroma: a conspiracy theory. *World J Gastroenterol* **20**, 11216-11229, doi:10.3748/wjg.v20.i32.11216 (2014).
229 Ballatori, N., Krance, S. M., Marchan, R. & Hammond, C. L. Plasma membrane glutathione transporters and their roles in cell physiology and pathophysiology. *Mol Aspects Med* **30**, 13-28, doi:10.1016/j.mam.2008.08.004 (2009).
230 Martinez-Outschoorn, U. E. *et al.* Oncogenes and inflammation rewire host energy metabolism in the tumor microenvironment: RAS and NFkappaB target stromal MCT4. *Cell Cycle* **12**, 2580-2597, doi:10.4161/cc.25510 (2013).
231 Cui, S. & Chang, P. Y. Current understanding concerning intestinal stem cells. *World J Gastroenterol* **22**, 7099-7110, doi:10.3748/wjg.v22.i31.7099 (2016).
232 Salama, P. & Platell, C. Colorectal cancer stem cells. *ANZ J Surg* **79**, 697-702, doi:10.1111/j.1445-2197.2009.05054.x (2009).
233 Zeki, S. S., Graham, T. A. & Wright, N. A. Stem cells and their implications for colorectal cancer. *Nat Rev Gastroenterol Hepatol* **8**, 90-100, doi:10.1038/nrgastro.2010.211 (2011).
234 Wang, F. *et al.* UHRF1 promotes cell growth and metastasis through repression of p16(ink(4)a) in colorectal cancer. *Ann Surg Oncol* **19**, 2753-2762, doi:10.1245/s10434-011-2194-1 (2012).
235 Hidalgo, M. Pancreatic cancer. *N Engl J Med* **362**, 1605-1617, doi:10.1056/NEJMra0901557 (2010).
236 Li, D. & Abbruzzese, J. L. New strategies in pancreatic cancer: emerging epidemiologic and therapeutic concepts. *Clin Cancer Res* **16**, 4313-4318, doi:10.1158/1078-0432.CCR-09-1942 (2010).
237 Geng, R. *et al.* Oxidative stress-related genetic polymorphisms are associated with the prognosis of metastatic gastric cancer patients treated with epirubicin, oxaliplatin and 5-fluorouracil combination chemotherapy. *PLoS One* **9**, e116027, doi:10.1371/journal.pone.0116027 (2014).
238 Sutton, P. *et al.* Proteomic analysis to identify biomarkers in the primary tumour that predict response to neoadjuvant chemotherapy in liver metastases. *Lancet* **385 Suppl 1**, S95, doi:10.1016/S0140-6736(15)60410-X (2015).
239 Awadallah, N. S. *et al.* NQO1 expression in pancreatic cancer and its potential use as a biomarker. *Appl Immunohistochem Mol Morphol* **16**, 24-31, doi:10.1097/PAI.0b013e31802e91d0 (2008).
240 Chen, S. H. *et al.* Gemcitabine-induced pancreatic cancer cell death is associated with MST1/cyclophilin D mitochondrial complexation. *Biochimie* **103**, 71-79, doi:10.1016/j.biochi.2014.04.004 (2014).
241 Obata, Y. *et al.* The epigenetic regulator Uhrf1 facilitates the proliferation and maturation of colonic regulatory T cells. *Nat Immunol* **15**, 571-579, doi:10.1038/ni.2886 (2014).
242 Gray, D. H. & Liston, A. Uhrf to Treg cells: reinforcing the mucosal peacekeepers. *Nat Immunol* **15**, 533-534, doi:10.1038/ni.2893 (2014).
243 Jaramillo, M. C. & Zhang, D. D. The emerging role of the Nrf2-Keap1 signaling pathway in cancer. *Genes Dev* **27**, 2179-2191, doi:10.1101/gad.225680.113 (2013).
244 Pearson, T. A. & Manolio, T. A. How to interpret a genome-wide association study. *JAMA* **299**, 1335-1344, doi:10.1001/jama.299.11.1335 (2008).
245 McWhinney, S. R. & McLeod, H. L. Using germline genotype in cancer pharmacogenetic studies. *Pharmacogenomics* **10**, 489-493, doi:10.2217/14622416.10.3.489 (2009).

246 Tatarian, T. *et al.* Cytoplasmic HuR Status Predicts Disease-free Survival in Resected Pancreatic Cancer: A Post-hoc Analysis From the International Phase III ESPAC-3 Clinical Trial. *Ann Surg*, doi:10.1097/SLA.0000000000002088 (2016).